Semiclassical theory of few- and many-body quantum systems with short-range interactions

DISSERTATION ZUR ERLANGUNG DES DOKTORGRADES DER NATURWISSENSCHAFTEN (DR. RER. NAT.) DER FAKULTÄT FÜR PHYSIK

DER UNIVERSITÄT REGENSBURG

vorgelegt von

Quirin Hummel aus

Mallersdorf-Pfaffenberg

im Jahr 2017

Promotionsgesuch eingereicht am: 05.05.2017

Die Arbeit wurde angeleitet von: Prof. Dr. Klaus Richter

Prüfungsausschuss:

Vorsitzender:	Prof. Dr. Christoph Strunk
Erstgutachter:	Prof. Dr. Klaus Richter
Zweitgutachter:	Prof. Dr. Ferdinand Evers
Weiterer Prüfer:	Prof. Dr. Tilo Wettig

Termin Promotionskolloquium: 23.10.2017

Für Ronja

A short note to the reader

Level of detail

When reading this thesis one may at some points experience an uncommon level of detail. As a matter of taste, I decided to create a rather self-contained handbook that can be actually used as a tool by anyone who is willing to do so. This decision was made especially in view of the colleagues involved in this project right now and potential students to study and continue this line of work in the future. I apologize to the reader in case he/she is more interested in the presentation of results and prefers a more superficial overview about methodical aspects. I beg for their understanding and kindly request them to scan the corresponding passages more superficially.

Used acronyms

To avoid confusion, I give here a short list of acronyms used throughout this work in chronological order:

DOS for **D**ensity **O**f **S**tates,

DFT for **D**ensity **F**unctional **T**heory,

BEC for **B**ose-**E**instein **C**ondensate,

NLSE for **N**onlinear **S**chrödinger **E**quation,

QPT for **Q**uantum **P**hase **T**ransition,

WKB for **W**entzel-**K**ramers-**B**rillouin,

EBK for **E**instein-**B**rillouin-**K**eller,

QCE for **Q**uantum **C**luster **E**xpansion,

ESQPT for **E**xcited-**S**tate **Q**uantum **P**hase **T**ransition,

LPA for **L**ocal **P**otential **A**pproximation,

BCS for **B**ardeen-**C**ooper-**S**chrieffer,

ROBDM for **R**educed **O**ne-**B**ody **D**ensity **M**atrix.

Contents

Introduction

The general topic of interest

To put the subject of interest into a very general light, I allow myself to start with a rather broadly formulated topic. The position of reductionism may be stated with a citation of P. W. Anderson [1]:

> *"The workings of our minds and bodies, and of all the animate or inanimate matter of which we have any detailed knowledge, are assumed to be controlled by the same set of fundamental laws, which except under certain extreme conditions we feel we know pretty well."*

As far as I can overlook from my experience, this point of view can be regarded widely accepted in the branch of natural sciences. In terms of theories one might formulate it in the following way: Despite in practice different theories are applied to explain phenomena on different levels of abstraction or scales, they all are believed to be implied by fundamental ones, albeit in a hidden and often incomprehensible way.

As Anderson points out in his essay, this type of reductionism does not lead to what he refers to as "constructionist" point of view. While there may be unique first principles and fundamental laws of nature that *determine* all phenomena on all scales, they cannot be applied methodologically to *reconstruct* the latter in general.

A typical situation that applies to – if not representing the essence of – this picture of emergent phenomena, are systems of particles that interact with each other.

While the basic principles and rules after which the system behaves might be known and even simple to formulate within one theory of choice, it is typically a hard if not impossible task to deduce from them the possibly rich collective phenomena that emerge or to predict the actual evolution of the system assuming knowledge of an initial state.

A typical scenario would be the following. If one augments the interacting particles to large numbers one might enter another layer of complexity, a new scale described by new theories in which the emergent phenomena of the previous might be treated as the new elementary entities or mechanisms.

Just to illustrate this point a bit, think for instance of sound waves as the elementary entities within an acoustic theory but actually emerging from interactions between individual molecules of a fluid. While the description in terms of wave equations may be a valid approximation in a macroscopically large system, it breaks down when only a small number of molecules is present. Then,

the description within the more fundamental theory usually becomes inevitable, demanding to treat the interplay of all constituents in a direct – not an effective – way.

It is this zone between successive layers of abstraction and also the precise way the two are connected that is as compelling to understand as it is challenging.

In the context of systems of mutually interacting particles this motivation applies already on the level of classical mechanics. If the particles are further demanded to be described quantum mechanically, the physical reality becomes even less intuitive from every-day experience, further exponentiating the motivations. To mention one aspect, with the indistinguishability of identical particles one introduces a concept without any classical analogue. The related (anti-)symmetry of fermions or bosons is a property addressing the quantum mechanical wave function of the whole system and has no direct meaningful counterpart on the classical level. But just like inter-particle interactions, the exchange symmetry is easily formulated as a fundamental law while having the potential to offer rich emergent phenomena. Consider for instance Bose-Einstein condensation, or even the every-day experience phenomenon of impenetrability of matter, mostly attributed to the indistinguishability of electrons and the implied Pauli exclusion. If one further combines the principles of quantum mechanics including indistinguishability with mutual interactions, a whole variety of directly observable non-trivial effects arises.

One striking example where distinctive properties on the very macroscopic level emanate from the interplay of these elementary mechanisms are neutron stars (see [2] for a historical introduction). While their existence is already predicted from indistinguishability alone, their mass-bounds and unique and rich internal structure are drastically influenced by interactions (see [3] for a recent review).

A prime example on a less cosmic but still macroscopic level is the effect of superconductivity [4] that does not have any classical analogue and strongly depends on mutual interactions which are needed to form cooper-pairs [5] of electrons, compound particles that can then in some circumstances be considered as bosons.

The fractional quantum Hall effect of two-dimensional electron gases is another example (see [6] for the Nobel lecture). Its origins are not yet fully revealed but have many proposals to be understood from interactions.

Another contemporary example are the many interesting effects one observes in optical lattices filled with ultracold atoms. Since the early stages when neutral atoms were trapped in optical lattices for the first time such experiments have evolved diversely (see [7, 8] for a review). In the meanwhile one has produced and measured transitions between Mott-insulating and superfluid phases [9] involving many atoms but also the propagation of few atoms, producing for instance such non-trivial phenomena as fermionization of bosons and the formation of repulsively bound pairs [10], an effect that is only possible due to the combination of interactions, symmetry and lattice discreteness. The high degree of control one has by now in such experimental setups has even made them a playground to simulate quantum mechanical effects of quantum systems on smaller scales. In this context they are considered as quantum simulators [11], *e.g.* for investigating interaction effects on conduction in condensed matter and the related many-body localization or even to simulate lattice gauge theories.

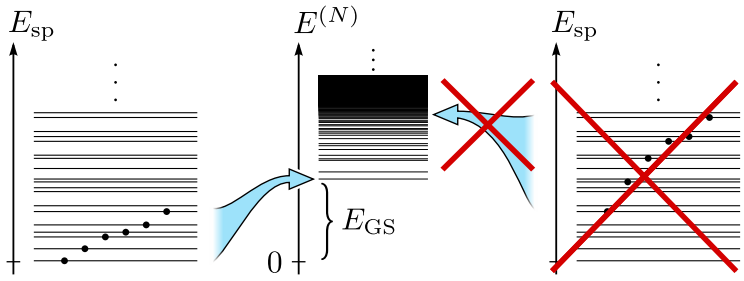

Fig. 1: Sketch of a typical mean-field picture of a (spinless) fermionic system. The lowest many-body energy levels $E^{(N)}$ are built up by independently occupying effective single-particle levels E_{sp} (left). For higher excitations the picture of independent particles becomes invalid (right). Typically, the density of states of the many-body spectrum (center) grows rapidly with the excitation.

This is by far not a complete list. Instead it is meant to emphasize the general interest in the subject, *i.e.*, systems of few or many interacting indistinguishable quantum particles.

The multitude of known methods and their limitations

This section is supposed to give an overview over important existing theoretical approaches to interacting quantum systems. As the available methods are too numerous this cannot be a complete list. Furthermore, the intention is not to provide detailed insights to the various non-trivial aspects inherent to each of the techniques and the great successes attributed to them. Only their general individual strengths, capabilities and limitations will be pointed at. For an expert's viewpoint I refer the reader to the respective literature.

Effectively independent particles

First of all, there is a variety of methods that treat many-body systems as effectively independent particles. The prime example being mean field descriptions, where the mutual influence of particles on each other due to interactions is simulated by an effective external potential. In a typical picture one would interpret the interacting ground state of a system as a starting point – a *vacuum* – on top of which effectively non-interacting quasi-particles build up the excitation spectrum. Especially in view of reproducing the correct excitation spectrum of the system as a whole, such descriptions become inappropriate when the latter only comprises a small number of particles (not quasi-particles). Figure 1 sketches the typical picture. While the lowest excitations in the spectrum of total energies might still be described to a satisfactory degree by occupying levels of the effective single-particle spectrum, this description becomes inappropriate for higher excitations. The deficiency has its origin in the fact that the mean field is associated to the ground state of the system and strictly speaking would have to be adjusted individually for each excitation. Another way to look at this is that the effects originating from residual interactions on top of the mean-field become non-negligible. These effects get enhanced if the number of particles is particularly small. If in addition the true eigenstates of the system are strongly

correlated the mean-field picture can be insufficient already for the lowest excitations, and the eigenenergies for which the picture does not apply can in general not be written as the sum of independent single-particle energies. To avoid confusion here I will completely drop the picture of independent particles. Energy dependent quantities like spectral densities, counting functions or similar are considered as related to the total energy of the system throughout this work. As a side-remark, Fig. 1 also illustrates qualitatively the fact that the density of total energies of a many-body system typically grows very rapidly so that for thermodynamic considerations of finite temperature the excited states become very important.

There is another practical problem associated with independent particle descriptions. Even when the particles at hand are genuinely non-interacting, the *analytic* description of the *average* density of states (DOS) is a non-trivial task when indistinguishability is taken into account. In the past, there was an interest on this quantity in the context of studying resonances of heavy nuclei, where an own research field developed to appropriately model the effective mean-field potential for nucleons, *e.g.*, by the class of Woods-Saxon potentials [12]. The analytic form of the collective DOS of all nucleons was found to be approximated by the Bethe formula [13]

$$\bar{\rho}_{\mathrm{Bethe}} = \frac{1}{\sqrt{48}Q} \exp\left(\sqrt{\frac{2\pi^2}{3}\rho_0 Q}\right) , \tag{1}$$

where Q is the (total) excitation energy. The derivation of this formula not only assumes independent (non-interacting) fermions, but also is only valid if the single-particle DOS at the Fermi energy can be considered as a constant ρ_0. Furthermore, another approximation is involved that limits the validity of (1) to the lowest excitations. Depending on the total number of particles, this restriction gets especially narrow in the few-particle sector, posing a strong restriction (see [14] for direct comparisons). If the assumption of constant single-particle level spacing holds not only on average but level-by-level, the DOS is related to the combinatorial problem of finding the number of restricted integer partitions[1]. However, for a generic system of not too many independent fermions or bosons, none of the assumptions holds, rendering the analytic prediction of the average DOS a non-trivial task. One finds here a limitation in the few-body sector when describing average spectra of (arbitrarily high) excitations.

Density functional theory

Another very commonly used approach is based on density functional theory (DFT) (see, *e.g.*, [16] or [17] for an introductory overview). The foundation of this theory is the seminal Hohenberg-Kohn theorem [18], which in its original formulation is an exact statement about interacting inhomogeneous electron gases. It states that (assuming a given specified interaction potential) a unique

[1] Interestingly, the problem of *unrestricted* integer partitions was analytically solved by Ramanujan and Hardy [15] in terms of the 24th roots of unity. The dominant term of their solution gives exactly the asymptotic expression (1). However, for restricted partitions apparently no general solution is known and one has to rely on recurrence relations. One expression for the restricted case will be given here by a polynomial found for the DOS of N free bosons in two dimensions (see section 1.1.4).

bijection exists between the external potential (which then specifies the system) and the electron density $n(\mathbf{r}) = N \int \mathrm{d}^3 r_2 \ldots \mathrm{d}^3 r_N |\Psi(\mathbf{r}, \mathbf{r}_2, \ldots, \mathbf{r}_N)|^2$ (the sum over spins is here omitted from notation) from the (non-degenerate) ground state Ψ of the system of N electrons. The density therefore is a unique representation of the full ground state wave function Ψ. While being a purely mathematical circumstance in the first place, it has been transfered to an applicable tool by recognizing the implication that the ground state energy has to be a unique functional of the density. If one knew this functional or a good approximation to it, it would then allow one to reduce the solution for the ground state energy to a problem in three rather than $3N$ coordinates – a huge simplification, *e.g.*, in view of the exponential growth of numerical computation times with the number of degrees of freedom. Further progress was made by Kohn and Sham [19] by expressing the system in terms of an exact reformulation as a number of effectively non-interacting fermions, where the effective external potential is itself a functional of the overall particle density, yielding a nonlinear optimization problem. The functional involved can then be split into a known part involving the external and interaction potential of the system and an unknown exchange correlation functional. It is this functional that makes the huge difference to descriptions dropping inter-particle correlations like the Hartree-Fock method [20, 21].

On the one hand, DFT has been widely and successfully used in many systems and is a major tool in modern research especially in determining the influence of variations of system parameters while many basic system characteristics are kept constant. On the other hand, it is still unclear if there exists a proper way to (approximately) determine the exchange correlation functional universally. To date, a huge multitude of different approximate functionals has been developed, each designed to work in specific classes of systems. This circumstance makes predictions with this method a non-trivial issue. When applied to a new system the first time, the use of a specific functional has to be either empirically guessed from experience with similar systems, chosen by generally identifying the approximations inherent to the functional as fitting to the system specifics, or has to be verified by independent ab-initio calculations or experimental measurements. Note that this issue is of lesser importance in systems that are known or expected to exhibit only weakly correlated particles.

Another limitation of time-independent DFT is that in its exact formulation, solving the Kohn-Sham equations for the ground state energy does not imply a solution for excited-state energies. Strictly speaking, the Kohn-Sham orbitals cannot literally be used as single-particle orbitals of a non-interacting system to determine excitations of the whole system. Doing so can only be an approximate description, yet it can serve as a starting point by providing a good basis for post DFT methods.

Perturbative approaches

Perturbative approaches consider interactions between particles as (small) perturbations of a decoupled theory that is taken as a starting point. Usually one attributes a coupling parameter to the interaction term in the Hamiltonian or the Lagrangian describing the theory and considers it as a small parameter. The effects from interaction on any property of interest – say, the ground state energy or a transition amplitude – are then included step by step by successive calcu-

lation of the coefficients of power series expansions in the coupling parameter. One might think of direct perturbation theory in the first quantized approach of Schrödinger or expansions in terms of Feynman diagrams in second quantized formulations like relativistic or non-relativistic quantum field theories.

Suppose a system under investigation is described by a renormalizable field theory and that one can properly define power series expansions in the coupling. Such perturbation expansions have been applied with great success in many areas. One prime example being quantum electrodynamics as the fundamental theory describing the coupling between electrically charged fermions and the electromagnetic field, where the dimensionless coupling parameter is as small as $\alpha_{\mathrm{em}} \approx 1/137$.

A heavy problem arises when the coupling cannot be considered a small parameter, so that a large number of terms in the corresponding power expansions have to be taken into account in order to describe a specific property accurately. Unfortunately the number of diagrams that have to be calculated grows in an extreme way (typically factorially!) with the power of the coupling parameter. For instance, this is one main reason why the description of the strong nuclear force within the quantum field theory of quantum chromodynamics involves such tremendous efforts. On the one hand this makes the description of nucleons and other baryons under natural conditions, *i.e.*, as bound systems of quarks and gluons at least partially rely on heavy use of simulations on the most powerful super computers ever built. On the other hand it is one of the reasons for the tremendous efforts taken to produce laboratory conditions in supercolliders under which the effective coupling becomes small enough to allow contact with experiments via perturbative expansions to test the foundations of the standard model of particle physics.

In experiments with ultracold atoms we will find another candidate in which arbitrarily large couplings are realized.

Classical field descriptions of Bose systems

An often used method especially to deal with Bose-Einstein condensates (BECs) of a large number of bosons under the influence of interactions is the description in terms of nonlinear Schrödinger equations (NLSEs). For instance this approach has been applied [22] to describe what is called a quantum phase transition (QPT) in one-dimensional attractively interacting Bose gases, where the ground state discontinuously changes its quality when a specific parameter is changed across a certain threshold. Formally this is attributed to similar mathematical mechanisms as in the description of second order phase transitions with Landau's theory [23].

The use of NLSEs like the Gross-Pitaevskii equation [24, 25] in describing quantum mechanical systems can either be considered as invoking the classical limit of quantized field theories or equivalently as the implication of a variational ansatz using product-wave functions with all bosons in the same single-particle state. Viewed as a classical limit, one has to think of the parameter that distinguishes the degree of "classicality" as not being Planck's quantum of action $\hbar$ but an effective quantity which turns out to vanish for large numbers of particles. From this perspective it becomes clear that nonlinear field descriptions correctly describe the true physics of a system only in the limit of infinitely many particles. This makes such approaches the "number one" analytical tool

in describing phase transitions and QPTs in macroscopically large systems close to the thermodynamic limit. Usually they are used to describe the ground state of a system, which becomes clear when viewed as the solution within a variational ansatz. To clarify this point a bit more in the following, I will adapt the interpretation as a classical limit. There may be additional solutions with higher energies. The different solutions thereby may be viewed as coexisting classical fixed point solutions residing in different minima (or other stationary points) of an – in this context infinite dimensional – potential landscape. If the fixed points correspond to maxima or saddle points they are dynamically unstable and do not allow for quantum states that reflect the classical solutions.

When relaxing the number of particles to a finite number N, each of the stable solutions would get associated a number of quantum excitations in what might typically be considered high dimensional potential wells. For large N these excitations generically are large in number with small spacings. Therefore in this regime, if there exist any higher energy solutions they correspond to (branches of) extremely highly excited states (with an excitation index growing with N). Therefore such solutions of higher energy are non-essential for macroscopic systems. The usual analytical approach to gain information about relevant excitations is the theory of Bogoliubov approximation [26–28]. It basically approximates the excitations around the fixed points by equidistant excitations of harmonic oscillators. Generically, for large systems $N \gg 1$, which corresponds to $\hbar_{\text{eff}} \ll 1$, the deviations from the quadratic approximation can be neglected.

The situation changes drastically if the system undergoes a QPT. This is attributed to a change in the qualitative character of the classical ground state solution of the NLSE. In the typical scenario of a second order transition this happens due to a bifurcation of the corresponding classical minimum, changing the signature of the Hessian from positive definiteness to an indefinite or negative definite form. The minimum becomes a saddle-point or even a maximum, rendering the classical solution unstable and therefore unavailable as quantum mechanical state. Beyond the point of transition it typically resides then in a neighboring minimum that has different physical characteristics.

When approaching the point of transition the harmonic frequency in at least one direction vanishes, leading to a breakdown of the Bogoliubov approximation. The description within the latter falsely predicts a collapse of all excitation energies to zero directly at the transition. If one considers the strict limit of $N \to \infty$ the breakdown happens only at the transition – a point of zero measure in parameter space – so that the approximation may be considered valid at any point arbitrarily close to the transition. It is actually this discontinuous feature of collapsing excitations and sudden change of the ground state energy that defines the QPT as such. In contrast to that, if the number of particles is large but finite, the description within Bogoliubov theory breaks down in a finite vicinity of the critical parameter.

Another signature of the breakdown is the width of the quantum ground state wave function in the field degrees of freedom (here considered classical) that gets drastically enhanced as the minimum widens from a quadratic to a higher-order dependence in at least one direction. The interpretation of this feature within Bogoliubov theory is that the many-body ground state can no longer be described as a condensate where almost all bosons occupy the same single-particle mode. Instead, the latter gets depopulated in favor of the occupa-

tion of other modes, resulting in a many-body state with non-trivial correlations between particles. This macroscopic decrease of the condensate fraction is called depletion of the condensate. It can be viewed as a physical reason – equivalent to the above considerations – for the breakdown of the Bogoliubov approximation, which relies on the ansatz of a product state without any correlations.

The excitation energies for finite N do not get arbitrarily close but show small but finite spacings, which have a non-trivial effect on physical observables. The analytic quantification of this finite-size precursor of a QPT is conceptually very hard up to impossible to attack within the Bogoliubov approach and demands to take into account genuine inter-particle correlations.

Exact analytical solutions in particular systems

For specific models of interacting systems there exist exact analytical solutions.

One example is the description of one-dimensional fermionic systems as Tomonaga-Luttinger liquid [29, 30], which admits an exact solution [31] arising from a linear single-particle dispersion. The requirement of constant single-particle level spacings and infinitely deep Dirac sea for the exact solution could be considered either as a restriction to a particular class of systems or again as an approximate description valid in the regime of large numbers of particles by linearization of generic single-particle dispersions at the Fermi energy.

Another class of solvable models especially related to this work is given by one-dimensional systems of bosons or fermions that are solvable by a Bethe ansatz (see [32] for the historical advent). Important examples are the Lieb-Liniger model [33, 34] of identical bosons on a line with contact interactions of zero range and periodic boundary conditions, the Gaudin-Yang model [35, 36], which is the fermionic counterpart for spin-1/2 particles and a "dynamical impurity model" of equal masses included in the latter as the case of maximized spin-imbalance, where one particle has a spin-polarization different from all the others. These models will be addressed in more detail later (see section 1.3.3 and section 1.4.3).

Here I want to emphasize that in general solvable models are very special and can be considered exceptional. For instance, adding external potentials instead of periodic boundary conditions or introducing mass imbalance renders the Lieb-Liniger and Gaudin-Yang model non-integrable. Nevertheless, one great opportunity they provide is to use them as benchmark for other methods. Moreover, as will be highlighted in the presented work (see section 1.5.3), there are ways to borrow exact results on fundamental analytic ingredients from the solvable models, then transferred to be used in non-solvable ones.

Numerical approaches

What can nowadays be considered the third main pillar of physical research besides theory and experiment is the field of computational physics. The role of this fast developing manifold of numerical approaches is somewhat fuzzily located between the two traditional branches of theoretical and experimental physics. One of the main reasons why numerical simulations have become so important are precisely the limitations of analytical theoretical approaches mentioned above. While the elementary mechanisms and therefore basic theories behind a phenomenon are known in many cases, the physical consequences – in

their complexity – are very often too hard or impossible to be reliably deduced by analytical methods.

In the context of interacting systems, it were the methods of self-consistent fields [37] that pushed the necessity of implementations in terms of numerical calculations. Even though the methods of Hartree and Hartree-Fock [20, 21, 37] do not take into account inter-particle correlations – beyond the ones purely related to exchange symmetry – they are in their usual iterative solution already only tractable as numerical implementations.

If correlations have to be taken into account – which is a basic demand within the presented work – one can rely on direct diagonalization techniques in truncated Hilbert spaces, often referred to as *configuration interaction*. Usually the truncation happens on the level of allowed single-particle orbitals. Truncation thereby most of the times is the only simplification, and these exact diagonalization methods offer great reliability in representing the actual system. Their obvious disadvantage is the extreme (exponential) growth in computation times with the number of particles or the cutoff in Hilbert space.

A lot of development has taken place in building a bridge between the methods of self-consistent fields and direct diagonalization by what is called *multi-configurational self-consistent fields* [37]. When one relaxes the restriction of the Hartree and Hartree-Fock method by allowing superpositions of a number of symmetrized product states one combines the quality due to optimization inherent from the variational nature of the self-consistent approach with the incorporation of correlated states on an effective level. This has been pushed to a level where sophisticated implementations like, *e.g.*, the multi-layer multi-configurational time-dependent Hartree method for bosons [38] allow to reliably simulate the non-trivial dynamics of correlated interacting few-boson clouds [39].

When simulating quantum fields a heavily used basic approach is given by discretization of space-time into a lattice of discrete points (and bonds) that index the quantum fields, which makes the number of quantum degrees of freedom finite. In many cases, such lattice approaches come with their own vast amount of non-trivial complications, one of the most prominent being the sign-problem [40], *e.g.*, inherent to quantum chromodynamics and related theories[2]. Therefore the idea of quantum simulations on lattices has created its own wide and living field of research (including an own arXiv section).

The trade-off that all numerical approaches come with is that explicit analytic dependencies on parameters are hidden: for any new set of parameters (that cannot be scaled out) one needs to repeat the corresponding calculations.

[2]Interestingly in some related models $(O(N), CP(N-1))$ coupled to a chemical potential it is possible by preceding analytical reformulation in terms of *dual variables* [41] to overcome the sign problem. This does not only make the subsequent quantum Monte Carlo simulations [42] numerically way more tractable, but also allows for alternative physical understanding of individual realizations involved in the sampling by a *world-line* interpretation of the dual variables. The latter can somewhat be considered an efficient rephrasing of which degrees of freedom are interpreted as elementary particles of the theory. Most interestingly, promising preliminary work [43] shows that the same ideas can be applied to the one-dimensional non-relativistic nonlinear Schrödinger field, closely related to the short-range interacting Bose gases mostly considered as applications in this thesis.

The power of semiclassics

The attempt of the project behind this thesis is to contribute to overcome some of these limitations. The intention is to introduce a focus on parameter ranges and properties that are – as far as I can overlook – not covered to a satisfactory degree by the majority of known methods in one way or another. In order to approach this still tremendous task, the ideas presented here are based on the concepts of semiclassical approximation. Specifying a particular class of simplified models (see the section after the next) will further reduce the generality in favor of allowing for explicit calculations and predictions when it comes to actual applications.

Filling the gap between waves and particles

The origins of semiclassics date back to the early stages when the quantum nature of the micro-world was just in the beginning of its discovery. When Franck and Hertz showed 1914 in their experiment [44] that the energies of an atom are restricted to discrete levels, the fundamentals of quantum mechanics were yet far from being uncovered. It was the model of Bohr [45], proposed one year before, that was supposed to be the correct theory to describe quantized energies of atoms. While still understanding the electrons in an atom as classical particles, his postulate of classical orbits being quantized to specific actions could now be seen as additionally attributing wave properties to them. In this sense, one can denote Bohr's model the first semiclassical description of a quantum system. With the subsequent generalization to elliptic orbits within the Bohr-Sommerfeld quantization rule [46] one was then able to fully reproduce the hitherto observed discrete spectrum of the hydrogen atom. These were the successful days of the "old quantum theory" which finally had to face a dead end when the various attempts of Bohr, Sommerfeld, Born, Kramers, Landé, van Vleck and others to apply it to the helium atom failed (see [47] for a historical overview).

It needed the collective ingenuity of Planck, Einstein, de Broglie, Born, Heisenberg, Schrödinger, and others to initiate the "new quantum theory". After the seminal development of Schrödinger's equation, the heuristic model of Bohr and Sommerfeld could be retrospectively identified as Wenzel-Kramers-Brillouin (WKB) or Einstein-Brillouin-Keller (EBK) quantization (see [48] for a review on the subject). As these descriptions are only available for systems with integrable classical counterparts, this connection further explained the failure of the old theory to describe the helium atom – a prime example of a non-integrable, chaotic three-body system. On the one hand, the approximations of WKB and EBK are formally connected to the true quantization in terms of Schrödinger's equation by considering Planck's quantum of action $\hbar$ as a small parameter (as compared to the typically way larger classical actions of a system). On the other hand, the final form of the quantization rules is purely given in terms of the classically allowed trajectories of the system and $\hbar$. Therefore they can be considered as the first *consciously* semiclassical approximations.

The value of semiclassics is thereby not only to be found in justifying older models. This framework is moreover able to build a bridge between the quantum and the classical world, which had been a riddle: how could the variety of bizarre-looking features of the former be smoothly connected to the compre-

hensibility of the latter in terms of everyday experience? Semiclassical approximations therefore can be considered to provide improved understanding and intuition for quantum mechanical processes, effects and properties.

The beauty with which semiclassical methods provide this bridge of comprehension and the power in its quantitative predictions was pushed to a climax in 1967 and the following years when Gutzwiller showed in his seminal works [49] (see [50] for historical developments) how to correctly apply them to approximate the quantum mechanical propagator. It had been before considered by van Vleck [51] as early as in 1928 to formulate such an approximation in terms of classical orbits using a probabilistic approach, but it was Gutzwiller who rigorously derived its corrected version on the basis of Feynman's [52] formulation as a path integral, dating back to 1948. By applying a stationary phase approximation in infinite dimensional path space he deduced what is now called the van Vleck-Gutzwiller propagator

$$K(\mathbf{q}^{\mathrm{f}}, \mathbf{q}^{\mathrm{i}}; t) = \sum_{\gamma:\, \mathbf{q}^{\mathrm{i}} \overset{t}{\mapsto} \mathbf{q}^{\mathrm{f}}} A_\gamma \mathrm{e}^{\mathrm{i}R_\gamma/\hbar}\,, \tag{2}$$

that surpasses the limitations imposed by naive application of the Ehrenfest theorem [53]. In his approximation the integral over all possible paths gets reduced to a coherent *sum* over amplitudes associated with all *classically allowed* trajectories γ connecting the initial and final points $\mathbf{q}^{\mathrm{i}}, \mathbf{q}^{\mathrm{f}}$ in coordinate space. It is this sum that expresses the capability of describing interference phenomena.

Furthermore, Gutzwiller showed [54] how one can use this propagator to approximately calculate the DOS of non-integrable, chaotic single-particle systems, which was a huge step in the history of semiclassics. The DOS thereby gets naturally split into two components, a fluctuating part that oscillates and averages to zero and a smooth part representing the DOS on average. The former – now famously known under the name Gutzwiller trace formula [see (1.9)] – is again purely formulated in terms of $\hbar$ and the classical orbits of the system with given energy and demanded to be *periodic*. The latter, which will have a main focus on in the first part of the thesis, is often attributed to the paths of vanishing length (see [55] for a review on this subject). Those were shown (again by Gutzwiller [49]) to comprise the dominant point-like paths spanning over the whole available phase space volume [56] on the one hand. On the other hand, additional paths of short length that are related to reflections very close to boundaries and alike are posing sub-dominant but still significant contributions [57] (more details on this point will be reviewed in section 1.1.2). By his insights, Gutzwiller created a whole new field in physics, dedicated to the subject now known as *quantum chaos*.

Providing quantitative predictions

One great new opportunity provided by Gutzwiller's trace formula was its complementary approximation to all methods known up to then. One special feature is for instance the analytic dependence on system parameters through the characteristics of orbits. Once those orbits are classified, their classical properties like actions, lengths, periods and stabilities are often known analytically, making the same single calculation cover whole ranges of parameters.

Another advantageous feature of the semiclassical description is related to the functional dependence on parameters. For instance contrasting perturbation

theory, the strength of a perturbing potential would be included to full extent from the beginning. Similarly, any system parameter – including $\hbar$ – appears in a non-perturbative way. It is mostly attributed to this non-trivial contribution in all orders of $\hbar$ that the trace formula proved itself way more accurate than expected in many cases of microscopic systems, where $\hbar$ could not be considered particularly small. A precursor of this general finding could be seen in the integrable versions of WKB and EBK in their accurate description of the hydrogen atom. In contrast to truncated power series the sum over periodic orbits has to be understood as an asymptotic series, where the most dominant effects are incorporated by the shortest, most stable orbits. Those usually give the gross shell structure of spectra representing fluctuations in the DOS on the scale of several mean-level spacings.

For an exhaustive and continuously actualized review on applications of periodic orbit theory, see [58]. Periodic orbits provide a way to interpret the harmonic analysis of quantum mechanical spectra in terms of classical actions and stabilities. This powerful technique was first successfully applied in atomic [59–62] and molecular [63] systems and microwave cavities [64]. After its early success, the periodic-orbit analysis of quantum mechanical spectra and wave functions (where periodic orbits manifest as scars [65]), has become a standard tool in mesoscopic [66, 67], chemical [68] and recently, many-body physics [69].

Describing universality

The application of semiclassical methods to understand the emergence of universal features of quantum systems is another branch where great successes have been achieved. According to random matrix theory (RMT), Hamiltonian matrices fall into a small number of universality classes represented by their fundamental symmetries – like, *e.g.*, time-reversal invariance (see, *e.g.*, [70]). The statistics of their eigenvalues were observed to be found in the spectra of specific quantum mechanical systems. It was the use of Gutzwiller's trace formula that substantiated this connection physically for arbitrary chaotic quantum systems of a single particle, which was up to then just a conjecture (see Bohigas, Giannoni and Schmit [71]). While in a first "diagonal" approximation [72] one could derive the leading order term of spectral form factors, it was a huge step [73] to elevate this connection to the next order by considering specific *pairs* of distinct but related orbits of similar action – now known under the name Sieber-Richter pairs. Since then, these universal considerations have been extended in several steps [74–83] by using generalizations of Sieber-Richter pairs to finally reproduce the full RMT result analytically [84] (up to the Heisenberg time T_{H}), underlining the depth with which interference effects are incorporated in semiclassical descriptions.

Other successful descriptions of universal properties of single-particle systems include weak localization [85–87] and anti-localization [88, 89], coherent backscattering [90] and the Loschmidt echo [91, 92] all based on the diagonal approximation. Moreover, Sieber-Richter pairs heave been used to calculate universal conductance fluctuations [93], transport of BECs through chaotic scattering regions [94] and conductance of chaotic conductors [95–97], the thermopower and conductance of Andreev billiards [98, 99] and the Loschmidt echo [100, 101].

There is yet another intriguing inference from semiclassical classification of uni-

versality that draws a connection to pure mathematics. The famous Riemann hypothesis [102] states that the non-trivial zeros of the Riemann zeta function $\zeta(s)$ are constricted to a specific line in the complex plane. While verified extensively by numerical calculation, it is still a big riddle if and how the conjecture could be proved[3]. The ζ-function can be reformulated to formally express the density of its zeros as an asymptotic series. When the formal analogy to a Gutzwiller trace was recognized this brought new life to an old proposal by Hilbert and Pólya (see [104] for a review on the subject). The idea is that one could possibly give a proof by finding a quantum mechanical system (described by a self-adjoint Hamiltonian) with a spectrum that resembles the ζ-zeros. There is, in addition, numerical evidence that the zeros share the same statistics with the eigenvalues of the Gaussian unitary ensemble. Together with this connection to RMT, the Bohigas-Giannoni-Schmit conjecture [71] underlines the basic idea and involvement of a semiclassical understanding. The implications from the analogy to semiclassics thereby helped to strongly narrow down the search for possible candidate systems beyond a pure classification of the universality class [104]. As a side project during the research presented in this thesis [105], one approach in this direction was the construction of a semiclassically exact infinite quantum graph, called the "butterfly graph" that was shown to have the exact same fluctuating part of the DOS as the density of zeros of the Riemann zeta function.

A complementary view to universality is given by the semiclassical determination of the average part of the DOS. Starting as early as in 1911 with Weyl [56] and further extended by Thomas and Fermi and later Balian and Bloch [57, 106], considerations on average classical phase-space volumes and local propagation in single-particle systems lead to the celebrated Weyl-expansion and extended Thomas-Fermi approximation in single-particle systems (see, *e.g.*, [107]). The term universality refers thereby not to classification of systems by regularity and chaos with particular fundamental symmetries. It rather classifies systems by basic geometric properties – like the available volume and surface of a cavity – not distinguishing between integrability or non-integrability of systems. This circumstance plays a crucial role in the presented work, as it will turn out that it allows for explicit calculations in non-solvable interacting models by connecting them to solvable counterparts.

Summarizing, one can say that semiclassical methods have not only been used to provide useful complementary physical insights to quantum mechanical systems. Rather, in the various successful applications to single-particle systems they have proved of value as accurate predictive analytical tools and there are still a lot of open potential applications. One of these seemingly has been itching many in the field of semiclassics for years now. It is the use of semiclassical methods – in the sense of fully accounting for quantum interference – in the context of interacting few- and many-body systems with all their power and beauty. This idea is not new, but a highly non-trivial one. First of all, the extended dimensionality of classical phase spaces heavily complicates already the classical description. Second, the quantum mechanical indistinguishability

[3]It is, in fact, one of the seven Millenium Prize Problems [103] stated by the Clay Mathematics Institute.

of identical particles in terms of (anti-)symmetric wave functions does not have a direct classical analogue and needs to be payed some special attention to.

Semiclassics in interacting systems

First quantization

The idea of applying semiclassical methods to interacting systems is not new. First of all, after the failure of Bohr-Sommerfeld quantization of the Helium atom, the successful application [108] of periodic orbit theory to it – almost 90 years later – was one of the great successes of semiclassics (see [47] for a more recent presentation). At the technical level a step was taken by Weidenmüller [109] in generalizing Gutzwiller's trace formula to the case of indistinguishable particles on a formal level. Thereby the sum over periodic orbits becomes a sum over exchange orbits, where particles interchange their roles within one period, which was again identified as parts of fully periodic orbits. On the level of universal applications this generalized trace formula was used to elevate the semiclassical calculation of the spectral statistics of RMT in the context of indistinguishability [110]. Making extensive use of Sieber-Richter pairs and their extensions, it was further possible to calculate the multi-lead transport of non-interacting BEC clouds through mesoscopic scattering regions [111], where universal Hong-Ou-Mandel profiles could be obtained displaying the effect of dephasing on the quantum-to-classical transition.

Another connection of semiclassical ideas and interacting systems can be found in DFT, where the Thomas-Fermi method [112] can be seen as the first DFT in the flavor of semiclassically counting phase-space volumes. With the introduction of the Kohn-Sham scheme the connection between semiclassics and DFT became a hidden one. But there is renewed interest in reconnecting the two strands, from which one expects new analytical foundations and improvements of approximate functionals [113, 114].

A different semiclassical approach within the formulation of first quantization attacks the *average* many-body DOS and related quantities. This line of work started with a configuration-space implementation for indistinguishable but non-interacting particles [14, 110] and is continued and extended to interacting systems here. As we will see, the inherent structure makes it especially amenable to the few-particle sector, where many-body techniques assuming large numbers of particles are inappropriate.

Second quantization

In the formulation of second quantization, identical particles of a system are represented as excitations of a single quantum field [115]. Similar to Feynman's path integral formulation [116] for a first-quantized quantum particle, a transition amplitude from one field configuration to another might be expressed as an integral over all possible (infinite-dimensional) field configurations in space-time. Thus, from this analogy with a single-particle system, it is not surprising that many attempts have been undertaken (see, *e.g.*, [21]), to apply stationary phase approximations – following the line of thought of Gutzwiller – in order to derive semiclassical approximations for field transition amplitudes and eventually a trace formula that would describe spectral properties. It is well known

that the continuum limit of quantum fields in general poses a very hard problem, even when one considers non-relativistic fields corresponding to particles that would obey Schrödinger's equation in the first quantized counterpart and most likely such problems will only get worse under the asymptotic nature of the semiclassical approximation. While one might still think of purely classical descriptions – as stationary points in field configuration space – yielding classical field equations, already this step shows to be particularly non-trivial in the case of an anti-commuting field describing fermions [21].

For bosonic systems on the other hand, the classical field equations can be obtained, yielding as field equation a NLSE, introduced by Gross and Pitaevskii [25] in the context of zero-range interacting non-relativistic bosons to describe interacting BECs, applicable – among other things – to superconductivity. Note that it was then not directly regarded as a classical limit but rather the variational solution of Schrödinger's equation with a product-state ansatz, where all bosons are assumed to occupy the same single-particle state. There is an important aspect crucially distinguishing such classical limits of quantum fields from their counterparts in first quantization. The regime where this classical limit emerges in the former is – in contrast to the formal limit of $\hbar \to 0$ in the latter – the regime of large numbers of particles N. This fact is sometimes expressed as the limit of an effective quantity $\hbar_{\text{eff}} \to 0$ and becomes less obscure by virtue of the correspondence of particles and field excitations. The experience from single-particle semiclassics is that the deviation from a true quantum system vanishes for high excitations, where most naturally the involved classical actions become very large. A similar thing happens to quantum fields, only that there high excitations imply many particles. Thus, in the above sense, mean field descriptions in terms of NLSEs like the Gross-Pitaevskii equation can be considered classical, valid in the limit $N \to \infty$, or equivalently, $\hbar_{\text{eff}} \to 0$. Such descriptions already offer a variety of rich physics, including superfluidity, vortices and QPTs and are also methodologically as compelling as challenging because of their non-trivial mathematical aspects (consider, *e.g.*, the field-integrability of the free one-dimensional NLSE [117]).

On the other hand, the effect of finite N on these emergent phenomena can disturb them in a non-trivial way not addressable by the classical field description. Moreover, also the description of excitations in terms of Bogoliubov approximation [26] is strictly valid only for $N \to \infty$ and – under certain circumstances – even breaks down for large but finite N. In the present context one might think of it as a "quasi-classical" description. Despite all non-triviality, beauty and richness that Bogoliubov excitations offer, and in deep respect for their finding, I allow myself to state this point in a provocative way, not to be taken too seriously: if Bohr would have applied the first-quantized pendant of Bogoliubov's idea, he would have come up with approximating hydrogen by a spring.

This is the point where semiclassics might help out. As mentioned, the continuum limit makes this task an especially hard one. But a first huge step was taken by finding the correct semiclassical descriptions of spatially discretized field theories [69, 118]. This has been first accomplished in the case of bosonic theories [119] and later in the case of fermions [120] which is more difficult to access. Up to now, this method has been applied to semiclassical propagation in Fock space [119], coherent backscattering and the consequent weak many-body localization [121] and other many-body phenomena [118].

In the presented work, this general approach will be used to describe finite-size precursors of critical quantum phenomena in an interacting bosonic system in terms of classically critical behavior. This application will show to allow for analytical description of specific properties in a regime inaccessible by conventional methods either because the number of particles is too large (*e.g.*, for numerics) or too small (because finite).

The value of simplified models – Experimental relevance

Large parts of the methodical developments found here are indeed formulated in a fundamentally quite general way. However, speaking of actual application, the scope of this work could only cover a small specific fraction of the vast amount of possible relevant applications that are now free to be tried out in coming future research. In the following I will give a brief characterization of the simplified models considered here in view of their relevance for describing realistic experiments.

First of all, there is the reduction of dimensionality from three to one. In all applications of the presented methods the motion of particles is constricted to a one-dimensional space. The second restriction concerns the type of mutual interactions. I will fully focus on zero-range interactions of Dirac delta type.

The relevance lies in experiments with ultracold neutral atoms in effectively one-dimensional traps, for which these model specifications are commonly used (see [8] for a review including more exhaustive lists of experimental realizations). For low temperatures only elastic scattering occurs and there are no ionization processes involved. Because of charge neutrality there are no long-range Coulomb interactions. Instead, one usually uses Feshbach resonances [122] by applying appropriate external magnetic fields. This introduces short-range interactions that can be tuned to virtually arbitrary strengths, ranging from seemingly non-interacting particles for out-of-resonance tuning to strongly attractive and strongly repulsive interactions, switching from one to the other directly at resonance.

It has become common practice to confine ultracold neutral atoms to clouds of effectively one dimension. Perpendicular degrees of freedom are then effectively frozen while motion or excitations in the longitudinal direction are still possible. The confining external potentials have for example been realized with optical traps using strongly focused laser beams [123, 124] or two-dimensional optical lattices of independent elongated tubes [125–128]. Over the last years the limits of such experiments have been pushed to the point where an atom-by-atom control over the trapped gases is possible [129–131]. This is of special relevance for the presented work because it allows for experiments in the few-particle sector, where a small, strictly fixed and measurable number of atoms is present in the system.

Other setups realized using optical lattices correspond to effective discretization of spatial degrees of freedom, pulling such experiments [9, 132] closer to discretized models like the Bose-Hubbard model [133]. For a review on the subject see [7], or [11] for a focus on quantum simulation. Also here, the degree of control over the experiments has evolved into a stage of atom-by-atom manipulation and measurement [10].

More recently another approach mapping to continuous space models is using micro traps, where atoms are confined by designed magnetic fields on microchips [134–136]. The designed harmonic confinement potentials thereby have frequencies that vary by orders of magnitude in the longitudinal and transversal directions, which again allows to confine the atoms to elongated, cigar-shaped clouds.

Moreover, also ring-trap structures have been realized [137, 138] which brings experiments closer to the solvable models of Lieb-Liniger and Gaudin-Yang that additionally assume periodic boundary conditions.

Among short-range interactions, contact interactions exhibit some special distinct features. Think for example of their exact cancellation between two fermions of same spin polarization due to Pauli exclusion. It might therefore still be questionable how valid it is to take them as model for realistic setups. However, the special features of delta interactions are not ruling them out as good models. One illustrative example was the direct observation of *fermionization* of two distinguishable (but identical) atoms[4] by strong repulsion [130]. Moreover, the corresponding fermionized Tonks-Girardeau gas of many strongly correlated bosons was realized [126, 127]. In many aspects, the bosons of such a gas act like non-interacting fermions. On the theoretical side this effect is very special to bosons or distinguishable particles in one spatial dimension with a repulsive delta-interaction that gets enhanced to be infinitely strong (see also section 1.4.1). This rather points out a special value of the model in the description of one-dimensional ultracold atomic gases.

Finally, I want to point out that the ideas, methods and some general results found here are not restricted to one spatial dimension and delta interactions. As an application, these simplifications are justified because of their particular experimental relevance. However, these restrictions are non-essential to the presented developments. Applications to three-dimensional systems and relaxing contact interactions to finite-range interactions – either specific or parametrized by scattering phases – are on the agenda of coming research.

[4]The distinction of the actually indistinguishable fermionic atoms thereby originates from occupying different hyperfine-states.

Structure of the thesis

The thesis is divided into two main parts.

Chapter 1 focuses on the average many-body DOS and related universal properties by developing and applying the method of quantum cluster expansion (QCE) based on the formulation in first quantization. It is structured as follows.

In section 1.1 the main concepts in the context of non-interacting particles are introduced and reviewed. After reviewing basic preliminary concepts in section 1.1.1 and the physical rationale behind dropping the discreteness of quantum mechanical spectra in section 1.1.2, the implications of indistinguishability in the many-body configuration space are addressed on the level of non-interacting particles in section 1.1.3. In section 1.1.4 a diagrammatic approach is introduced and the general calculus for cavities is applied and compared to exact spectra to demonstrate the basic quality and range of validity of the QCE. After an extension including external potentials (section 1.1.5) the superiority over grand-canonical descriptions in the few-body sector is demonstrated in section 1.1.6.

Section 1.2 considers then the consistent treatment of interaction effects on the methodical level that keeps a degree of generality without specifying the spatial dimensionality or the type of interactions. After reviewing the known hierarchical expansion of Ursell into interaction effects in section 1.2.1, they are introduced into the diagrammatics in section 1.2.2. The general implications of the Ursell expansion in the many-body configuration space are then considered, where the notion of interacting irreducible clusters emerges as fundamental object. In section 1.2.3 the general calculus is formulated in terms of irreducible diagrams, putting an emphasis on the generally applicable combinatorial aspects. The truncation to first order QCE is introduced in section 1.2.4, only allowing single pairs of particles to interact at a time while fully incorporating quantum degeneracy through indistinguishability. A generic dimensional analysis in section 1.2.5 is shown to imply specific scaling properties on individual clusters and the description of the system as a whole that makes thermodynamic calculation especially amenable. From this argument one additionally identifies the general regime in energy where first-order QCE becomes asymptotically exact.

The actual applications start in section 1.3, where the model systems are specified to be one-dimensional with contact interactions. After pointing out the experimental relevance and analytical accessibility of these specifications in section 1.3.1, the explicit analytic results from the calculus in first order QCE are presented in section 1.3.2 and consistency with Pauli exclusion is shown. As

explicit application, comparisons with exact spectra of the Lieb-Liniger model are presented in section 1.3.3. A corresponding comparison of the mechanical equation-of-state in thermal equilibrium further demonstrates on the one hand the accuracy and strengths of the method due to its non-perturbative character and the full inclusion of indistinguishability and on the other hand its deficiencies due to truncation to first order and the loss of system-specific features due to universality.

In section 1.4, extensions are considered where a special emphasis emerges on the analytical accessibility of non-solvable systems within the QCE description. First, a known exact Bose-Fermi duality is used in section 1.4.1 to develop a strong coupling expansion that becomes exact in the fermionization limit of infinite repulsion. Comparisons with the Lieb-Liniger model are presented, showing that the combined bounds given by weak- and strong-coupling expansion allow for identifying an exact point of cross-over between weak- and strong-coupling regimes, where the method becomes least accurate, which represents a *lower* bound to its quality. In section 1.4.2 the consistent application of integrability-breaking external confinements is addressed by minimal manipulation of the general formalism, especially allowing for the explicit analytic description of non-integrable systems. This clarifies one major strength of the QCE and its inherent disregard of spectral discreteness: As a theory that does not distinguish between integrability and non-integrability, it boils down the properties of systems exactly so much that one recovers analytic solvability in their universally accessible information. This is the point where the method becomes a predictive tool, where exact numeric solutions are extremely exhaustive in computation time and are strongly restricted to a small number of particles and excitation energies. Emphasis is put on the experimentally relevant and non-solvable case of harmonic confinements. In section 1.4.3 the restriction to one particle species is relaxed, which includes the extension to spin-1/2 fermionic systems. Maximized spin-imbalance is considered as a special case and it is pointed out that, due to universality, the description includes non-solvable systems with mass-imbalance.

The approach finds its climax in applicability by further being extended in section 1.5 on the methodical level. In section 1.5.1 it is shown how to consistently incorporate non-universal effects by minimal manipulation while keeping the advantages of the universal expansion. The application to the thermodynamics in the Lieb-Liniger model benchmarks the approach and underlines the accuracy on *arbitrary* scales, reaching from extreme quantum degeneracy to classical scales. An energy shifting method is developed in section 1.5.2 from a complementary ansatz, that is then fully determined by the smallest clusters of QCE. This analytically motivated and substantiated method allows the QCE to come of age, overcoming the problems in intermediate coupling regimes and for larger numbers of particles, while all information that is needed is carried by the smallest irreducible clusters. Comparison with numerics (close to intractability) in a non-solvable harmonically confined Bose system highlights the transition of QCE from a reproducing to a predictive tool. This efficient usage of smallest clusters culminates in section 1.5.3, when it is demonstrated how solvable models – here Lieb-Liniger together with its thermodynamic solution by Yang and Yang – can be used to obtain irreducible clusters of higher order also in the non-solvable case, fully accounting for the interaction effects of three particles and more. By applying a subsequent second order energy shifting, virtually

perfect accuracy on arbitrary parameter ranges is found.

Finally, section 1.6 addresses the applicability to spatially dependent quantities like non-local pair correlations. This section stands out from the rest of this part, as it puts a focus on the many-body sector while keeping the quality of the non-perturbative character. After the general representation of one-body observables (section 1.6.1) and two-body observables (section 1.6.2) in terms of irreducible clusters, an explicit analytic formula for non-local pair-correlations is obtained that is restricted to temperatures far above quantum degeneracy but accurately valid – as can be seen from a comparison with published numerics – for arbitrary coupling strengths, reaching from perfect bunching of ideal bosons to perfect anti-bunching in the fermionization regime.

A summary and outlook of the part on QCE is given in section 1.7.

Chapter 2 considers the specific model of the one-dimensional Bose gas with attractive contact interactions on the ring. Complementary to the description of universality related to average spectra within the QCE, here I focus on a full semiclassical treatment based on second quantization, targeting the regime of large but finite numbers of particles, capable to describe the finite-size precursors of a QPT and an excited-state QPT (ESQPT) in the system that are related to a spontaneous symmetry breaking due to enhanced particle bunching.

Section 2.1 reviews the general semiclassical method of EBK quantization in integrable systems.

In section 2.2 the specific model is introduced, including a truncation in single-particle momentum space.

The proper classical counterpart of the second quantized model with three degrees of freedom is deduced in section 2.3 with an emphasis on its constants of motion, the corresponding integrability and appropriate transformations into polar coordinates in order to simplify the theoretical description.

In section 2.4 the issue of effective quanta of action is briefly addressed with an emphasis on the functional dependence $\hbar_{\text{eff}} \sim 1/\tilde{N}$ in the model. This anticipates the many-particle regime as the regime of validity as the classical quantity $\tilde{N}$ will later be identified with the number of bosons.

The structure of the six-dimensional classical phase space is the subject of section 2.5. First, the reduction of the available phase space to a minimal representative is addressed in section 2.5.1, including the effective reduction form three to one degree of freedom and the restrictions induced by the description in polar coordinates and the implied topological phase space doubling. In section 2.5.2 the non-interacting limit is quantized within EBK implying the general identification of two of the degrees of freedom as system parameters, corresponding to the total number of bosons and the total angular momentum in the system. A study of the phase-space structure for vanishing total angular momentum and arbitrary coupling strengths in section 2.5.3 identifies a critical point of a classical transition. The subcritical regime thereby is smoothly connected to the non-interacting case, showing the same class of orbits ("*librations*"), whereas the supercritical regime displays a separatrix structure, allowing for an additional class of tori ("*vibrations*") that is not smoothly connected to the subcritical regime. The similarities and special features of the case of finite total angular momentum are pointed out in section 2.5.4.

The EBK quantization is then applied to the model with vanishing total angular momentum in section 2.6. First, the correct quantization of librations

is carried out in section 2.6.1. After that, the more difficult quantization of vibrations is the subject of section 2.6.2, involving the careful analysis of the topological aspects of elementary loops. In section 2.6.3 the two quantization rules for librations and vibrations are combined to be represented by a single common quantum number. It is further emphasized that the discontinuous jumping of the quantized classical orbits from one class to the represent the semiclassical picture of the finite-size version of the QPT and ESQPT and can be used to semiclassically define a single point of a finite-size transition rather than a crossover.

The obtained semiclassical quantization rules are then applied to calculate spectra in section 2.7. Section 2.7.1 focuses on the ground state energy in a comparison to exact numerics and the mean-field prediction, here to be understood as the classical limit. Low-lying spectra are analyzed in section 2.7.2 showing on the one hand the quantitative quality of the semiclassical approach by comparing to exact numerics and on the other hand its capability to describe the finite-size features directly at the transition, where the approximation using Bogoliubov-like excitations is shown to break down.

In order to enhance the analytical simplicity of the full semiclassical quantization and consequently allow for analytical refinement of predictions, in section 2.8 the asymptotics in the regime of large numbers off particles are explored. After obtaining an asymptotic expression for the critical couplings for the ground state and excited states in section 2.8.1, Bogoliubov-like asymptotics of excitation energies are deduced by expansions in classical phase space for the subcritical and supercritical regimes in section 2.8.2 and section 2.8.3, respectively. Since the latter break down at the transition, a more thorough asymptotic analysis of the lowest excitation energy is given in section 2.8.4, based on an asymptotic scaling property that the phase space exhibits when one stays at the point of transition during the increase of the number of particles. A power-law scaling with N involving unique semiclassically determined coefficients is obtained as a prediction of the energy gap and its location in the coupling parameter space. Comparison to numerics verifies then the scaling. However, the quantitative accuracy saturates with finite relative errors of $\sim 10\%$ and $\sim 1\%$ in the gap and its location, respectively. The asymptotic scaling property is held responsible for the remaining deficiency by making the exact gap influenced by "deep quantum effects" that cannot be overcome by increasing N (or equivalently by decreasing $\hbar_{\text{eff}}$). In section 2.8.5 the large-N asymptotics of the level spacings close to the finite-size ESQPT are obtained by a universal separatrix quantization. Comparison to numerics shows full agreement and further considerations on extreme asymptotics allow to associate a unique time-scale with the ESQPT. Showing similarities to the Ehrenfest time of chaotic systems, this time scale gets interpreted as local Ehrenfest time where the dynamical stability exponent of the instability induced by the separatrix takes the role of a Lyapunov exponent.

The investigations on the asymptotic behavior around the ESQPT are applied to obtain the "scrambling time" in a quench of the non-interacting ground state in section 2.9. As a time scale for the evolution of inter-particle correlations it is shown to be asymptotically given by the local Ehrenfest time related to the instability. The statement is verified by a comparison to exact numerics.

Finally, in order to overcome the saturated deficiency of a semiclassical description of the energy gap at the finite-size QPT, it is shown in section 2.10

how one can apply a requantization of the classical system in the regime of asymptotic scaling, yielding an asymptotic Schrödinger equation. The universal solution yields then a correction of the unique coefficients shown to be in perfect agreement with exact numerics.

A summary and outlook of the part is given in section 2.11.

I close this work with a general conclusion on the subject.

Chapter 1

The canonical QCE for few-body systems

1.1 The non-interacting case of indistinguishable particles

This section is intended to guide the reader into the subject and is to large part reviewing known concepts (for a more detailed introduction see, *e.g.*, [21]) and previous work by the author. More conceptual details on the non-interacting case can be found in [14, 110].

1.1.1 Preliminary concepts

Particle exchange symmetry in first quantization

One approach considered in this work to describe physical properties of interacting many-body systems on the footing of first quantized formulation is the QCE. This means we consider a quantum system of a fixed number N of (identical) particles described by a many-body state $|\Psi\rangle$ as an element of a Hilbert space $\mathscr{H}_N$ that is constructed as the N-fold tensor product[1]

$$\mathscr{H}_N = \mathscr{H}_1^{\otimes N} = \underbrace{\mathscr{H}_1 \otimes \cdots \otimes \mathscr{H}_1}_{N\text{times}} \tag{1.1}$$

of single-particle Hilbert spaces $\mathscr{H}_1$. A many-body state may then be represented by its wave function

$$\Psi(\mathbf{q}_1, \mathbf{q}_2, \ldots, \mathbf{q}_N) = \left(\langle \mathbf{q}_1| \otimes \langle \mathbf{q}_2| \otimes \cdots \langle \mathbf{q}_N|\right)|\Psi\rangle\,, \tag{1.2}$$

in (multi-dimensional) configuration space, where $\langle \mathbf{q}_i| \in \mathscr{H}_1^*$ are dual single-particle states represented as bras in Dirac notation strictly localized at positions

[1] If the particles considered are not identical they may or may not live kinematically in different spaces, which one would have to account for by (tensorially) multiplying the appropriate single-particle Hilbert spaces.

$\mathbf{q}_i = (q_i^{(1)}, \ldots, q_i^{(D)})$ living in D spatial dimensions. A specific system is then defined by a self-adjoint Hamiltonian operator

$$\hat{H} = \underbrace{\sum_{i=1}^{N} \hat{H}_i^{(1)}}_{\text{non-interacting}} + \underbrace{\sum_{i<j} U_{ij}(\hat{\mathbf{q}}_i - \hat{\mathbf{q}}_j)}_{\text{two-body interactions}} , \tag{1.3}$$

consisting of the non-interacting part that is separable with respect to the different particles described by their single-particle Hamiltonians $\hat{H}_i^{(1)}$ and the interacting part that is restricted to two-body interactions throughout this work. In addition, some boundary conditions on the wave function might be prescribed.

Two identical particles i and j share the same basic properties (like mass or spin) and moreover follow the same dynamical routes if they are interchanged. This is expressed by the commutation relation

$$[\hat{H}, \hat{P}_{ij}] = 0 , \tag{1.4}$$

where $\hat{P}_{ij}$ is a permutation operator that interchanges particle i and j. This notion of indistinguishability just expresses the fact that identical particles behave in the same way, which is true on the classical level as much as on the quantum level. But there is a deeper meaning to indistinguishability in quantum mechanics that misses a direct analogue in the classical world: the additional constraint that any physical realization should belong to a specific symmetry class regarding permutations. Any physically realized state $|\Psi\rangle$ has to be either totally symmetric or antisymmetric *w.r.t.* interchanging any two particles of the same species:

$$\hat{P}_{ij}|\Psi\rangle = \pm|\Psi\rangle . \tag{1.5}$$

Particle species that are symmetric or antisymmetric then yield thermodynamic Bose-Einstein statistics or Fermi-Dirac statistics [139], respectively, and are therefore called bosons or fermions, respectively. From classical every-day experience it may seem bizarre that even dynamically independent particles always are connected (*entangled*) in this non-detachable way, as long as they belong to identical species. This peculiarity gets weakened when one recognizes that the first quantized description of identical particles presented here emerges as an effective low-energy theory from more fundamental theories. The latter being quantum field theories, where identical particles are nothing else than elementary excitations of one single (quantum) field that is unique to a whole particle species. The spin-statistic theorem [139] states that particles of integer spin obey Bose statistics while half-integer spin corresponds to fermions. For later reference I prefer here to remark that it is nevertheless (perfectly) possible to speak of spin-less fermions (antisymmetric) despite the fact that this would formally correspond to a spin of zero, which is integer. At least in cases where spin does not interact with spatial degrees of freedom this can be thought of as fully spin-polarized fermions, where all spins are aligned together and neglected as dynamical information. If, furthermore, the spin observables of all particles commute with the Hamiltonian, one can even consider identical particles separated into collections for each (orthogonal) spin-polarization, each of which then acts as an individual spin-less particle species with its exchange symmetry inherited from the original species carrying spin.

Advantage and trade-off of the first-quantized description – Few-body systems

This subsection is intended to give a first insight in the regime where the approach at hand is considered appropriate. Also the several aspects of the theory introduced later go hand in hand to maintain a consistent picture of where it is most applicable.

First, in the first-quantized approach, each system naturally has a specified number of particles N already on the kinematic level as opposed to formulations in second quantized formulations, where the number of particles is instead a dynamical observable $\hat{N}$. This makes it especially well-suited for the description of closed systems, *i.e.*, systems in microcanonical or canonical equilibrium.

Second, the number of degrees of freedom here is always finite, as it is usually given by the total dimension ND of classical configuration space. This is in contrast to the second-quantized descriptions, where the number of degrees of freedom usually blows up to infinity, as any possible single-particle mode $|\phi\rangle$ of an arbitrarily chosen single-particle basis $\{|\phi\rangle\}$ spanning $\mathscr{H}_1$ gets addressed an extra degree of freedom. This means they are infinite in number for continuous systems, and more severely they are even uncountable when the system is unbound (*e.g.*, particles in free space). This poses a restriction to the analytical tractability of continuous systems in second quantized form. The latter is for example better-suited to cases where one is interested in specific regimes of system parameters where a restricted (finite) number of single particle modes suffices in approximately describing system features one is focused on.

The trade-off in first quantization is that one has to take care of particle exchange symmetry explicitly, which usually introduces sums over all possible permutations of identical particles. As a consequence the number of terms one has to take into account in specific analytic calculations can grow heavily with the number of particles, rendering the quantum cluster approach cumbersome for large numbers of particles.

All in all these three considerations already show that the approach is predestined for treating interacting *few-body* systems in the continuum. Especially then effective descriptions where the number of particles is not strictly fixed are doomed to fail as are mean-field treatments, rendering the first quantized description a good candidate to fill this gap.

The opposite case is the one of large numbers of particles in systems that can (up to some extent) be described using truncated bases of a finite number of single-particle modes. In chapter 2 one such application will be shown where the second quantized formulation drastically can simplify a semiclassical description.

The need of simplification

Interacting quantum systems of the form (1.3) are analytically very hard to treat in general and usually need some way of simplification, unless they fall into the rare class of quantum integrable systems. In this approach, all observations are restricted to properties that are related to the *smooth* part of spectra. This means that in this description two properties of exact spectra are neglected. First, the exact values of eigenenergies are neglected so that any information about fluctuations about evenly distributed energies is dropped. Second, the discreteness of spectra itself is neglected. In single-particle systems,

this is achieved using a well-developed toolbox of semiclassical standard techniques, which I will review in the subsequent subsection. Thereby a focus is put on interpreting spectrally smooth quantities as short-time dynamical information. Establishing this connection provides the key feature that lies at the core of all considerations regarding the QCE. It will allow for extending the well-understood single-particle methods to include indistinguishability of identical particles (see section 1.1.3). Furthermore it will naturally lead the way to the appropriate inclusion of inter-particle interactions (see section 1.2) and also the impact of external potentials in a consistent way.

1.1.2 The short(-time) story about smoothness

The exact discrete spectrum of any (bound) quantum system defined by its Hamiltonian $\hat{H}$ and appropriate boundary conditions can be represented by the exact DOS [20]

$$\rho(E) = \sum_n \delta(E - E_n)\,, \tag{1.6}$$

with E_n being the exact eigenenergies obeying Schrödinger's equation

$$\hat{H}|\Psi_n\rangle = E_n|\Psi_n\rangle \tag{1.7}$$

for eigenstates $|\Psi_n\rangle$ that obey the given boundary conditions.Consider then a separation

$$\rho(E) = \bar{\rho}(E) + \rho_{\text{fluc}}(E) \tag{1.8}$$

of (1.6) into an average part $\bar{\rho}$ and a fluctuating part ρ_{fluc} that oscillates around zero and vanishes on average. In the present approach the focus is then on the mean DOS $\bar{\rho}(E)$ while ignoring any knowledge of $\rho_{\text{fluc}}(E)$.

In single-particle systems the ambiguities inherent in the separation (1.8) are overcome in a semiclassical treatment, where the fluctuating part is approximated by the sum [50]

$$\rho_{\text{fluc}}(E) \approx \rho^{\text{scl}}_{\text{fluc}}(E) = \sum_\gamma A_\gamma \cos\left(\frac{1}{\hbar}S_\gamma(E) + \frac{\pi}{4}\nu_\gamma\right) \tag{1.9}$$

over (classes of) periodic orbits γ in the classical counterpart of the quantum system with their actions S_γ, stabilities A_γ and Maslov-indexes ν_γ all defined classically. This approximation was proposed in a two-fold way that distinguishes the underlying classical systems with respect to their integrability. For integrable systems the form (1.9) was derived by Berry and Tabor [50] starting from the semiclassical EBK torus quantization prescription [140]. Astonishingly, even in the case of classical chaos, which usually renders the corresponding quantum system especially hard to treat, the form (1.9) holds and was derived in the seminal works of Gutzwiller based on several subsequent stationary phase approximations, starting in path space in a Feynman path integral representation of the quantum propagator [141], all of which are assuming fast variations of classical action integrals compared to Planck's quantum of action $\hbar$. This is often referred to as taking the formal limit $\hbar \to 0$. It is then not too surprising that – given the common form of $\rho^{\text{scl}}_{\text{fluc}}(E)$ – the smooth part $\bar{\rho}(E)$ is semiclassically defined in *exactly* the same way in the two cases of integrable and non-integrable systems. The so-called Thomas-Fermi approximation is the basic method for

calculating the mean part of DOS. It does not distinguish between integrable and non-integrable systems at all – neither on the derivational, the methodical nor the practical level. It offers a way of counting classically available phase space volumes at a specific energy E in units of Planck cells of volume $(2\pi\hbar)^f$, where f is the number of degrees of freedom, and it is related to short-time quantum dynamics in an intriguing way. For a non-relativistic particle in D spatial dimensions described by the time-independent Hamiltonian

$$\hat{H} = H(\hat{\mathbf{p}}, \hat{\mathbf{q}}) = \frac{\hat{\mathbf{p}}^2}{2m} + U(\hat{\mathbf{q}}) \tag{1.10}$$

it is given by

$$\begin{aligned} \bar{\rho}_{\mathrm{TF}}(E) &= \frac{1}{(2\pi\hbar)^D} \int \mathrm{d}^D q \int \mathrm{d}^D p \; \delta(E - H(\mathbf{p}, \mathbf{q})) \\ &= \frac{1}{\Gamma(D/2)} \left(\frac{m}{2\pi\hbar^2}\right)^{\frac{D}{2}} \int \mathrm{d}^D q \; [E - U(\mathbf{q})]^{\frac{D}{2}-1} \theta(E - U(\mathbf{q}))\,, \end{aligned} \tag{1.11}$$

where $\theta(x)$ is the Heaviside step function and $\Gamma(x)$ is the gamma function. A different way of looking at the mean DOS is by relating it to the quantum propagator from an initial point $\mathbf{q}^{\mathrm{i}}$ to a final point $\mathbf{q}^{\mathrm{f}}$ in real space

$$K(\mathbf{q}^{\mathrm{f}}, \mathbf{q}^{\mathrm{i}}; t) = \langle \mathbf{q}^{\mathrm{f}} | \mathrm{e}^{-\frac{\mathrm{i}}{\hbar}\hat{H}t} | \mathbf{q}^{\mathrm{i}} \rangle \tag{1.12}$$

by exploiting the exact relation between the full DOS (1.6) and the Fourier transform of the trace of the propagator

$$\begin{aligned} \rho(E) &= \frac{1}{2\pi\hbar} \int \mathrm{d}t \; \mathrm{e}^{\frac{\mathrm{i}}{\hbar}Et} \sum_n \mathrm{e}^{-\frac{\mathrm{i}}{\hbar}E_n t} = \mathscr{F}_{\mathrm{t}}\left[\mathrm{tr}\, \mathrm{e}^{-\frac{\mathrm{i}}{\hbar}\hat{H}t}\right](E) \\ &= \mathscr{F}_{\mathrm{t}}\left[\int \mathrm{d}^D q \; K(\mathbf{q}, \mathbf{q}; t)\right](E)\,. \end{aligned} \tag{1.13}$$

Since smoothing the DOS means focusing on slow variations with the energy, the Fourier transform translates this to short times t. Note that t can here be positive and negative, using the bilateral definition (1.12) of the propagator that allows for negative times as well as positive times. An alternative to the dynamical formulation (1.13) is the thermodynamical formulation

$$\rho(E) = \mathscr{L}_\beta^{-1}[Z(\beta)](E) = \mathscr{L}_\beta^{-1}\left[\int \mathrm{d}^D q \; K(\mathbf{q}, \mathbf{q}; t = -\mathrm{i}\hbar\beta)\right](E) \tag{1.14}$$

using the inverse Laplace transform $\mathscr{L}^{-1}$ of the canonical partition function[2]

$$Z(\beta) = \mathrm{tr}\, \mathrm{e}^{-\beta\hat{H}} = \sum_n \mathrm{e}^{-\beta E_n}\,, \tag{1.15}$$

which is simply related to (1.13) by identifying inverse temperature $\beta = 1/k_{\mathrm{B}}T$ with imaginary time by $\beta = \mathrm{i}t/\hbar$. This identification shows that smoothness in

[2] Throughout this work the bilateral form of the Laplace transform $\mathscr{L}_E = \int_{-\infty}^{\infty} \mathrm{d}E\, \mathrm{e}^{-\beta E}(\cdot)$ is used, which also keeps the information about negative energies. The inverse $\mathscr{L}_\beta^{-1}$ of the bilateral transformation then naturally gives the correct behavior at negative energies, so that, *e.g.*, $\mathscr{L}_\beta^{-1}[\beta^{-\nu}](E) = \Gamma(\nu)^{-1} E^{\nu-1}\theta(E)$ contains the Heaviside step function $\theta(E)$ as a factor.

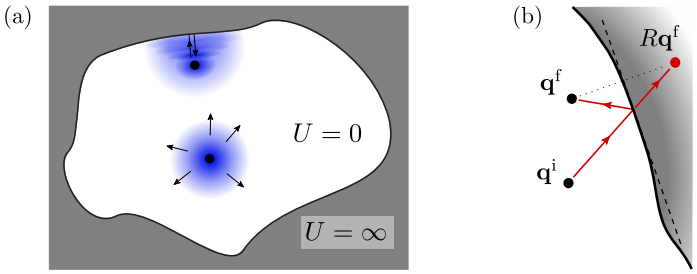

Fig. 1.1: (a) The two dominant contributions from short-time dynamics of localized wave packets in quantum billiards: locally free propagation and interference with boundary-reflected waves. (b) Direct reflection on a locally flat boundary as the leading-order correction to short-time propagation in quantum billiards.

energy, or equivalently short-time dynamics, may also be understood as "high-temperature" behavior in the thermodynamic sense. As will be seen later, this formulation is misleading as it sounds way to restrictive on the range of validity in temperature.

To make the relation of smoothness in energy to short-time dynamics more explicit and show what exactly is the short-time propagator that has to be used to obtain (1.11) we move to an even simpler system.

Quantum billiards

A non-relativistic quantum billiard in D dimensions is a system of a quantum particle of the form (1.10) defined by its domain $\Omega \subset \mathbb{R}^D$ on which the potential vanishes $U = 0$ and some specification for boundary conditions on the wave function at the boundary $\partial\Omega$, usually chosen to be of one of three types. They can be of Dirichlet type, which constrains $\psi(\mathbf{q}) = 0$ for $\mathbf{q} \in \partial\Omega$. They can be of Neumann type, constraining the perpendicular derivative $\nabla_q \psi(\mathbf{q}) \cdot \mathbf{n} = 0$, where $\mathbf{n}$ is an arbitrary normal vector on the boundary. Or they can be a mixture of both, meaning the piecewise combination of Dirichlet and Neumann boundary conditions.

A wave packet localized deep in the interior of the billiard will start to spread and disperse, but for short times it basically evolves like a free particle (since $U = 0$ in the interior). The situation changes when it is initially located close to the boundary, where it will feel immediate interference with reflections from the latter. The two situations are illustrated in Fig. 1.1a and lead to two different contributions to the DOS.

First, assuming locally free propagation

$$K(\mathbf{q}^{\mathrm{f}}, \mathbf{q}^{\mathrm{i}}; t) \approx K_0(\mathbf{q}^{\mathrm{f}}, \mathbf{q}^{\mathrm{i}}; t) = \left(\frac{m}{2\pi\hbar \mathrm{i} t}\right)^{\frac{D}{2}} \exp\left[\frac{\mathrm{i}m}{2\hbar t}(\mathbf{q}^{\mathrm{f}} - \mathbf{q}^{\mathrm{i}})^2\right] \tag{1.16}$$

in the interior and employing it in (1.13) yields a dominant contribution

$$\bar{\rho}_{\mathrm{V}}(E) = \left(\frac{m}{2\pi\hbar^2}\right)^{\frac{D}{2}} \frac{V_D}{\Gamma\left(\frac{D}{2}\right)} E^{\frac{D}{2}-1}\theta(E) = \bar{\rho}_{\mathrm{TF}}(E)\,, \tag{1.17}$$

where the D-volume $V_D = \int_\Omega \mathrm{d}^D q$ enters because free propagation renders the integrand in (1.13) invariant under arbitrary translations in the billiard. The

contribution (1.17) matches *exactly* the Thomas-Fermi approximation (1.11), establishing locally free propagation as the definition of dominant short-time dynamical information.

The reflections on the boundary are in a first approximation taken into account by assuming the boundary to be locally flat. The interference with the reflected wave is then included in the spirit of the image charge method by a modification

$$K(\mathbf{q}^{\mathrm{f}},\mathbf{q}^{\mathrm{i}};t) \approx K_0(\mathbf{q}^{\mathrm{f}},\mathbf{q}^{\mathrm{i}};t) \pm \underbrace{K_0(R\mathbf{q}^{\mathrm{f}},\mathbf{q}^{\mathrm{i}};t)}_{\text{reflected wave}} \tag{1.18}$$

of the free propagator with another free propagation where the final point is reflected *w.r.t.* the boundary (see Fig. 1.1b). The sign stands for Neumann (+) and Dirichlet (-) boundary conditions, respectively. This naturally splits the spatial integral in (1.13) into an integral along the $D-1$ dimensions of the surface of the billiard, under which the integrand is again invariant, and the perpendicular direction. In the perpendicular direction, the integral over the reflected propagator converges fast with increasing distance from the boundary if propagation time is assumed to be short in a sense. Thus one can neglect the influence of other parts of the boundary, *e.g.*, in the form of multiple reflections or curvature and corners or edges of the boundary in this first approximation. This implies that one extends the integral in perpendicular direction to infinity, yielding the first boundary correction

$$\begin{aligned}\bar{\rho}_{\mathrm{S}}(E) &= \pm\mathscr{F}_{\mathrm{t}}\left[\int_{\partial\Omega}\mathrm{d}^{D-1}q_{\parallel}\int_0^\infty \mathrm{d}q_\perp\ \left(\frac{m}{2\pi\hbar it}\right)^{\frac{D}{2}}\mathrm{e}^{-\frac{2m}{i\hbar t}q_\perp^2}\right](E)\\ &= \pm\frac{1}{4}\left(\frac{m}{2\pi\hbar^2}\right)^{\frac{D-1}{2}}\frac{S_{D-1}}{\Gamma\left(\frac{D-1}{2}\right)}E^{\frac{D-1}{2}-1}\theta(E)\,,\end{aligned} \tag{1.19}$$

where S_{D-1} is the ($D-1$-dimensional) surface "area" $\int_{\partial\Omega}\mathrm{d}^{D-1}q$ of the billiard. So, again, invariance of a specific propagation *w.r.t.* translation along some manifold results in the measure of this manifold as a prefactor. Moreover, the exponents of the energy and other prefactors are systematically determined by the dimensionality of those manifolds. This already indicates the general significant importance of *invariant* manifolds in the context of the mean DOS. So far, we met the two cases of invariant manifolds of the billiard domain Ω itself as a D-dimensional representative with measure V_D and the $D-1$-dimensional billiard boundary $\partial\Omega$ with measure S_{D-1}. But in general, depending on D, there are more such manifolds which contribute to the mean DOS. In two dimensions, *e.g.*, contributions originating from the curvature or corners of the boundary can be understood as the (degenerate) case of 0-dimensional (point-like) manifolds and are also adding to the smooth DOS. A treatise on the contributions in a three dimensional billiard assuming smooth boundaries can be found in [57], a generalization to higher dimensions including intrinsic curvature contributions can be found in [106].

In general, the common convention (substantiated by some general arguments [142]) is to include all contributions down to the point-like invariant manifolds in the mean DOS. In principle, one could go on and calculate even higher order corrections by multiple-reflection analysis, but common sense is that one would start to include information about periodic orbits of the system which would introduce over-counting in the semiclassical splitting (1.8). The

sum of all smooth contributions down to the point-like ones in quantum billiards is known as the *Weyl-expansion*

$$\bar{\rho}(E) = \underbrace{\bar{\rho}_{\mathrm{V}}(E)}_{\text{Thomas-Fermi}} + \bar{\rho}_{\mathrm{S}}(E) + \dots , \tag{1.20}$$

where every term is determined by basic geometric properties of the system.

The following sections will show that the importance of invariant manifolds is carried over to systems of identical particles, even when interactions are included.

Smooth potentials

Also in the presence of smooth single-particle potentials $U(\mathbf{q})$ the Weyl asymptotic of the single-particle DOS given by the Thomas-Fermi approximation (1.11) has a formulation by means of inverse Laplace transform of short-time propagation.

In the short-time regime the corresponding single-particle propagator comes as a phase-modification of the free propagator (1.16) given by the eikonal approximation [143]

$$K(\mathbf{q}^{\mathrm{f}}, \mathbf{q}^{\mathrm{i}}; t) \approx \left(\frac{m}{2\pi \mathrm{i}\hbar t}\right)^{\frac{D}{2}} \exp\left[\frac{\mathrm{i}m}{2\hbar t}|\mathbf{q}^{\mathrm{f}} - \mathbf{q}^{\mathrm{i}}|^2 - \frac{\mathrm{i}}{\hbar} t \int_0^1 \mathrm{d}s\, U(\mathbf{q}(s))\right] , \tag{1.21}$$

where the influence of the external potential U is approximated by the average corresponding phase accumulated along the straight path $\mathbf{q}(s) \coloneqq \mathbf{q}^{\mathrm{i}} + (\mathbf{q}^{\mathrm{f}} - \mathbf{q}^{\mathrm{i}})s$ connecting the initial and final configuration linearly.

The eikonal approximation (1.21) can be obtained from the van Vleck-Gutzwiller propagator (2) assuming that the classical orbits of the free case, *i.e.*, straight lines, remain unchanged. This is a valid assumption for smooth contributions to the DOS as the latter correspond to short times t.

The approach simplifies further when used in (1.13) or (1.14) because for identical initial and final point $\mathbf{q}^{\mathrm{i}} = \mathbf{q}^{\mathrm{f}} = \mathbf{q}$ the short-time effect of the potential is

$$K(\mathbf{q}, \mathbf{q}; t) \approx \left(\frac{m}{2\pi \mathrm{i}\hbar t}\right)^{\frac{D}{2}} \exp\left[-\frac{\mathrm{i}}{\hbar} U(\mathbf{q}) t\right] . \tag{1.22}$$

This means that in this approximation the external smooth potential is taken into account as a (locally) constant shift in the energy that changes with the position $\mathbf{q}$ of the localized wave packet. This is consistent with the short-time philosophy since it corresponds to the assumption that for short times the main contribution of the localized wave packet spreads over a region small enough to assume the potential to be constant there. In the single-particle context one only needs to know the "diagonal part" (1.22) and use it in the general relation (1.13) or (1.14) to reproduce (1.11). Thus, the approximate form (1.21) of the propagator contains more information than needed in this context. It is one possible choice to serve as an origin of (1.22). But in the many-body context, as will become clear later (see section 1.1.5), the eikonal approximation is needed to argue in which sense a similar approximation to the DOS will be appropriate. The corresponding way of incorporating external potentials will be referred to as *local potential approximation* (LPA).

1.1.3 The geometrical side of exchange symmetry

Indistinguishable particles

Consider now N identical, indistinguishable particles in a quantum billiard. Any physically realized state is either symmetric or antisymmetric under the exchange of any two particles, depending on whether they are bosons (+) or fermions (−):

$$\hat{P}|\Psi_\pm\rangle = (\pm 1)^P\,|\Psi_\pm\rangle\,, \qquad (-1)^P \coloneqq \mathrm{sgn}(P) \tag{1.23}$$

for any permutation $P \in S_N$ (S_N here denotes the symmetric group, not to be confused with the D-dimensional surface S_D in different context), where $\hat{P}$ is the corresponding permutation operator acting on many-body states. The physical spectrum of such a system is, strictly speaking, a subspectrum of the full Hamiltonian corresponding to the correct symmetry. It is obtained by restricting to those eigenenergies that correspond to the appropriate subspace of Hilbert space. Let $\hat{\mathbb{1}}_\pm = \hat{\mathbb{1}}_\pm^\dagger = \frac{1}{N!}\sum_{P\in S_N}(\pm 1)^P\hat{P}$ be the projector onto the subspace of correct symmetry. Restricting the trace in the general relation (1.13) (which holds also for many distinguishable particles understood as an effectively high dimensional system) to this subspace is equivalent to replacing the time evolution operator $\hat{U}(t) = \exp(-\frac{\mathrm{i}}{\hbar}\hat{H}t)$ and the propagator by their symmetry-projected analogues

$$\hat{U}_\pm(t) \coloneqq \hat{\mathbb{1}}_\pm\hat{U}(t)\hat{\mathbb{1}}_\pm = \hat{\mathbb{1}}_\pm\hat{U}(t)\,, \tag{1.24}$$

$$K_\pm^{(N)}(\mathbf{q}^\mathrm{f},\mathbf{q}^\mathrm{i};t) \coloneqq \frac{1}{N!}\sum_{P\in S_N}(\pm 1)^P\,K^{(N)}(P\mathbf{q}^\mathrm{f},\mathbf{q}^\mathrm{i};t)\,, \tag{1.25}$$

where the coordinates $\mathbf{q}_j^{\mathrm{i/f}}$ of all particles are subsumed to

$$\mathbf{q}^{\mathrm{i/f}} = (\mathbf{q}_1^{\mathrm{i/f}},\ldots,\mathbf{q}_N^{\mathrm{i/f}})\,. \tag{1.26}$$

In (1.24), the commutation of the time evolution operator and the symmetry projector due to $[\hat{P},\hat{H}] = 0$, and idempotence of $\hat{\mathbb{1}}_\pm$ have been used. If the exact propagator is used this leads to the exact bosonic or fermionic DOS

$$\rho_\pm^{(N)}(E) = \sum_n \delta\Big(E-E_{\pm,n}^{(N)}\Big) = \mathscr{F}_\mathrm{t}\left[\frac{1}{N!}\sum_{P\in S_N}(\pm 1)^P\int \mathrm{d}^{ND}q\,K^{(N)}(P\mathbf{q},\mathbf{q};t)\right](E)\,, \tag{1.27}$$

where $\{E_{\pm,n}^{(N)}\}$ are the eigenenergies of the full many-body Hamiltonian (1.3) that correspond to states with the demanded symmetry. Eq. (1.27) gets thermodynamically formulated as

$$\rho_\pm^{(N)}(E) = \mathscr{L}_\beta^{-1}\Big[Z_\pm^{(N)}(\beta)\Big](E) \tag{1.28}$$

in terms of the bosonic or fermionic canonical partition function

$$Z_\pm^{(N)}(\beta) = \sum_n \mathrm{e}^{-\beta E_{\pm,n}^{(N)}} = \int \mathrm{d}^{ND}q\,K_\pm^{(N)}(\mathbf{q},\mathbf{q};t=-\mathrm{i}\hbar\beta)\,. \tag{1.29}$$

Thus symmetry requires taking wave propagation over finite distances into account, as $P\mathbf{q}\neq\mathbf{q}$ in general.

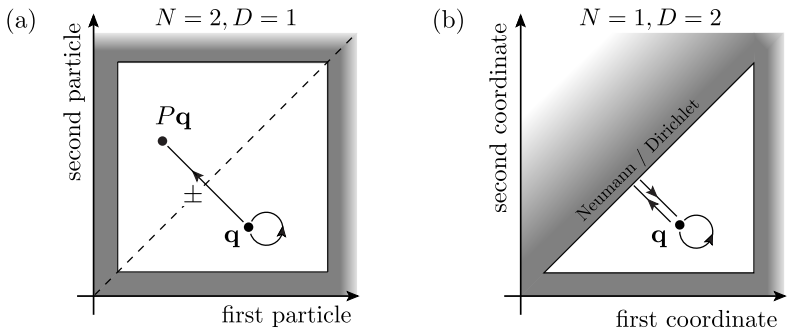

Fig. 1.2: (a) A system of two bosons (+) or fermions (−) ($N = 2$) on a straight line ($D = 1$) involves two contributions to the symmetrized propagator and is equivalent to (b) a single particle ($N = 1$) in a triangularly shaped billiard ($D = 2$) that corresponds to the fundamental domain with Neumann or Dirichlet boundary condition on the boundary segment that corresponds to the symmetry line.

Case study: two identical particles in one dimension

To get a feeling on the geometrical aspects of particle exchange symmetry, consider as a simple example a one-dimensional system of two bosons (+) or fermions (−) confined to a line of length L with hard wall (Dirichlet) boundary condition on both end points. The only two permutations are the identity and the exchange of the two particles. Figure Fig. 1.2a illustrates the two corresponding contributions to the propagator. Because of the (anti-)symmetry of the wave function $\Psi(q_1, q_2)$ with respect to the symmetry line $q_1 = q_2$, the wave function in the full domain $(q_1, q_2) \in \Omega = [0, L]^2$ is completely determined by its content in one fundamental domain by application of exchange permutation. One choice of fundamental domain here could be $\mathcal{F}_2 = \{(q_1, q_2) \in \Omega \mid q_1 > q_2\}$. Depending on the statistics, the (anti-)symmetry of the wave function implies the vanishing of either the wave function (fermions) or its normal derivative on the symmetry line $q_1 = q_2$. This establishes an exact quantum mechanical mapping between the one-dimensional two-body system and a two-dimensional single-particle system in the fundamental domain with additional Neumann or Dirichlet boundary condition that has to be imposed along the symmetry line illustrated in Fig. 1.2b. In this exact mapping the identity as permutation corresponds to the locally free propagation leading to the Thomas-Fermi term (1.17) while the exchange permutation maps to the correction due to reflection on the boundary (1.19). Thus in this simple case the smooth part of the spectrum is fully determined by standard Weyl-expansion methods and the correction due to symmetry-related permutations can be understood as reflection-related Weyl-like boundary corrections. Naturally, the question arises if similar mappings allow for calculation of the smooth DOS in arbitrary non-interacting D-dimensional N-particle billiards by applying standard Weyl expansion methods.

A similar system as discussed above with a slightly complicating modification would be two have two identical particles on a ring ($q_1 \in S^1, q_2 \in S^1$) so that the full domain $\Omega = S^1 \times S^1$ is a torus. The symmetry-related contributions to the propagator are illustrated in Fig. 1.3a where the torus is described as a square in the Euclidean plane with topological (oriented) identification of opposite sides.

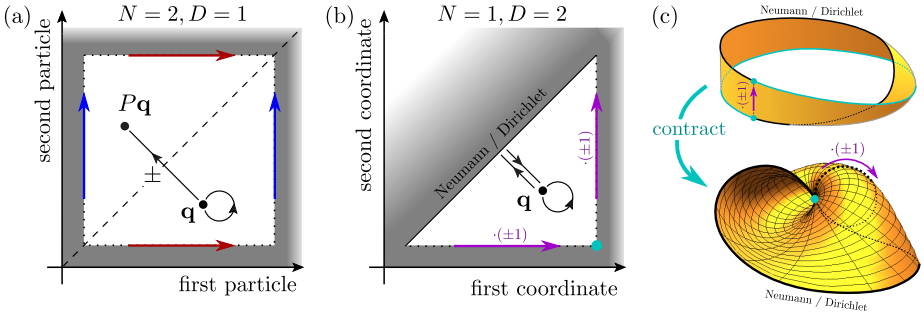

Fig. 1.3: (a) A system of two bosons (+) or fermions (−) ($N = 2$) on a circle ($D = 1$) involves two contributions to the symmetrized propagator. The torus structure is described in the plane by indicating oriented identification of points on opposite sides with colored arrows, where identical color means identification and the orientation of arrows indicates which points on one line are mapped to which ones on the other line. The system is equivalent to (b) a single particle ($N = 1$) on a billiard ($D = 2$) that corresponds to the fundamental domain with Neumann or Dirichlet boundary condition on the boundary segment that corresponds to the symmetry line. The symmetry relation induces an additional identification of reflected sides (red and blue arrows) and results in an identification of the two remaining sides of the fundamental domain (purple arrows) where in the fermionic case the wave function is subject to a phase jump of π when crossing the line of identification. (c) The corresponding object is a degenerate Möbius strip with one half of its boundary (colored in cyan) contracted to a point ("*Möbius cone*").

Also this system has an exact mapping to a two-dimensional single-particle system by moving to the fundamental domain, which is again constructed by setting $q_1 > q_2$ but now inherits a more complicated topology from the (oriented) identification of opposite sides. The symmetry *w.r.t.* to $q_1 = q_2$ induces an additional oriented identification of reflected sides (see Fig. 1.3b), but it connects two different fundamental domains, so that in the fermionic case the (two-dimensional) wave function has a change of sign. This makes the two-dimensional "billiard" a complicated object. It is a degenerate case of a Möbius strip, where one half of its boundary is contracted to a single point as illustrated in Fig. 1.3c, which I feel free to call a Möbius cone (in accordance with the untwisted situation of forming a cone out of a cylinder by contracting one of its boundaries). It still has a single boundary on which exchange symmetry imposes again Neumann or Dirichlet boundary conditions for bosons or fermions, respectively. Despite the more complicated topology, the Weyl expansion would not depend on the way the billiard is connected, since the method is based on local considerations whereas the topological aspects characterize the system on a global level. On the one hand, this shows the power that lies in the generality of the Weyl expansion, or better, of considerations on the smooth DOS. On the other hand, it is not clear from first sight if the additional phase jump condition in the fermionic case has an impact on the smooth DOS, because standard Weyl-expansion methods do not consider such unusual situations. Indeed, it will turn out that the phase jump has no effect on the smooth level, but strictly speaking this statement has to be proven explicitly. This circumstance already indicates that many-body billiards cannot be addressed using standard Weyl expansion in general. Instead, one needs a purpose-built method to address the

effects of exchange symmetry on the average DOS.

A short excursion to fundamental domains and discrete symmetries

Fundamental domains are a general concept of describing quantum systems obeying arbitrary discrete symmetries. In general, each such symmetry is associated with a group $G = \{\hat{g}\}$ of symmetry operations $\hat{g}$ that leaves the system itself invariant but not necessarily its wave content. Formally speaking, this means that $[\hat{g}, \hat{H}] = 0$ but the actual actions on physically realized states $|\Psi\rangle \mapsto \hat{g}|\Psi\rangle$ are left undetermined. I only consider here the case of symmetries that correspond to point transformations. This includes for instance the discrete translational symmetry of an infinite or periodic lattice as well as discrete rotational symmetries or, as in the present case, a more abstract symmetry in high-dimensional space that corresponds to particle exchange. The spectra $\{E_n\}_{n\in\mathbb{N}}$ and corresponding eigenstates $\{|\Psi_n\rangle\}_{n\in\mathbb{N}}$ of discretely symmetric systems naturally decompose into subspectra $\{E_n^{(s)}\}_{n\in\mathbb{N}}$, one for each *symmetry class* s that characterizes the behavior of the corresponding eigenstates $\{|\Psi_n^{(s)}\rangle\}_{n\in\mathbb{N}}$ under symmetry operations $\hat{g}$. Mathematically speaking the symmetry classes s of states correspond to the *irreducible representations* of the symmetry group G [144]. In the context of bosonic and fermionic exchange symmetry the *one-dimensional* irreducible representations are the only relevant ones, for which the action of $\hat{g}$ is given by scalar multiplication

$$\hat{g}|\Psi_n^{(s)}\rangle = \chi_s(\hat{g})|\Psi_n^{(s)}\rangle\,, \tag{1.30}$$

where $\chi_s : G \to \mathbb{C}$ is the *linear character* of the representation s.

A fundamental domain is then given by a subset $\mathcal{F} \subset \Omega$ of the full (configurational) space Ω that *disjointly*[3] reproduces the latter under application of all elements of the symmetry group

$$\Omega = \dot{\bigcup_{\hat{g}\in G}} g(\mathcal{F})\,, \tag{1.31}$$

where each point transformation $\hat{g}$ as a linear operator is uniquely identified with a map $g : \Omega \to \Omega$ by $|g(\mathbf{q})\rangle := \hat{g}|\mathbf{q}\rangle$. Furthermore the boundaries of $\mathcal{F}$ that are related by symmetry operations are identified, which can introduce non-trivial topology (see, *e.g.*, the example of two particles on a ring before). The corresponding topologically identified object will often be referred to as the *wrapped* fundamental domain. The full dynamics of the system is then determined by the dynamics in the fundamental domain, where one has to apply additional boundary conditions on the wave function at the boundary of the fundamental domain. These boundary conditions depend on the symmetry class and correspond to the actions of the group elements that relate identified points on the boundary $\partial\mathcal{F}$.

To make this concept more explicit in a probably more familiar context we will briefly go through an important application in solid state physics. For a generic periodic lattice (I do not consider additional rotational or reflection

[3] Strictly speaking, the equivalence to the disjoint union is only true up to a set of zero measure that corresponds to the boundaries of $\mathcal{F}$, that are either missing or multiply counted in (1.31), depending on whether $\mathcal{F}$ is defined as closed or open set.

symmetries here), the representations s are given by the discrete set of possible quasi-momenta $\mathbf{k}$ in the Brillouin zone of the reciprocal lattice. The group elements, which are translations, are indexed by their integer coefficients n_i of all lattice basis vectors $\mathbf{a}_i$ spanning the lattice. The representations are all one-dimensional and the group actions or characters are then roots of unity corresponding to the phase relation between two distant elementary cells of the lattice.

$$\hat{g}_{\mathbf{n}}|\Psi_{\mathbf{k}}\rangle = \chi_{\mathbf{k}}(\hat{g}_{\mathbf{n}})|\Psi_{\mathbf{k}}\rangle = \mathrm{e}^{\mathrm{i}\mathbf{k}\cdot(n_1\mathbf{a}_1+\ldots+n_D\mathbf{a}_D)}|\Psi_{\mathbf{k}}\rangle\,. \tag{1.32}$$

The fundamental domain is one elementary cell with a wave function of symmetry class $\mathbf{k}$ undergoing phase jumps $\mathrm{e}^{\mathrm{i}\mathbf{k}\cdot\mathbf{a}_i}$ when switching to opposite sides of the elementary cell (by a translation by $\mathbf{a}_i$).

In the present case of indistinguishable particles, the group of symmetries is the *symmetric group* S_N of all $N!$ permutations $\hat{P}$ acting on N-particle states. The symmetric groups for $N > 2$ are not decomposable into one-dimensional irreducible representations only. But the two classes corresponding to bosonic $(+)$ and fermionic $(-)$ exchange symmetry, which are one-dimensional representations, always exist. The additional higher-dimensional representations are not considered here, as they are not of physical relevance in the present context. The actions of permutations on the two symmetry classes $(\pm)$ are

$$\hat{g}_P|\Psi_\pm\rangle = \hat{P}|\Psi_\pm\rangle = (\pm 1)^P|\Psi_\pm\rangle\,, \tag{1.33}$$

where $(-1)^P = \operatorname{sgn} P$ is the sign of the permutation P. Leaving the spatial dimensionality D arbitrary, the construction of a fundamental domain involves an ordering of the particles by *just one* of the spatial components. One possible choice is

$$\mathcal{F}_N \coloneqq \left\{\mathbf{q} = (\mathbf{q}_1, \ldots, \mathbf{q}_N) \in \Omega^N \;\middle|\; q_1^{(1)} < q_2^{(1)} < \ldots < q_N^{(1)}\right\}, \tag{1.34}$$

which orders the particles by their first spatial component. If an ordering is not possible in Ω (*e.g.*, on a ring $\Omega = S^1$) one can describe Ω in Euclidean space with additional identifications (see the case of two particles on a ring before).

Geometry of many indistinguishable particles on a line

One-dimensional systems play a very special role from the point of view of fundamental domains, corresponding boundary identifications and induced conditions on wave functions. The construction (1.34) makes clear that the boundaries of $\mathcal{F}_N$ are given by the conditions $q_i^{(1)} = q_j^{(1)}$ for any two particles i and j, meaning when any particle passes another one regarding *one* of the spatial components. In a one-dimensional system, this means that on any point on the boundary at least two particles collide, because they share all their coordinates: There are no additional dimensions allowing them to avoid each other. This fact has a deep impact on the behavior of wave functions on the boundary.

In the fermionic case, the antisymmetry and the corresponding Pauli principle dictates that the many-body wave function has to vanish on all (symmetry related) boundaries. In the bosonic case, the total symmetry demands many-body wave functions to have vanishing normal derivatives at the (symmetry-related) boundaries of $\mathcal{F}_N$. This allows one to fully account for the indistinguishability of particles by moving to the reduced space $\mathcal{F}_N$ and applying

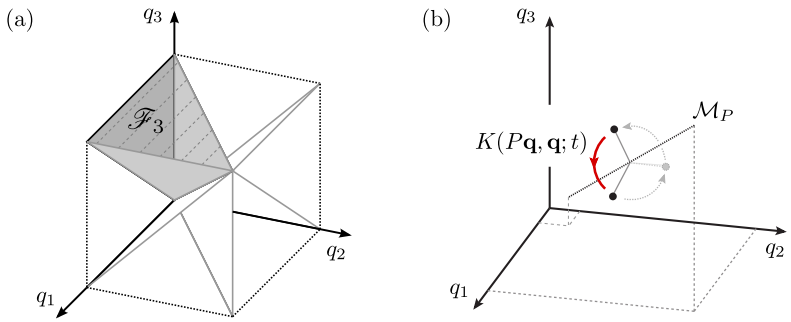

Fig. 1.4: Three particles on a line ($N = 3$, $D = 1$). (a) Fundamental domain $\mathcal{F}_3$ bounded by symmetry planes $q_1 = q_2$ and $q_2 = q_3$ (light gray) and physical boundaries $q_1 = 0$ and $q_3 = L$ (dark Grey and shaded). (b) The invariant manifold of the cyclic permutation $P = (1\,2\,3)$ of all three particles and the corresponding propagation amplitude.
The obsolete superscript $^{(1)}$ for the specification of a spatial component has been omitted.

Dirichlet or Neumann boundary conditions on the (symmetry-related) boundaries for fermions or bosons, respectively. Figure 1.4a shows the example of a fundamental domain of three particles on a line. Interpreting it as a three-dimensional cavity with appropriate boundary conditions would then allow to calculate the smooth DOS of the three-particle system using the Weyl expansion of three-dimensional quantum billiards. Although the mapping to N-dimensional cavities with Neumann- or Dirichlet-type boundary conditions holds for one-dimensional systems of arbitrary number of particles N, it introduces complications that – on a general level – have not been addressed systematically in the literature, and in the particular context of identical particles were the subject of the reviewed work [14]. As indicated already in the case $N = 3$, the effective high-dimensional cavities exhibit corners, edges, and generalized analogues of singular features of all possible dimensions. This circumstance renders the mapping to fundamental domains in the context of Weyl expansions for identical particles in one dimension an academic formulation rather than an applicable opportunity for practical purposes.

Geometrical aspects in arbitrary dimensions D

If the spatial dimension is larger than one ($D > 1$), the situation changes drastically compared to the above discussion on one-dimensional systems. The boundaries of the fundamental domain $\mathcal{F}_N$ are still given by the conditions $q_i^{(1)} = q_j^{(1)}$, but now particles do not collide everywhere on the boundary, because of the freedom of independent choice of all the other spatial components $q_i^{(2)}, \ldots, q_i^{(D)}$. This means that two *distinct* points on the boundary $\partial\mathcal{F}_N$ can be connected by symmetry, where the wave function takes values related by either unity or sign inversion rather than imposing an actual *boundary condition* on it. For example, the manifolds on which a fermionic wave function takes values zero (later called *invariant manifolds*, the skeleton of *cluster zones*) are defined by the collision condition of particles (in all their coordinates). This gives these manifolds a dimension less than $ND-1$, the dimension of an actual

boundary that is able to separate regions in full configuration space. Instead, the largest possible dimension of such a manifold is $(N-1)D$ for the collision of exactly two particles, which are rather embedded in the (symmetry-related) boundaries $\partial\mathcal{F}_N$ than coinciding with them. Thus, for higher-dimensional systems ($D > 1$), even on the level of principal prospects, it is not possible to reformulate the problem of many-body billiard system in a way that standard Weyl calculus in terms of Neumann or Dirichlet boundary conditions applies.

This emphasizes the necessity of an independent calculus that is applicable for arbitrary N and D. The development of this calculus, which is based on a description using (1.27) or (1.28) in the full domain instead of the fundamental one, started in [14] and will be reviewed in the following. Despite the fact that the invariant manifolds are not appropriate objects to formulate actual boundary conditions in general, they still play a crucial role in the systematic calculation of smooth contributions to the DOS.

Invariant manifolds and cluster zones

In the above example of two particles on a line (see Fig. 1.2 and discussion) the correction to $\bar{\rho}_-(E)$ due to the exchange permutation (see (1.27)) is related to the propagation in the vicinity of the symmetry line $q_1 = q_2$ just as the inclusion of wave reflections in a single-particle billiard only affects the short-time propagation near the physical boundary. The symmetry line is characterized by the invariance under the exchange permutation $P = (1\,2)$ of particle 1 and 2, so that the distance $|P\mathbf{q} - \mathbf{q}|$ becomes zero. This is the very reason to assume short-time contributions to come from its vicinity. The concept of invariant manifolds is extended to the general case by finding the manifolds associated with each permutation P, defined by

$$\mathcal{M}_P = \left\{\mathbf{q} \in \Omega^N \;\middle|\; |P\mathbf{q} - \mathbf{q}| = 0\right\}. \tag{1.35}$$

The manifolds $\mathcal{M}_P$ are invariant under the action of P, hence the name. Any permutation P can be written as a composition of commuting cycles (see for example [144])

$$P = \sigma_1 \cdots \sigma_l \tag{1.36}$$

acting on distinct sets of particle indexes of sizes $n_1, n_2, \ldots, n_l$. Hence $\mathcal{M}_P$ is the manifold defined by the coincidence of the coordinates of all particles associated with each cycle

$$\mathcal{M}_P = \bigcap_{k=1}^{l} \left\{\mathbf{q} \in \Omega^N \;\middle|\; \mathbf{q}_i = \mathbf{q}_j \quad \forall i,j \in I_k\right\}, \tag{1.37}$$

where I_k is the set of particle indexes affected by σ_k. As a simple example take the permutation $P = (1\,3\,4)\,(2\,5)$, whose associated manifold $\mathcal{M}_P$ corresponds to the condition (see figure 1.5)

$$\left(\mathbf{q}_1 = \mathbf{q}_3 = \mathbf{q}_4\right) \wedge \left(\mathbf{q}_2 = \mathbf{q}_5\right). \tag{1.38}$$

Another example is shown in Fig. 1.4b, which shows the invariant manifold $\mathcal{M}_P$ for a specific permutation P and depicts the corresponding contribution to the symmetrized propagator (1.25) in the case of three particles on a line. As argued

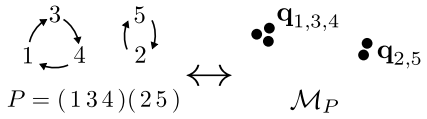

Fig. 1.5: Example of the correspondence between the cycle decomposition of a permutation P and the invariant manifold $\mathcal{M}_P$ pictured as the associated clustering of particles.

above, in contrast to the symmetry line in the one-dimensional two-particle case (see Fig. 1.2 and discussion), these manifolds in general cannot be regarded as a boundary or surface in coordinate space in the sense of dividing the space into distinct parts. The vicinities of these invariant manifolds will be referred to as *cluster zones*. All particles associated with a particular cycle index set I_k will be subsumed using the notion of a *cluster*. A system that is arranged in a particular cluster zone is composed of l clusters, each associated with a cycle in P. Each cluster k is composed of n_k particles according to the length of the cycle σ_k.

The propagation close to $\mathcal{M}_P$ will not depend on shifting the position parallel to $\mathcal{M}_P$. This holds at least as long as one does not get too close to the single-particle billiard boundaries to be included later. For the moment, only consider the locally free propagation (referred to as the "*unconfined*" case or the *bulk* contribution) for which this invariance is exact, whereas later additional contributions from physical boundary reflections or external potentials will be included on top of that (referred to as the "*confined*" case).

Furthermore, in a strict treatment the invariance of propagation along the invariant manifolds is also broken in the case of interactions. However, this construction is based on the intuition that, when restricting to short-range interactions, the propagation can be assumed to be invariant along $\mathcal{M}_P$ as long as one does not get too close to other invariant sub-manifolds. In other words, as long as the coordinates corresponding to different cycles do not become too close, that is, the different clusters should not "collide". Equivalently, as will be seen later, implied by the short-range assumption of interactions, one can split the exact propagator into a non-interacting part and hierarchically ordered interaction corrections in a way that these corrections are localized in specific cluster zones. Those can then in principle be included completely separately from the non-interacting propagation (or hierarchically lower-level corrections). By this separation, in each hierarchical step, one maintains *exact* invariance along the corresponding manifolds $\mathcal{M}_P$. Deviations thereof that are manifest in the full propagator are then pushed to and absorbed into higher-level hierarchical corrections which become less and less dominant. This way of expanding the many-body propagator into an hierarchy of corrections is the key concept at the heart of the QCE and is at this point just mentioned briefly as a preview.

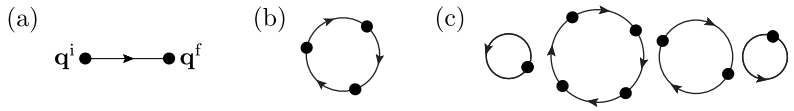

Fig. 1.6: (a) single-particle-propagator $K_0^{(1)}(q^{\mathrm{f}}, q^{\mathrm{i}}; t)$; (b) example for the contribution A_n from a single cycle (here $n = 3$); (c) example for the contribution $A_{\mathfrak{N}}$ from a specific clustering (here $\mathfrak{N} = \{1, 1, 2, 4\}, N = 8$); The value of a diagram is defined as the product of all its single-particle with all involved (non-terminal) points eventually integrated over the available space. Names of non-terminal points are dropped since they are not an argument of the diagram.

1.1.4 The non-interacting quantum billiard and emergent ground-state energies

Bulk contribution

The dominant contribution to the full N-particle propagator $K^{(N)}$ in (1.25) and (1.27) is given by neglection of physical boundary effects (reflections on walls) and interaction effects. In this first step the only many-body aspect to be addressed is the explicit inclusion of exchange symmetry while boundary and interaction effects can then later be included as additional, sub-dominant contributions to the propagator. Thus, also with interactions and reflections, the non-interacting, unconfined consideration stays the main contribution with its own right to exist.

In order to keep an overview of the large number of possible contributions and to make their meaning more intuitive I introduce a diagrammatic description. A selection of basic contributions in the non-interacting case are translated into diagrammatics is depicted in Fig. 1.6. The non-interacting part $K_0^{(N)}$ of the propagator factorizes into single-particle propagators (see Fig. 1.6a) and the contribution to the canonical partition function $Z_{\pm}^{(N)}$ (1.29) corresponding to a permutation $P \in S_N$ is a product of cluster contributions, each involving a subset of the particles as large as the cycle lengths in the cycle decomposition (1.36) of P. Let $\mathfrak{N}_P$ denote the multiset with elements $n_k \in \mathbb{N}, k = 1, \ldots, l$ corresponding to the lengths of the l cycles of a permutation $P \in S_N$. Clearly $\sum_{k=1}^{l} n_k = N$ and $|\mathfrak{N}| = l$ and we may use $\mathfrak{N}$ without subscript wherever the assignment is clear from context. The contribution to the trace of the propagator from any cycle of length n_k is the amplitude (see Fig. 1.6b)

$$\mathcal{A}_{n_k}(t) = \int \mathrm{d}^D q_1 \ldots \mathrm{d}^D q_{n_k} \prod_{i=1}^{n_k} K_0^{(1)}(\mathbf{q}_{i+1}, \mathbf{q}_i; t) = \int \mathrm{d}^D q \, K_0^{(1)}(\mathbf{q}, \mathbf{q}; n_k t)\,, \tag{1.39}$$

where the semigroup property

$$\int \mathrm{d}^D q \; K^{(1)}(\mathbf{q}^{\mathrm{f}}, \mathbf{q}; t_2) K^{(1)}(\mathbf{q}, \mathbf{q}^{\mathrm{i}}; t_1) = K^{(1)}(\mathbf{q}^{\mathrm{f}}, \mathbf{q}^{\mathrm{i}}; t_1 + t_2) \tag{1.40}$$

of the single-particle propagator and the identification $\mathbf{q}_{n_k+1} := \mathbf{q}_1$ has been used. In order to ease notation a relabeling of particle indexes has been applied in the integration variables.

Neglecting physical boundaries and smooth potentials, (1.39) is explicitly

calculated using the free propagator (1.16) to be

$$\mathcal{A}_{n_k}(t) = n_k^{-\frac{D}{2}} V_D \left(\frac{m}{2\pi \mathrm{i}\hbar t}\right)^{\frac{D}{2}} , \tag{1.41}$$

or equivalently, in terms of thermodynamic formulation to be used in (1.28),

$$\mathcal{A}_{n_k}(-\mathrm{i}\hbar\beta) = n_k^{-\frac{D}{2}} \frac{V_D}{\lambda_{\mathrm{T}}^D} = Z^{(1)}(n_k\beta) , \tag{1.42}$$

where

$$\lambda_{\mathrm{T}} = \sqrt{2\pi\hbar^2\beta/m} \tag{1.43}$$

is the thermal de Broglie wavelength. The expressions (1.41) and (1.42) show that each cluster (diagrammatically depicted by Fig. 1.6b) can be regarded as a single entity. It contributes to the partition function or the smooth DOS like a single particle that can invariantly be moved along the single-particle configuration space Ω, yielding its volume V_D as measure[4] of the invariant manifold corresponding to the n_k particles of the cluster. Also, the dimensionality of this invariant manifold corresponds to the dimensionality D of Ω, resulting in the same exponent in the dependence on t or β. The number of participating particles only enters as a prefactor, which could also be interpreted as a reduction of the mass of the effective cluster entity by a factor n_k. While this relation might seem counter-intuitive at first sight, it becomes a bit less puzzling when considering an effectively reduced mass as a fastening in the spreading of a wave packet, that is, in some sense more loosely bound for a larger number of particles in the cluster. This interpretation of acceleration of the spreading by a factor n_k holds for an arbitrary single-particle system, reflected by the general expression (1.42) in terms of the single-particle partition function $Z^{(1)}$ of multiple inverse temperature β, which is purely a consequence of the general semigroup property (1.40).

The full contribution to the non-interacting partition-function corresponding to a permutation is then (see Fig. 1.6c)

$$\mathcal{A}_{\mathfrak{N}}(-\mathrm{i}\hbar\beta) = \prod_{n\in\mathfrak{N}} \mathcal{A}_n(-\mathrm{i}\hbar\beta) \tag{1.44}$$

while the partition function is

$$\begin{aligned} Z_{0,\pm}^{(N)}(\beta) &= \frac{1}{N!} \sum_{\mathfrak{N}\vdash N} (\pm 1)^{N-|\mathfrak{N}|} c_{\mathfrak{N}}^{(N)} \mathcal{A}_{\mathfrak{N}}(-\mathrm{i}\hbar\beta) \\ &= \frac{1}{N!} \sum_{\mathfrak{N}\vdash N} (\pm 1)^{N-|\mathfrak{N}|} c_{\mathfrak{N}}^{(N)} \prod_{n\in\mathfrak{N}} Z^{(1)}(n\beta) . \end{aligned} \tag{1.45}$$

Here, the sum runs over all partitions $\mathfrak{N}$ of N and

$$c_{\mathfrak{N}}^{(N)} := \frac{N!}{\prod_{n\in\mathfrak{N}} n \prod_n m_{\mathfrak{N}}(n)!} \tag{1.46}$$

[4] Up to a constant factor $n_k^{D/2}$ [14].

denotes the number of permutations of N with a cycle decomposition corresponding to $\mathfrak{N}$, where $m_{\mathfrak{N}}(n)$ is the multiplicity of n in $\mathfrak{N}$. Again the expression (1.45) in terms of $Z^{(1)}$ holds for arbitrary single-particle systems. Evaluating (1.45) in the case of a quantum billiard yields then the explicit result

$$Z_{0,\pm}^{(N)}(\beta) = \sum_{l=1}^{N} z_{\pm,l}^{(N,D)} \left(\frac{V_D}{\lambda_{\mathrm{T}}^D}\right)^l \tag{1.47}$$

with coefficients

$$z_{\pm,l}^{(N,D)} = (\pm 1)^{N-l} C_l^{(N,D)}/l!\,, \tag{1.48}$$

where the index l corresponds to the number of clusters the total number of particles is divided into, or equivalently the number of cycles in a permutation. To relax notation I may omit any of the sub- and superscripts N, D or $\pm$, writing, *e.g.*, $z_l = z_l^{(N)} = z_{\pm,l}^{(N,D)}$ whenever these dependencies are clear from context. The universal coefficients $C_l^{(N,D)}$ are given by

$$C_l^{(N,D)} = \sum_{\substack{\mathfrak{N}\vdash N \\ |\mathfrak{N}|=l}} \frac{l!}{\prod_n m_{\mathfrak{N}}(n)!} \Big(\prod_{n\in\mathfrak{N}} \frac{1}{n}\Big)^{\frac{D}{2}+1} = \sum_{\substack{n_1,\ldots,n_l=1 \\ \sum n_k = N}}^{N} \Big(\prod_{k=1}^{l} \frac{1}{n_k}\Big)^{\frac{D}{2}+1} \tag{1.49}$$

and result from direct calculation (1.42) together with summing up all contributions with the same number l of clusters, irrespective of their individual sizes, absorbing the coefficients (1.46). A full combinatorial derivation of (1.49) as well as a recursive method of their fast calculation for larger N can be found in [14].

Taking the (bilateral) inverse Laplace transform by the connection (1.28) then gives the smooth unconfined non-interacting many-body DOS

$$\bar{\rho}_{\pm}^{(N)}(E) = \rho_0 \sum_{l=1}^{N} \frac{z_l}{\Gamma\big(\frac{lD}{2}\big)} (\rho_0 E)^{\frac{lD}{2}-1} \theta(E)\,, \tag{1.50}$$

where for convenience I introduced the unit of density in energy (implying an associated unit of energy)

$$\rho_0 = \frac{m(V_D)^{\frac{2}{D}}}{2\pi\hbar^2}\,, \tag{1.51}$$

which corresponds roughly to the level spacing at the lower end of the single-particle spectrum, which has a Weyl volume term

$$\bar{\rho}^{(1)}(E) = \rho_0 \frac{(\rho_0 E)^{\frac{D}{2}-1}}{\Gamma\left(\frac{D}{2}\right)}\,. \tag{1.52}$$

The expressions (1.47) and (1.50) are the main result in the non-interacting unconfined case and have been conducted in the previous work [110].

Boundary reflections

In the following we consider the extension of (1.50) in the context of billiard systems by including physical boundary effects. To leading order those are incorporated as direct reflections on the boundary that is locally assumed to be

flat. Analogous to the perimeter (or surface) correction term $\bar{\rho}_{\mathrm{S}}$ in the single-particle Weyl expansion (1.20), such reflections (1.18) can be included on the level of the single-particle propagator.

The derivation of the corresponding corrections to (1.47) and (1.50) under the assumption of locally flat boundaries can be performed directly by incorporating the additional geometrical features into the propagation in cluster zones. Thereby all possible subsets of particles for any clustering due to a specific permutation have to be chosen to contribute via reflected single-particle propagation $K_0^{(1)}(R\mathbf{q}^{\mathrm{f}}, \mathbf{q}^{\mathrm{i}}; t)$ whereas the others contribute by direct free propagation. Although this is a possible way to proceed that leads to the correct expressions in the end, it gets lengthy and seems a bit long-winded. Therefore, an alternative but equivalent derivation can be chosen here. It is based on the fact that also the exact confined single-particle propagator obeys the semigroup property (1.40) as well as the free propagator. This means, the reduction (1.39) of cluster contributions to just one single-particle propagation with altered time $t \mapsto n_k t$ holds also for the confined propagator. There is just one subtlety that has to be taken care of, namely that the semigroup property (1.40) applies only for *exact* propagators of an arbitrary single-particle system. But instead, here an approximation (1.18) to the propagator is used that corresponds to its short-time dynamics in the vicinity of boundaries. One can show [14] then that, indeed, this approximation also obeys the same property when one takes the assumption of locally flat boundaries to the level of the intermediate coordinate that is integrated over. In this way, one allows the intermediate integration to be split into directions parallel to the boundary and a direction perpendicular to it and then the effective propagator (1.18) locally corresponds indeed to the exact propagator of an actual system, namely a particle moving in free space with an additional infinitely extended flat wall. Thus, each cluster contribution reads

$$\begin{aligned}\mathcal{A}_{n_k}(t) &= \int \mathrm{d}^D q_1 \ldots \mathrm{d}^D q_{n_k} \prod_{i=1}^{n_k} \left(K_0^{(1)}(\mathbf{q}_{i+1}, \mathbf{q}_i; t) \pm K_0^{(1)}(R\mathbf{q}_{i+1}, \mathbf{q}_i; t) \right) \\ &= \int \mathrm{d}^D q \, \left(K_0^{(1)}(\mathbf{q}, \mathbf{q}; n_k t) \pm K_0^{(1)}(R\mathbf{q}, \mathbf{q}; n_k t) \right) ,\end{aligned} \tag{1.53}$$

indicating that also in the presence of boundary effects, each cluster can be regarded as an entity that either propagates freely or gets reflected on the boundary *as a whole*, whereas in the first place every single particle inside a cluster is left with this choice. On the formal level, this subsummation simplifies the calculus significantly.

To make the long story short, after a similar analysis as in the unconfined case and further combinatorial manipulations the resulting expressions read

$$Z_{\pm}^{(N)}(\beta) = \sum_{l=1}^{N} \sum_{l_{\mathrm{V}}=0}^{l} z_{l,l_{\mathrm{V}}} \left(\frac{V_D}{\lambda_{\mathrm{T}}^D} \right)^{l_{\mathrm{V}}} \underbrace{\left(\pm \frac{S_{D-1}}{4\lambda_{\mathrm{T}}^{D-1}} \right)^{l-l_{\mathrm{V}}}}_{\text{Neumann / Dirichlet surface term}} \tag{1.54}$$

and

$$\bar{\rho}_{\pm}^{(N)}(E) = \rho_0 \sum_{l=1}^{N} \sum_{\substack{l_{\mathrm{V}}, l_{\mathrm{S}}=0 \\ \sum l_i = l}}^{l} \frac{z_{l,l_{\mathrm{V}}} \gamma^{l_{\mathrm{S}}}}{\Gamma(\lambda)} (\rho_0 E)^{\lambda-1} \theta(E) , \tag{1.55}$$

where $\lambda = l_{\mathrm{V}} D/2 + l_{\mathrm{S}}(D-1)/2$ and $l = l_{\mathrm{V}} + l_{\mathrm{S}}$. The additional dimensionless geometrical parameter

$$\gamma = \pm \frac{S_{D-1}}{4(V_D)^{1-1/D}} \tag{1.56}$$

represents the ratio of the surface S_{D-1} to the volume V_D of the billiard. The plus(minus) sign in the surface term in (1.54) and (1.56) refers to Neumann (Dirichlet) conditions at the physical boundary not to be confused with the symmetry class under particle exchange, which is absorbed into $z_{l,l_{\mathrm{V}}}$. The interpretation of each term in (1.54) and (1.55) is that $l = l_{\mathrm{V}} + l_{\mathrm{S}}$ is the total number of clusters the particles get partitioned into according to permutations and the index l_{V} represents the number of clusters that contribute by free propagation all over the billiard Ω whereas l_{S} indexes the number of clusters that contribute via reflection on the boundary $\partial\Omega$. The confined generalization of the dimensionless numerical coefficients

$$z_{l,l_{\mathrm{V}}} \coloneqq (\pm 1)^{N-l} \frac{C^{(N,D)}_{l,l_{\mathrm{V}}}}{l_{\mathrm{V}}!(l-l_{\mathrm{V}})!} \tag{1.57}$$

involves the generalized universal coefficients

$$C^{(N,D)}_{l,l_{\mathrm{V}}} \coloneqq \sum_{\substack{n_1,\ldots,n_l=1 \\ \sum n_k = N}}^{N} \Big(\prod_{k=1}^{l_{\mathrm{V}}} \frac{1}{n_k} \Big)^{\frac{D}{2}+1} \Big(\prod_{k=l_{\mathrm{V}}+1}^{l} \frac{1}{n_k} \Big)^{\frac{D}{2}+\frac{1}{2}}, \tag{1.58}$$

which, as their unconfined counterparts (1.49), can be calculated efficiently using a recurrence relation [14].

In the case of $D = 1$ the terms corresponding to $l_{\mathrm{V}} = 0$ correspond to a overall point-like invariant manifold and have to be replaced according to the rule

$$\frac{(\rho_0 E)^{\frac{l_{\mathrm{S}}(D-1)}{2}-1}}{\Gamma\Big(\frac{l_{\mathrm{S}}(D-1)}{2}\Big)} \theta(E) \overset{D\to 1}{\longrightarrow} \delta(\varrho_0 E)\,, \tag{1.59}$$

and in (1.56) the surface S_0 has to be taken as the number of boundary points, which would be two for a finite line and zero for the one-sphere topology. The reason for this replacement simply lies in the fact that a point-like contribution is constant as a function of inverse temperature β while the inverse Laplace transform of a constant breaks ranks by yielding a Dirac-delta distribution rather than a power law. This circumstance has its single-particle analogue, *e.g.*, in the curvature and corner correction in the Weyl expansion of a two-dimensional billiard that are also delta-like [106, 107]. For consistency, one can check that the expression (1.50) for the unconfined case can easily be reobtained as the special case $\gamma = 0$ by recognizing that $C^{(N,D)}_{l,l_{\mathrm{V}}=l} = C^{(N,D)}_{l}$.

The same result (1.55) would be obtained by utilizing a convolution formula by Weidenmüller [109] where one directly uses the information of boundary corrections on the level of the single-particle DOS in Weyl expansion (1.20). Applying the convolution formula thereby implicitly assumes the semigroup property of the short-time propagator used for boundary corrections and is therefore equivalent to the approach shown here. The corresponding derivation can be found in [14].

The naive volume term

Before analyzing the full expressions (1.50) and (1.55) one should stress what is actually one of the main questions that will be answered there: What is the role and the importance of all the sub-leading contributions originating from clusterings? In single-particle systems usually the situation is as follows. The leading (or volume) term, given by the Thomas-Fermi approximation (1.17), not only gives the asymptotic behavior of the DOS for large E but usually suffices in describing it in a very wide range of energies. Only when one comes close to $E = 0$, the corrections from the boundary become important. One of their main effects is to effectively account for the shift of ground-state energies, which are naturally larger when the wave function is constrained to be zero-valued (Dirichlet boundary condition) along the boundary as compared to Neumann conditions. This means that, typically, if one would estimate the location of discrete energy levels using only the volume term, the effect of higher-order corrections only has a noticeable impact in the regime of the lowest few of those levels. If one ignores the accuracy at the very few lowest levels, the Thomas-Fermi approximation (or Weyl volume term) gives a sufficient description.

This gives rise to the natural question about the importance of all higher-order corrections in (1.50) and (1.55) related to clusterings of particles. How strong is their impact? How valid is the truncation to the leading term

$$\begin{aligned}\bar{\rho}_{\mathrm{V}}^{(N)}(E) &= \frac{1}{N!}\rho_0^{\frac{ND}{2}}\frac{E^{\frac{ND}{2}-1}}{\Gamma\left(\frac{ND}{2}\right)}\theta(E) \\ &= \frac{1}{N!}\bar{\rho}_{\mathrm{TF}}(E)\end{aligned} \tag{1.60}$$

that corresponds to $l = N$ (each particle in its own cluster)? Or, equivalently, how valid is the Thomas-Fermi approximation (or Weyl volume term) (1.17) in the ND-dimensional fundamental domain $\mathcal{F}_N$ (1.34)? As one could naively expect (1.60) to be widely sufficient in analogy to the single-particle situation I will refer to this term as the *naive volume term*.

Emergence of ground state energies and the importance of higher-order clusterings

This subsection focuses on applying formulae (1.50) and (1.55) and investigating the effect of higher-order symmetry corrections on the many-body DOS. As a representative I choose here the spatial dimensionality to be $D = 2$, of special interest in the context of mesoscopic physics, where, in the long term, one might for instance think of applications to confined two-dimensional electron gases in semiconductor heterostructures [145] or two-dimensional superconducting structures (see, *e.g.*, [146, 147] for renewed interest due to realizations either in boundary layers or as mono- or few-atomic, or molecular layers) with effective bosonic description due to Cooper pairing [5]. Furthermore, the asymptotically constant single-particle DOS of two-dimensional billiards is a valuable special feature, not only because it simplifies calculus but interestingly because it opens the possibility to make connections to number theory. Namely, asymptotics for the distribution of (restricted) partitions of integers can be obtained. Establishing this connection and comparison with formerly known results goes beyond the scope of this thesis and can be looked up in [14, 110].

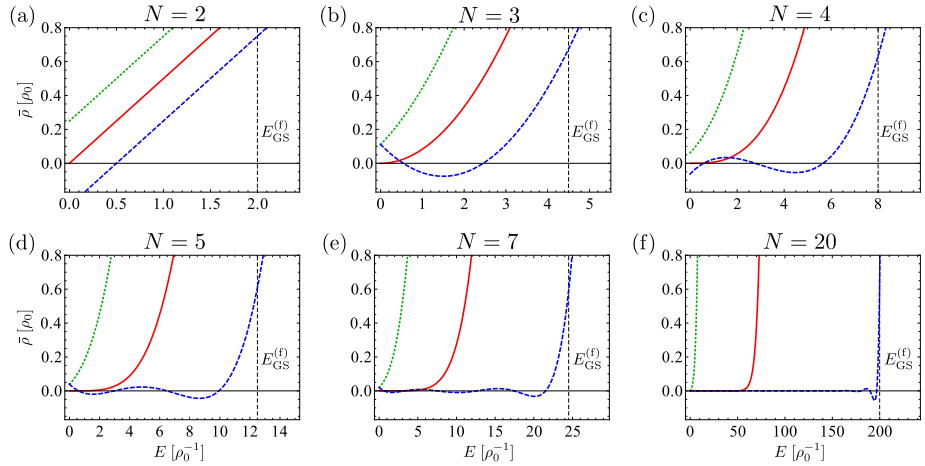

Fig. 1.7: Symmetry-projected two-dimensional DOS without boundary corrections (1.50), for bosons (green, dotted) and fermions (blue, dashed) in comparison to the naive volume term (1.60) (red, solid) for various numbers of particles. The vertical dashed black line marks the particular expected many-body ground state energy $E_{\mathrm{GS}}^{(\mathrm{f})}$ (1.61) for fermions. Densities $\bar{\rho}$ and energies E are measured in units of the constant single-particle density ρ_0 (1.52) and (1.51), and its inverse ρ_0^{-1}, respectively.

For $E > 0$ the unconfined DOS (1.50) in $D = 2$ is a polynomial of degree $N - 1$ in energy with coefficients that are just rational numbers. The numerical coefficients (1.48) can be summed up to their exact rational values for any explicit pair of indexes N and l.

Figure 1.7 shows the two-dimensional non-interacting unconfined mean DOS for particle numbers varying from $N = 2$ to 20. The bosonic and fermionic cases (1.50) are shown in comparison to the naive volume term (1.60).

Already for $N = 2$ Fig. 1.7a shows that the symmetry correction $l = 1$ gives a qualitative push in the right direction. With respect to the naive volume term $l = N = 2$ (1.60) the zero point of the fermionic density is shifted to higher energies, which can be regarded as a precursor of a finite fermionic many-body ground state energy. On the contrary, the bosonic density is shifted to lower energies, which accords to the full counting of many-body levels corresponding to shared single-particle energies in contrast to the naive volume term, where these are counted with a factor of $1/N!$, even if they cannot be permuted in $N!$ ways due to the identity of some of the single-particle energies, the most extreme example being the ground state, where all particles occupy the same mode. Figures 1.7b–f show the cases $N = 3$ to 20 particles. In the fermionic case the lower powers in E in the polynomial (1.50) produce oscillations around the axis $\bar{\varrho} = 0$. These oscillations get smaller in amplitude and larger in number with increasing particle number, approximating a zero-valued DOS. The finite DOS is effectively shifted to higher energies and an energy gap opens that coincides with the expected fermionic many-body ground state energy $E_{\mathrm{GS}}^{(\mathrm{f})}$ calculated by counting single-particle levels by virtue of the smooth single-particle DOS $\bar{\rho}^{(1)}(E)$. It is defined by

$$E_{\mathrm{GS}}^{(\mathrm{f})} = \int_{-\infty}^{\bar{E}_{\mathrm{F}}} \mathrm{d}E'\ \bar{\rho}^{(1)}(E')E'\,, \tag{1.61}$$

where the Fermi energy $\bar{E}_{\mathrm{F}}$ is determined through

$$N = \int_{-\infty}^{\bar{E}_{\mathrm{F}}} \mathrm{d}E' \; \bar{\rho}^{(1)}(E') \,. \tag{1.62}$$

Instead of explicitly filling up single-particle energy levels, in the geometrical approach pursued here, the many-body ground state energy occurs as a consequence of exchange symmetry systematically incorporated in the propagator. The corrections from cluster-zone propagations are sufficient to generate the expected ground state energy. This is not obvious in the first place, since the QCE approach is based on the mean DOS in the semiclassical limit, disregarding the discrete nature of the energy levels. When increasing N, the symmetry projected DOS at $E = E_{\mathrm{GS}}^{(\mathrm{f})}$ is observed to keep moderate values $\bar{\varrho}_{-}(E_{\mathrm{GS}}^{(\mathrm{f})}) \approx \mathcal{O}(1)$ while the DOS based on the naive volume term apparently grows exponentially with N at this energy. In contrast to the fermionic density the bosonic density does not exhibit oscillations. There, the polynomial in E has only positive coefficients and the density is effectively shifted to lower energies as expected intuitively for bosons.

Again, the emergent fermionic energy gap accurately reproduces the ground state energy, indicated by crossing the axis $\rho = \rho^{(1)} = \rho_0$, which is in agreement with the fact that, regarding discrete spectra, the first excited many-body level should be roughly one single-particle mean level spacing above the many-body ground state level, while the small values of $\bar{\rho}_{-}(E)$ for $E \lesssim E_{\mathrm{GS}}^{(\mathrm{f})}$ result from large cancellations between terms in the sum (1.50) with different values of l. Therefore the behavior of the DOS in this regime is very sensitive to incomplete summation and all terms are required to reproduce the DOS correctly, as can be looked up to more detail in [110]. This emphasizes the importance of all cluster contributions. To the extreme end, the naive volume term (1.60) shows to be several orders of magnitude off in extremely wide range of energies already for very small numbers of particles and with even increasing insufficiency with N. But also all the sub-dominant contributions from very large clusters (meaning very small l) turn out to be an input of major importance. As explicitly shown in [110], any slight deviation in the coefficients in (1.50) from (1.48) destroys the correct description, especially around the ground state energy $E_{\mathrm{GS}}^{(\mathrm{f})}$ – a circumstance that makes it even more impressing that the short-time dynamical information alone is sufficient to accurately reproduce average ground state energies in a universal manner, while the discrete nature of actual spectra has been completely ignored. This shows an important feature at the core of the whole approach: The QCE has a way larger range of validity than one might expect from its conceptual basis. Despite the fact that generally, semiclassical approaches are considered to asymptotically describe physical reality in the high-energy regime we have here a coincidence down to universally expected many-body ground state energy. In a sense the descriptive power of the approach goes even beyond, as also below $E = E_{\mathrm{GS}}^{(\mathrm{f})}$ the absence of any energy level is predicted by effectively vanishing DOS. The small oscillations are thereby artifacts that integrate to zero. Also the corresponding naive assumption that, from the thermodynamic point of view, the approach would lead to a high-temperature description is proven wrong in this sense. While the information about the exact positions of energy levels is dropped, their average distribution is correctly reflected up to the extreme limits. What is lost seems to be only the

discreteness of many-body spectra itself and system-specific fluctuations that may manifest in the accurate location of exact ground state energies that can fluctuate around the universal value $E = E_{\mathrm{GS}}^{(\mathrm{f})}$ with system-specific parameters (for example ones that specify the exact shape or global topology of the billiard) or the number of particles.

To further test the descriptive power of the method we move on to compare with actually calculated exact (non-interacting) many-body levels. To do so, in the following, the QCE is applied to a quantum billiard system bringing along the analysis of confinement effects. In Fig. 1.8 the effect of boundary corrections is shown by means of the level counting function

$$\mathcal{N}(E) = \int_{-\infty}^{E} \mathrm{d}E' \, \bar{\rho}_{-}(E') \,. \tag{1.63}$$

Compared are counting functions $\mathcal{N}(E)$ based on several calculations for $N = 12$ particles in two dimensions. I choose here a logarithmic scaling of $\mathcal{N}$ in the plot, which exaggerates the oscillations around $\mathcal{N} = 0$ (negative values are displayed as logarithm of their absolute value) and moderates the extreme growth for $E > E_{\mathrm{GS}}^{(\mathrm{f})}$ to comparable values. The exaggerated oscillations as an artifact of vary small magnitude are no physical feature. The functions can be considered effectively zero-valued there. First of all, I compare the smooth DOS based on the bulk contribution (1.50) (blue dashed curve) with the confined result given by expression (1.55) (black dotted) for Dirichlet boundary conditions with a geometrical perimeter-to-area ratio (1.56) of $\gamma = -\sqrt{\pi}/2$. This is the smallest possible parameter for flat, simply-connected billiards, since it is the one of a circular billiard. The curve incorporating boundary contributions is basically shifted to higher energies, enlarging the energy gap. Again the universally expected ground state energy $E_{\mathrm{GS}}^{(\mathrm{f})}$, this time calculated using the single-particle Weyl expansion (1.20) with perimeter correction, is reproduced very well. Interestingly, already for this minimal γ the deviations from the unconfined case are rather strong. Thus, naturally the question arises whether the assumption of locally flat boundaries gives a sufficient description of an actual billiard or whether additional corrections would lead to further rather strong deviations, making the treatment of boundary curvature non-negligible. To answer this question the exact quantum mechanical levels of a circular billiard have been used to compute the non-interacting fermionic many-body levels shown by the green staircase function. The deviation is a slight shift, considerably smaller than the deviation of the confined from the unconfined case. The additional comparison with exact levels of a billiard with the shape of a cylinder barrel with same γ as the circle, serving as an example of a 2D system without curvature[5], shows perfect agreement with the smooth part[6](see inset of Fig. 1.8).

An analysis of the $E_{\mathrm{GS}}^{(\mathrm{f})} = E_{\mathrm{GS}}^{(\mathrm{f})}(N, \gamma, \chi)$ in two dimensions for the unconfined and confined cases with and without curvature, specified by the Euler character χ [106], indicates the relative importance of the corresponding contributions in the smooth DOS. The smooth ground state energy involving a Dirichlet type

[5]The absence of curvature can be seen in the single-particle expansion given by Balian and Bloch [106], where the corresponding correction is proportional to the Euler characteristic χ of the billiard, which happens to be one for a disk and zero for a cylinder barrel.

[6]Note that in this geometry the minimal value of γ could be underrun, which is not contradictory since it is not flat and simply connected.

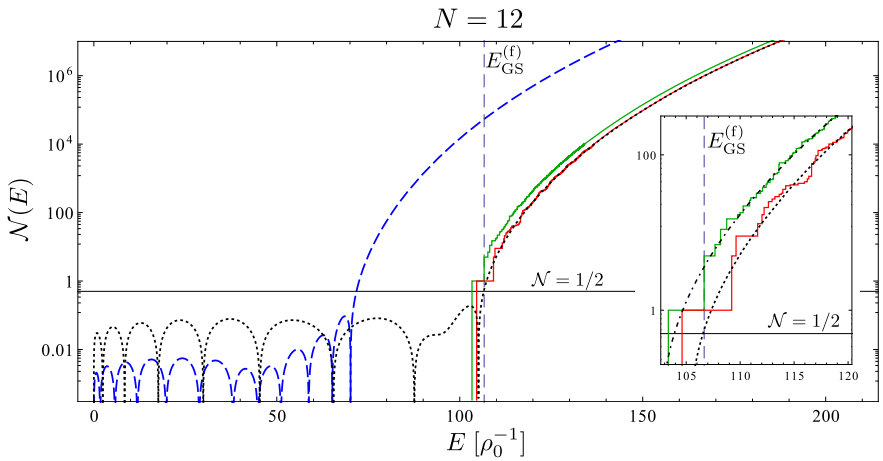

Fig. 1.8: Level counting function (1.63) for 12 fermions. The blue dashed curve shows the smooth part without confinement corrections. The black dotted curve includes boundary corrections with a geometrical parameter $\gamma = -\sqrt{\pi}/2$, which corresponds to a circular billiard. The green staircase (left) shows the exact non-interacting many-body levels of the circular billiard with Dirichlet boundary condition. The red staircase (right) shows the exact levels of a cylindrical billiard with same geometrical parameter. The dash-dotted black curve in the inset shows the smooth part shifted to lower energies corresponding to the shift of $E_{\rm GS}^{(\rm f)}$ due to curvature effects (1.65).

perimeter correction without curvature ($\chi = 0$) reads

$$E_{\rm GS}^{(\rm f)}(N,\gamma,0) = E_{\rm GS}^{(\rm f)}(N,0,0)\,\left(\sqrt{1+a}+\sqrt{a}\right)^3\left(\sqrt{1+a}-\frac{1}{3}\sqrt{a}\right), \qquad a = \frac{|\gamma|}{\sqrt{\pi N}}\,. \tag{1.64}$$

The inclusion of the curvature correction $\chi\delta(E)/6$ [106] in the single-particle DOS yields the ground state energy $E_{\rm GS}^{(\rm f)}(N,\gamma,\chi) = E_{\rm GS}^{(\rm f)}(N-\chi/6,\gamma,0)$. Comparing the correction due to the perimeter ($\chi = 0$) with the further correction due to curvature,

$$\frac{E_{\rm GS}^{(\rm f)}(N,\gamma,\chi) - E_{\rm GS}^{(\rm f)}(N,\gamma,0)}{E_{\rm GS}^{(\rm f)}(N,\gamma,0) - E_{\rm GS}^{(\rm f)}(N,0,0)} = -\frac{\sqrt{\pi}\chi}{8|\gamma|}\sqrt{\frac{1}{N}} + \frac{\chi}{16N} + \mathcal{O}\big(N^{-\frac{3}{2}}\big)\,,$$

indicates that curvature contributions in general get suppressed for increasing particle number. Based on this observation, the smooth part of the many-body DOS including curvature in $D = 2$ might be approximated by simply shifting the many-body DOS (including perimeter corrections) by

$$\Delta E = E_{\rm GS}^{(\rm f)}(N,\gamma,\chi) - E_{\rm GS}^{(\rm f)}(N,\gamma,0)\,. \tag{1.65}$$

The corresponding function is plotted as dashed-dotted curve in the inset of Fig. 1.8. This way of incorporating boundary curvature as an effective shift in the total energy basically shows perfect agreement. Without going into detail, I anticipate the quality of this method here as one motivation for a generalized, less trivial version of shifting total energies. This method is developed and

discussed later in section 1.5.2 and will serve as a valuable tool to incorporate interactions in a simplified manner.

1.1.5 External potentials in local approximation

The local potential approximation for clusters

So far we only considered the non-interacting QCE of billiard systems, meaning with flat (or zero) external potential in the allowed domain Ω, either unconfined (1.50) or with confinement induced through boundary conditions (1.55) rather than a confining potential. On the single-particle level we already discussed the usual way of incorporating smooth potentials $U_{\text{ext}}(\mathbf{q})$ (1.10) in the mean DOS consistent with the focus on short-time dynamics (see section 1.1.2). There, the eikonal approximation (1.21) (see, *e.g.*, [143]) to the single-particle propagator leads to the inclusion of potentials that are locally constant over the relevant spread of wave packets for short times. This way, the effect of potentials was implemented as just a phase in the "diagonal part" of the single-particle propagator (1.22). In the single-particle context the dependence of this phase on the location $\mathbf{q}$ is special, because the initial and final coordinate $\mathbf{q}^{\text{i}}$ and $\mathbf{q}^{\text{f}}$ coincide. In contrast, for cluster propagations that correspond to cycles involving more than one particle, the single-particle propagations are not diagonal in this sense but rather involve finite distances. Similar as when confinement corrections were introduced in the billiard systems, the question arises, whether the effect on a (non-interacting) cluster contribution also shows up purely on the diagonal single-particle level in (1.39) after exploiting the semigroup property (1.40).

After relabeling particle indexes the contribution (1.39) coming from a cycle P of length n in eikonal approximation is

$$\begin{aligned}
&\int \mathrm{d}^{nD}q\, K(P\mathbf{q},\mathbf{q};t) = \\
&\quad \Big(\frac{m}{2\pi \mathrm{i}\hbar t}\Big)^{\frac{nD}{2}} \int \mathrm{d}^{D}q_1 \cdots \int \mathrm{d}^{D}q_n \, \exp\left[\frac{\mathrm{i}}{\hbar}\frac{m}{2t}\Big(|\mathbf{q}_2-\mathbf{q}_1|^2+\cdots+|\mathbf{q}_1-\mathbf{q}_n|^2\Big)\right] \\
&\times \exp\left[-\frac{\mathrm{i}t}{\hbar}\int_0^1 \mathrm{d}s\,\Big(U_{\text{ext}}\big((\mathbf{q}_2-\mathbf{q}_1)s+\mathbf{q}_1\big)+\cdots+U_{\text{ext}}\big((\mathbf{q}_1-\mathbf{q}_n)s+\mathbf{q}_n\big)\Big)\right].
\end{aligned} \tag{1.66}$$

Now another approximation to this object exploiting $t \to 0$ is given by the saddle point method identifying the second exponential as smooth function compared to the first one. Thus the saddle point is given by the quadratic form only

$$\frac{\partial}{\partial q_i^{(d)}}|P\mathbf{q}-\mathbf{q}|^2 = 0 \qquad \forall i,d \tag{1.67}$$

$$\Leftrightarrow\ q_{i+1}^{(d)} - q_i^{(d)} = 0 \qquad \forall i,d\,, \tag{1.68}$$

with $\mathbf{q}_{n+1} := \mathbf{q}_1$.

Thus the dominant contribution originates from the region around the configuration where all particles of the cluster coincide in their coordinates. For the saddle point, this is the D-dimensional freedom of simultaneous translation of all particles, which can be split off as the location of one of the involved particles.

After integrating all the remaining coordinates in saddle point approximation one finds

$$\int \mathrm{d}^{nD}q\, K(P\mathbf{q},\mathbf{q};t) \approx n^{-\frac{D}{2}} \left(\frac{m}{2\pi\mathrm{i}\hbar t}\right)^{\frac{D}{2}} \int \mathrm{d}^{D}q_1\, \exp\left[-\frac{\mathrm{i}t}{\hbar} n U_{\mathrm{ext}}(\mathbf{q}_1)\right] . \quad (1.69)$$

So, indeed, within this consistent approximation, the effect of potentials show up on the diagonal single-particle level

$$\mathcal{A}_{n_k}(t) = \int \mathrm{d}^{D}q\, K^{(1)}(\mathbf{q},\mathbf{q};n_k t)\,, \quad (1.70)$$

using $K^{(1)}(\mathbf{q},\mathbf{q};t) \simeq \mathrm{e}^{-\frac{\mathrm{i}}{\hbar}U_{\mathrm{ext}}(\mathbf{q})t} K_0^{(1)}(\mathbf{q},\mathbf{q};t)$, where K_0 refers to unconfined free propagation. Another way of expressing this fact is that, within the saddle-point approximation considering short times, the single-particle propagator in eikonal approximation (1.21) fulfills the semigroup property (1.40).

Equivalently, a separation into center-of-mass and relative coordinates could be performed, where relative coordinates are integrated as free propagation and the influence of the external potential is on the level of the center of mass, which may be closer to interpretation. Anyhow, physically speaking, for cluster propagation over short times external potentials act as if an n-cluster was united as a single entity at one point $\mathbf{q}_1$ feeling the n-fold potential there. In other words, the potential can effectively be considered locally constant over the relevant spread of a cluster, which is the reason to refer to this method as *LPA*.

Homogeneous potentials

Of special interest in experimental realizations is the class of homogeneous potentials of degree μ

$$U_{\mathrm{ext}}(\mathbf{q}) = w^{\mu} U_{\mathrm{ext}}(\mathbf{q}/w)\,, \qquad w \in \mathbb{R}^{+}\,, \quad (1.71)$$

that includes harmonic confinements $\mu = 2$ often realized in optical or magnetic traps for ultracold neutral atoms (see introduction for references).

The homogeneity property (1.71) allows to calculate (1.70) to be

$$\begin{aligned} \mathcal{A}_n(t) &= n^{-\frac{d}{2}} V_{\mathrm{eff}} \left(\frac{m}{2\pi\mathrm{i}\hbar t}\right)^{\frac{d}{2}}\,, \\ \mathcal{A}_n(-\mathrm{i}\hbar\beta) &= n^{-\frac{d}{2}} \frac{V_{\mathrm{eff}}}{\lambda_{\mathrm{T}}^{d}}\,, \end{aligned} \quad (1.72)$$

which has exactly the same form as the expressions (1.41) and (1.42) without external potential. The effect of the homogeneous potentials then enters just as a replacement of the dimensionality D and the D-volume V_D by the effective quantities

$$\begin{aligned} d &= D + \frac{2}{\mu} D\,, \\ V_{\mathrm{eff}} &= (2\hbar^2/m e_0)^{D/\mu} \int \mathrm{d}^{D}q \exp(-U_{\mathrm{ext}}(\mathbf{q})/e_0)\,, \end{aligned} \quad (1.73)$$

where e_0 is an arbitrary unit of energy introduced to make the exponent dimensionless. For practical purposes it can simply be set to unity. The effective

volume is a d-volume considering units but represents (up to an undetermined constant factor) the D-volume enclosed by a equipotential surface. This identification can be easily seen in the relation between effective volumes corresponding to a potential $U_{\text{ext}}(\mathbf{q})$ and its scaled version $U'_{\text{ext}}(\mathbf{q}) = U_{\text{ext}}(\mathbf{q}/w)$, which happens to be $V'_{\text{eff}} = w^D V_{\text{eff}}$.

The corresponding partition function in LPA reads

$$Z_{0,\pm}^{(N)}(\beta) = \sum_{l=1}^{N} z_{\pm,l}^{(N,d)} \left(\frac{V_{\text{eff}}}{\lambda_T^d}\right)^l , \quad z_{\pm,l}^{(N,d)} = (\pm 1)^{N-l} C_l^{(N,d)}/l! , \tag{1.74}$$

where the definition (1.49) of the universal constants $C_l^{(N,d)}$ is unchanged since it only accounts for the combinatorial issues of collecting different clusterings. Again, I may omit the scripts N, d and $\pm$ whenever they are clear from context and I emphasize that one should keep in mind to use the effective dimension in case homogeneous external potentials are applied. The special case of zero external potential (without confinement corrections) is included as $\mu \to \infty$, $d = D$, and with the available physical volume $V_{\text{eff}} = V_D$. Correspondingly, the mean many-body DOS of identical particles confined by a homogeneous potential reads

$$\bar{\rho}_{\pm}^{(N)}(E) = \rho_0^{\text{eff}} \sum_{l=1}^{N} \frac{z_l}{\Gamma\left(\frac{ld}{2}\right)} (\rho_0^{\text{eff}} E)^{\frac{ld}{2}-1} \theta(E) , \tag{1.75}$$

in LPA, where the effective volume enters in the energy-scale

$$\rho_0^{\text{eff}} = \frac{m(V_{\text{eff}})^{\frac{2}{d}}}{2\pi\hbar^2} . \tag{1.76}$$

As a last point of this subsection, I would like to stress again that the approximation involved in the LPA is fully consistent with the short-time consideration of local propagations. Therefore, this "approximation" does not introduce an actual deviation as long as one is interested in quantities related to smooth spectra only. This statement will be supported later by comparisons with exact spectra in such systems.

1.1.6 The superiority to grand canonical descriptions

Before we leave the stage of non-interacting systems and move on to actually use the cluster structure to incorporate the effect of genuine mutual interactions among particles, I briefly focus here on implications on thermodynamical considerations of non-interacting systems. The emphasis will thereby be on the fact that systems of few identical particles whose number N is strictly fixed demand thermodynamical descriptions within the canonical ensemble. This is opposed to the description within grand canonical ensembles where N is subject to thermal fluctuations, which is usually preferred especially in non-interacting systems. The reason for the usual preference lies in the fact that the non-interacting grand canonical partition function allows for an exact single-particle level-wise summation of occupation numbers on an analytical level:

$$\begin{aligned} Z_{\text{G},\pm} &= \sum_{\{n_i\}\in O_{\pm}^{\mathbb{N}}} \prod_i \mathrm{e}^{-\beta(\epsilon_i-\mu)n_i} = \prod_i \left(1 \mp \mathrm{e}^{-\beta(\epsilon_i-\mu)}\right)^{\mp 1} , \\ O_+ &= \mathbb{N}_0 , \quad O_- = \{0,1\} , \end{aligned} \tag{1.77}$$

where the upper sign refers to bosons and the lower one to fermions, respectively. The usual argument is then that for a large (average) number of particles $\langle N \rangle$, the relative thermal fluctuations $\delta N / \langle N \rangle$ become small, so that grand canonical and canonical descriptions are assumed to be equivalent in the thermodynamic limit, making both descriptions equivalently applicable to actual macroscopic many-body systems. There are, however, important situations where the grand canonical description fails. First, if the number of particles is considerably small (speaking of few-body systems which are one focus of modern experimental studies), the thermal fluctuations of N cannot be neglected and can have a rather strong impact on the physics. Second, it has been shown [148, 149] that the thermal fluctuations in the occupation numbers of single-particle levels heavily diverge from the canonical description *even in the thermodynamic limit*. These effects are non-negligible and play a special role in the context of BEC fluctuations. A third point is a practical issue that appears when one wants to express several thermodynamic quantities as functions of the (mean) number of particles $\langle N \rangle$. Then one has to rely on inversions of power-expansions in the fugacity $\mathrm{e}^{\beta\mu}$, which leads to cumbersome expressions that have to be truncated. This underlines once again that it is time to go beyond the grand canonical formalism for the description of experimentally relevant situations.

The mentioned intrinsic problems of the grand canonical formalism will be demonstrated in a special case. First, I introduce scaled variables that are natural to the description of thermodynamics. The (thermally) scaled volume is defined as

$$\tilde{v} = \frac{V_{\mathrm{eff}}}{\lambda_{\mathrm{T}}^d} \,. \tag{1.78}$$

The pressure in terms of the canonical partition function Z (1.15), (1.29) is defined as [139]

$$P(V_{\mathrm{eff}}, \beta, N) = \frac{1}{\beta} \frac{\partial}{\partial V_{\mathrm{eff}}} \log Z(V_{\mathrm{eff}}, \beta, N) \,, \tag{1.79}$$

here generalized to the context of homogeneous potentials. In general I will treat V_{eff} as the quantity reflecting the volume of the system also for other quantities, like isothermal compressibility

$$\kappa_{\mathrm{T}} = -\frac{1}{V_{\mathrm{eff}}} \left(\frac{\partial V_{\mathrm{eff}}}{\partial P} \right)_{T,N} = -\frac{1}{V_{\mathrm{eff}}} \left(\frac{\partial P(V_{\mathrm{eff}}, \beta, N)}{\partial V_{\mathrm{eff}}} \right)^{-1} . \tag{1.80}$$

Consider now a system of non-interacting bosons confined by a harmonic trap of frequency ω in one dimension, for which

$$\tilde{v} = \frac{1}{\beta \hbar \omega} \,. \tag{1.81}$$

This special case admits a fully exact analytic solution within the canonical ensemble which will be compared to two different approaches. The first approach is the canonical description based on neglecting spectral discreteness using (1.74). The second approach is the usual, textbook grand canonical description based on the mean DOS. The exact canonical partition function can be easily calculated to be [139]

$$Z_{\mathrm{ex}} = \mathrm{e}^{-\beta\hbar\omega \frac{N}{2}} \prod_{n=1}^{N} \frac{1}{1 - \mathrm{e}^{-\beta\hbar\omega n}} = \mathrm{e}^{-\tilde{v}^{-1} \frac{N}{2}} \prod_{n=1}^{N} \frac{1}{1 - \mathrm{e}^{-\tilde{v}^{-1} n}} \,, \tag{1.82}$$

whereas the smooth version based on the canonical QCE in LPA (1.74) reads

$$Z_{\mathrm{C}} = \sum_{l=1}^{N} z_l \left(\frac{1}{\beta\hbar\omega}\right)^l = \sum_{l=1}^{N} z_l \tilde{v}^l \,. \tag{1.83}$$

The exact grand canonical partition function is given by

$$\log Z_{\mathrm{G}} = -\sum_{n=0}^{\infty} \log\Big(1 - z\mathrm{e}^{-\beta\hbar\omega(n+1/2)}\Big) \tag{1.84}$$

as a function of the fugacity

$$z = \mathrm{e}^{\beta\mu} \,, \tag{1.85}$$

for chemical potential μ. As mentioned, to make (1.84) comparable to (1.83) one must omit discreteness by introducing the mean DOS on the single-particle level which yields the standard smooth version [139]

$$\log Z_{\mathrm{G}} = \tilde{v}\,\mathrm{Li}_{\frac{d}{2}+1}(z) = \frac{1}{\beta\hbar\omega}\,\mathrm{Li}_2(z) = \tilde{v}\,\mathrm{Li}_2(z) \,, \tag{1.86}$$

where $\mathrm{Li}_s(z) = \sum_{k=1}^{\infty} z^k/k^s$ is the polylogarithm and the first equation is here generalized to hold for homogeneous single-particle potentials.

The goal is now first to extract the mechanical equation of motion out of (1.83) or (1.84), meaning the pressure as a function of the (effective) volume V_{eff}, the temperature or its inverse $\beta = (k_{\mathrm{B}}T)^{-1}$ and the number of bosons N, which has to be taken as its thermal average in the grand canonical case. In the smooth canonical case this procedure is straight forward and yields the *closed* expression

$$P_{\mathrm{C}}(V_{\mathrm{eff}}, \beta, N) = \frac{k_{\mathrm{B}}T}{V_{\mathrm{eff}}} \frac{\sum_{l=1}^{N} l z_l \tilde{v}^l}{\sum_{l=1}^{N} z_l \tilde{v}^l} \,, \tag{1.87}$$

which holds in general using (1.74) and the specific expression for the non-interacting harmonically confined bosons in one dimension is obtained by identifying (1.78). In the smooth grand canonical case, the dependence on $\langle N\rangle$ is hidden, which needs extra effort to make it explicit. The pressure and average number of particles in the grand canonical ensemble are generally given by [139]

$$\begin{aligned} P_{\mathrm{G}}(V_{\mathrm{eff}}, \beta, z) &= \frac{1}{\beta}\left(\frac{\partial \log Z_G}{\partial V_{\mathrm{eff}}}\right)_{\beta,z} = \frac{1}{\beta\lambda_{\mathrm{T}}^d}\,\mathrm{Li}_{\frac{d}{2}+1}(z) \,, \\ \langle N\rangle_{\mathrm{G}} &= z\left(\frac{\partial \log Z_G}{\partial z}\right)_{V_{\mathrm{eff}},\beta} = \frac{V_{\mathrm{eff}}}{\lambda_{\mathrm{T}}^d}\,\mathrm{Li}_{\frac{d}{2}}(z) \,, \end{aligned} \tag{1.88}$$

which leaves power expansions in the fugacity that are typical for grand canonical descriptions. They are best written in dimensionless form for the scaled pressure $\beta\lambda_{\mathrm{T}}^d P_{\mathrm{G}}$ and the *thermal particle density* $\tilde{n} = \lambda_{\mathrm{T}}^d \langle N\rangle_{\mathrm{G}}/V_{\mathrm{eff}}$ as

$$\begin{aligned} \beta\lambda_{\mathrm{T}}^d P_{\mathrm{G}} &= c_1 z + c_2 z^2 + c_3 z^3 + \dots \,, \\ \tilde{n} &= c_1 z + 2c_2 z^2 + 3c_3 z^3 + \dots \,, \\ c_k &\coloneqq k^{-\frac{d}{2}-1} \,. \end{aligned} \tag{1.89}$$

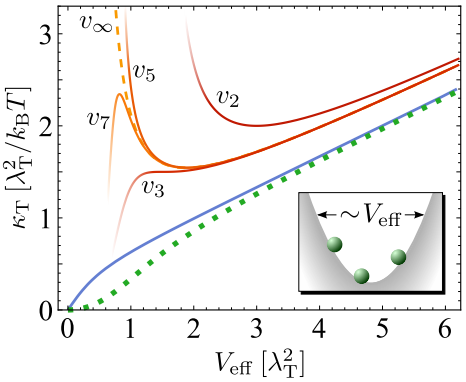

Fig. 1.9: Isothermal compressibility (1.80) of the ideal Bose gas with harmonic confinement and $N = 3$ particles. While the QCE (solid, blue) using (1.74) and (1.87) fits the numerical values (dotted, green) down to the condensation regime, the virial expansions (1.90) (here denoted v_k) to various orders k (solid, red-orange tones) give unphysical results. Discreteness effects are not taken into account.

To relate the two quantities $P_{\rm G}$ and $\tilde{n}$ in order to arrive at a mechanical equation of state, one needs to invert the fugacity expansion for the thermal particle density $\tilde{n}$. The ansatz is therefore a power expansion

$$\beta\lambda_{\rm T}^d P_{\rm G} = a_1\tilde{n} + a_2\tilde{n}^2 + a_3\tilde{n}^3 + \dots \tag{1.90}$$

of the pressure in terms of $\tilde{n}$. The quantity $\tilde{n}$ measures the number of particles in a box of the size of the thermal de Broglie wavelength $\lambda_{\rm T}$, which means the ansatz is an expansion around the regime of dilute gases far away from quantum degeneracy. Therefore I will here use the notions of low temperature, high density and small volume synonymously in the sense of the quantum degenerate regime.

The present case of the ideal Bose gas in a homogeneous potential (1.90) admits an exact analytical solution for the a_k [139] and can in principle be summed up to arbitrary order. The situation changes when interactions are taken into account, where the full fugacity expansions (1.89) usually are not known but instead have to be truncated after a few terms (usually two or three). The corresponding inversions, known as *virial expansions*, are then strongly bound in their validity to the regime of truly high temperatures. This incapability of grand canonical virial expansion is a serious issue on the practical level. While in principle they might be defined, it is merely impossible to perform the actual calculations that would go beyond the extreme classical regime. It has to be emphasized that this is not just the issue of calculating higher-order interaction contributions (corresponding to canonical partition functions of larger and larger number of particles) but already happens on the level of particle exchange symmetry. Only in the fully non-interacting case considered here an explicit solution to all (thermally scaled) virial coefficients a_k, accounting for quantum statistics apart from the ideal classical gas, can be given. This is the practical issue of fugacity inversion, virial expansions and consequent high temperature description inherent to the grand canonical description. But even if this problem is bypassed, which can be done in the non-interacting case, there remains the systematic problem of inappropriate number fluctuations that can lead to

significantly wrong physical descriptions. To underline this point, Fig. 1.9 shows the isothermal compressibility (1.80) of $N = 3$ non-interacting bosons in a one-dimensional harmonic oscillator. Not only the truncated virial expansion in the grand canonical formalism fails to describe the gas appropriately already at moderately low temperatures but also the full summation to infinite order spuriously predicts that the gas can be compressed infinitely easily at very low temperatures. This wrong result lies in the nature of the grand canonical formalism allowing particles to thermally exit the gas. At the same time, the smooth canonical description (1.87) is capable of describing the compressibility of the gas qualitatively correct for arbitrarily low temperatures despite neglection of discreteness in the single-particle spectrum. It also shows good quantitative quality in a very wide range. Only at extremely large particle densities deep in the quantum degenerate regime of Bose-Einstein condensation the lack of discreteness becomes quantitatively manifest.

1.1.7 Resumée

In the previous section we have seen how under the only approximation of neglecting the discreteness of spectra one can systematically find the canonical and microcanonical descriptions of non-interacting systems of a fixed number of indistinguishable particles in terms of the canonical partition function (1.47), (1.54) and (1.74) or the smooth many-body DOS (1.50), (1.55) and (1.75). From a methodical point of view this involved the partitioning of all particles into clusters that corresponded to the cycle decompositions of all permutations of N particles. These clusterings showed to be a valid concept because they allowed for a physical understanding and interpretation, a systematic organization and last but not least the explicit calculation of the possible contributions. Neglecting the discreteness thereby could be understood as focus on short-time dynamics or equivalently "high" temperatures and, since it corresponds to a semiclassical asymptotic description of the actual DOS, "high" energies. By application of the general calculus we have observed the emergence of universally expected many-body ground state energies and good agreement with spectral and thermodynamic properties in specific systems in a range of parameters (energy or temperature) that reached far beyond the original expectation. These observations make the general method of cluster expansions a valuable tool to describe gases of indistinguishable particles all the way down deep into the quantum degenerate regime. This value became explicit in the non-interacting case of ideal quantum gases, which sets the stage to incorporate the effect of mutual interparticle interactions on the same level of approximation, meaning by neglecting discreteness or equivalently looking at the short-time dynamics.

1.2 Interaction effects

1.2.1 Expansion in Ursell operators

The purpose now is to account for effects due to mutual interactions. First, I will specify which details about interactions are here intended to describe and which are regarded to be unnecessary in order to fit consistently into the framework established for non-interacting systems. After that I will review the general concept of expansions in Ursell operators, underlining the fact that it meets these requirements.

The general idea is to incorporate interaction effects in a non-perturbative way, avoiding any power series expansions in interaction coupling parameters, so that in principle also strong interactions can be described. The needed input in the formalism [see (1.27)] is the knowledge of the propagator of N particles, which is sufficient to know on the level of interacting but distinguishable particles, denoted by the propagation amplitude

$$K^{(N)}((\mathbf{q}_1^{\mathrm{f}},\ldots,\mathbf{q}_N^{\mathrm{f}}),(\mathbf{q}_1^{\mathrm{i}},\ldots,\mathbf{q}_N^{\mathrm{i}});t)=\langle\mathbf{q}_1^{\mathrm{f}},\ldots,\mathbf{q}_N^{\mathrm{f}}|\mathrm{e}^{-\frac{\mathrm{i}}{\hbar}\hat{H}t}|\mathbf{q}_1^{\mathrm{i}},\ldots,\mathbf{q}_N^{\mathrm{i}}\rangle \quad (1.91)$$

between N-body states of the (unsymmetrized) Hilbert space $\mathscr{H}_N$ (1.1) that are localized at initial and final positions $\mathbf{q}_1^{\mathrm{i}},\ldots,\mathbf{q}_N^{\mathrm{i}}$ and $\mathbf{q}_1^{\mathrm{f}},\ldots,\mathbf{q}_N^{\mathrm{f}}$, respectively. The flow of time evolution thereby is determined by a general interacting Hamiltonian of the form (1.3). Assuming the knowledge of the interacting distinguishable propagator (1.91) one could in principle go on and account for the particle exchange symmetry again by applying permutations to a version of (1.91) that is reduced to its short-time behavior.

There are two obvious problems with this direct approach. First, since interacting systems are in general very hard to describe analytically, the knowledge of exact N-body propagators represents the exceptionally small class of what feels like a zero-measure set in the vast sea of possible interacting non-relativistic quantum systems (simultaneously specified by the symmetry class $\pm$, the dimensionality D, the external confinement U_{ext} and the type of interactions U_{ij}). There are nevertheless solvable interacting systems, and I will specifically choose one later (see section 1.3) that allows not only for performing explicit calculations (see section 1.3.2), but will open the door to take the analytical information on the solvable model and transfer it to non-soluble systems in a consistent and meaningful way later (see section 1.4.2). Second, using a fully interacting propagator (1.91) directly would destroy the factorization of all particles into independent cluster contributions, which we learned to understand as a very valuable feature in the non-interacting case. It would be in strong contrast to the physical point of view, from which the cluster structure should also serve as the structure that organizes interaction effects. In the cluster zones particles are close to collision, so that the effect of interactions (assuming that they fall off with distance) becomes strongest there and might be negligible outside the cluster zones. This already hints in the right direction. A reasonable way of accounting for interactions here should follow in a way that uses the non-interacting case as a starting point, and the effect of interactions should then be introduced as a *modification* in terms of extra contributions. Furthermore, if one could, as a first dominant contribution, include the effect of interactions in a way that it affects only two-particles at a time it would directly fit to clusterings with clusters made out of maximally two particles. Then, in the embedded

higher-order cluster zones, where more particles or clusters are close to collision, one would have to account for additional interaction effects that go beyond the pairwise level. By now, the need of some hierarchical structure behind this splitting into different interaction contributions corresponding to particular cluster zones becomes immanent.

Indeed, the way of decomposing interaction effects in exactly the desired way has been considered previously by Ursell [150]. He developed the systematic way of expanding the propagator (1.91) of a distinguishable N-particle system in what is today known as the expansion in Ursell operators. To ease notation, I will define the latter in terms of time evolution operators rather than specifying a specific basis representation by using propagators. The time evolution operator of a single particle for a fixed time t is defined as

$$\hat{K}^{(1)} = \mathrm{e}^{-\frac{\mathrm{i}}{\hbar}\hat{H}^{(1)}t}\,. \tag{1.92}$$

In order to distinguish between the action of operators on different particle subspaces of $\mathscr{H}_N$ I specify the corresponding particle index i as an argument:

$$\hat{K}^{(1)}(i) = \mathrm{e}^{-\frac{\mathrm{i}}{\hbar}\hat{H}_i^{(1)}t} = \underbrace{\hat{\mathbb{1}}\otimes\cdots\otimes\hat{\mathbb{1}}}_{i-1}\otimes\underbrace{\mathrm{e}^{-\frac{\mathrm{i}}{\hbar}\hat{H}^{(1)}t}}_{i\text{-th position}}\otimes\underbrace{\hat{\mathbb{1}}\otimes\cdots\otimes\hat{\mathbb{1}}}_{N-i}\,, \tag{1.93}$$

where $\hat{\mathbb{1}}$ is the identity and $\hat{H}^{(1)}$ the single-particle Hamiltonian both acting on the single-particle Hilbert space $\mathscr{H}_1$. Similarly I denote with

$$K^{(n)}(i_1,\ldots,i_n) = \exp\left[-\frac{\mathrm{i}}{\hbar}\left(\sum_{i\in\{i_1,\ldots,i_n\}}\hat{H}_i^{(1)} + \sum_{\substack{i,j\in\{i_1,\ldots,i_n\}\\ i<j}}\hat{U}_{ij}\right)t\right], \tag{1.94}$$

the time evolution operator that only acts on n particles $i_1,\ldots,i_n$. Since the particles are all identical, the interaction potential is the same for all pairs of particles. I denote this fact by

$$\hat{U}_{ij} =: U_{\mathrm{int}}(\hat{\mathbf{q}}_i - \hat{\mathbf{q}}_j) \tag{1.95}$$

for a unique interaction potential function U_{int}.

The idea of Ursell operators then offers a quantum mechanical equivalent of classical cluster expansions [139] for the partition function of distinguishable particles on the level of operators.

The Ursell operators $\hat{U}^{(n)}$ (not to be confused with the potential U_{int} or $\hat{U}_{ij}$) are constructed in the following way. First the single-particle Ursell operator carries the full time-evolution of a single particle:

$$\hat{K}^{(1)} = \hat{U}^{(1)}\,. \tag{1.96}$$

The two-particle Ursell operator $\hat{U}^{(2)}$ is then implicitly defined by whatever has to be added to the factorizing non-interacting part:

$$\hat{K}^{(2)}(1,2) = \underbrace{\hat{U}^{(1)}(1)\hat{U}^{(1)}(2)}_{\text{non-interacting}} + \hat{U}^{(2)}(1,2)\,. \tag{1.97}$$

The corresponding decomposition of the three-body propagator

$$\begin{aligned}\hat{K}^{(3)}(1,2,3) = &\underbrace{\hat{U}^{(1)}(1)\hat{U}^{(1)}(2)\hat{U}^{(1)}(3)}_{\text{non-interacting}} \\ &+ \hat{U}^{(2)}(1,2)\hat{U}^{(1)}(3) + \hat{U}^{(2)}(1,3)\hat{U}^{(1)}(2) + \hat{U}^{(2)}(2,3)\hat{U}^{(1)}(1) \\ &+ \hat{U}^{(3)}(1,2,3)\end{aligned} \tag{1.98}$$

is similar and gives insight in the way a hierarchical structure emerges. First, the effect of interactions on all pairs of particles is taken into account using the two-body (or second order) Ursell operator $U^{(2)}$. Whatever remains to be added to complete the fully interacting three-body time evolution is defined as $U^{(3)}$. In the same way the implicit definition for arbitrary order n is

$$\hat{K}^{(n)}(1,\ldots,n) = \sum_{\mathfrak{I}\vdash\{1,\ldots,n\}} \prod_{I\in\mathfrak{I}} \hat{U}^{(|I|)}(i_1,\ldots,i_{|I|})\,, \tag{1.99}$$

where $\mathfrak{I}$ runs over all set partitions of the full index set $\{1,\ldots,n\}$, so that each element $I \in \mathfrak{I}$ is an index subset of size $|I| \leq n$ comprising indexes $\{i_1,\ldots,i_{|I|}\}$. The picture is that one gathers all possible clusterings of particles, starting from the trivial one of N independent single-particle clusters and then – step by step – moving downwards addressing higher-order clusterings by taking clusters that are independent in one layer and merging them in the subsequent layer. In each step one assigns to each cluster the modifications due to interactions one has to add on top of the interaction effects that are already included by considering all partitions of this cluster into smaller parts in previous steps.

In order to explicitly express the Ursell operators in terms of exact time-evolution operators one has to recursively invert (1.99). Demonstrating this explicitly for the second- and third-order Ursell operators gives

$$\begin{aligned}\hat{U}^{(2)}(1,2) &= \hat{K}^{(2)}(1,2) - \hat{K}^{(1)}(1)\hat{K}^{(1)}(2)\,, \\ \hat{U}^{(3)}(1,2,3) &= \hat{K}^{(3)}(1,2,3) \\ &\quad - \hat{K}^{(1)}(1)\hat{K}^{(2)}(2,3) - \hat{K}^{(1)}(2)\hat{K}^{(2)}(1,3) - \hat{K}^{(1)}(3)\hat{K}^{(2)}(1,2) \\ &\quad + 2\hat{K}^{(1)}(1)\hat{K}^{(1)}(2)\hat{K}^{(1)}(3)\,.\end{aligned} \tag{1.100}$$

For arbitrary n the unique inversion gives (see, *e.g.*, [151])

$$\hat{U}^{(n)}(1,\ldots,n) = \sum_{\mathfrak{I}\vdash\{1,\ldots,n\}} (-1)^{|\mathfrak{I}|-1}(|\mathfrak{I}|-1)! \prod_{I\in\mathfrak{I}} \hat{K}^{(|I|)}(i_1,\ldots,i_{|I|})\,, \tag{1.101}$$

where $|\mathfrak{I}|$ is the number of clusters the n particles are grouped into in a particular partition $\mathfrak{I}$.

I have here decided to separate particle exchange symmetry from the considerations on the hierarchical inclusion of interactions. This may seem circumstantial at first sight because of the similarity in the structure of clustering particles. One might think that it would be advantageous to merge both effects together in a single step by considering time evolution and Ursell operators in the symmetry projected subspaces of $\mathscr{H}_N$ directly. Indeed, this has been previously considered on the general methodical level [151] for systems of *large*

volume, while as far as I know, and especially in the recent literature [152–154], explicit applications are apparently rare – in particular beyond a pure two-body interaction effect [155, 156] – and have been considered only in the many-body scheme, based on grand canonical approaches focusing on virial-type of expansion that are inappropriate for the few-body sector. It has been argued [151] that in principle the combination of interaction and symmetry does not change the relations (1.99) at all, only that they are then relations between the symmetry-projected versions of the $\hat{K}^{(n)}$ and $\hat{U}^{(n)}$. While the combined approach might in general be appealing in its cleanness, I still prefer to separate the effects of interactions and symmetry. The reason is that one of the goals of this work is to find actual applications with explicit calculations. Then, naturally, to find higher-order Ursell operators $\hat{U}^{(n)}$ with $n \geq 3$ is a hard task (the three-body problem, that is impossible to perform analytically in most cases). The separation of symmetry and interaction effects offers then the possibility *to fully account for the quantum statistical aspects – valid down to the quantum degenerate regime, as shown in section 1.1.6 – while at the same time weak (or moderate) interactions can be considered only up to the pairwise level* by neglecting Ursell operators of order three or larger. This kind of truncation of interactions while keeping all symmetry effects is what will be referred to as the *first-order* QCE, which will be addressed in detail in section 1.2.3. Before developing the corresponding calculus I will briefly discuss the geometrical aspects of the expansion in Ursell operators when one represents time evolution in coordinate space.

1.2.2 The geometrical side of short-range interactions

The representation of Ursell operators in coordinate space gives the (hierarchically organized) interacting contributions to propagators

$$\Delta K^{(n)}(\mathbf{q}^{\mathrm{f}}, \mathbf{q}^{\mathrm{i}}; t) = \langle \mathbf{q}^{\mathrm{f}} | \hat{U}^{(n)}(1, \ldots, n) | \mathbf{q}^{\mathrm{i}} \rangle \tag{1.102}$$

for the initial and final n-body configurations $\mathbf{q}^{\mathrm{i}} = (\mathbf{q}^{\mathrm{i}}_1, \ldots, \mathbf{q}^{\mathrm{i}}_n)$ and $\mathbf{q}^{\mathrm{f}} = (\mathbf{q}^{\mathrm{f}}_1, \ldots, \mathbf{q}^{\mathrm{f}}_n)$, respectively. The explicit expression for the fully interacting distinguishable N-particle propagator is therefore

$$K^{(N)}(\mathbf{q}^{\mathrm{f}}, \mathbf{q}^{\mathrm{i}}; t) = \sum_{\mathfrak{I} \vdash \{1,\ldots,N\}} \prod_{I \in \mathfrak{I}} \Delta K^{(|I|)}(\mathbf{q}^{\mathrm{f}}_{i_1,\ldots,i_{|I|}}, \mathbf{q}^{\mathrm{i}}_{i_1,\ldots,i_{|I|}}; t)\,, \tag{1.103}$$

with the multi-index notation

$$\mathbf{q}_{i_1,\ldots,i_{|I|}} = (\mathbf{q}_{i_1}, \ldots, \mathbf{q}_{i_{|I|}}) \tag{1.104}$$

and the single-particle identification

$$\Delta K^{(1)} \equiv K^{(1)}\,, \tag{1.105}$$

that implies in particular

$$K^{(2)}(\mathbf{q}^{\mathrm{f}}, \mathbf{q}^{\mathrm{i}}; t) = K^{(1)}(\mathbf{q}^{\mathrm{f}}_1, \mathbf{q}^{\mathrm{i}}_1; t) K^{(1)}(\mathbf{q}^{\mathrm{f}}_2, \mathbf{q}^{\mathrm{i}}_2; t) + \Delta K^{(2)}(\mathbf{q}^{\mathrm{f}}, \mathbf{q}^{\mathrm{i}}; t)\,. \tag{1.106}$$

To keep an overview over possible contributions and to allow for easy physical interpretation of different terms the diagrammatic approach introduced

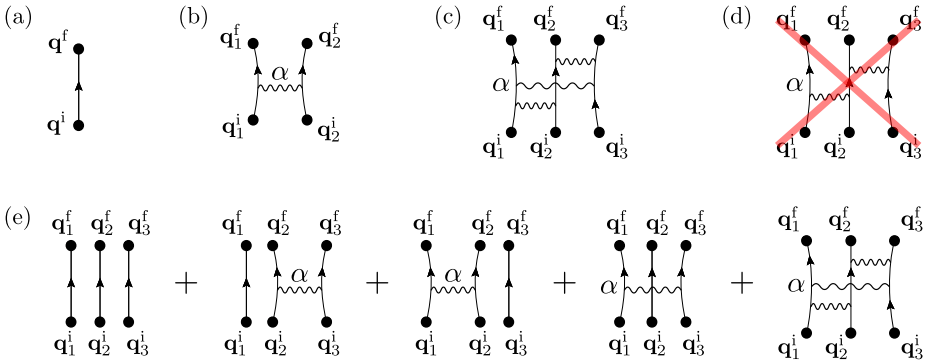

Fig. 1.10: Diagrams representing propagation amplitudes. (a) A single particle propagator $K^{(1)}(\mathbf{q}^{\mathrm{f}}, \mathbf{q}^{\mathrm{i}}; t)$ exactly the same as in Fig. 1.6. (b) The interacting part $\Delta K^{(2)}(\mathbf{q}^{\mathrm{f}}, \mathbf{q}^{\mathrm{i}}; t)$ of the distinguishable two-body propagator. (c) The three-body interaction effect of a third-order Ursell operator $U^{(3)}$ as propagation amplitude $\Delta K^{(3)}$. (d) Example of an invalid diagram. It does not correspond to a partition $\mathfrak{I}$ into Ursell contributions (see (1.99)) since particle 2 in the middle would participate in two different second-order terms, which is not possible. (e) The diagrammatic representation of the fully interacting three-body propagator corresponding to the time evolution operator (1.98) as the finite hierarchical expansion in the different interaction contributions.

in section 1.1.4 (see Fig. 1.6) has to be extended. Each (open) propagation amplitude (1.102) gets associated with a diagram comprising (terminal) points that represent initial and final positions of single particles, each of which get assigned the coordinates as they are arguments of the diagram. They are connected through solid lines connecting points corresponding to the same particle index. Assigning an arrow to each line distinguishes the direction of propagation, or in other words, tells initial and final position apart. The order of Ursell operators is then visualized by curly lines that mutually connect the propagation lines of all particles evolving under a specific Ursell operator. The curly lines may additionally be marked with a variable representing a coupling parameter (I will typically choose α as the symbol). Disconnected parts of a diagram are then multiplied to give the value the full separable diagram as the product of irreducible parts. A selection of diagrams clarifying this definition is given in Fig. 1.10. Emphasis should be made here that, despite the similarity in appearance, the diagrammatics introduced here differ from Feynman diagrams in a very important point. The interaction contributions in the QCE are *not* just perturbative contributions in the sense of contributions within a certain power of a coupling parameter α. As a consequence, they are always given as *finite* expansions whereas perturbative expansions are infinite series of diagrams of unboundedly increasing order (and therefore increasing complexity and combinatorial number). The case that demonstrates this fact in the most obvious way is the propagation of two particles, where a single interaction contribution (the diagram in Fig. 1.10b) gives the full amplitude (including all orders of α).

The expansion in Ursell operators becomes especially useful when the interparticle interaction is of a short-range type in the sense that particles that are well separated behave like independent particles. Similarly, going one step further, two groups of particles that are well separated will asymptotically behave as independent clusters that only locally are affected by mutual interactions

within each group. Furthermore, the propagation of individual particles over long distances is suppressed for short times. This should not be understood as a strict statement since, *e.g.*, the propagation amplitude (1.16) of a single free particle is constant in modulus all over space at each point in time. But the statement becomes true when initial or final coordinates get smeared either by convolution with some wave packet envelope function or, more relevant here, by integration over all of the coordinate space. The reason is that the further the distance over which the particles propagate, the faster they oscillate in the complex phase. The consequence is that the value of a contribution corresponding to a specific partition $\mathfrak{I}$ in (1.103) into interaction effects (1.102) (represented by diagrams, examples of which are shown in Fig. 1.10) is peaked around the region in coordinate space where all particles corresponding to connected parts of diagrams are close to each other. This is exactly what defines the cluster zones that emerged in the same sense but in the context of cyclic propagations due to exchange permutations. Naturally the notion of *clusters* gets extended by this observation. Each irreducible part of a diagram will be called a cluster. This does not necessarily have to be by virtue of interactions. Once we introduce again permutations in the "diagonal" part of the propagator (setting $\mathbf{q}^{\mathrm{f}} = \mathbf{q}^{\mathrm{i}}$) the final coordinates become a permutation of the initial ones

$$\mathbf{q}^{\mathrm{f}} \mapsto P\mathbf{q}^{\mathrm{i}} = (\mathbf{q}^{\mathrm{i}}_{P(1)}, \ldots, \mathbf{q}^{\mathrm{i}}_{P(N)})\,. \tag{1.107}$$

Then individual particles within an (irreducible) cluster can be either connected by interaction effects (curly lines in diagrams) or exchange propagation (linking final coordinates of particles to the initial coordinates of other particles).

The separation of interaction effects and symmetry effects that are hierarchically organized in a similar way has also been considered previously on the methodical level [156] in the thermodynamic limit of large systems $N, V_D \to \infty$ with $N/V_D = \text{const}$. Nevertheless, here, a connection is drawn that seems to be unobserved so far and which is crucial in order to make the method applicable by allowing for explicit calculations in the few-body regime of small numbers of particles N. In my opinion this connection offers a special value, convinced that one major power of the method lies in the description of few-body systems where the superiority to more traditional descriptions like mean-field plus quasi-particle pictures becomes most significant and versatile. What enters the stage again now is the focus on average (universal) properties of interacting systems in the sense of neglecting the discreteness and the exact location of the total-energy levels, and rather considering smooth many-body DOS. As was extensively argued in the previous section 1.1, this corresponds to short-times in the dynamical sense which can also be understood as effective large extent in the system size V_D. This means that instead of taking exact interacting propagators $K^{(N)}$ of confined systems one can stick to their analogues that are infinitely extended in space which are usually easier to obtain analytically. This is true on the non-interacting level and especially extends to interacting systems. The very heart of this chapter is based on the observation that one can take the information on interacting propagators in infinitely extended systems and use it in systems of *arbitrarily small size*, as long as one is interested in properties related to mean DOS. The finite volume V_D then enters in calculus by replacing the divergent coordinate integrals corresponding to the invariance of whole clusters *w.r.t.* simultaneous translations. Alternatively, one can use the infinite-system propagators to discuss thermodynamics down to temperatures

where the thermal de Broglie wavelength becomes comparable to the system size $\lambda_{\mathrm{T}}^D \sim V_D$.

1.2.3 The canonical QCE

General calculus, organization in cluster zones and diagrammatics

The goal is to calculate traces of symmetrized propagators (1.25) used to finally yield the many-body DOS or canonical partition function by virtue of (1.27) or (1.29), respectively. Thus we focus on the trace

$$\int_{\Omega^N} \mathrm{d}^{ND}q\; K_{\pm}^{(N)}(\mathbf{q},\mathbf{q};t) = \frac{1}{N!}\sum_{P\in S_N}(\pm 1)^P \int \mathrm{d}^{ND}q\; K^{(N)}(P\mathbf{q},\mathbf{q};t)\,. \quad (1.108)$$

Using the expansion (1.103) in Ursell contributions, that expression reads

$$\begin{aligned}\int_{\Omega^N} \mathrm{d}^{ND}q\; K_{\pm}^{(N)}(\mathbf{q},\mathbf{q};t) &= \frac{1}{N!}\sum_{P\in S_N}(\pm 1)^P \sum_{\mathfrak{I}\vdash\{1,\ldots,N\}} \int_{\Omega^N} \mathrm{d}^{ND}q\; \Delta K^{\mathfrak{I}}(P(\mathbf{q}),\mathbf{q};t)\,,\\ \Delta K^{\mathfrak{I}}(P(\mathbf{q}),\mathbf{q};t) &= \prod_{I\in\mathfrak{I}} \Delta K^{(|I|)}\Big(\mathbf{q}_{P(i_1),\ldots,P(i_{|I|})},\mathbf{q}_{i_1,\ldots,i_{|I|}};t\Big)\,,\end{aligned} \quad (1.109)$$

using the multi-index notation (1.104). In the trace (1.109) every particle index appears exactly twice, once as an initial point and once as a final point. In the diagrammatic approach this means that every point representing a particle coordinate $\mathbf{q}_i$ has exactly one propagation-line ending at it and one starting at it. The corresponding diagrams are therefore only closed diagrams in the sense that there are no terminal points. In addition all the particle coordinates have to be integrated over the allowed domain Ω. Therefore I set the diagrammatic rule that the coordinates of all non-terminal points have to be integrated and hence do not need labels in the diagram because they are just integration variables.

As mentioned in the previous subsection, the combined grouping of particles due to symmetry (see section 1.1.4) and interaction effects leads to the extended notion of (irreducible) clusters, within which all particles are connected by either one or the other effect, or both. A selection of valid closed irreducible cluster diagrams is given in Fig. 1.11. Before writing formal expressions I will briefly review what is the mechanism behind this clustering and the resulting consequences.

On the level of symmetry, the clustering happens by linking two particles i and j together if one gets transfered to the other by virtue of a particular exchange permutation P, expressed as $j = P(i)$. Since we consider the "diagonal part" $\mathbf{q}^{\mathrm{f}} = \mathbf{q}^{\mathrm{i}} = \mathbf{q}$ this link implies that particle i propagates from $\mathbf{q}_i$ to the initial location $\mathbf{q}_j = \mathbf{q}_{P(i)}$ of the other particle. The contribution coming from a propagation where the single-particle position $\mathbf{q}_i$ is transfered to $\mathbf{q}_j$ is concentrated on the region where the two positions are close to each other and can be neglected when moving the two positions apart. This circumstance is surely a true fact for independent (non-interacting) particles and is a natural

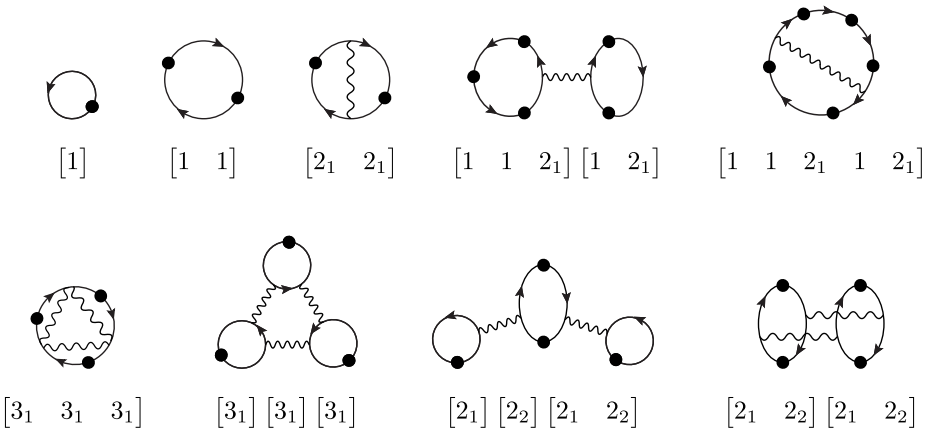

Fig. 1.11: Selection of closed irreducible cluster diagrams that contribute to the trace (1.109) of of the fully symmetrized and interacting propagator. The value of each diagram is given by the rules defined for open amplitudes (see section 1.2.2 and Fig. 1.10). All points are non-terminal and (up to an arbitrary single one) have to be integrated over full space $\mathbb{R}^D$. The integral of the remaining one over the domain Ω is performed virtually by adding a factor V_D due to translational invariance. Below each diagram is a representing symbolic cluster structure (A.236) defined in appendix A.

assumption to all particles participating in a Ursell contribution individually[7].

On the level of interactions the clustering is a bit more obvious and has already been discussed in detail in section 1.2.2. The effect of (short-range) interactions on particles is assumed to become negligible when the particles are separated far apart.

The main consequence of clustering is that the distances between constituents can be integrated (as relative coordinates) over full space $\mathbb{R}^D$, ignoring any finiteness of the full domain Ω. This is the exact analogue to the calculus behind the single-particle surface correction (1.19) in the Weyl expansion where the integration of the coordinate perpendicular to the boundary $\partial\Omega$ gets extended to infinity. Also there, increasingly fast phase oscillations of the propagation amplitude with propagation distance induced fast convergence of the perpendicular integral with the upper limit, so that the latter could be taken as infinity. Without external potentials (to be added later in section 1.4.2) the homogeneity of space then makes the propagation amplitude of a cluster invariant to simultaneous translation of all cluster particles, which formally would lead to a divergent spatial integral if the integration domains of all coordinate would be extended to full space. Instead, only relative coordinates should be extended whereas a

[7]This assumption has to be distinguished from the assumption that the effect of (short-range) interactions vanishes between particles that are separated far apart. As an illustration, consider the interaction effect on two particles that are close to each other initially and also finally, meaning there are quantum paths where both are close to each other all the time, making interaction non-negligible. But still, if their final positions are distant from the initial ones, the propagation amplitude from the interaction effect is considered to oscillate increasingly fast with the separation, as is the case with non-interacting propagations. The physical interpretation of this assumption is that switching on interactions does not enable localized many-body wave packets to immediately spread over large distances. Instead, the effective spread of wave packets is assumed to be bounded by the time of flight.

center-of-mass coordinate is kept inside the finite domain Ω. Since the integrand, which is the propagation amplitude, is independent of the center-of-mass coordinate, this one integral simply gives the full measure V_D. Equivalently, in order to ease notation, one can treat one of the particle coordinates $\mathbf{q}_i$ directly as the invariant one, yielding the volume V_D and perform the integrals of all other particle coordinates over full space $\mathbb{R}^D$, avoiding the introduction of center-of-mass and relative coordinates which is cumbersome for more than two particles. When it comes to the consistent inclusion of smooth external potentials (see section 1.4.2) the same simplification will turn out to be possible.

Similar to the non-interacting case (1.45) one can formally organize the partition function of N identical particles in partitions into clusters

$$Z_{\pm}^{(N)}(\beta) = \frac{1}{N!} \sum_{\mathfrak{N} \vdash N} (\pm 1)^{N-|\mathfrak{N}|} c_{\mathfrak{N}}^{(N)} \prod_{n \in \mathfrak{N}} \mathcal{A}_n(-\mathrm{i}\hbar\beta)\,, \tag{1.110}$$

where now the amplitudes are given as symmetry-weighted sums

$$\mathcal{A}_n(t) = \sum_{\substack{\mathfrak{C} \\ |\mathfrak{C}|=n}} (\pm 1)^{l(\mathfrak{C})-1} M_{\mathfrak{C}} \mathcal{A}_{\mathfrak{C}}(t) \tag{1.111}$$

over all irreducible cluster diagrams $\mathcal{A}_{\mathfrak{C}}(t)$ that are indexed by their internal cluster structure $\mathfrak{C}$. The dependence on the symmetry class $\pm$ has been dropped from notation of the sums $\mathcal{A}_n$ for simplicity. The internal cluster structure $\mathfrak{C}$ specifies how the particles within a diagram are connected by symmetry and interaction. Two equivalent cluster structures correspond to the same unique diagram. The sum runs over such equivalence classes of (irreducible) cluster structures $\mathfrak{C}$ for clusters of size n and the $M_{\mathfrak{C}}$ are purely combinatorial factors that account for multiplicity of equivalent clusters in the sum. The number of symmetry-related cycles $l(\mathfrak{C})$ within a cluster determines its symmetry weight.

A formalization of cluster structures by symbolic indexation is given in appendix A. It allows to organize all possible cluster structures, the explicit calculation of multiplicities $M_{\mathfrak{C}}$ (A.268) and the proper formal definition of the values $\mathcal{A}_{\mathfrak{C}}$ (A.255) of corresponding diagrams. As an important example, the complete set of possible irreducible three-clusters including their symbolic cluster structures and the related combinatoric factors is shown in Fig. 1.12.

1.2.4 First-order QCE

Definition and general significance

Since one basic assumption are genuine two-body interactions (as contrasted to interaction potentials that are non-separable into pairs of particles they involve), a natural supposition is that the influence of higher orders of interaction effects gets increasingly suppressed if the coupling strength is not too large. This means, in a first attempt, consider vanishing interaction effects $\Delta K^{(u)} \approx 0$ in (1.109) [and (A.255) in appendix A] of higher order $u \geq 3$ which will leave a pairwise approximation to the full cluster expansion. A further possible truncation of the expansion in clusters is to assume that the interaction affects only two particles at a time, meaning, here we only consider (besides the non-interacting

$\mathfrak{C}$	$\mathcal{A}_{\mathfrak{C}}$	$\#_P$	$\#_{\mathfrak{I}}^{(P)}$	$\#_{P,\mathfrak{I}}$	$M_{\mathfrak{C}}$
$\left[1\ \ 1\ \ 1\right]$		2	1	2	1
$\left[1\ \ 2_1\right]\left[2_1\right]$	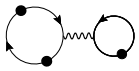	3	2	6	3
$\left[1\ \ 2_1\ \ 2_1\right]$		2	3	6	3
$\left[3_1\right]\left[3_1\right]\left[3_1\right]$	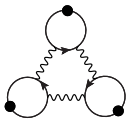	1	1	1	$\frac{1}{2}$
$\left[3_1\right]\left[3_1\ \ 3_1\right]$	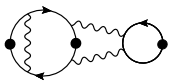	3	1	3	$\frac{3}{2}$
$\left[3_1\ \ 3_1\ \ 3_1\right]$		2	1	2	1

Fig. 1.12: The six possible irreducible clusters of size three. Each is associated with a symbolic cluster structure $\mathfrak{C}$, the corresponding diagram (representing the amplitude $\mathcal{A}_{\mathfrak{C}}$), and its combinatorial factor $M_{\mathfrak{C}}$. By virtue of the symbolic indexation the latter can be calculated in terms of "essential relabelings" $\#_{P,\mathfrak{I}}$, which are composed of relabelings $\#_P$ that yield distinct permutations P and the relabelings $\#_{\mathfrak{I}}^{(P)}$ that give distinct interaction partitions $\mathfrak{I}$ under a constrained permutation. See appendix A for details on symbolic cluster structures and the involved combinatorics.

part) interaction partitions

$$\mathfrak{I} = \big\{\{k,l\}\big\} \cup \bigcup_{i\neq k,l} \big\{\{i\}\big\}\,, \quad 1 \leq k,l \leq N, k \neq l\,, \tag{1.112}$$

so that only one second-order term $\Delta K^{(2)}$ occurs in (1.109) or (A.255). Because a separate consideration of symmetry and interaction effects in the whole approach was chosen, we are able to allow for all symmetry-related cycle structures despite the interaction truncation (1.112). The approximation specified in this way is probably the strongest non-trivial direct simplification within the method that still includes direct interaction effects. Therefore this approximation is what will be referred to as the QCE of *first order*. We will see that it has still a rich structure and demands non-trivial calculus in application (see section 1.3.2), and gives accurate results in certain regimes. Furthermore, because of the inclusion of all symmetry effects it is in principle still capable to include non-trivial physics related to interactions down to ultra-low temperatures or energies, because quantum degeneracy is well described by the cycle structures in the non-interacting case (see section 1.1.4 and section 1.1.6). This truncation naturally restricts the range of validity to a weakly interacting regime but still in a non-perturbative way, so that already in first order the range of well-described interaction strengths α is superior to a truncated perburbative expansion in powers of α, as it contains information about interaction effects in all orders $\mathcal{O}(\alpha^n), n \in \mathbb{N}_0$. Moreover, there are methodical extensions based on the first-order truncation that will for example allow for applications to ultra-strong interactions (see section 1.4.1) and even arbitrary interaction strengths (see section 1.5.2) to mention two.

Formal structure

Besides the non-interacting clusters, which are given as single-cycle structures $\mathfrak{C} = \big[1 \;\; \cdots \;\; 1\big]$ (see appendix A for the notation) with $\mathcal{A}_\mathfrak{C}$ given by (1.41) or (1.42) [or (1.72) in the case of homogeneous external potentials] the clusters in first order come in two classes. The interaction effect may link together two particles that are involved in either the same or in two different cycles of P, referred to as *intra-* and *inter-cycle* clusters, respectively. They are specified by two numbers n_1 and n_2 and are symbolically given by (see appendix A)

$$\mathfrak{C}^{\text{intra}}_{n_1,n_2} = \big[\underbrace{1 \;\; \cdots \;\; 1 \;\; 2_1}_{n_1} \;\; \underbrace{1 \;\; \cdots \;\; 1 \;\; 2_1}_{n_2}\big]\,, \tag{1.113}$$

$$\mathfrak{C}^{\text{inter}}_{n_1,n_2} = \big[\underbrace{1 \;\; \cdots \;\; 1 \;\; 2_1}_{n_1}\big] \big[\underbrace{1 \;\; \cdots \;\; 1 \;\; 2_1}_{n_2}\big]\,. \tag{1.114}$$

The corresponding diagrams are shown in Fig. 1.13. Their combinatorial factors

$$M_{\mathfrak{C}^{\text{intra/inter}}_{n_1,n_2}} = \frac{n_1+n_2}{1+\delta_{n_1 n_2}} \tag{1.115}$$

are the same and both cases exhibit the same cluster equivalence *w.r.t.* interchanging n_1 and n_2:

$$\mathfrak{C}^{\text{intra/inter}}_{n_1,n_2} = \mathfrak{C}^{\text{intra/inter}}_{n_2,n_1}\,. \tag{1.116}$$

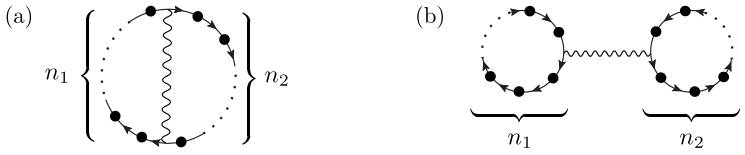

Fig. 1.13: The two classes of interacting cluster diagrams in the QCE of first order: (a) The intra-cycle cluster where the interaction effect happens between two particles within the same cycle. (b) The inter-cycle structure where the interaction effect between two particles links two distinct cycles together to a single large cluster.

As an abbreviation for the corresponding contributions I write

$$\mathcal{A}^{\text{intra/inter}}_{n_1,n_2} := \mathcal{A}_{\mathfrak{C}^{\text{intra/inter}}_{n_1,n_2}} . \tag{1.117}$$

Altogether, the sum of all interacting clusters of size n in first-order QCE is

$$\Delta\mathcal{A}_n = \sum_{\substack{n_1\leq n_2\\ n_1+n_2=n}} \frac{n}{1+\delta_{n_1 n_2}} \left(\mathcal{A}^{\text{intra}}_{n_1,n_2} \pm \mathcal{A}^{\text{inter}}_{n_1,n_2}\right) = \frac{n}{2} \sum_{n_1=1}^{n-1} \left(\mathcal{A}^{\text{intra}}_{n_1,n-n_1} \pm \mathcal{A}^{\text{inter}}_{n_1,n-n_1}\right) . \tag{1.118}$$

Basic combinatorics combining (1.118) and (1.110) show that the non-interacting parts of all clusterings sum up to non-interacting partition functions (1.45) of correspondingly smaller number of particles. This way, the first order QCE correction to the canonical partition function can be written

$$\Delta Z^{(N)}_{\pm} = \sum_{n=2}^{N} (\pm 1)^n Z^{(N-n)}_{0,\pm} \sum_{n_1=1}^{n-1} \frac{\mathcal{A}^{\text{inter}}_{n_1,n-n_1} \pm \mathcal{A}^{\text{intra}}_{n_1,n-n_1}}{2} , \tag{1.119}$$

where I omitted the explicit dependence on β and $t = -\mathrm{i}\hbar\beta$. Eq. (1.119) recursively generates the first order correction to $Z^{(N)}_{\pm}$ depending on non-interacting partition functions of smaller particle numbers and the sum of irreducible diagrams of all sizes $n = 2, \ldots, N$. This can be understood as a special case of the general recursive formula in terms of irreducible diagrams in the full QCE without truncation where in first order (1.119) the interaction effect only enters in the irreducible diagrams that are split off from the partitions into clusters, while the partition functions of smaller numbers of particles are taken as the non-interacting ones. Additionally, the interaction effect to each irreducible cluster is just on the level of one pairwise Ursell contribution $\Delta K^{(2)}$.

1.2.5 Generic dimensional scaling in the QCE

Before we turn to the application of the first-order QCE to a specific model a general useful feature of the method that does not depend on the specific form of the interactions[8]is the subject of the current section. A detailed dimensional analysis shows that besides the linear scaling with the available volume V_D further natural universal scaling properties of cluster diagrams $\mathcal{A}_{\mathfrak{C}}$ are inevitable.

[8]As long as they are short-ranged in the sense that interaction effects $\Delta K^{(n)}$ can be integrated up to infinite distance between particles due to fast convergence instead of restriction to finite domains.

Generic scaling of spatial potentials and propagators

This universal scaling, discussed in detail in [157], originates in a generic scaling inherent to any non-relativistic system described by a Hamiltonian of the form

$$\hat{H} = \hat{T} + U(\hat{\mathbf{q}}) \tag{1.120}$$

with an arbitrary (total) number of spatial degrees of freedom D_{tot}, where the kinetic term defined by its operational action

$$\langle \mathbf{q}|\hat{T} = -\sum_{i=1}^{d} \frac{\hbar^2}{2m_i} \nabla_{q,i}^2 \langle \mathbf{q}| \tag{1.121}$$

may involve different masses m_i for different spatial directions.

Without specifying the exact form of the potential U in the Hamiltonian (1.120) or correspondingly the interaction potential between particles, the only demand is that the function U depends on just one coupling parameter that has a physical dimension other than unity. It may further depend on Planck's constant $\hbar$ and a mass m but besides that only dimensionless parameters $\boldsymbol{\lambda}$ are presumed to be involved. In case more than just one mass are entering the Hamiltonian (*e.g.*, for different particle species or anisotropic mass tensors) the dependence on various masses m_i can be substituted by a dependence on one reference mass (then simply called m) and a number of dimensionless parameters $\boldsymbol{\lambda}$ representing the ratios between the actually participating masses and m. A further assumption is that the coupling parameter can be given in the form of a characteristic energy denoted α. In total, the generic assumption is that one can write

$$U(\mathbf{q}) = U(\alpha, \hbar, m, \boldsymbol{\lambda}; \mathbf{q})\,, \tag{1.122}$$

with units $[\alpha] = [E]$, $[\lambda_j] = 1$, $[q_i] = [x]$, and $[U(\mathbf{q})] = [E]$. Exceptions of (1.122) are potentials that are homogeneous functions of $\mathbf{q}$ of degree -2, namely the (anisotropic) $\sim 1/q^2$ potential, Dirac-Delta potentials $\sim \delta^{(2)}\Big(\sum_{ij} a_{ij} \binom{q_i}{q_j}\Big)$ involving two dimensions, linear combinations of the mentioned, and maybe other more exotic constructions. The reason for this exception is that those potentials intrinsically are given by dimensionless couplings that cannot be transformed into energy-like couplings α by means of the available constants. At the same time this means that such potentials yield scale-invariant Hamiltonians which need to be regularized to give them physical meaning. To achieve that, usually the regularized forms are equipped with a physical parameter of the system that is to be modeled [158, 159]. This parameter must not be dimensionless and is often given as a bound state energy or a scattering length. Therefore also those exceptional cases are in their final regularized physically meaningful versions again admitting the form (1.122). Under this generic assumption a general dimensional analysis (see supplemental material of [157]) shows that the potential can be written in the form

$$U(\alpha, \hbar, m, \boldsymbol{\lambda}; \mathbf{q}) = \alpha\, u\Big(\boldsymbol{\lambda}, \sqrt{4\pi\beta\alpha}\mathbf{x}\Big)\,, \tag{1.123}$$

where u is the potential scaled to a dimensionless quantity that is itself a function of dimensionless arguments only. They involve the inverse temperature

$\beta = 1/k_\mathrm{B}T$ that has been introduced to scale the positions $\mathbf{q}$ to dimensionless coordinates

$$\mathbf{x} := \frac{1}{\lambda_\mathrm{T}}\mathbf{q} \tag{1.124}$$

by means of the thermal de Broglie wavelength

$$\lambda_\mathrm{T} = \left(\frac{m}{2\pi\hbar^2\beta}\right)^{-\frac{1}{2}} . \tag{1.125}$$

A thorough analysis of the implications of the generic scaling on the Schrödinger equation and hence quantum dynamics of the system (see supplemental material of [157]) allows one to write a generic scaling property of propagation amplitudes. For the discussion on the universal scaling consider the evolution of quantum states in the system described by (1.120) in imaginary time $t = -\mathrm{i}\hbar\beta$. The corresponding (non-unitary) evolution operator for a fixed *relaxation "time"* β is $\mathrm{e}^{-\beta\hat{H}}$. As abbreviation I identify the notations

$$K(\mathbf{q}^\mathrm{f}, \mathbf{q}^\mathrm{i}; \beta) \equiv K(\mathbf{q}^\mathrm{f}, \mathbf{q}^\mathrm{i}; t = -\mathrm{i}\hbar\beta) \tag{1.126}$$

for any propagation amplitude K. The consequence of the dimensional scaling is that the full propagator in imaginary time β as a function of the additional parameter α can be written in the form

$$K_\alpha(\mathbf{q}^\mathrm{f}, \mathbf{q}^\mathrm{i}; \beta) = \lambda_\mathrm{T}^{-D_\mathrm{tot}} \tilde{k}(\lambda_\mathrm{T}^{-1}\mathbf{q}^\mathrm{i}, \lambda_\mathrm{T}^{-1}\mathbf{q}^\mathrm{f}; \beta\alpha) . \tag{1.127}$$

For simplicity I dropped the dependence on dimensionless parameters $\boldsymbol{\lambda}$ in $\tilde{k}$ which can always exist implicitly. The significant property of (1.127) is that the scaled propagator $\tilde{k}$ only depends on the interaction parameter via the product $\beta\alpha$.

In the following section, the scaling property (1.127) will be used to derive universal scaling properties for QCE contributions.

Universal scaling properties of QCE

Since (1.127) is a general property regardless of the dimension D_tot and explicit form of the potential U, it holds also for the propagator of systems of N distinguishable particles in D spatial dimensions. The total effective dimensionality is then $D_\mathrm{tot} = ND$ and one identifies $U(\mathbf{q}) = \sum_{ij} U_{ij}(\mathbf{q}_i - \mathbf{q}_j)$ as an interaction potential relating different particles. Remarkably this holds also if the interaction is applied only on a subset of particles. Because of that, also the linear combination of two propagators where the interaction links different subsets of particles in the two cases are still subject to the general scaling (1.127) with $\beta\alpha$. The simplest illustration of this statement is the propagator of a two-particle system in the non-interacting and interacting case, respectively. Both obey the scaling and hence their difference, which is nothing else than the Ursell contribution $\Delta K^{(2)}$, does as well. In general, by virtue of (1.101), this enables us to write Ursell operators of arbitrary order n as

$$\Delta K_\alpha^{(n)}(\mathbf{q}^\mathrm{f}, \mathbf{q}^\mathrm{i}; \beta) = \lambda_\mathrm{T}^{-nD} \Delta\tilde{k}^{(n)}(\mathbf{x}^\mathrm{f}, \mathbf{x}^\mathrm{i}; \beta\alpha) . \tag{1.128}$$

Moving to the indistinguishable case, an arbitrary cluster contribution $\mathfrak{C}$ involves a product of Ursell operators and the final configurations are given as a

permutation of the initial configuration $\mathbf{q}^{\mathrm{f}} = P(\mathbf{q}^{\mathrm{i}})$. This means the integrand for an arbitrary cluster of size n is given by

$$\Delta K_\alpha^{\mathfrak{I}}(P(\mathbf{q}), \mathbf{q}; \beta) = \lambda_{\mathrm{T}}^{-nD} \Delta \tilde{k}^{\mathfrak{I}}(P(\mathbf{x}), \mathbf{x}; \beta\alpha)\,, \tag{1.129}$$

where $\Delta K^{\mathfrak{I}}$ denotes a product of Ursell operators (1.128) corresponding to an interaction partition $\mathfrak{I}$ (restricted to the n particles of the cluster) [see (1.109)] and $\Delta \tilde{k}^{\mathfrak{I}}$ denotes its scaled version. The details of the relation between cluster structures, permutations and interaction partitions are extensively addressed in section 1.2.3 and are of minor importance for the current discussion. The contribution from the n-cluster is then the amplitude

$$\mathcal{A}_{\mathfrak{C}}(\alpha, \beta) = \int_\Omega \mathrm{d}^D q_1 \ldots \int_\Omega \mathrm{d}^D q_n \Delta K_\alpha^{\mathfrak{I}}(P(\mathbf{q}), \mathbf{q}; \beta)\,. \tag{1.130}$$

Since we talk about a single cluster, there is only one invariant direction in $\mathbf{q}$-space for the integrand, which corresponds to the center-of-mass motion. Otherwise the integral (1.130) would be separable into distinct cluster-contributions per definition.

Focusing on the short-time dynamics and neglecting physical boundary effects, the integration domains are extended to infinity for all particles but one (here chosen as $\mathbf{q}_1$). The integrand is invariant *w.r.t.* $\mathbf{q}_1$ which yields the volume V_D of the domain Ω. A scaling of integration variables to the dimensionless ones (1.124) yields for the amplitude (1.130)

$$\mathcal{A}_{\mathfrak{C}}(\alpha, \beta) = \frac{V_D}{\lambda_{\mathrm{T}}^D} \underbrace{\int \mathrm{d}^D x_2 \ldots \mathrm{d}^D x_n\; \Delta \tilde{k}^{\mathfrak{I}}\big(P(\mathbf{0}, \mathbf{x}_2, \ldots, \mathbf{x}_n), (\mathbf{0}, \mathbf{x}_2, \ldots, \mathbf{x}_n); \beta\alpha\big)}_{=: \mathcal{I}(\beta\alpha, P, \mathfrak{I})}\,, \tag{1.131}$$

where the integral $\mathcal{I}$ is a function of $\beta\alpha$ only and the purely combinatorial structural quantities P and $\mathfrak{I}$. As discussed in detail in section 1.2.3, the pair $(P, \mathfrak{I})$ comes in equivalence classes of internal cluster structures $\mathfrak{C}$ that yield equivalent amplitudes. By means of this identification we are free to define

$$a_{\mathfrak{C}}(\beta\alpha) =: n^{D/2} \mathcal{I}(\beta\alpha, P, \mathfrak{I})\,, \tag{1.132}$$

so that we arrive at the universal scaling of generic cluster amplitudes

$$\mathcal{A}_{\mathfrak{C}}(\alpha, \beta) = n^{-D/2} \frac{V_D}{\lambda_{\mathrm{T}}^D} a_{\mathfrak{C}}(\beta\alpha)\,, \tag{1.133}$$

with some dimensionless function a that characterizes the internal effect of interaction in the cluster structure $\mathfrak{C}$. In contrast, the prefactor characterizes the cluster as a unified entity as in the non-interacting case. Correspondingly one could interpret the functions $a_{\mathfrak{C}}(\beta\alpha)$ as factors that alter how loosely or tightly clusters are bound compared to the non-interacting ones in the sense of measuring the time-dependence of their spreading or equivalently their local damping in density as $\rho(\mathbf{q}, t) \sim |\mathcal{A}_{\mathfrak{C}}(\alpha, \beta = \mathrm{i}t/\hbar)|^2 / V_D^2$.

From these considerations I feel free to call the functions $a_{\mathfrak{C}}(\beta\alpha)$ *cluster damping factors*. The generic scaling provides exact knowledge of how the spreading or density decay gets speeded up or slowed down with the coupling

strength. The spreading receives a speed-up that increases linearly with the coupling parameter α. Depending on whether the strength of interaction increases or decreases with α, one has an acceleration or deceleration of cluster damping due to the interaction. A sign inversion in α might even switch between a spreading and collapsing behavior.

Note that these considerations on damping and spreading focus on particle clusters as combinatorial objects that contribute to the dynamics of the whole cloud of N particles in a combined and therefore rather hidden way. Therefore it is hard to say, in general, whether the considerations on dynamics of clusters can be transferred to a physical picture of quasiparticle-like structures and the physics of the system as a whole.

Using the scaling for all cluster structures directly leads to a corresponding scaling

$$Z_{\pm}^{(N)}(\beta) = \sum_{l=1}^{N} [z_l + \Delta z_l(\beta\alpha)] \left(\frac{V_D}{\lambda_T^D}\right)^l . \tag{1.134}$$

of the interacting partition function in QCE to arbitrary order, where the effect $\Delta z_l(\beta\alpha)$ of interaction on the coefficients is determined by the cluster damping factors $a_{\mathfrak{C}}(\beta\alpha)$ of all cluster structures. The full explicit relation reads

$$\Delta z_l(\beta\alpha) = \frac{(\pm 1)^{N-l}}{l!} \sum_{\substack{\mathbf{n}\in\mathbb{N}^l \\ ||\mathbf{n}||_1 = N}} \left(\prod_{k=1}^{l} n_k^{-\frac{D}{2}-1}\right) \left[\prod_{k=1}^{l} a_{n_k}(\beta\alpha) - 1\right], \tag{1.135}$$

with the one-norm $||\mathbf{n}||_1 = \sum_{k=1}^{l} n_k$ and the (symmetry-weighted) summation of all damping factors of size n to

$$a_n(\beta\alpha) = \sum_{\substack{\mathfrak{C} \\ |\mathfrak{C}|=n}} (\pm 1)^{l(\mathfrak{C})-1} M_{\mathfrak{C}} a_{\mathfrak{C}}(\beta\alpha) . \tag{1.136}$$

In particular in first-order QCE they are given by

$$\Delta_1 z_l(\beta\alpha) = \sum_{n=2}^{N-l+1} (\pm 1)^{n-1} n^{-\frac{D}{2}} z_{l-1}^{(N-n)} \frac{1}{2} \sum_{n_1=1}^{n-1} \left(a^{\text{intra}}_{n_1,n-n_1}(\beta\alpha) \pm a^{\text{inter}}_{n_1,n-n_1}(\beta\alpha)\right) \tag{1.137}$$

in terms of the intra- and inter-cycle damping factors, consistently with the general relation (1.133) defined as

$$a^{\text{intra/inter}}_{n_1,n-n_1}(\beta\alpha) = n^{D/2} \frac{\lambda_T^D}{V_D} \mathcal{A}^{\text{intra/inter}}_{n_1,n-n_1}(\alpha,\beta) . \tag{1.138}$$

Again, the implicit dependence of the coefficient functions (1.135) and (1.137) on N, D and symmetry $\pm$ is omitted and will be added as scripts when they are not clear from context.

One strong implication of the scaling (1.134) is that the mechanical equation of state, as it is given by differentiation *w.r.t.* the volume (1.79), generically can be directly written as closed expression also in the fully interacting system:

$$P(V_D,\beta,N,\alpha) = \frac{k_B T}{V_D} \frac{\sum_{l=1}^{N} l[z_l + \Delta z_l(\beta\alpha)]\left(\frac{V_D}{\lambda_T^D}\right)^l}{\sum_{l=1}^{N} [z_l + \Delta z_l(\beta\alpha)]\left(\frac{V_D}{\lambda_T^D}\right)^l} . \tag{1.139}$$

When expanding (1.139) in inverse powers of $V_D/\lambda_{\mathrm{T}}^D$ one gets the ideal gas equation as the dominant term and corrections that correspond to the virial expansion in the grand canonical formalism with the difference that finite N corrections are exactly incorporated in the coefficients. But the true strength of (1.139) lies in the fact that one does not have to do such a high-temperature (or equivalently low-density) expansion which cuts the applicability to the quantum degenerate regime. Instead one can take the *closed* and *finite* expression of the canonical QCE whereas the grand canonical formalism does not allow for such a direct approach and forces one to take the detour over fugacity inversion and virial expansion. The general discussion of this comparison between canonical QCE and grand canonical descriptions was already given in section 1.1.6 in the context of independent but indistinguishable particles and was purely based on the similar form of the equation of state. The generic scaling therefore extends all of this discussion to the interacting case even without specifying which type of interaction is inherent in the model.

Another strong implication is found when switching to the domain of energy rather than temperature by means of inverse Laplace transform of (1.134). The generic impact of interactions to the form of the mean many-body DOS is again found to be a change of coefficients in the expansion in powers of the volume V_D:

$$\begin{aligned}\bar{\rho}_{\pm}^{(N)}(E) &= \sum_{l=1}^{N}\left[\frac{z_l}{\Gamma\left(\frac{lD}{2}\right)}+f_l\left(\frac{E}{\alpha}\right)\right]\frac{1}{E}\left(\frac{mE}{2\pi\hbar^2}\right)^{\frac{lD}{2}}V_D^l\theta(E)\\ &= \rho_0\sum_{l=1}^{N}\left[\frac{z_l}{\Gamma\left(\frac{lD}{2}\right)}+f_l\left(\frac{E}{\alpha}\right)\right](\rho_0 E)^{\frac{lD}{2}-1}\theta(E)\,,\end{aligned} \tag{1.140}$$

where the effect of interactions lies purely in the modification of coefficients by interaction-specific functions $f_l = f_{\pm,l}^{(N,D)}$ that depend only on the ratio E/α. As for the constant coefficients the scripts N, D and $\pm$ are omitted whenever clear from context. For comparisons with exact or numerically calculated spectra it is more convenient to use the level counting function $\bar{\mathcal{N}}(E) = \int_{-\infty}^{E}\mathrm{d}E'\bar{\rho}(E')$ rather than the DOS $\bar{\rho}(E)$. One may write

$$\bar{\mathcal{N}}(E) = \sum_{l=1}^{N}\left[\frac{z_l}{\Gamma\left(\frac{lD}{2}+1\right)}+g_l\left(\frac{E}{\alpha}\right)\right](\rho_0 E)^{\frac{lD}{2}}\theta(E)\,. \tag{1.141}$$

The coefficient modifications as functions of the scaled energy $\epsilon := E/\alpha$ are then given by

$$\begin{aligned}f_l(\epsilon) &= \epsilon^{1-\frac{lD}{2}}\,\mathscr{L}_{\mathrm{s}}^{-1}\left[\Delta z_l(s)s^{-\frac{lD}{2}}\right](\epsilon)\,,\\ g_l(\epsilon) &= \epsilon^{-\frac{lD}{2}}\,\mathscr{L}_{\mathrm{s}}^{-1}\left[\Delta z_l(s)s^{-\frac{lD}{2}-1}\right](\epsilon)\,,\end{aligned} \tag{1.142}$$

where the functions $\Delta z_l(s)$ are taken from (1.134). In case of the first-order QCE they are given by (1.137). The coefficients for the DOS and the counting function are related by

$$\epsilon^{1-\frac{lD}{2}}f_l(\epsilon) = \frac{lD}{2}g_l(\epsilon)+\epsilon\frac{\mathrm{d}}{\mathrm{d}\epsilon}g_l(\epsilon)\,. \tag{1.143}$$

Note that a general consequence of (1.140) or (1.141) is that the effect of interactions gets suppressed either when the total energy $E \gg \alpha$ or $E \ll \alpha$ for interaction potentials that vanish for $\alpha \to 0$ or $\alpha \to \infty$, respectively. Or vice versa the interactions dominantly impact the low-energy physics or the high-energy physics in the two cases, respectively. Within the framework of QCE these two types of interactions can be directly observed as vanishing correction terms:

$$\begin{aligned} \lim_{\alpha\to 0} U_{\text{int}} = 0 \quad &\Rightarrow \quad \lim_{E\to\infty} f_l\left(\frac{E}{\alpha}\right) = \lim_{\alpha\to 0} f_l\left(\frac{E}{\alpha}\right) = 0\,, \\ \lim_{\alpha\to \infty} U_{\text{int}} = 0 \quad &\Rightarrow \quad \lim_{E\to 0} f_l\left(\frac{E}{\alpha}\right) = \lim_{\alpha\to\infty} f_l\left(\frac{E}{\alpha}\right) = 0\,, \end{aligned} \tag{1.144}$$

and similarly for g_l.

Closing this section, one should stress one important point. We have seen generic dimensional scaling in the QCE in the various facets of *i)* cluster damping behavior (1.133) with interaction-induced enhanced or suppressed spreading or even collapsing of clusters; *ii)* scaling in the partition function (1.134); *iii)* the consequent finite expression for the interacting quantum gas equation (1.139); *iv)* and the scaling of the DOS (1.140) allowing for direct identification of low- or high-energy dominating interactions. Crucial to the feasibility of all these is again the short-time focus and short-range assumption on the interactions, since it allows for extending integrals over distances between interacting particles to infinity. If the finiteness of the system would be taken into account for relative coordinates in clusters, this would possibly introduce additional length-scales, complicating the situation and destroying the generic scaling at least partially.

1.3 Application: Repulsive contact interactions in 1D

1.3.1 Demand and opportunity

Definition of the model

In this section I will introduce the application of the general QCE approach to a specific type of interactions, *i.e.*, contact interactions. Furthermore the spatial dimensionality is restricted to one. Throughout the rest of this work, this will be the setup to do explicit calculations of diagrams and derived system properties, which will turn out to be sufficient to fill the scope with its various aspects. As a system specification consider the N-particle Hamiltonian in spatial coordinate representation

$$\hat{H} = \sum_{i=1}^{N} \left(-\frac{\hbar^2}{2m_i} \frac{\partial^2}{\partial q_i^2} + U_{\mathrm{ext}}(q_i) \right) + \frac{\hbar^2}{2m} \sqrt{\frac{2m\alpha}{\hbar^2}} \sum_{i<j} \delta(q_i - q_j) \,, \tag{1.145}$$

where m_i are the masses of particles (that may differ in general) living in one-dimensional space with an arbitrary external potential U_{ext}. The interaction potential that affects all pairs of particles is specified to be a Dirac delta distribution of their mutual distances. The strength of this interaction is given by the prefactor, represented in the form (1.145) by the parameter α, which has the dimension of an energy. The physical constants involved in the prefactor give the interaction term correct units. The mass m is thereby some reference mass in case m_i differ from each other. This delta-type of interaction has zero range in the sense of potential width. It therefore perfectly fits the QCE requirement of being of short range. Nevertheless it affects the quantum propagation of two particles over finite distance in the sense that the dynamics of their common wave function in the relative coordinate is not only affected point-like.

Furthermore, this type of interaction does not have a reasonable classical analogue, which makes it especially interesting from a methodical point of view in the context of semiclassical approximations.

Relevance of contact interactions

Delta interactions are not an uncommon way to model realistic three-dimensional short-range interacting systems. In three dimensions one often identifies pure s-wave scattering with it because of its spherical symmetry [20]. The s-wave scattering of two particles is fully determined by the scattering phase shift $\delta_{\mathrm{s}}(k)$ between the incident and outgoing scattering states in the relative coordinates as a function of their wave number k. If one further considers the low-energy regime of scattering or equivalently low temperatures in an equilibrated system, the scattering phase is asymptotically determined by a single parameter, usually specified by the scattering length [20]

$$a_{\mathrm{s}} = -\lim_{k \to 0} \frac{\tan \delta_{\mathrm{s}}(k)}{k} \,. \tag{1.146}$$

The informative value of a_{s} can for example be seen in the fact that the total cross section for the two-particle scattering is (in the low-energy regime) solely

determined by the scattering length according to

$$\sigma_{\mathrm{tot}} = 4\pi a_{\mathrm{s}}^2 \,. \tag{1.147}$$

For a realistic system in the low-energy regime one can then identify the actual s-wave scattering length as an experimentally accessible parameter and model the interaction with a contact interaction (1.145) that produces the same scattering length by matching its prefactor.

The effective description with contact interactions is of special experimental relevance for ultracold neutral atoms in traps (see [8, 160] for reviews on the subject or the introduction for more references). For low temperatures only elastic scattering occurs and there are no ionization processes involved. The atoms are therefore considered as composite particles described by just one spatial location (as a classical or quantum degree of freedom) as if they were single entities in disregard of their internal structure. Because of charge neutrality the long-range Coulomb interactions between elementary particles are saturated within the individual atoms, and no Coulomb-type interaction between two atoms is present. There are, however, other effective interactions present between neutral atoms. Despite neglecting internal structures from the explicit final description, they can still be origin of effective interactions. There is for instance the van der Waals force that originates in internal charge separations within each atom that are mediated as inter-atomic force by electromagnetic dipole-dipole interaction. Furthermore, also small-scale Coulomb repulsion of hull electrons and effective repulsion due to Pauli exclusion are present when two atoms come extremely close.

Feshbach resonances [122] pose another experimentally very important type of inter-atomic interaction involving internal degrees of freedom, where the atoms can be tuned arbitrarily close to resonance by applying appropriate external magnetic fields. Using this method it is possible to introduce mutual short-range interactions that can be tuned in their scattering length to virtually arbitrary values. The accessible interactions thereby range from seemingly non-interacting particles for specific out-of-resonance tuning to strongly attractive and strongly repulsive interactions, switching from one to the other directly at resonance, a situation which is commonly referred to as unitarity.

Relevance of the one-dimensional model

The reduction of three dimensions to one is, further, of experimental relevance for effectively one-dimensional traps (see introduction for references). In such experiments the motion of constituents is strongly confined in two of the three directions. In these degrees of freedom the corresponding transversal excitations have large mean level spacings and can at low temperatures be regarded frozen. In a strict sense, this is already a conceptually incorrect statement because it assumes separation into transversal and longitudinal degrees of freedom, not valid in the presence of interactions. However, this decoupling becomes valid in the asymptotic scattering states of two interacting atoms, where the spatial separation renders them effectively non-interacting. While higher transversal modes are involved during a scattering process, the system can still be considered quasi one-dimensional as long as they are frozen for the individual atoms before and after the scattering.

To map such an experimental setup to the appropriate model, one needs to specify the coupling strength in the delta potential. The transversal confinement thereby affects the effective coupling strength in the one-dimensional description in a two-fold way. First, the stronger the confinement, the harder it is for two atoms to sidestep each other and therefore the stronger the effective interaction. I consider here the experimentally relevant situation of harmonic confinement $U_{\mathrm{conf}}(\mathbf{q}) = \frac{1}{2}m\omega_\perp^2\mathbf{q}_\perp^2$ in the transversal coordinates $\mathbf{q}_\perp = (q_\perp^{(1)}, q_\perp^{(2)})$ with frequency $\omega_\perp$. The relation to the energy-like coupling α in (1.145) for repulsive interaction under the assumption $a_s \ll \sqrt{\hbar/m\omega_\perp}$ on the scattering length (1.146) is

$$\alpha = 8ma_s^2\omega_\perp^2\,, \tag{1.148}$$

where the remnants of perpendicular motion are taken into account in an effective manner by integrating out transversal directions [161], with the remaining effect being a plain rescaling of the coupling depending on the frequency $\omega_\perp$ of the transversal harmonic confinement. Second, for scattering lengths a_s comparable with the confinement width, additional confinement-induced resonances [162] – driven by the transversal dynamics during scattering – render two atoms impenetrable at finite a_s. While the one-dimensional description is not affected by the resonances, they result in the modified effective coupling [161, 162]

$$\alpha = 8ma_s^2\omega_\perp^2\left(1 - C\frac{a_s}{\sqrt{2\hbar/m\omega_\perp}}\right)^{-2} \tag{1.149}$$

for repulsive interaction, where $C = 1.4603\ldots$.

One should note that if one wants to use the delta potential as model in more than one dimension directly, one needs to regularize the interaction, because otherwise its effect becomes infinitely strong [159]. This circumstance can be understood in the following way. Suppose one replaces the (isotropic) delta-potential by a regularized finite non-singular potential. Take for example a spherical potential well with fixed "integrated depth" $V_\delta U_\delta$, where V_δ is the volume of the well and U_δ the value of the potential inside the well. The width of the well, or correspondingly its volume V_δ may be considered as a cut-off parameter. We are now interested in the limit of zero cutoff. When one takes the limit of smaller and smaller wells this reproduces a delta-type potential, but at the same time the effect on the scattering of such a construction changes with the size instead of being constant (if the dimension is larger than one). For $D = 2, 3$ this leads to an infinitely strong effect in the limit $V_\delta \to 0$, *e.g.*, in the sense of a diverging scattering length [159] or bound state energy for attractive interaction. Thus, in this scheme, to obtain a finite effect to the scattering behavior (*e.g.*, reflected by the scattering length or bound state energy that one intends to model) one would have to introduce a renormalization factor that decreases to zero in a specific way when the cutoff goes to zero [158, 163]. One possible scheme that is often used is to replace the interaction by a pseudopotential of Huang type [164], which has been shown to be equivalent to a renormalization due to a momentum-space cutoff of the bare Dirac delta interaction [165]. In one way or another, to make delta potentials meaningful models of real physical interactions in $D = 2, 3$ one has to regularize them.

Integrability and analytical amenability – A special opportunity

On the theoretical side, the modeling using delta interactions has a special value in the sense that it offers the opportunity of extensive analytic calculations. One reason for that is the quantum integrability in the bosonic case of vanishing external potential but periodic or Dirichlet [166] boundary conditions. In the most prominent case of periodic boundary conditions this model of N contact-interacting bosons on a ring is known as the Lieb-Liniger model [33, 34] and admits a solution in terms of a Bethe ansatz (see section 1.3.3). Despite the possibility of exact analytic solution the goal here still is to do QCE for several reasons. First of all, the quantum integrability offers the opportunity of testing the method in a well-controlled environment. Second, the QCE does not explicitly depend on the assumptions making the Lieb-Liniger model solvable. Therefore, once we have gained experience and results for QCE with contact interactions this knowledge may later be provided in systems which do not allow for analytic solution. As a little anticipating motivation, this implies the very important case of confining external potentials (see section 1.4.2).

For the scope of this section, only first-order corrections within the cluster expansion are considered. For this we only need to extract the second-order Ursell operator $\hat{U}^{(2)}$. The propagator of $N = 2$ distinguishable particles of mass m in one-dimensional free space with delta interaction gets separated. One factor represents the center-of-mass motion given as the free propagator of a particle of total mass $2m$. The other factor represents the motion in the relative coordinate given as the propagation of a particle of reduced mass $m/2$ in presence of a delta barrier placed in one-dimensional free space. As a matter of fact, the latter is known exactly [167] and has a closed analytic form given as a free propagator plus a deviation, which naturally fits to the separation of non-interacting motion and interaction effect. The deviation gives then exactly what is needed to determine $\hat{U}^{(2)}$. Throughout this chapter, only repulsive contact interactions are considered, for which one obtains [168]

$$\begin{aligned} K^{(2)}(\mathbf{q}^{\mathrm{f}},\mathbf{q}^{\mathrm{i}};t) &= K_0^{(2)}(\mathbf{q}^{\mathrm{f}},\mathbf{q}^{\mathrm{i}};t) + \Delta K_\alpha^{(2)}(\mathbf{q}^{\mathrm{f}},\mathbf{q}^{\mathrm{i}};t)\,, \\ \Delta K_\alpha^{(2)}(\mathbf{q}^{\mathrm{f}},\mathbf{q}^{\mathrm{i}};t) &= -\sqrt{\alpha}\sqrt{\frac{m}{2\hbar^2}}\left(\frac{m}{2\pi\mathrm{i}\hbar t}\right)\exp\left(\frac{\mathrm{i}m}{\hbar t}\left(Q^{\mathrm{f}}-Q^{\mathrm{i}}\right)^2\right) \\ &\quad\times\int_0^\infty \mathrm{d}y\,\exp\left(-\sqrt{\frac{m}{2\hbar^2}}\sqrt{\alpha}y+\frac{\mathrm{i}m}{4\hbar t}\left(|\Delta q^{\mathrm{f}}|+|\Delta q^{\mathrm{i}}|+y\right)^2\right), \end{aligned} \tag{1.150}$$

with the center-of-mass and relative coordinates given by

$$\begin{aligned} Q^{\mathrm{i,f}} &:= \frac{1}{2}\left(q_1^{\mathrm{i,f}}+q_2^{\mathrm{i,f}}\right), \\ \Delta q^{\mathrm{i,f}} &:= q_1^{\mathrm{i,f}}+q_2^{\mathrm{i,f}}, \end{aligned} \tag{1.151}$$

respectively. To reduce notation, I express the interacting part of the two-body propagator in imaginary time $t = -\mathrm{i}\hbar\beta$ (or equivalently the heat kernel with

inverse temperature β)

$$\Delta K_\alpha^{(2)}(\mathbf{q}^{\mathrm{f}},\mathbf{q}^{\mathrm{i}};t=-\mathrm{i}\hbar\beta) = -\sqrt{\beta\alpha}\lambda_{\mathrm{T}}^{-2}\mathrm{e}^{-2\pi(X^{\mathrm{f}}-X^{\mathrm{i}})^2} \times \int_0^\infty \mathrm{d}u\ \exp\Big[-\sqrt{\pi\beta\alpha}u - \frac{\pi}{2}\left(|\Delta x^{\mathrm{f}}|+|\Delta x^{\mathrm{i}}|+u\right)^2\Big] \tag{1.152}$$

in scaled coordinates

$$\begin{aligned} X^{\mathrm{i,f}} &:= \frac{1}{2}\left(x_1^{\mathrm{i,f}}+x_2^{\mathrm{i,f}}\right), \\ \Delta x^{\mathrm{i,f}} &:= x_1^{\mathrm{i,f}}-x_2^{\mathrm{i,f}}, \\ x_i &:= \lambda_{\mathrm{T}}^{-1}q_i, \end{aligned} \tag{1.153}$$

which confirms the general scaling law (1.128) for the propagation of interaction effects in the case of repulsive delta interaction.

The direct analytic availability of the two-particle interaction effect (1.150) alone emphasizes the value of using this model while later this is pushed to the extreme when elevated to arbitrary high orders by making connection with the integrable model (see section 1.5.3).

1.3.2 Contact interactions in first-order QCE

The thermal equilibrium quantities

Using the explicit expression for the interacting part of the two-body propagator (1.150) for the contact interaction potential (1.145), the value of intra-cluster diagrams $A^{\mathrm{intra}}_{n_1,n_2}$ defined in (1.117) (see also Fig. 1.13a) is found to be

$$A^{\mathrm{intra}}_{n_1,n_2} = -\frac{L}{\lambda_T n^{\frac{1}{2}}}\frac{\sqrt{2\beta\alpha}}{4\pi}\int_0^\infty \mathrm{d}r \int_{-\infty}^\infty \mathrm{d}z \int_0^\infty \mathrm{d}u \times \exp\left[-\frac{1}{8}z^2 - \sqrt{\frac{\beta\alpha}{2}}u - \frac{1}{8}(|\bar\nu z+r|+|r|+u)^2\right], \tag{1.154}$$

where $L=V_1$ is the available length of the one-dimensional system and n and $\bar\nu$ are related to the numbers of particles involved in the process by

$$\bar\nu = \sqrt{(2n_1n_2-n_1-n_2)/n}, \quad n=n_1+n_2. \tag{1.155}$$

Expression (1.154) is found after using the semigroup convolution property (1.40) on all consecutive single-particle propagators reducing the cluster diagram to a maximum number of four constituents (see Fig. 1.14), some of which have altered (effective) masses (or equivalently modified propagation times). The remaining integration variables determine the distance between the two interacting particles in a scaled version, where $r=x_2-x_1$ is their (scaled) initial relative coordinate and $z=((x_2-x_1)+(x_2'-x_1'))/\bar\nu$ their (scaled) average relative coordinate during the process. The (scaled) change $X=(x_1+x_2)-(x_1'+x_2')$ in the center-of-mass of the two interacting constituents contributes in a non-interacting way, since it does not interfere with the interaction-dependent evolution of their distance. It has therefore been integrated as a Gauss integral

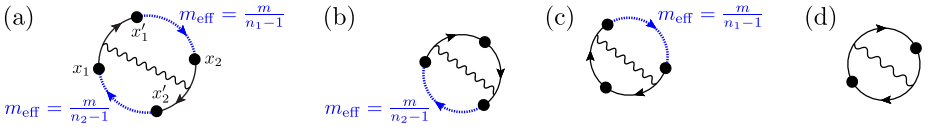

Fig. 1.14: Reduced effective cluster diagrams one obtains out of the general intra-cluster diagram (see Fig. 1.13a) after convolution of consecutive single-particle propagators. One gets four different cases (three are truly distinct) depending on the original number of constituents. (a) $n_{1,2} \geq 2$ reduces to an effective four-cluster. The $x_i^{(\prime)}$ label the (scaled) coordinates of the constituents. (b) $n_1 = 1, n_2 \geq 2$ reduces to an effective three-cluster as well as the case (c) $n_1 \geq 2, n_2 = 1$. (d) $n_{1,2} = 1$ is not reduced and remains a 2-cluster. Single particle propagators of effective masses are marked with broken blue thick lines. All four cases are subsumed to the integral (1.154).

to arrive at (1.154). The remaining variable u, taken over from the two-body propagator (1.152) (with some scaling) can be interpreted as an auxiliary length inserted at the location of the delta peak, which has to be traveled additionally (by the relative coordinate) in a free propagating manner with a weight $\sim \sqrt{\alpha}$ given by the coupling strength. Although some intermediate integrations involved to get from (A.255) to (1.154) are absent if $n_1 = 1$ or $n_2 = 1$, the resulting expression (1.154) also includes those cases.

Analogue considerations can be made on the inter-cycle cluster diagrams and lead to the exact identity

$$\mathcal{A}^{\rm intra}_{n_1,n_2} = \mathcal{A}^{\rm inter}_{n_1,n_2} =: \mathcal{A}_{n_1,n_2}\,, \tag{1.156}$$

which is a special feature of the delta-type interaction and implies the redundancy of delta-interactions characteristic for *spinless fermions*. This special implication of the Pauli exclusion principle is thereby confirmed within QCE of first order, instead of being imposed explicitly. In the cluster expansion this happens by rendering the sum (1.118) of all (first-order) irreducible diagrams of a specific size null, since $\mathcal{A}^{\rm intra}_{n_1,n-n_1} - \mathcal{A}^{\rm inter}_{n_1,n-n_1} = 0$. While, as a physical fact, this circumstance is expected we find it here as a non-trivial cancellation effect confirming the whole approach.

Finally, the multiple integrals for the intra-cycle cluster diagram (1.154) can be reduced by further manipulations. It has the universal scaling form (1.133) predicted for general interactions in section 1.2.5, reading

$$\mathcal{A}_{n_1,n_2}(\alpha,\beta) = \frac{L}{\lambda_{\rm T} n^{\frac{1}{2}}} a_{n_1,n_2}(\beta\alpha) \tag{1.157}$$

with the damping factor

$$\begin{aligned} a_{n_1,n_2}(s \coloneqq \beta\alpha) = \frac{2}{\pi}\tan^{-1}\bar{\nu} - 1 + \frac{2\bar{\nu}^2}{\sqrt{\pi(1+\bar{\nu}^2)}}\sqrt{s} \\ - \frac{2}{\sqrt{\pi}}\bar{\nu}\sqrt{s}\mathrm{e}^s\,\mathrm{erfc}(\sqrt{s}) + \frac{2}{\sqrt{\pi}}(1-2\bar{\nu}^2 s)F_{\bar{\nu}}(s)\,, \end{aligned} \tag{1.158}$$

where I introduced the thermal interaction strength $s = \beta\alpha$, which is the key dimensionless parameter determining the effect of interactions (see section 1.2.5

for the general argument). The remaining integral is defined by[9]

$$F_{\bar{\nu}}(s) = \mathrm{e}^{(1+\bar{\nu}^2)s} \int_0^\infty \mathrm{d}z\, \mathrm{e}^{-(z-\bar{\nu}\sqrt{s})^2}\, \mathrm{erfc}(\sqrt{s}+\bar{\nu}z)\,, \tag{1.159}$$

and therefore setting $\bar{\nu} = 0$ one recovers the case involving only two particles $\mathcal{A}_{1,1} = \frac{L}{\lambda_\mathrm{T}} \frac{1}{\sqrt{2}}(-1+\mathrm{e}^s\,\mathrm{erfc}(\sqrt{s}))$ on a line [168]. By using this definition of $F_{\bar{\nu}}(s)$ in a_{n_1,n_2} in (1.158) or (1.157) and substituting the latter into the coefficients $\Delta_1 z_l$ (1.137) or the recursion (1.119) one obtains an analytical non-perturbative expression for the canonical partition function of N bosons in one dimension with contact interaction in the absence of confining elements such as external potentials or boundary conditions.

Properties of the many-body spectrum

Given the explicit expression for the damping factors (1.158) and hence for the coefficients $\Delta_1 z_l^{(N)}$ by (1.137) one can then turn to determine the influence of interactions on the DOS by calculating the coefficients (1.142). Unfortunately the remaining integral (1.159) in thermal representation cannot be expressed in terms of elementary functions. In contrast to that, surprisingly, when one turns to the energy representation, the inverse Laplace transforms of its several variations involved when calculating the coefficient functions f_l and g_l reduce to elementary functions. I give here the result for the coefficient functions g_l in the counting function. The corresponding derivation can be found in appendix C. The coefficient functions f_l for the DOS are then related by (1.143). One can write

$$g_l^{(N)}(\epsilon) = \sum_{n=2}^{N-l+1} \frac{1}{\sqrt{n}} z_{l-1}^{(N-n)} \sum_{n_1=1}^{n-1} b_{\bar{\nu}}^{(l)}(\epsilon)\,, \tag{1.160}$$

where the $z_{l-1}^{(N-n)}$ are the coefficients (1.48) of the non-interacting partition functions. The functions $b_{\bar{\nu}}^{(l)}(\epsilon)$ only depend on the cluster index l representing the total number of clusters the N particles are divided into, the size n of the interacting cluster and its distribution of particles into cycles specified by n_1 [see (1.155) for the relation with $\bar{\nu}$]. I may omit the dependence on $\bar{\nu}$ when clear from context. These functions are the spectral representation of the combined damping factors of all clusters

$$b^{(l)}(\epsilon) = \epsilon^{-\frac{l}{2}}\, \mathscr{L}_\mathrm{s}^{-1}\left[s^{-\frac{l}{2}-1} a_{n_1,n_2}(s)\right](\epsilon)\,. \tag{1.161}$$

To maintain a minimal degree of overview one can split the coefficients into four contributions

$$b^{(l)}(\epsilon) = \sum_{j=1}^{4} b_j^{(l)}(\epsilon) \tag{1.162}$$

corresponding to the four terms in (1.158) [see (C.289) in appendix C]. The index j should not be confused with the dependence on $\bar{\nu}$, which has been omitted from notation here.

[9] For specific applications – especially in the regime of strong coupling s – the alternative forms (B.285) and (B.286) of (1.159), derived in appendix B, drastically improve accuracy and stability in the numerical integration.

The first one reads

$$b_1^{(l)}(\epsilon) = \left(\frac{2}{\pi}\tan^{-1}\bar{\nu} - 1\right)\frac{\theta(\epsilon)}{\Gamma\left(\frac{l}{2}+1\right)} + \frac{2\bar{\nu}^2}{\sqrt{\pi(1+\bar{\nu}^2)}}\frac{\theta(\epsilon)}{\Gamma\left(\frac{l}{2}+\frac{1}{2}\right)\sqrt{\epsilon}}\,. \tag{1.163}$$

The second part

$$\begin{aligned} b_2^{(l)}(\epsilon) = &-\frac{2\bar{\nu}}{\sqrt{\pi}}\frac{\left(1+\frac{1}{\epsilon}\right)^{\frac{l}{2}-\frac{1}{2}}}{\Gamma\left(\frac{l}{2}+\frac{1}{2}\right)\sqrt{\epsilon}}h_\lambda(\epsilon) \\ &+ \frac{2\bar{\nu}}{\pi}\sum_{k=1}^{\lfloor\frac{l}{2}\rfloor}\frac{\Gamma\left(\frac{l}{2}-k+\frac{1}{2}\right)}{\Gamma\left(\frac{l}{2}-k+1\right)\Gamma\left(\frac{l}{2}+\frac{1}{2}\right)}\left(1+\frac{1}{\epsilon}\right)^{k-1}\frac{\theta(\epsilon)}{\epsilon}\,, \end{aligned} \tag{1.164}$$

distinguishes between odd and even cluster number l through the definition

$$h_\lambda(\epsilon) = \begin{cases} \frac{2}{\pi}\theta(\epsilon)\tan^{-1}(\sqrt{\epsilon}) & : \quad \lambda = \frac{1}{2}\,, \\ \theta(\epsilon) & : \quad \lambda = 0\,, \end{cases} \tag{1.165}$$

where

$$\lambda = \frac{l}{2} \bmod 1 = \begin{cases} \frac{1}{2} & : \quad l \text{ odd}\,, \\ 0 & : \quad l \text{ even}\,. \end{cases} \tag{1.166}$$

Here $\lfloor q \rfloor$ denotes the integer $n \leq q$ that is closest to q.

The third term involves inverse Laplace transforms $\mathscr{L}_{\mathrm{s}}^{-1}[s^{-n/2}F_{\bar{\nu}}(s)](\epsilon)$ of the integral (1.159) which can be initially solved for $n = 0, 1, 2$ and then taken to arbitrary $n \in \mathbb{N}_0$ by virtue of the solution of a recurrence relation. The result reads

$$\begin{aligned} b_3^{(l)}(\epsilon) = \frac{\left(1+\frac{1+\bar{\nu}^2}{\epsilon}\right)^{\frac{l}{2}}}{\Gamma\left(\frac{l}{2}+1\right)}\Bigg[t_\lambda(\epsilon) - \frac{1}{\sqrt{\pi}}\sum_{k=1}^{\lceil\frac{l}{2}\rceil}\Gamma(k-\lambda)\left(1+\frac{1+\bar{\nu}^2}{\epsilon}\right)^{\lambda-k} \times \\ \times\left(\frac{\sqrt{\pi}}{2}b_2^{(2(k-\lambda))}(\epsilon) + \frac{\sqrt{1+\bar{\nu}^2}}{\Gamma\left(k-\lambda+\frac{1}{2}\right)}\frac{\theta(\epsilon)}{\sqrt{\epsilon}}\right)\Bigg]\,, \end{aligned} \tag{1.167}$$

where $\lceil q \rceil$ denotes the integer $n \geq q$ that is closest to q and the function t_λ is defined as

$$t_\lambda(\epsilon) = \begin{cases} \frac{2}{\pi}\theta(\epsilon)\tan^{-1}\left(\frac{1}{\bar{\nu}}\sqrt{1+\frac{1+\bar{\nu}^2}{\epsilon}}\right) & : \lambda = \frac{1}{2}\,, \\ \frac{2}{\pi}\theta(\epsilon)\left[\tan^{-1}\left(\sqrt{\frac{\epsilon}{1+\bar{\nu}^2}}\right)\right. & \\ \qquad \left. + \tan^{-1}\left(\sqrt{\frac{\bar{\nu}^2}{1+\epsilon}}\right) - \tan^{-1}\bar{\nu}\right] & : \lambda = 0\,. \end{cases} \tag{1.168}$$

The fourth term has a simple relation to the third one by

$$b_4^{(l)}(\epsilon) = -2\bar{\nu}^2\frac{1}{\epsilon}b_3^{(l-2)}(\epsilon) \tag{1.169}$$

for all $l \in \mathbb{N}$, where for $l = 1, 2$ this involves the evaluation of (1.167) for $l = -1, 0$, for which the latter is also valid.

1.3.3 Application to the Lieb-Liniger model

The Lieb-Liniger model – A perfect benchmark candidate

The model introduced and solved by Lieb and Liniger [33, 34] is one of the most paradigmatic examples of solvable interacting systems. It describes a one-dimensional gas of total length L of a fixed number N of non-relativistic indistinguishable particles satisfying Bose-Einstein statistics being subject to contact interactions and periodic boundary conditions. I will here briefly review the definition of the model and its solution and point out its use for the present purposes. In coordinate representation it is described by the Hamiltonian (after scaling to appropriate units)

$$\hat{H}_{\mathrm{LL}} = -\sum_{j=1}^{N} \frac{\partial^2}{\partial x_j^2} + 2c \sum_{1\leq i<j\leq N} \delta(x_i - x_j) \tag{1.170}$$

acting on a wave function $\Psi(x_1, \ldots, x_N)$ together with the symmetry condition

$$\Psi(x_1, \ldots, \underbrace{x_i}_{\text{position } i}, \ldots, \underbrace{x_j}_{\text{position } j}, \ldots, x_N) = \Psi(x_1, \ldots, \underbrace{x_j}_{\text{position } i}, \ldots, \underbrace{x_i}_{\text{position } j}, \ldots, x_N) \tag{1.171}$$

for all pairs $i < j$ and the periodic boundary condition

$$\Psi(x_1, \ldots, \underbrace{x_i + L}_{\text{position } i}, \ldots, x_N) = \Psi(x_1, \ldots, \underbrace{x_i}_{\text{position } i}, \ldots, x_N) \tag{1.172}$$

w.r.t. to each individual particle i. The constant $c \geq 0$ determines the strength of the interactions and is related to the coupling-parameter α in (1.145) by

$$c = \sqrt{\frac{m\alpha}{2\hbar^2}}\,. \tag{1.173}$$

The model admits an exact analytic solution in terms of a Bethe ansatz [32]

$$\Psi(x_1, \ldots, x_N) = \sum_{P\in S_N} a_P \exp\left(\mathrm{i}\sum_{j=1}^{N} k_{P(j)} x_j\right) \tag{1.174}$$

for the wave function in the fundamental domain (1.34) given by the simplex comprising all points that satisfy

$$0 \leq x_1 \leq \ldots \leq x_N \leq L\,. \tag{1.175}$$

The solution for the permutation coefficients a_P together with the quasi-momenta $k_1, \ldots, k_N$ is found by satisfying the boundary conditions

$$\lim_{x_j \to x_{j+1}^-} \left(\frac{\partial}{\partial x_{j+1}} - \frac{\partial}{\partial x_j}\right) \Psi = c\Psi\big|_{x_j = x_{j+1}}\,, \quad (x_{N+1} \coloneqq x_1) \tag{1.176}$$

on the boundaries $x_j = x_{j+1}$ of the simplex that are imposed by the delta interactions (1.170) in combination with the symmetry condition (1.171). It has been shown [169] that all solutions are of the form

$$a_P = \prod_{1\leq i<j\leq N} \left(1 + \frac{\mathrm{i}c}{k_{P(i)} - k_{P(j)}}\right) \tag{1.177}$$

with (scaled) eigenenergies

$$\tilde{E} = \sum_{j=1}^{N} k_j^2 \,, \tag{1.178}$$

related to the eigenergies E of (1.145) by $E = \hbar^2 \tilde{E}/2m$. The quasi-momenta k_j are determined by the periodic boundary condition (1.172) and satisfy a set of coupled transcendental equations. For repulsive interaction $c \geq 0$ assumed here, the k_j are all real which allows to rewrite the transcendental equations as

$$Lk_j = 2\pi I_j - 2\sum_{i=1}^{N} \arctan\left(\frac{k_j - k_i}{c}\right) \,, \quad j = 1, \ldots, N \,, \tag{1.179}$$

where all possible solutions are now ordered by a set of quantum numbers

$$I_1 < I_2 < \ldots < I_N \,, \quad I_j \in \begin{cases} \mathbb{Z} & : \; N \text{ odd} \,, \\ \mathbb{Z} + \frac{1}{2} & : \; N \text{ even} \,, \end{cases} \tag{1.180}$$

that are either integer when N is odd or half integers when N is even. This ordering by quantum numbers is an essential simplification that allows for efficiently finding large complete sets of energy levels (1.178) by numerically solving the coupled equations (1.179), also for moderately large numbers of particles. If one allows for attractive interactions, in principle the solution still exists, but the k_j have to be allowed to be complex, which does not allow for an ordering of solutions in terms of quantum numbers like (1.179). Throughout this chapter, in the context of QCE, I stick to the case of repulsive contact interactions, but issues of numerically solving for spectra in the attractive case will become important again in chapter 2.

Historically, the Lieb-Liniger model was introduced to benchmark approximate methods for interacting systems like Bogoliubov approximation [26] and this is exactly how it will be used here. As a first benchmark, it will provide insight in how far one can get with the crudest approximation within QCE, which is the first order calculated in section 1.3.2. As a fortunate coincidence, the exact details of the Lieb-Liniger model are extremely well fitted for testing the QCE with delta interactions. This is because the periodic boundary conditions render the system borderless. One can think of it as bosons moving on a ring rather than a line, a boundary condition that has no effect on the smooth DOS as compared to Dirichlet or Neumann conditions. The short-time dynamics and hence the smooth DOS – determined by local behavior – are not affected by the periodicity which one has to go once around the whole circle to feel.

The many-body spectral density

As in the non-interacting case (see section 1.1.4), the counting function $\mathcal{N}(E) = \int_{-\infty}^{E} \mathrm{d}E' \rho(E')$ is better-suited for comparisons with exact spectra than the DOS $\rho(E)$. Eq. (1.141) together with the explicit expressions given in section 1.3.2 gets compared with the staircase functions corresponding to the counting functions of exact spectra numerically calculated using the analytic solution (1.179). Figure 1.15 shows the case $N = 3$ in the full regime of coupling strengths ranging from $\alpha = 0$ to $\alpha \to \infty$. For $\alpha = 0$ the ideal periodic one-dimensional Bose gas is obtained, smoothly reproduced by the non-interacting QCE (1.50). When

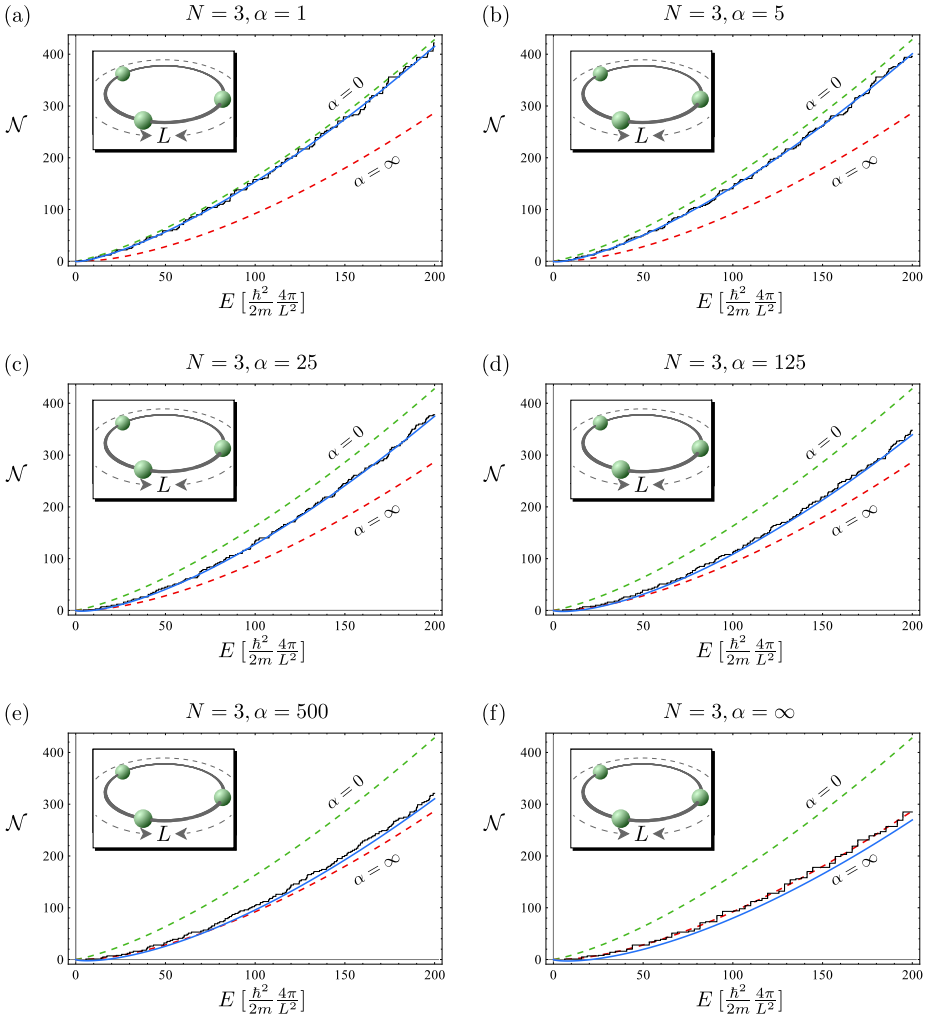

Fig. 1.15: Counting function of the exact many-body energies in the Lieb-Liniger model of $N = 3$ bosons (black staircase) for various interaction strengths $\alpha = 1, 5, 25, 125, 500, \infty$ in units of $\rho_0^{-1} = \frac{\hbar^2}{2m}\frac{L^2}{4\pi}$ and the corresponding analytic functions (1.141) given by first-order QCE (solid blue) with the explicit form given in section 1.3.2. The non-interacting QCE (1.50) for bosons (dashed green) and fermions (dashed red) pose an average bound for the exact levels corresponding to the limits $\alpha = 0$ and $\alpha \to \infty$, respectively.

the repulsive interaction gets enhanced, all eigenenergies increase continuously as expected, which effectively pushes the graph of the counting function to larger energies. The QCE calculation thereby follows rather accurately, where the effective shifting of energies is not implemented as such directly but instead is a collective effect induced by the (energy-dependent) modification of the coefficients of the corresponding polynomial in $(\rho_0 E)^{1/2}$. For $\alpha \to \infty$ the spectrum of the Lieb-Liniger model exactly corresponds to an ideal periodic Fermi gas [170], an effect commonly referred to as *fermionization*. The Bose gas in this hardcore limit, which is also known by the name Tonks-Girardeau gas [171], is smoothly reproduced by the fermionic non-interacting QCE (1.50). The interacting QCE to first order shows overall very good agreement. In the limit $\alpha \to \infty$ the interacting bosonic QCE to first order is not expected to coincide with the fermionic non-interacting QCE, since the truncation of three-body interaction effects $\Delta K^{(3)}$ from the three-clusters becomes an increasingly important deficiency. It is rather the full expansion including higher orders that should, due to the fermionization of the exact spectra, coincide with the non-interacting fermionic expansion. Therefore it is systematically expected that for very strong couplings the first-order expansion deviates. The significance of the deviation is but very small and even stays finite in the hardcore limit $\alpha \to \infty$, an important property that strongly distinguishes it from perturbative expansions, which by construction are doomed to diverge in this limit.

Figure 1.16 shows the case of slightly increasing number of bosons N. For each value a moderate coupling strength is chosen in a way that $N^2\alpha$ as a rough estimate for the interaction energy in the system is kept constant to allow for a comparison of physically similar situations. The deviations of first order QCE from the exact spectra get larger for increasing number of bosons, which is not surprising, since a strongly increasing fraction of possible cluster diagrams is omitted by the truncation of the cluster expansion to first order.

Still, even in this crude truncation, despite the strong growth of the counting function with the energy for larger N, the deviation keeps seemingly more or less constant. As a consequence the relative error drops off rapidly for increasing energy which confirms the general statement (1.144) from the universal scaling analysis of QCE in section 1.2.5. The given delta interaction potential belongs to the class of potentials that vanish for $\alpha \to 0$, which have the strongest impact in the low-energy regime.

Equation of state – Thermal equilibrium

The subject of this subsection is the (closed) Lieb-Liniger system in thermal equilibrium. I explicitly stick to the description within the canonical ensemble with a small and strictly fixed number of particles N. As argued before (see section 1.1.6), especially in the few-body regime the physics crucially differ from the grand canonical description. Thus, although there exists a solution of the model that is very well suited for grand canonical thermodynamic descriptions *in the thermodynamic limit* [172, 173] by what is called the thermodynamic Bethe ansatz, it is inappropriate for the current purpose. Instead, I will again employ the solution by solving the transcendental (but algebraic) system of equations (1.179) to benchmark the QCE with truncation to first order (described in section 1.3.2) and thereby point out its weaknesses, strengths and potential to improve.

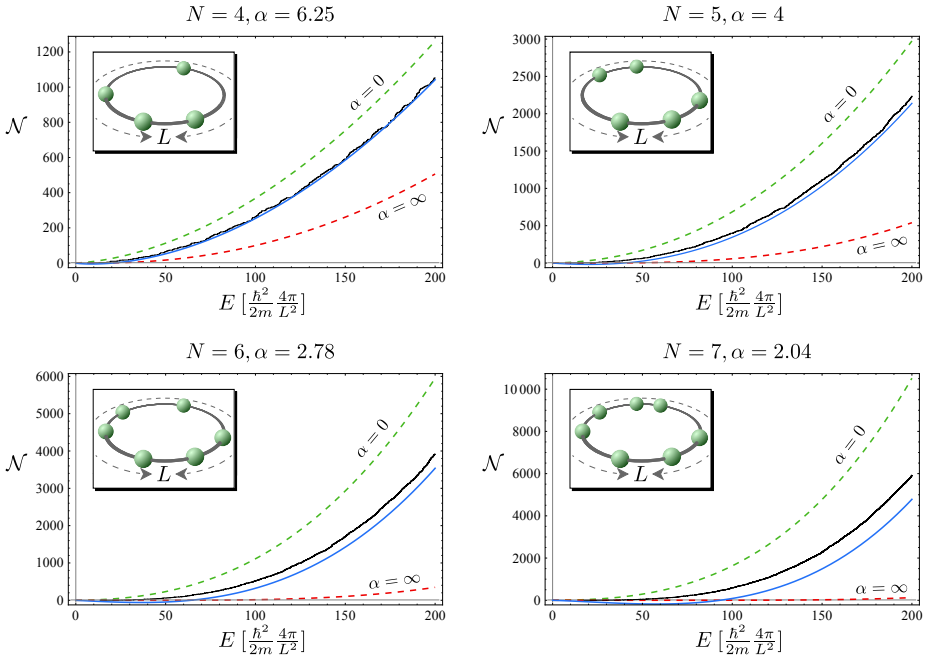

Fig. 1.16: Counting function of the exact many-body energies in the Lieb-Liniger model of $N = 4, 5, 6, 7$ bosons (black staircase) for interaction strengths α (given in units of $\rho_0^{-1} = \frac{\hbar^2}{2m}\frac{L^2}{4\pi}$) moderately chosen such that $N^2\alpha = \text{const}$ in the four plots. The corresponding analytic functions (1.141) are given by first-order QCE (solid blue) with the explicit form given in section 1.3.2. The non-interacting QCE (1.50) for bosons (dashed green) and fermions (dashed red) pose an average bound for the exact levels corresponding to the limits $\alpha = 0$ and $\alpha \to \infty$, respectively.

Figure 1.17 shows the mechanical equation of state $P(L, T, \alpha)$ in thermal equilibrium determined by the canonical partition function $Z(L, T, \alpha)$ (1.29) via (1.79). Within the cluster expansion it is given by (1.134) and (1.139). The comparison is done for the case $N = 3$. Because of the general dimensional scaling discussed in section 1.2.5, when the volume (length L) of the system is measured in units of the thermal de Broglie wavelength λ_{T}, the functional dependence on the coupling strength purely involves the thermal interaction strength $s = \beta\alpha$. This applies to the QCE as well as to the exact solutions (1.179). When a specific temperature is fixed, Fig. 1.17a–e shows the pressure as a function of the system volume L for different coupling parameters α, ranging from the non-interacting case $\alpha = 0$ over weak, intermediate and strong coupling to the (practically) fermionized case of ultra-strong coupling $\alpha = 10^8$.

Already the non-interacting case (see Fig. 1.17a) clarifies an important point about the QCE in general. Namely, as a universal description, the latter is in its pure form not able to resolve system specific features that are characterized beyond the dimensionality, system size, particle number and type of interaction. Such non-universal features show up in the exact location of many-body energies, which are scattered around the universal distribution in a specific way. In some cases the associated fluctuations of exact levels may be considered as if being stochastically distributed without a significant systematic effect on the physics. This is for example the case for the harmonically confined ideal Bose gas discussed in section 1.1.6 (see Fig. 1.9). In other cases, there may be a systematic way in which the exact levels are distributed and produce a strong influence on physical observables. For temperatures above the regime of deep quantum degeneracy, such system specifics are washed out by larger sets of many-body eigenstates and their energies. In contrast to that, for ultra-low temperatures, the equilibrium physics get dominated by the ground state of the system and the lowest excitations, which gives system specific properties the chance to pop up. In the Lieb-Liniger system discreteness shows up in an extreme way. The strong qualitative and quantitative deviations between exact numerics and QCE in the deep condensation regime $L \approx \lambda_{\mathrm{T}}$ of the non-interacting system in Fig. 1.9a can be physically explained in the following way. When the system gets shrunken the independent bosons increasingly occupy the single particle ground state. This single particle ground state is of zero energy with a wave function of constant value in $[0, L[$. Because its energy is in particular not depending on the size L, it results in arbitrary compressibility, displayed by the vanishing of the pressure at zero size $L = 0$, where the thermal ensemble is fully composed of bosons in the zero mode. The effect is that this system will collapse when a certain threshold in length or temperature is gone below (under non-vanishing external pressure). This effect is a pure consequence of the periodic boundary condition[10], which is a non-universal property.

For repulsive interaction $\beta\alpha > 0$ the full collapse is prevented, so that the gas eventually becomes incompressible as $L/\lambda_{\mathrm{T}} \to 0$. The repulsion due to interaction and effective "attraction" due to (finite-size) Bose-Einstein "condensation" in a zero-mode are thereby competing effects. Above a certain thermal coupling strength $\beta\alpha \approx 0.5$ (see Fig. 1.17c) the repulsion is strong enough to prevent

[10] For realistic systems of elongated gases of cold atoms it is questionable if the collapse can be considered as a physical effect or rather an artifact. Still, atoms in ring-shaped traps in principle might be capable of exhibiting this behavior when temperatures are low enough and the trap size is large enough so that its finiteness does not influence the transversal modes.

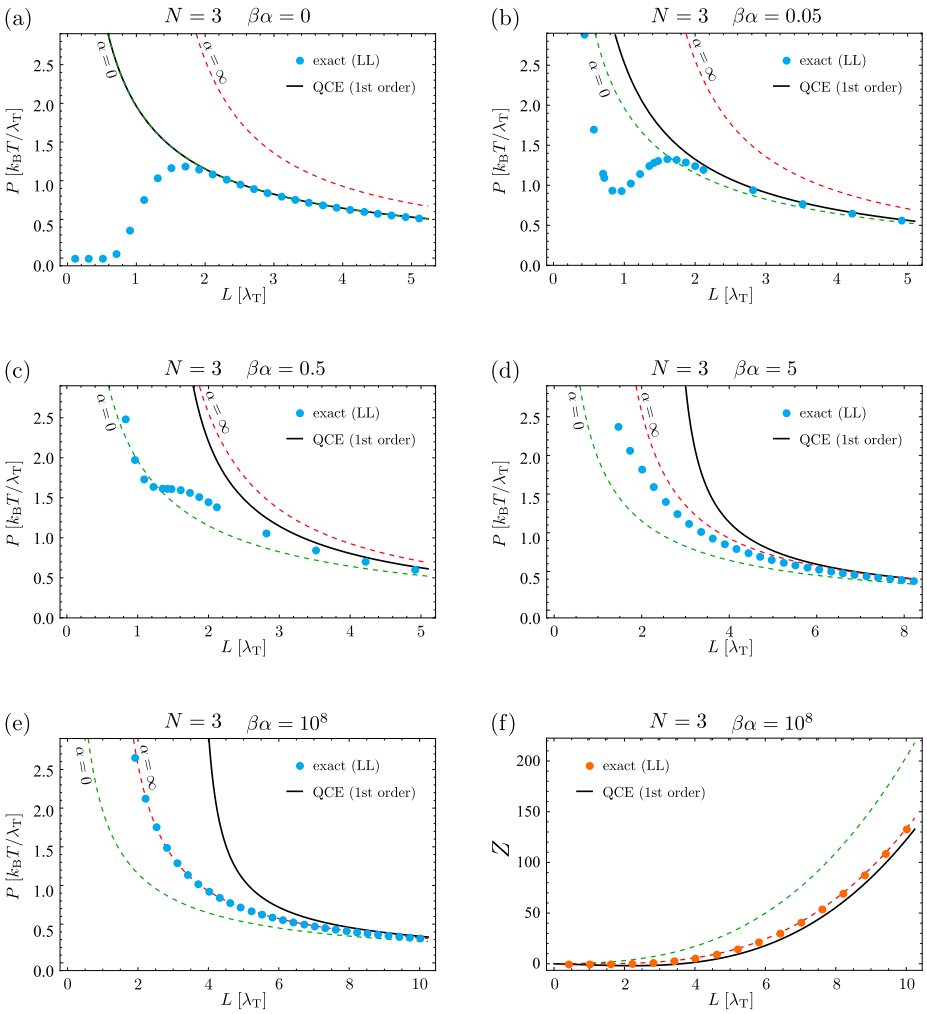

Fig. 1.17: (a)–(e) Mechanical equation of state $P(L)$ in the Lieb-Liniger model of $N = 3$ bosons for thermal interaction strengths $\beta\alpha = 0, 0.05, 0.5, 5, 10^8$. The samples of the exact curve (blue dots) were calculated using several thousand exact many-body levels for each by repeated numerical solution of the (algebraic) analytic equations (1.179). This is demanded to converge to a negligible error within the whole plotted range of lengths L/λ_T (or equivalently temperatures, if L is considered fixed). The corresponding analytic functions (1.139) are the first-order truncation of QCE (solid black) with the explicit form given by the coefficient functions $\Delta_1 z_l^{(N)}$ in (1.137). Above the non-universal condensation regime the non-interacting QCE (using (1.47)) for bosons (dashed green) and fermions (dashed red) pose an average bound for the exact pressure corresponding to the limits $\alpha = 0$ and $\alpha \to \infty$, respectively.

even a partial collapse by rendering the pressure a monotonous function of the system size. For couplings far above this critical value (see Fig. 1.17d,e) the physics get dominated by the repulsive interaction, outweighing the effective attraction from Bose statistics in the presence of periodic boundary conditions. This renders the system characteristics closer to universal behavior also in the quantum degenerate regime $L \lesssim \lambda_{\mathrm{T}}$, indicated by the overall smoothness in the graph of $P(L, T, \alpha)$. So far we are not able to explicitly confirm the last conjecture in the regime of strong but finite couplings because the truncation to first order makes the cluster expansion approach invalid. The deviation in the partition function (see Fig. 1.17f) is rather small in magnitude, comparable to the deviation in the spectral counting function (see Fig. 1.15) even for (practically) infinite interaction strength. However, the induced deviation one observes in the pressure is rather strong in this regime. Nevertheless, in the limit of infinite interactions we directly observe verifiable universality. As in the study of the counting function, also here the exact numerics are very well described by the non-interacting QCE (1.45) of an ideal Fermi gas.

Resumée

In the previous subsections the strengths and weaknesses of the QCE and its truncation to first order in particular have been benchmarked against numerical calculations. Summarizing them I also want to point out the several prospects of further improving the approach. This way this little interlude shall serve as a motivator by allowing a quick glance into the upcoming methodical progress.

To start with the strengths, first of all we have seen good agreement for few particles with weak to moderate interactions in the many-body DOS or counting function and in thermal equilibrium in the pressure at temperatures above condensation.

Second, from an analytic point of view the QCE comes with the universal scaling property (1.134), (1.140) and (1.141). On the one hand this implies the general analytic identification of regimes of increased validity, here confirmed as the regimes of high energy or temperatures above condensation. This way the QCE gets granted a certain basic amount of control over its predictive power in general. On the other hand, the expansion in powers of the volume allows for a closed finite expression for the pressure (1.139).

Third, since the QCE is a non-perturbative approach, it interpolates between an excellent description in the non-interacting limit and a *finite* deficiency in the limit of infinitely strong coupling. This finiteness has become evident in both the spectral counting function and the thermal properties determined by the partition function.

The most obvious weakness of the first-order approximation regards its inaccuracy for intermediate to strong couplings. What indicates great potential to improve at this point is the observation of perfect universal description within the non-interacting fermionic QCE in the extreme limit $\alpha \to \infty$. Indeed, we will see later (see section 1.4.1) how the effect of fermionization can be exploited to elevate the first-order expansion to an applicable theory in both, the weak and strong coupling regime.

For increasing numbers of particles N the first-order approximation misses too many interacting cluster diagrams which drastically limits the range of well-described interaction strengths. The spectral comparison shows a great

difference in the quality of describing a ($N = 3$)-system as compared to larger numbers of particles. There is also some potential to improve inherent to this observation. One can argue that the first-order calculation works especially well in the case $N = 3$ because it lies within a class of higher quality approximations of the full expansion. Consider an approximation where first-order diagrams are allowed in all clusters simultaneously rather than in just one cluster at a time. I will refer to this scheme as the *independent pairing* approximation (see the outlook in section 1.7), which is not explicitly applied in this work but instead serves here only as a thinkable theoretical improvement. For $N = 3$ there are no additional diagrams from independent pairing compared to first order, which distinguishes this case qualitatively from $N \geq 4$. The scheme of independent pairing as well as other higher-order truncations are in general better suited to describe thermal properties than spectral ones. The reason is that the former involve *products* (see (1.110)) of independent cluster contributions $\mathcal{A}_{\mathfrak{C}}$ rather than *convolutions* thereof[11]. This reduces the analytical tractability of thermal higher-order descriptions to the analytic knowledge of isolated cluster diagrams. In contrast to that, the spectral higher-order description might in most cases involve integrals of arbitrary multiplicity up to $N - 3$ without elementary solution. For the spectral description, even for intermediate couplings and arbitrary numbers of particles another great potential is covered in the generic scaling and the fermionization. In section 1.5.2 an approximate method is developed that brings the whole range of interactions into reach considering the universal spectral density.

The last weakness to mention was shown in its probably most extreme form in Fig. 1.17: the limitation to universal properties. The system-specific physics, potentially observable in the regime of ultra-low temperatures cannot be described by the pure QCE based on short-time dynamics. We have seen and argued that such non-universal features are related to the discreteness of the spectrum and especially influenced by the exact behavior of the ground state of the system. Recognizing the origin of non-universality is where another potential to improve sets in. In section 1.5.1 a method is developed that allows for inclusion of non-universality while keeping all the advantages of the QCE by introducing rudimentary, analytical information about the lowest exact eigenenergies of the system.

Before turning to the development of these methodical advances, the next section is committed to extending the applicability of QCE in the presence of repulsive contact interactions by widening the set of systems it applies to. A special role is taken by the extension to the fermionization regime in section 1.4.1. While it is a methodical extension in the first place, it can be understood as application of the normal first-order QCE to a different system. Furthermore, this extension poses a general and strong improvement of the QCE for all systems to come. Hence it is already attached to the next section as a starter.

[11] The inverse (bilateral) Laplace transform of a product is the convolution $\mathscr{L}_\beta^{-1}[A(\beta)B(\beta)](E) = \int \mathrm{d}E' \, \mathscr{L}_\beta^{-1}[A(\beta)](E - E') \, \mathscr{L}_\beta^{-1}[B(\beta)](E')$ of the individual inverse Laplace transforms.

1.4 Extensions I: Systems

1.4.1 Fermionization regime and the Tonks-Girardeau gas

Full fermionization – The Tonks-Girardeau gas

One observation in the comparison of exact numerics in the Lieb-Liniger model with QCE calculations in the last section was that the hardcore limit of infinite coupling strength $\alpha \to \infty$ in its universal properties (disregarding discreteness) coincided with a non-interacting fermionic system very well reproduced by the non-interacting QCE (1.50) and (1.47) for fermions (see Fig. 1.15f and Fig. 1.17e,f). There is indeed a deeper truth at the bottom of this observation, a known effect commonly referred to as *fermionization*. This effect is inherent in all bosonic one-dimensional systems with an interaction that becomes point-like impenetrable and apart from that stays finite [170]. A summary of this well-known analytical peculiarity is given in the following. The point is that impenetrability at zero distance means that the many-body wave function becomes zero-valued whenever two or more particles coincide in their coordinates, which can be interpreted as Pauli exclusion principle of spinless fermions. Furthermore, if the system is one-dimensional, this is equivalent to imposing Dirichlet boundary conditions on all of the boundaries of the fundamental domain $\mathcal{F}_N$ (1.34) (see section 1.1.3) that are related to collisions, the same boundary condition one would obtain from antisymmetry in the fermionic (spinless) equivalent. The wave function in the full domain Ω^N is then obtained by applying all permutations on the fundamental domain without sign inversion because of the bosonic symmetry *w.r.t.* exchange. The wave function of the fermionic equivalent therefore is related to the one in the bosonic theory by exact identity

$$\Psi_-^{\text{eff}}(\mathbf{q}) = \Psi_+^{(\alpha\to\infty)}(\mathbf{q}) \quad \text{if} \quad \mathbf{q} \in \bigcup_{\substack{P\in S_N \\ \operatorname{sgn} P=1}} P(\mathcal{F}_N) \tag{1.181}$$

in the fundamental domain and even permutations thereof and by sign-inversion

$$\Psi_-^{\text{eff}}(\mathbf{q}) = -\Psi_+^{(\alpha\to\infty)}(\mathbf{q}) \quad \text{if} \quad \mathbf{q} \in \bigcup_{\substack{P\in S_N \\ \operatorname{sgn} P=-1}} P(\mathcal{F}_N) \tag{1.182}$$

in domains obtained by odd permutations.

The non-collisional boundaries of $\mathcal{F}_N$ that are not related to collisions are subject to physical boundary conditions each individual particle is subject to. Periodic boundary conditions like in the Lieb-Liniger model take a special role posing a small complication there. Under their presence one fundamental domain can be reached from another one by a path $\mathbf{q}(t)$ without any collision of particles or hitting physical boundaries. This means there are boundaries of $\mathcal{F}_N$ that are identified and therefore are intersecting surfaces rather than actual boundaries. The example of two indistinguishable particles on a circle has been considered in section 1.1.3, where this intersecting surface was pictured in Fig. 1.3 by the lines colored in purple. The identification of those surfaces corresponds to a single cyclic permutation $P = \begin{pmatrix} 1 & 2 & \dots & N \end{pmatrix}$ of all particles with a sign $(-1)^P = (-1)^{N+1}$. The implication is the condition of sign inversion

$$\Psi(q_N, q_1, \dots, q_{N-1}) = (\pm 1)^{N+1}\Psi(q_1, \dots, q_N) \tag{1.183}$$

at these surfaces that only periodic systems of an even number of true fermions are subject to. Note that (in contrast to antisymmetry of fermions at collisional boundaries) the sign-inversion at these surfaces does not imply a zero-valued wave function, since the latter do not have to be continuous functions there. On the contrary, what has to be actually demanded is continuity and differentiability of the function one obtains locally when it is sign-inverted on one side of the surface. In the case of hardcore interacting bosons, the sign inversion is *not* present and has to be corrected to establish equivalence.

The conclusion is the following. Assume one starts from an interacting bosonic theory in one dimension with ring topology S^1 and increases the interaction to the hardcore limit in the sense above. Then one obtains a system equivalent to a fermionic theory with otherwise identical system specifications with the one exception that in the case of an even number of particles one has to impose an additional (discontinuous) sign-inversion on the fermionic wave function at the non-collisional intersecting surface related to the periodic boundary condition.

Then the corresponding fermionic theory is equivalent in the sense of the identification of wave-functions (1.181) and (1.182), which in particular implies that the systems are isospectral

$$E^{\mathrm{eff}}_{-,n} = E^{(\alpha\to\infty)}_{+,n} \tag{1.184}$$

with identical modulus of their eigenfunctions

$$|\Psi^{\mathrm{eff}}_{-,n}(\mathbf{q})|^2 = |\Psi^{(\alpha\to\infty)}_{+,n}(\mathbf{q})|^2\,, \quad \forall \mathbf{q} \in \Omega^N\,. \tag{1.185}$$

In the special case of delta interaction the fermionic theory is non-interacting, since the only effect of the infinitely strong delta barriers on the collisional boundaries of $\mathcal{F}_N$ is to impose Dirichlet conditions. The corresponding fermionized (but strictly speaking still bosonic) gas is known by the name Tonks-Girardeau gas [170, 171]. Moreover in the case of an even number of hardcore bosons plus periodic boundary conditions the sign-inversion on the periodicity boundaries of $\mathcal{F}_N$ is a condition that can be considered a global property, since it does not matter where exactly this sign-inversion happens. The only demand is that an overall change in sign happens *at some point* along a path that connects two classical configurations related by a single cyclic permutation. One can think of such a path as moving all particles sitting at initial positions on a circle in the *same direction* (*e.g.*, clockwise) exactly as much until they sit at the initial positions of their next neighbor. A lower bound for the length of such a path is reached when all particles are equally distributed along the circle. Then the traveled distance (in N-dimensional full configuration space) is $L/\sqrt{N}$, which is of the order of the system size. Therefore the local short-time quantum dynamics are not affected by the sign-inversion. This is the exact analogue of the irrelevance of the periodic boundary condition to the short-time dynamics in the bosonic Lieb-Liniger model. It explains the success of the non-interacting fermionic QCE in exactly reproducing the universal behavior of the Tonks-Girardeau gas (see Fig. 1.15f and Fig. 1.17e,f).

The argument of system-sized path-lengths that do not affect the universal properties (local propagation, short-time dynamics or smooth DOS) – in its inversion – also clarifies the non-applicability of the fermionization in higher

dimensions $D \geq 2$. There, two classical configurations that are related by exchange of two particles can be reached by paths of arbitrary short length avoiding any collision of particles with each other or physical boundaries. Although the vanishing wave function of hard-core bosons at the collisional manifolds (invariant manifolds $\mathcal{M}_P$) could as well be interpreted as Pauli exclusion principle of spinless fermions, this mapping is not valid in the vicinity of these manifolds (cluster zones). The condition of sign-inversion along arbitrarily short paths that exchange two particles in a system of spinless fermions makes a difference also in *local* quantities, meaning it alters the short-time dynamics compared to hard-core bosons, making a mapping between the two impossible or at least burying it in the analytics in a non-trivial way. To be sure, the hard-core bosonic system is then not simply equivalent to the non-interacting fermionic system by means of the mappings (1.184) and (1.185). It remains an open question whether it is possible to draw a connection of more hidden type between hard-core bosons and fermions for $D \geq 2$.

The fermionization in $D = 1$ is a very special effect about one-dimensional systems and interaction potentials that become point-like impenetrable but otherwise stay finite (in contrast to, *e.g.*, Coulomb interactions or dipole-dipole interactions that diverge for arbitrary distances). For this reason one may ask if this effect is of physical relevance in experimentally accessible systems. This question is best answered with a reference to actually conducted experiments [126, 127], where this strongly correlated system was realized in gases of many ultracold bosonic neutral atoms in elongated traps. In addition, the equivalent of this effect on distinguishable particles was directly observed on a single pair of ultracold atoms [130]. Once again, this confirms the validity of the delta-interaction model in describing cold-atom systems in one dimension.

Partial fermionization

Beyond the identification of hardcore contact-interacting bosonic systems with non-interacting fermionic systems there exists an extended mapping between bosonic and fermionic theories with way more far-reaching consequences for the present context of cluster expansions. While still restricted to one-dimensional systems it lifts the applicability from the zero-measure set of infinite coupling to the whole world of arbitrary coupling strengths $\alpha \in \mathbb{R}^+$. It has been shown [174] that a one-dimensional contact-interacting bosonic theory exactly maps to a fermionic theory with an effective interaction of inverse strength with the additional sign-inversion (see previous subsection) in case of an even number of bosons with periodic boundary condition. The equivalence is thereby a mapping in the same sense (1.181) and (1.182) as in the fully fermionized case with the same implications of isospectrality (1.184) and identical joint probability densities (1.185). By this mapping a bosonic theory with strongly repulsive contact interactions can be understood (in its relevant aspects) as a fermionic theory with a weak, residual, mutually attractive interaction. The effective fermionic interaction potential thereby is also point-like and hence short-ranged. As the delta interaction can be understood as a boundary condition in the relative coordinates so can the fermionic interaction. For the bosonic side, exchange symmetry plus delta interaction demands continuity of the wave function and a specifically related discontinuity in the derivative at vanishing distance (the collisional boundaries of $\mathcal{F}_N$). In contrast to that, for the fermionic side, the

effective interaction imposes continuity in the derivative of the wave function combined with a specifically related jump in the wave function itself. This mapping can be directly seen when sign inversion is applied to the bosonic situation on one side of the collisional boundary. As has been shown in [174] the corresponding effective interaction potential can be explicitly given as the limit of a series of three infinitely close delta potentials where the coupling parameter α of the bosonic delta interaction appears in a reciprocal manner, so that the effective fermionic interaction vanishes in the hard-core limit $\alpha \to \infty$.

The main consequence of this generalized mapping is that a strongly interacting bosonic theory can be considered as a weakly interacting fermionic one, where the truncation to a single interaction event at a time (first-order QCE) applies. The new ingredient one needs is then the second-order Ursell operator $\tilde{U}^{(2)}$ (or equivalently the interacting part $\Delta\tilde{K}^{(2)}$ of the propagator) for two distinguishable particles being subject to the effective interaction. In the following, I will show how general, rather abstract, considerations allow to fully relate the effective two-body propagator back to the bosonic one.

The strong coupling cluster expansion

The analysis given here is a review of the one given in [157]. Here, I will refer to the effective attractive point-like interaction for fermions simply as the anti-delta interaction. For the purpose of describing it within the QCE it suffices to know the two-body propagator of distinguishable particles in free space $\Omega = \mathbb{R}$ with mutual anti-delta interaction. This corresponds to the (local) short-time analysis where global boundary conditions (like periodicity on a circle or hard walls) are neglected. For the current purpose it suffices to consider the case of $N = 2$ particles exclusively, thus the superscript $^{(2)}$ is omitted throughout this subsection. First, for any two-body propagator K on $\mathbb{R}^2$ I define the swapping operation denoted by $\bar{K}$ as

$$\overline{K}((q_1', q_2'), (q_1, q_2); t) = \begin{cases} K((q_1', q_2'), (q_1, q_2); t) & \text{for } (q_1 - q_2)(q_1' - q_2') \geq 0, \\ -K((q_1', q_2'), (q_1, q_2); t) & \text{for } (q_1 - q_2)(q_1' - q_2') < 0\,, \end{cases} \tag{1.186}$$

which gives a relative sign inversion when the two particles have to cross each other along any classical path from (q_1, q_2) to (q_1', q_2') and therefore changes the symmetry class of K. A propagator that is symmetric under particle exchange (*e.g.*, in its final configuration) becomes antisymmetric under (1.186) and vice versa. Now consider the interacting propagator K of two distinguishable particles subject to the δ-interaction. It is built from its symmetric part K_+ and its antisymmetric part K_- *w.r.t.* to particle exchange,

$$K = K_+ + K_-\,, \tag{1.187}$$

where $K_+(K_-)$ are determined by restriction of the time-evolution operator to symmetric(antisymmetric) eigenfunctions $\psi_\pm(R, r)$ of the two-body system, and R, r denote center-of-mass and relative coordinates, respectively. The delta interaction only has an effect on the symmetric wave functions $\psi_+(R, r)$, whereas the antisymmetric ones are unaffected $\psi_-(R, r) = \psi_{0,-}(R, r)$, thus we write

$$K_+ = K_{0,+} + \Delta K_\alpha\,, \tag{1.188}$$

$$K_- = K_{0,-}\,, \tag{1.189}$$

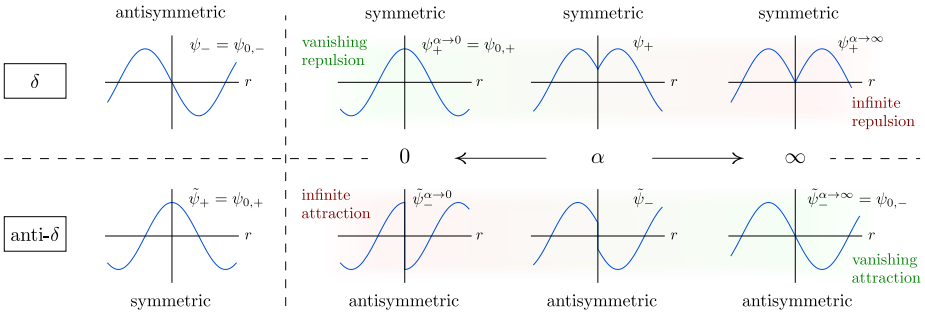

Fig. 1.18: Representative wave functions in the relative coordinate r for two distinguishable particles with delta interaction (upper row) and anti-delta interaction (lower row), respectively. While the antisymmetric, respectively symmetric wave functions are unaffected by the interaction (left), the effect on the functions of complementary symmetry ranges from vanishing to infinitely strong repulsion and attraction, respectively (right). The conditional sign inversion (1.191) maps between the effects of delta and anti-delta interaction (right). While delta interactions have vanishing effect for $\alpha \to 0$, the anti-delta case becomes non-interacting for $\alpha \to \infty$.

where $K_{0,\pm}$ denotes the (anti-)symmetric part (1.25) of the non-interacting propagator and ΔK_α the modification to the symmetric part due to finite interaction.

For the anti-delta interaction (which will be denoted by a tilde) one has unaffected symmetric wave function

$$\tilde\psi_+(R,r) = \psi_{0,+}(R,r)\,, \tag{1.190}$$

whereas the antisymmetric wave functions $\tilde\psi_-(R,r)$ feel the interaction in form of a jump discontinuity at vanishing relative distance r of the particles. Because of the exact mapping, those antisymmetric wave functions are equivalent with the symmetric ones for the delta interaction with a conditional sign-inversion

$$\tilde\psi_-(R,r) = \mathrm{sign}(r)\psi_+(R,r)\,. \tag{1.191}$$

By this construction one manages to have the exact mapping between delta-interacting bosons and anti-delta-interacting fermions that at the same time guarantees that the anti-delta interaction vanishes for $\alpha \to \infty$ also for distinguishable particles and not only for fermions. The mutual relations are depicted in Fig. 1.18 by sketching examples of wave functions showing also the disappearance and infinite enhancement of the two types of interactions in the respective limits. The identity (1.190) and the sign-inversion (1.191) in the wave functions are then reflected in the propagator $\tilde K$ of two distinguishable particles with anti-delta interaction through its (anti-)symmetric parts

$$\begin{aligned} \tilde K_+ &= K_{0,+}\,, \\ \tilde K_- &= \overline{K}_+ = \overline{K}_{0,+} + \overline{\Delta K}_\alpha\,, \end{aligned} \tag{1.192}$$

as

$$\tilde K = K_{0,+} + \overline{K}_{0,+} + \overline{\Delta K}_\alpha\,. \tag{1.193}$$

For first-order QCE calculations one needs then only the modification $\Delta\tilde{K}_\alpha$ of the propagator due to anti-delta interaction, thus we write

$$\begin{aligned}\tilde{K} &= K_0 + \Delta\tilde{K}_\alpha \\ &= K_{0,+} + K_{0,-} + \Delta\tilde{K}_\alpha\,,\end{aligned} \tag{1.194}$$

and obtain the final result

$$\Delta\tilde{K}_\alpha = \overline{K}_{0,+} + \overline{\Delta K}_\alpha - K_{0,-}\,, \tag{1.195}$$

which is a fully antisymmetric propagator *w.r.t.* particle exchange (in one of the configurations – initial *or* final). A simple test of this result can be done in the limit $\alpha \to \infty$ where the symmetric propagator for delta interaction becomes just the swapped version of the free antisymmetric propagator

$$K_{0,+} + \Delta K_\alpha \xrightarrow[\alpha\to\infty]{} \overline{K}_{0,-}\,, \tag{1.196}$$

so that

$$\Delta\tilde{K}_\alpha \xrightarrow[\alpha\to\infty]{} 0\,, \tag{1.197}$$

which means the fermionic theory is non-interacting in this limit, confirming the full fermionization effect.

Using the relation (1.195) in the calculation of the corresponding QCE diagrams involved in the cluster contribution $\tilde{A}_{(n_1,n-n_1)}(s)$ for the fermionic theory one gets then a replacement of the damping factors $a_{n_1,n_2} \mapsto \tilde{a}_{n_1,n_2}$ given by (see (1.158) for comparison)

$$\begin{aligned}\tilde{a}_{n_1,n_2}(s) = &-\frac{2}{\pi}\frac{\bar{\nu}}{1+\bar{\nu}^2} - \frac{2\bar{\nu}^2}{\sqrt{\pi(1+\bar{\nu}^2)}}\sqrt{s} \\ &+ \frac{2}{\sqrt{\pi}}\bar{\nu}\sqrt{s}\mathrm{e}^s\,\mathrm{erfc}(\sqrt{s}) + \frac{2}{\sqrt{\pi}}(1+2\bar{\nu}^2 s)F_{\bar{\nu}}(s)\end{aligned} \tag{1.198}$$

and consequently the replacement of coefficient functions $g_l(E) \mapsto \tilde{g}_l(E)$ in the energy representation given by the contributions (see section 1.3.2 for comparison)

$$\begin{aligned}\tilde{b}_1^{(l)}(\epsilon) &= -\frac{2}{\pi}\frac{\bar{\nu}}{1+\bar{\nu}^2}\frac{\theta(\epsilon)}{\Gamma(\frac{l}{2}+1)} - \frac{2\bar{\nu}^2}{\sqrt{\pi(1+\bar{\nu}^2)}}\frac{\theta(\epsilon)}{\Gamma(\frac{l}{2}+\frac{1}{2})\sqrt{\epsilon}}\,, \\ \tilde{b}_2^{(l)}(\epsilon) &= -b_2^{(l)}(\epsilon)\,, \\ \tilde{b}_3^{(l)}(\epsilon) &= b_3^{(l)}(\epsilon)\,, \\ \tilde{b}_4^{(l)}(\epsilon) &= -b_4^{(l)}(\epsilon)\,,\end{aligned} \tag{1.199}$$

which can then be used in (1.160) and (1.141) together with the non-interacting fermionic coefficients

$$z_{-,l}^{(n)} = (-1)^{n-l} z_{+,l}^{(n)} \tag{1.200}$$

to get the corresponding counting functions in the fermionization regime.

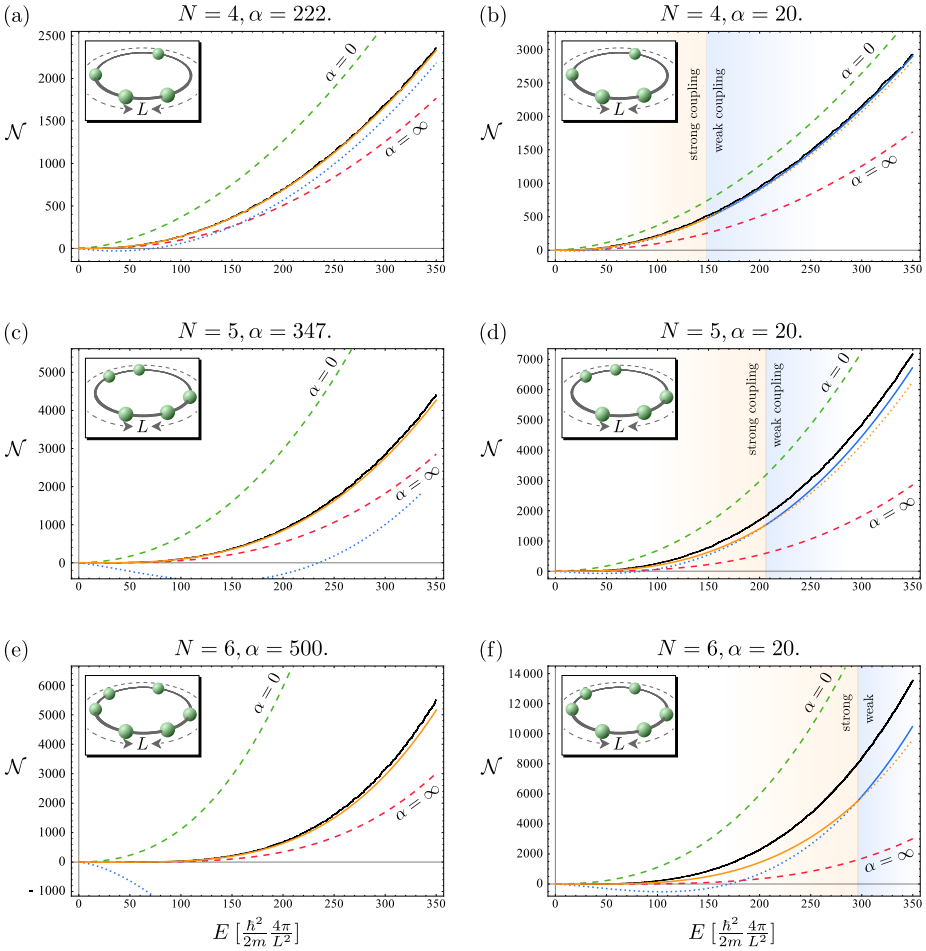

Fig. 1.19: Counting function of the exact many-body energies (black staircase) in the Lieb-Liniger model with (top to bottom) $N = 4, 5$ and 6 bosons for various interaction strengths α. left: (a),(c),(e) strong coupling regime with $\alpha = 222., 347., 500.$ chosen such that $N^2/\alpha \approx$ const over the three plots. right: (b),(d),(f) intermediate coupling regime with $\alpha = 20$. The corresponding analytic functions (1.141) either given by the (effective fermionic) first-order strong-coupling QCE (orange) with the explicit form given by (1.199) used together with (1.160) and (1.200) or the direct first-order QCE (blue) for weak couplings with the explicit form given in section 1.3.2. The non-interacting QCE (1.50) for bosons (dashed green) and fermions (dashed red) pose the universal bound (on average) for the exact levels corresponding to the limits $\alpha = 0$ and $\alpha \to \infty$, respectively. The weak- and strong-coupling QCE curves are plotted solid in the regimes where they are of superior quality and dotted where they are of inferior quality compared to the other cluster expansion, respectively. Coupling strengths α are given in units of $\rho_0^{-1} = \frac{\hbar^2}{2m}\frac{L^2}{4\pi}$.

Application

Figure 1.19 shows the counting functions calculated by exact numerics in the Lieb-Liniger model in direct comparison with first-order QCE calculations in the standard (weak-coupling) expansion and the strong-coupling expansion, which corresponds to the effective fermionic theory by the mapping described in the previous subsections. Since the effective fermionic attractive anti-delta interaction vanishes in the limit $\alpha \to \infty$, the generic scaling consideration state that the description within strong-coupling QCE should become more accurate for *low energies* in contrast to the weak-coupling expansion. In other words, at the lower end of the spectrum the bosons effectively behave like non-interacting fermions, while the influence from the anti-delta interaction increases with energy. At some point the description by the weak-coupling expansion becomes superior in quality and then increases monotonously in quality for growing energy. I allow myself to use this distinction to define the weak- and strong-coupling regimes. Like the first-order weak-coupling expansion, also the first-order strong-coupling expansion systematically underestimates the average universal value of the counting function[12]. Therefore the point where both analytic curves cross each other defines the border between weak- and strong-coupling regime. This border between the two regimes is the point where the overall description by first-order QCE reaches its minimum in quality. The further one moves away from this intermediate coupling regime the better the respective description becomes. One could even think of the graphs of the weak- and strong-coupling QCE as asymptotes of the counting function of the true averaged (or universal part of) the spectrum. The systematic tendency of underestimating and the take-over between weak- and strong-coupling descriptions enhance the predictive power of the QCE in numerically intractable regimes by posing essential lower bounds for the average spectral density, whereas an upper bound is given by the ideal bosonic gas described by the non-interacting QCE.

Furthermore, the strong-coupling extension allows to bypass the complete breakdown of the (weak-coupling) QCE to first order in the regime of strong couplings and low energies especially present for "larger" numbers of particles (see, *e.g.*, the fail of the bosonic QCE in the shown regime of Fig. 1.19). An accurate description in the intermediate coupling regime for $N \gtrsim 6$ still stays out of reach of the first-order approximation. A method addressing the intermediate regime is presented in section 1.5.2.

Figure 1.20 shows the application of the strong coupling expansion to the mechanical equation of state in the Lieb-Liniger model is shown. The result is a strong increase in the quality of the description in the universal regime $L \gtrsim \lambda_{\mathrm{T}}$ for larger repulsions. The non-universality in the condensation regime of this model naturally stays badly described by the QCE, because it is dominated by system specific behavior related to the spectral discreteness. However, this is not in contradiction to the statement – based on the general dimensional scaling

[12]This underestimation is expected to be a rigid feature when changing the number of particles, coupling strengths and even external potentials. The reason is that one can think of it as depending on the sign of next-to-leading order corrections to the first-order QCE. Given by the coefficient of V_D^{N-2} those involve pairs of interacting two-body clusters and a three-body cluster. Since these terms contribute to the same order of V_D, the sign of their sum should be unaffected by N or the system size and even homogeneous external potentials as those will later show to correspond to replacement of dimensionality and system size by effective quantities only (see section 1.4.2).

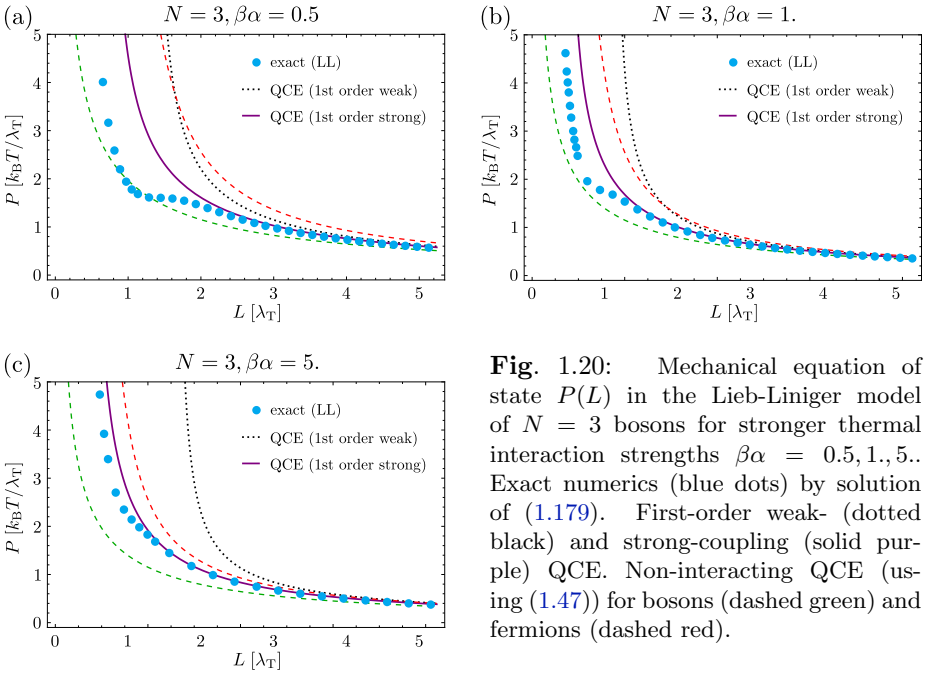

Fig. 1.20: Mechanical equation of state $P(L)$ in the Lieb-Liniger model of $N = 3$ bosons for stronger thermal interaction strengths $\beta\alpha = 0.5, 1., 5.$. Exact numerics (blue dots) by solution of (1.179). First-order weak- (dotted black) and strong-coupling (solid purple) QCE. Non-interacting QCE (using (1.47)) for bosons (dashed green) and fermions (dashed red).

considerations – that the first-order approximation in the strong-coupling expansion becomes better and better when going to lower temperatures, since it is only a statement about universal features. Nevertheless, the strong-coupling cluster expansion in this context only makes sense down to $L \approx \lambda_T$ as well, because in this regime even the non-interacting fermionic universal pressure diverges. The reason is that the exact partition function becomes extremely small-valued, which is represented in the cluster expansion by spurious, extremely small but noticeable oscillations around zero analogous to the ones observed on fermionic DOS (see Fig. 1.7 and discussion). A zero in the partition function produces a pole in the pressure.

So far one can consider the QCE in the regime of ultra-low temperatures $L \lesssim \lambda_T$ as being dominated by artifacts rendering it meaningless. A method addressing system specific discreteness effects in combination of the universal description through the QCE is presented in section 1.5.1.

1.4.2 Harmonic confinement and other external potentials

Eikonal approximation with interactions

Similar to the non-interacting case (see section 1.1.5) the inclusion of smooth external potentials $\sum_{j=1}^{N} U_{\text{ext}}(\mathbf{q}_j)$ is here boiled down to the eikonal approximation for fully interacting (distinguishable) propagators $K^{(N)}$. Considering the system as an effective (ND)-dimensional system of a single particle allows

for including U_{ext} by standard eikonal approximation as

$$K^{(N)}(\mathbf{q}^{\text{f}},\mathbf{q}^{\text{i}};t) \approx K^{(N)}_{\text{int}}(\mathbf{q}^{\text{f}},\mathbf{q}^{\text{i}};t)\exp\left[-\frac{\mathrm{i}t}{\hbar}\int_0^1 \mathrm{d}s\ \sum_{j=1}^{N} U_{\text{ext}}\big((\mathbf{q}^{\text{f}}_j-\mathbf{q}^{\text{i}}_j)s+\mathbf{q}^{\text{i}}_j\big)\right], \tag{1.201}$$

where

$$K^{(N)} \xrightarrow[U_{\text{ext}}\to 0]{} K^{(N)}_{\text{int}} \tag{1.202}$$

is the fully interacting distinguishable N-particle propagator neglecting the external potential, which I refer to as the *internal* propagator. The eikonal approximation (1.201) for the full propagator gets then inherited by the Ursell operators in coordinate representation. When $K^{(N)}$ is decomposed into hierarchic interaction effects according to (1.99) within (1.201), each Ursell propagator gets assigned a corresponding phase factor

$$\Delta K^{(n)}(\mathbf{q}^{\text{f}},\mathbf{q}^{\text{i}};t) \approx \Delta K^{(N)}_{\text{int}}(\mathbf{q}^{\text{f}},\mathbf{q}^{\text{i}};t)\exp\left[-\frac{\mathrm{i}t}{\hbar}\int_0^1 \mathrm{d}s\ \sum_{j=1}^{n} U_{\text{ext}}\big((\mathbf{q}^{\text{f}}_j-\mathbf{q}^{\text{i}}_j)s+\mathbf{q}^{\text{i}}_j\big)\right], \tag{1.203}$$

where $\Delta K^{(n)}$ are Ursell operators derived from the full propagators $K^{(\leq n)}$ using (1.101) and $\Delta K^{(n)}_{\text{int}}$ are the resulting expressions when solving the recursion using the *internal* fully interacting propagators $K^{(\leq n)}$.

It is now crucial to recognize that $\Delta K^{(n)}_{\text{int}}(\mathbf{q}^{\text{f}},\mathbf{q}^{\text{i}};t)$ is *strongly peaked*[13] considering short-time dynamics.

In a single irreducible cluster the integrand decomposes into Ursell contributions specified by a index partition $\mathfrak{I} \vdash \{1,\ldots,n\}$ (which is here considered to only involve the n particles of a single cluster) according to (1.109), each of which can then be approximated by (1.203). The corresponding integrand is again strongly peaked in the above sense when

$$\bigwedge_{I\in\mathfrak{I}} (P\mathbf{q}_I = \mathbf{q}_I) \tag{1.204}$$

simultaneously for all $I \in \mathfrak{I}$. Because the cluster is fully connected by permutation and/or Ursell contributions, the condition (1.204) is equivalent to the collision of all constituents

$$\mathbf{q}_1 = \mathbf{q}_2 = \ldots = \mathbf{q}_n\,. \tag{1.205}$$

Under the integral $\int_{\Omega^n} \mathrm{d}^{nD}q$ this condition leaves one coordinate undetermined (I choose q_1) which can be thought of describing the position of the cluster as a whole.

The next steps are similar to the non-interacting case in section 1.1.5 but, instead of applying stationary phase approximation, here all information about $\Delta K^{(n)}_{\text{int}}$ is kept. As an approximation I assume consistently with the short-time focus that for smooth enough potentials the integrand decouples. The smoothly

[13] It is peaked in the sense of smearing out coordinates, because the "peak" usually shows up as a stationary phase rather than a maximum in amplitude. Alternatively one can switch to imaginary time (or thermal description), where the corresponding heat kernels $K(\mathbf{q}^{\text{f}},\mathbf{q}^{\text{i}};-\mathrm{i}\hbar\beta)$ are then literally peaked in amplitude.

varying exponential containing information about the external potential thereby gets evaluated at the peak (1.205) and therefore depends only on the single coordinate $\mathbf{q}_1$. In contrast to that, the internal strongly peaked part that contains all the information about the exchange and interaction effects in the cluster structure does not depend on $\mathbf{q}_1$ at all. It is invariant under simultaneous translation of all constituents since it is deduced from $K_{\mathrm{int}}^{(n)}$. Neglecting any external potential corresponds to assuming homogeneity of space.

Similar to the LPA without interaction (see section 1.1.5) the physical interpretation is that as far as concerns the influence of smooth external potentials the cluster can be regarded as a single particle feeling the n-fold potential at a single point $\mathbf{q}_1$ in space. This is consistent with the short-time philosophy of the QCE since for short times the relevant spread of the cluster is small compared to the scale of variations in the external potential.

The local potential approximation with interactions

The analysis in this subsection partially coincides with the one I have given in the supplemental material of [157]. As in the section on universal scaling properties of the QCE without external potential (see section 1.2.5) we switch to the thermal description in terms of the inverse temperature β using notation as in (1.126). The assumption of cluster-wise locally constant potentials separates the amplitude (1.130) as

$$\mathcal{A} = \mathcal{A}_{\mathrm{int}}\mathcal{A}_{\mathrm{ext}}\,. \tag{1.206}$$

On the one hand one gets an *internal part*

$$\mathcal{A}_{\mathrm{int}} = \lambda_{\mathrm{T}}^{D}\int \mathrm{d}^{D}q_2\ldots\mathrm{d}^{D}q_n\;\Delta K_{\alpha,\mathrm{int}}^{\mathfrak{J}}(P(\mathbf{0},\mathbf{q}_2,\ldots,\mathbf{q}_n),(\mathbf{0},\mathbf{q}_2,\ldots,\mathbf{q}_n);\beta)\,, \tag{1.207}$$

that has one of the coordinates fixed, while one extends the integration over the others to infinity. The internal part does not feel any external potential and yields exactly the same integral $\mathcal{I}(\beta\alpha,P,\mathfrak{J})$ as in (1.131) when applying the generic scaling (1.129).

The *external part* on the other hand is

$$\mathcal{A}_{\mathrm{ext}} = \int \mathrm{d}^{D}q_1 K_{\mathrm{ext},n}^{(1)}(\mathbf{q}_1,\mathbf{q}_1;\beta)\,, \tag{1.208}$$

which corresponds to a single particle feeling the n-fold external potential. The short-time effect of the external potential is thereby considered as a locally constant energy shift

$$K_{\mathrm{ext},n}^{(1)}(\mathbf{q}_1,\mathbf{q}_1;\beta) \simeq \lambda_{\mathrm{T}}^{-D}\mathrm{e}^{-\beta n U_{\mathrm{ext}}(\mathbf{q}_1)}\,. \tag{1.209}$$

In general, applying the universal scaling considerations (see section 1.2.5) to the external potential one finds that

$$\mathcal{A}_{\mathrm{ext}} = n^{D/2}\xi(\sqrt{n\beta\alpha_{\mathrm{ext}}}) \tag{1.210}$$

with a dimensionless function ξ and the strength of the external potential characterized by a energy-like parameter α_{ext}. As in the non-interacting LPA a special role is taken by homogeneous external potentials (1.71) for which

$$\mathcal{A}_{\mathrm{ext}} = \left(n^{-d/2}\frac{V_{\mathrm{eff}}}{\lambda_{\mathrm{T}}^{d}}\right)n^{D/2}\,, \tag{1.211}$$

with the same definitions (1.73) of effective dimension d and effective volume V_{eff}.

In total, within the LPA, the contribution (1.130) from a specific cluster in homogeneous external potentials has the form

$$A_{\mathfrak{C}}(\alpha,\beta) = n^{-d/2}\frac{V_{\text{eff}}}{\lambda_{\text{T}}^{d}}a_{\mathfrak{C}}(\beta\alpha)\,, \tag{1.212}$$

where the internal cluster structure $\mathfrak{C}$ does not depend on any system parameters and the dependence on the interaction is again completely absorbed into the (local) damping factors $a_{\mathfrak{C}}$ that are exactly the same as in the corresponding system without external potential.

The full QCE expressions (1.134) and (1.140) from generic scaling are therefore still applicable where the LPA demands the replacement $D \mapsto d, V_D \mapsto V_{\text{eff}}$ by effective parameters all around. The final expression for the partition function in LPA is

$$Z_{\pm}^{(N)}(\beta) = \sum_{l=1}^{N}[z_{\pm,l}^{(N,d)} + \Delta z_{\pm,l}^{(N,d)}(\beta\alpha)]\left(\frac{V_{\text{eff}}}{\lambda_T^d}\right)^{l}. \tag{1.213}$$

and correspondingly

$$P_{\text{eff}}(V_{\text{eff}},\beta,N,\alpha) = \frac{k_{\text{B}}T}{V_{\text{eff}}}\frac{\sum_{l=1}^{N} l[z_{\pm,l}^{(N,d)} + \Delta z_{\pm,l}^{(N,d)}(\beta\alpha)]\left(\frac{V_{\text{eff}}}{\lambda_{\text{T}}^{d}}\right)^{l}}{\sum_{l=1}^{N}[z_{\pm,l}^{(N,d)} + \Delta z_{\pm,l}^{(N,d)}(\beta\alpha)]\left(\frac{V_{\text{eff}}}{\lambda_{\text{T}}^{d}}\right)^{l}}\,, \tag{1.214}$$

where the (effective) pressure has to be understood as the intensive thermodynamic dual of the effective volume V_{eff}. The literal interpretation as pressure has sense for confining homogeneous potentials U_{ext} since V_{eff} is proportional to the D-volumes enclosed by equipotential surfaces. In the spectral representation the generic expressions in LPA are

$$\bar{\rho}_{\pm}^{(N)}(E) = \rho_0^{\text{eff}}\sum_{l=1}^{N}\left[\frac{z_{\pm,l}^{(N,d)}}{\Gamma\left(\frac{ld}{2}\right)} + f_{\pm,l}^{(N,d)}\left(\frac{E}{\alpha}\right)\right](\rho_0^{\text{eff}}E)^{\frac{ld}{2}-1}\theta(E)\,, \tag{1.215}$$

for the many-body DOS and

$$\bar{\mathcal{N}}(E) = \sum_{l=1}^{N}\left[\frac{z_{\pm,l}^{(N,d)}}{\Gamma\left(\frac{ld}{2}+1\right)} + g_{\pm,l}^{(N,d)}\left(\frac{E}{\alpha}\right)\right](\rho_0^{\text{eff}}E)^{\frac{ld}{2}}\theta(E)\,. \tag{1.216}$$

for the corresponding counting function with the effective unit of density ρ_{eff} given by (1.76). The non-interacting coefficients [given by (1.74)] appearing in all the LPA expressions (1.213), (1.214), (1.215) and (1.216) are adjusted to the effective dimension as well. In case of first-order QCE in one dimension also the functions (1.161) building up the coefficient functions (1.160) have to be modified to the effective dimension according to

$$g_{\pm,l}^{(N,d)}(\epsilon) = \sum_{n=2}^{N-l+1} n^{-\frac{d}{2}} z_{\pm,l-1}^{(N-n,d)} \sum_{n_1=1}^{n-1} b_{\bar{\nu}}^{(ld)}(\epsilon)\,, \tag{1.217}$$

Again, as in the LPA without interactions, the case of zero external potential is included as $d = D$ and $V_{\text{eff}} = V_D$.

One has to stress one point. The given QCE formalism in LPA enables a very important application – especially when making contact with experimental realizations: Realistic external confinement potentials can now be applied. In exact treatments this makes a most *significant difference*, generically rendering *solvable* systems in the presence of contact interactions *non-soluble*. In contrast, the straight-forward consistent implementation in QCE comes as a *slight modification*, maintaining all the general, convenient analytical properties of the framework.

Application to harmonically confined contact-interacting bosons

A special role within the class of homogeneously scaling external potentials is taken by harmonic confinements $U_{\text{ext}}(q) = m\omega^2 q^2/2$ in one dimension especially when combined with contact interactions. This case has an effective dimension of $d = 2$, an effective (two-dimensional) volume $V_{\text{eff}} = 2\pi\hbar/(m\omega)$ and a corresponding effective single-particle density $\rho_0^{\text{eff}} = 1/\hbar\omega$. There are basically three reasons why this type of system is exceptional for applications of the QCE.

First, it is of particular experimental relevance, since cold neutral atoms in traps are usually realized by harmonic trapping potentials. In elongated traps the transversal frequencies exceed the longitudinal one by orders of magnitude. At low temperatures the transversal motion is frozen out, leaving quasi-one-dimensional systems where the harmonic trapping in longitudinal direction is still noticeable by the physics as such.

Second, the cluster expansion in spectral representation is especially tractable in this case. This is because the effective dimension $d = 2$ is an integer, so that all coefficient functions $f_l(E/\alpha)$ and $g_l(E/\alpha)$ are built by the analytically explicit expressions $b^{(2l)}$ [see (1.217), (1.161) and following]. The derivation of these functions heavily depends on a recursion demanding integer superscripts. In contrast to that, I do here not provide analytic expressions for non-integer d.

Third, including a harmonic confinement transforms the solvable Lieb-Liniger model into a non-integrable system without analytic solution (if $N > 2$). This poses a great opportunity to demonstrate one of the great strengths of the QCE as a theory that does not distinguish between integrable and non-integrable systems. In a sense, it boils down the properties of a system exactly so much that one recovers analytic solvability in its universally accessible information. This is the point where the QCE becomes a predictive tool, where exact numeric solutions are extremely exhaustive in computation time and are strongly restricted to a small number of particles and computed excitations.

Figure 1.21 shows the comparison of the first-order QCE with the numerically calculated lowest levels in a system of $N = 3$ and $N = 4$ bosons with contact interaction in a harmonically confined trapping potential. By application of the strong-coupling QCE in LPA for the stronger couplings one gets full agreement in the whole range of interaction strengths $\alpha \geq 0$. The numerical calculation of exact levels is based on an exact diagonalization with a truncation of the single-particle eigenbasis of the harmonic oscillator. The point-like character of the contact interaction thereby poses a strong complication. Consider the Fourier decomposition of the delta potential, which contains all momenta (or wavenumbers) with equal strength. If one similarly decomposes single-particle wave functions into momentum modes this means that the interaction couples two particles with arbitrary momenta with the same strength disregarding how

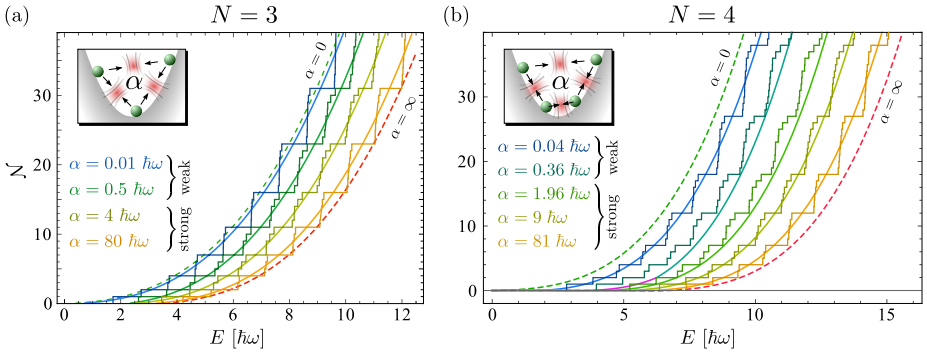

Fig. 1.21: Counting function of the exact many-body energies of (a)$N = 3$ and (b)$N = 4$ harmonically trapped bosons (staircase) with repulsive contact interaction of varying strengths α. Corresponding analytic functions given by the QCE in LPA (solid) applied either as weak- or as strong-coupling expansion. For the case $N = 4, \alpha = 0.36\hbar\omega$ the QCE changes from strong- (purple) to weak-coupling (dark turquoise) at $E \approx 6.23\hbar\omega$. The non-interacting QCE (1.50) for bosons (dashed green) and fermions (dashed red) pose the universal bound (on average) for the exact levels corresponding to the limits $\alpha = 0$ and $\alpha \to \infty$, respectively.

far the momenta are separated. Similarly, when decomposing in the eigenbasis of the harmonic oscillator, single-particle states of very different quantum number are strongly coupled. In other words, highly excited modes in the single-particle basis are needed to resolve the true nature of the delta interaction potential, which makes a pure truncation of single-particle modes inapplicable. The numerical calculations presented here in the context of contact interactions in harmonically confined systems circumvent this complication by an effective interaction potential approach that has been used as a tool in a similar way previously (see [175] for the original context of nuclear interactions, and, *e.g.*, [176] for an application in one dimension with contact interactions). In a sense, the two-body interaction potential gets altered to partially compensate for the deficiency in exact diagonalization due to truncation of the basis. This is achieved by virtue of the exact solution of two contact-interacting bosons in a harmonic oscillator potential [177]. The ansatz is, given a specific truncation of single-particle modes, to modify the finite two-body interaction matrix (represented in the truncated harmonic oscillator basis) in a ways that the correct two-body eigenenergies and (finite truncations of the) two-body eigenstates are obtained in the $N = 2$-system by construction. The so-obtained effective two-body interaction matrix is then used as mutual interaction in a larger system with $N > 2$. This way one partially compensates for the deficiency in describing point-like structures in truncated Hilbert spaces. In the case $N = 2$, the deficiency is even set to zero. The trade-off of this modification is that one looses some amount of control because the approximate N-body eigenenergies are not guaranteed to pose an upper bound for the actual exact spectra. On the other hand, when one increases the cutoff, one observes fast convergence of calculated levels. The dependence of the calculated many-body levels with the cutoff then serves as an estimation of the residual error. The calculations presented in this chapter are all converged to virtually imperceptible error within the scale of the shown plots, hence the absence of error bars.

To close this section, one can emphasize again that due to the LPA the first order QCE becomes a predictive tool in regimes of weak an strong coupling for "larger" numbers of particles $N \gtrsim 8$. Also the prediction of the universal part of whole spectra up to arbitrarily large energies is a remarkable feature. For larger particle numbers, the quality of the QCE in describing intermediate interactions still lacks accuracy. In section 1.5.2 an approximate method to address arbitrary coupling strengths and numbers of particles will be presented.

1.4.3 Multiple species – Spins, Gaudin-Yang model and dynamical impurities

In this section the set of systems addressable by first-order QCE gets extended to the case of multiple particle species (s in number) with individually fixed number of particles $N_1, \ldots, N_s$. Each species thereby consists of indistinguishable particles that can be either (spinless) bosons or fermions while any two different species are distinguishable from each other. Mutual interactions are further allowed to be present within each species and between particles of different species. Thereby the coupling strengths may differ for all possible pairs of species.

First-order QCE for multiple species

In first order, only one interaction event takes place at a time. This can either happen within one species (as inter- and also intra-cycle contribution) or between two particles of different species (then only as inter-cycle contribution, since permutations do not mix particles of different species). For this setup the first-order contribution from QCE to the overall partition function can be reduced to

$$\begin{aligned}\Delta Z^{(N_1,\ldots,N_s)}_{\sigma_1,\ldots,\sigma_s} &= \sum_{i=1}^{s} \Delta Z^{(N_i)}_{\sigma_i} \prod_{j\neq i} Z^{(N_j)}_{0,\sigma_j} \\ &+ \sum_{i<j} \sum_{n_i=1}^{N_i} \sum_{n_j=1}^{N_j} \sigma_i^{n_i-1} \sigma_j^{n_j-1} \mathcal{A}^{\text{inter}}_{n_i,n_j} \left[Z^{(N_i-n_i)}_{0,\sigma_i} Z^{(N_j-n_j)}_{0,\sigma_j} \prod_{k\neq i,j} Z^{(N_k)}_{0,\sigma_k} \right] ,\end{aligned} \tag{1.218}$$

by exploiting the combinatorial properties of the symmetric groups S_{N_i} involved for each individual species. The non-interacting part is the product

$$Z^{(N_1,\ldots,N_s)}_{0,\sigma_1,\ldots,\sigma_s} = \prod_{j=1}^{s} Z^{(N_j)}_{0,\sigma_j} \tag{1.219}$$

of individual species. The $\sigma_i = \pm 1$ in (1.218) and (1.219) reflect the quantum statistics within species i. In the given general form, (1.218) is valid for arbitrary short-ranged interactions addressable with the QCE approach using (1.119). The interaction-related two-body information then finds its way into (1.218) through the diagrammatic calculation of $\mathcal{A}^{\text{inter}}_{n_1,n_2}$ and $\mathcal{A}^{\text{intra}}_{n_1,n_2}$ (see Fig. 1.13) depending on the interacting part of the propagator of two particles living in free space and being subject to the specific interactions.

In the case of delta interactions, expression (1.158) with (1.212) can be used in (1.218). Special care has to be taken if some of the particle species are

allowed to differ in mass. Then one has to take care of the correct masses m_i in all calculations. This is done by substituting the corresponding thermal de Broglie wavelength $\lambda_{\mathrm{T}} \to \lambda_{\mathrm{T}}^i$ in all expressions involving only one species i on the one hand. I denote the modified quantities with a tilde and one finds the two trivial substitutions

$$\begin{aligned} \tilde{Z}_{0,\sigma_i} &= Z_{0,\sigma_i}|_{\lambda_{\mathrm{T}} \to \lambda_{\mathrm{T}}^i} \,, \\ \Delta\tilde{Z}_{\sigma_i} &= \Delta Z_{\sigma_i}|_{\lambda_{\mathrm{T}} \to \lambda_{\mathrm{T}}^i} \,, \end{aligned} \tag{1.220}$$

with the corresponding thermal de Broglie wavelength

$$\lambda_{\mathrm{T}}^i = \left(\frac{2\pi\beta\hbar^2}{m_i}\right)^{\frac{1}{2}} . \tag{1.221}$$

On the other hand, the inter-cycle contributions $\mathcal{A}^{\mathrm{inter}}_{n_i,n_j}$ [see (1.154) since inter- and intra-cycle diagrams coincide in value for delta interaction] between two different species i and j have to be altered by the prescription

$$\tilde{\mathcal{A}}^{\mathrm{inter}}_{n_i,n_j} = \left(\frac{M_{ij}}{4\mu_{ij}}\right)^{\frac{1}{2}} \mathcal{A}^{\mathrm{inter}}_{n_i,n_j}\Big|_{\substack{\lambda_{\mathrm{T}} \to \tilde{\lambda}_{\mathrm{T}}^{ij} \\ n \to \tilde{n}_{ij} \\ \bar{\nu} \to \tilde{\bar{\nu}}_{ij}}} , \tag{1.222}$$

where the modified quantities

$$\begin{aligned} \tilde{\lambda}_{\mathrm{T}}^{ij} &= \left(\frac{\pi\beta\hbar^2}{\mu_{ij}}\right)^{\frac{1}{2}} , \\ \tilde{n}_{ij} &= \frac{2m_{ij}^{\mathrm{tot}}}{M_{ij}} , \\ \tilde{\bar{\nu}}_{ij} &= \sqrt{\frac{M_{ij}}{m_{ij}^{\mathrm{tot}}} n_i n_j - 1} , \end{aligned} \tag{1.223}$$

are defined in terms of the reduced and total mass

$$\begin{aligned} \mu_{ij} &= \frac{m_i m_j}{m_i + m_j} , \\ M_{ij} &= m_i + m_j \end{aligned} \tag{1.224}$$

of two representatives of the different species and the total cluster-mass

$$m_{ij}^{\mathrm{tot}} = n_i m_i + n_j m_j \,. \tag{1.225}$$

Naturally, it is also possible to put different interaction-strengths α_{ij} between different species, and so on.

Spin species and the Gaudin-Yang model

An especially interesting case is the one of indistinguishable particles carrying spin under absence of spin-orbit coupling. Then the individual spin-polarizations are conserved and the particles separate into sub-species of specific spin-polarization (magnetic spin quantum number). To put it in another way, the particles

become distinguishable by spin-polarization. The special case of N spin-1/2 fermions with mutual delta interactions and periodic boundary conditions is called the Gaudin-Yang model.

This model, similar to the Lieb-Liniger model, also admits a solution in terms of a Bethe ansatz [35, 36], where the solution involves the group-theoretical aspects of the symmetric group S_N and is constructed in the following way. First one solves a system of N indistinguishable (spinless) particles restricted to a Hilbert sub-space that corresponds to an arbitrary irreducible representation of S_N. These involve the one-dimensional representations of the totally symmetric and totally antisymmetric states (called the trivial and sign-representation, respectively) but also higher-dimensional representations. This includes the solutions of Lieb-Liniger and the ideal periodic Fermi gas (because of Pauli principle) as the trivial and sign-representation, respectively, but non-trivially extends to all other representations. In the setup of spin-1/2 fermions all solutions are then totally antisymmetric *w.r.t.* simultaneous exchange in the orbital and spin-degrees of freedom. Separating the orbital part from the spin part, one searches for all the irreducible representations in the orbital part and combines each with the corresponding (complementary) irreducible representation assigned to the spin wave functions to get the overall sign-representation of totally anti-symmetric states in the tensor product of the orbital and spin part. In the case of a fixed total spin population imbalance $N_\uparrow - N_\downarrow$ (with $N = N_\uparrow + N_\downarrow$ fixed), the enumeration of all combinations of irreducible representations reduces to a second eigenvalue problem which Yang [36] solved by another application of Bethe's hypothesis introducing $N_\downarrow$ *spin-rapidities* λ_i as new variables in addition to the quasi-momenta k_i (without loss of generality one can choose $N_\uparrow \geq N_\downarrow$). This way, one ends up with a system of $N + N_\downarrow$ coupled transcendental complex but algebraic equations for the k_i and λ_i. The corresponding total eigenenergy of the system for one specific solution is then $E = \hbar^2/(2m)\sum_{i=1}^{N} k_i^2$. For repulsive coupling, the quasi-momenta k_i are real as in the solution of the repulsive Lieb-Liniger, but the spin-rapidities λ_i are allowed to be complex, which makes the numerical solution of these equations a lot harder. As an additionally complicating consequence, the solutions cannot be strictly ordered by quantum numbers on the level of the equations in advance to the actual search for the solutions (as in the attractive Lieb-Liniger model).

The Gaudin-Yang model is of equal experimental relevance as the Lieb-Liniger model, since it can be realized by fermionic ultracold atoms in elongated traps in two opposite hyperfine states where contact interaction is again tuned by Feshbach resonance. Further interest in this model is gained when one relaxes the restriction to repulsive interactions. Then one obtains a model that exhibits a non-trivial crossover from weakly-bound Bardeen-Cooper-Schrieffer-like (BCS-like) pairs to tightly bound larger molecules. For an extensive review on the subject of one-dimensional atomic Fermi gases, starting from fundamental theoretical aspects, the description by the Gaudin-Yang model over inherent physical phenomena up to the many experimental realizations, see [160].

In the context of QCE, the universal properties of the Gaudin-Yang model can then be described by the special case $s = 2$ of (1.218) with $N_1 = N_\uparrow, N_2 = N_\downarrow, \sigma_1 = -1, \sigma_2 = -1$. As has been discussed in section 1.3 the effect of delta interactions within a (spinless) fermionic species vanishes (also within first-order), so that the first term on the RHS of (1.218) is zero due to $\Delta Z_-^{(N_\uparrow)} =$

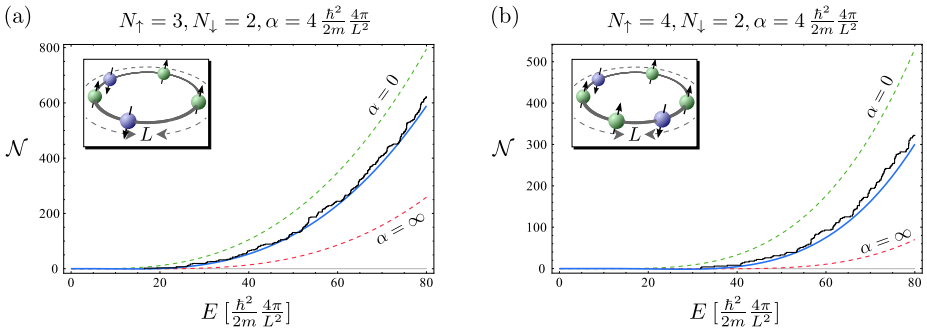

Fig. 1.22: Counting function in the (integrable) Gaudin-Yang model with (a)$N_\uparrow = 3, N_\downarrow = 2$ and (b)$N_\uparrow = 4, N_\downarrow = 2$ particles. Exact analytic solution (black staircase) compared to the first-order QCE (solid blue) obtained from (the inverse Laplace transform) of (1.226). Non-interacting QCE (dashed green) and the (combinatorially corrected) non-interacting QCE of spinless fermions corresponding to the generalized fermionization (1.227) (dashed red).

$\Delta Z_-^{(N_\downarrow)} = 0$. The overall effect of the interactions (in first order) is then given by[14]

$$\Delta Z_{-,-}^{(N_\uparrow,N_\downarrow)} = \sum_{n_\uparrow=1}^{N_\uparrow}\sum_{n_\downarrow=1}^{N_\downarrow}(-1)^{n_\uparrow+n_\downarrow}\mathcal{A}_{n_\uparrow,n_\downarrow}Z_{0,-}^{(N_\uparrow-n_\uparrow)}Z_{0,-}^{(N_\downarrow-n_\downarrow)}\,, \tag{1.226}$$

using the amplitude (1.158), (1.212) for delta interaction and the non-interacting partition functions (1.74). As a side remark, I note that by using the LPA with $D \mapsto d = 2$ and $V_D \mapsto V_{\text{eff}} = 2\pi\hbar/(m\omega)$, the QCE calculation (1.226) can easily be transfered to the non-integrable and non-solvable model of contact-interacting spin-1/2 fermions in a harmonic quasi-one-dimensional trap. A comparison with the integrable Gaudin-Yang model is shown in Fig. 1.22. The hardcore limit of $\alpha \to \infty$ in the Gaudin-Yang model corresponds to a generalized fermionization effect between the distinguishable spin-up and spin-down fermions. In the sense of isospectrality (1.184), as found in bosonic systems, the system becomes equivalent to a system of non-interacting spinless (or fully spin-polarized) fermions

$$Z_{-,-}^{(N_\uparrow,N_\downarrow)} \xrightarrow[\alpha\to\infty]{} \frac{N!}{N_\uparrow!N_\downarrow!}Z_{0,-}^{(N)}\,, \tag{1.227}$$

up to a purely combinatorial global factor (in the partition function and therefore also in the DOS and counting function) that accounts for the fact that the particles of different spin are still distinguishable from each other. On the level of exact spectra this factor has to be understood as a degeneracy of each (non-interacting) many-body level corresponding to the distribution of the N different occupied orbital single-particle modes on the two sets of $N_\uparrow$ and $N_\downarrow$ spin-states.

[14]There is an alternative way on the level of the cluster expansion that uses the above mentioned decomposition into combined irreducible representations related to spin and orbital degrees of freedom not shown here because of the limited scope. In the sum over irreducible representations the group characters have then to taken into account. It can then be shown that this group theoretical approach is equivalent to the presented formulation in terms of two distinguishable spinless fermionic species.

The dynamical impurity model

Another interesting case included in the class of periodic one-dimensional multiple-species systems with contact interactions is given by the dynamical impurity model. This model describes a number of non-interacting indistinguishable fermions each of which interacts point-like with just *one* additional particle that can be considered as a mediator of indirect mutual interactions. Similarly this additional particle can be considered as an impurity on which the non-interacting particles can scatter individually and that can move dynamically rather than having a fixed position, hence the name of the model. There are two distinct cases of the dynamical impurity model. First, if the mass of the impurity m_{I} coincides with the other masses m, the model is solvable and integrable [178] and corresponds to a Gaudin-Yang model with maximum spin-imbalance $N_\uparrow = N-1, N_\downarrow = 1$. Second, if the mass of the impurity differs from the rest one obtains a different model without known solution and which exhibits non-integrability regarding level statistics [179]. This offers again a great opportunity for both, testing the QCE for equal masses and using it as a predictive tool for different masses. Once again, because of the focus on universal (or equivalently smooth or short-time) properties, the QCE does not distinguish between integrability and non-integrability. Here, the ratio of the two masses would simply appear as an analytic parameter. What makes this model in this context especially appealing is that the two cases are smoothly connected by the limit $m_{\mathrm{I}} \to m$, offering a system where one could analyze smooth emergence of non-integrability. In this way, one might be able to give better insight on how strongly the amount of non-universality is influenced by integrability in a continuous way, a line of thought I postpone to future work.

Another specialty makes the dynamical impurity model attractive for the application of QCE. No multiple pairs of interacting particles contribute to the full expansion (because of fermionic symmetry) similar to the three-particle Lieb-Liniger model (see Fig. 1.15 and discussion in the Resumée of the embedding subsection). Because of that, the expansion up to first order is expected to catch already most of the interaction effects, making it a potentially accurate tool also for larger numbers of particles.

Figure 1.23 shows the comparison of the spectral density in the integrable (equal masses) dynamical impurity model with the corresponding first-order QCE calculation for in total $N = 7$ particles. Because of the strong increase in the counting function I have chosen a logarithmic plotting (similar to Fig. 1.8). Again, the correspondingly exaggerated artificial oscillations below the ground state energy are not a physical feature and can be considered effectively zero-valued due to their small magnitude. One observes basically full agreement over the whole range of interactions by application of the first-order weak-coupling QCE. This confirms the statement above that due to the absence of multiple pair contributions in the full expansion, the truncation to first order catches most of the interaction effects.

There is yet another reason that makes the dynamical impurity model attractive as it includes a limiting case of essentially different physics. If one considers $m_{\mathrm{I}}/m \to \infty$ one expects to obtain a static impurity, effectively yielding a system of $N-1$ non-interacting particles each of which is under the influence of a scatterer. Unfortunately this decoupling of fermions in the limit of static impurity cannot be shown within the first-order cluster expansion. Nevertheless, for

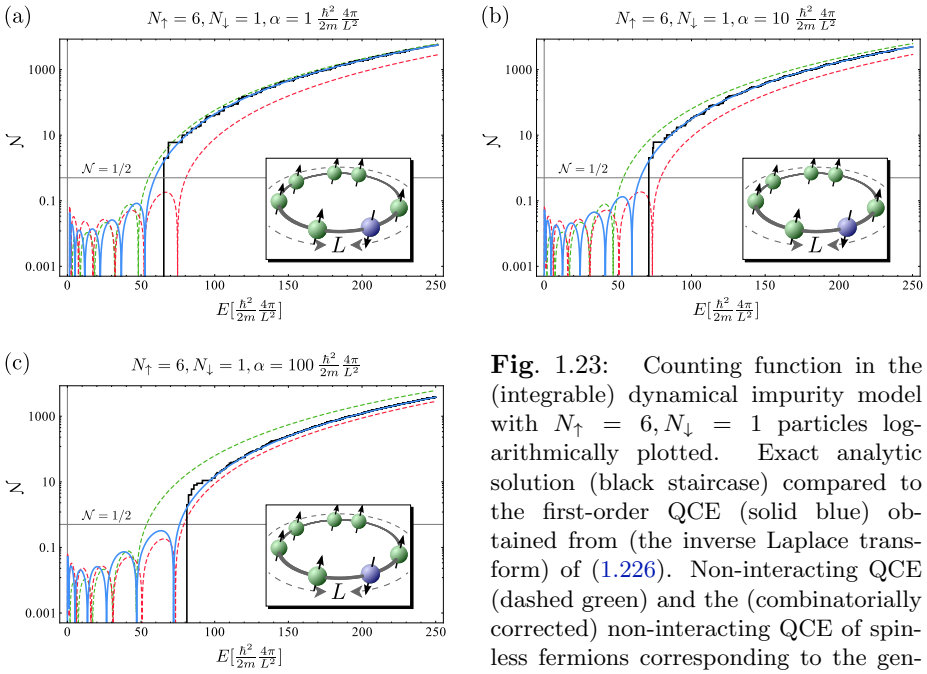

Fig. 1.23: Counting function in the (integrable) dynamical impurity model with $N_\uparrow = 6, N_\downarrow = 1$ particles logarithmically plotted. Exact analytic solution (black staircase) compared to the first-order QCE (solid blue) obtained from (the inverse Laplace transform) of (1.226). Non-interacting QCE (dashed green) and the (combinatorially corrected) non-interacting QCE of spinless fermions corresponding to the generalized fermionization (1.227) (dashed red).

a better understanding of the essence of the first-order expansion, it is worthwhile to deeper investigate the reason for this. From first order (1.226) of a $(N+1)$-dynamical impurity model with unequal masses (see (1.220)–(1.225) for replacements) one gets

$$Z_-^{(N,1)} \overset{\text{first order}}{=} \tilde{Z}_0^{(1)} \underbrace{\left[Z_{0,-}^{(N)} + \sum_{n=1}^{N} (-1)^{n+1} \frac{\tilde{\mathcal{A}}_{n,1}}{\tilde{Z}_0^{(1)}} Z_{0,-}^{(N-n)} \right]}_{\xrightarrow[m_{\mathrm{I}}/m \to \infty]{?} Z_{0,-}^{\prime(N)}} . \tag{1.228}$$

The question would then be to what extent the part in brackets decouples in the sense that it corresponds to a non-interacting (denoted by subscript 0) fermionic (denoted by subscript $-$) system with altered (denoted by a prime) single-particle dynamics. From the case $N = 1$ it is then evident that this altered single-particle system would have to be given by

$$Z_0^{\prime(1)}(\beta) = \operatorname{tr} K^{\prime(1)}(t = -\mathrm{i}\hbar\beta) = Z_0^{(1)}(\beta) + \frac{\tilde{\mathcal{A}}_{1,1}(\beta)}{\tilde{Z}_0^{(1)}(\beta)} , \tag{1.229}$$

corresponding to a *dressing* of the single-particle propagator with the interaction with the impurity (depicted in Fig. 1.24a). The corresponding N-particle partition function of dressed fermions would then be given by the general non-interacting formula (1.45), based on convolutions of single-particle propagators in cycles, which, by virtue of the semigroup property, can be fully expressed in terms of (1.229). A comparison with the first-order QCE expression (1.228)

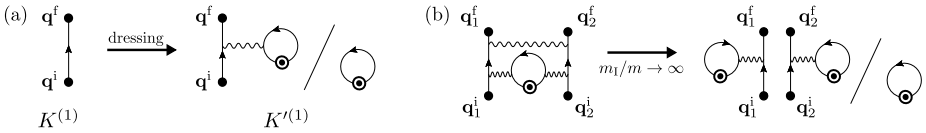

Fig. 1.24: (a) Dressing of the single-particle propagator $K^{(1)}$ with the interaction with the impurity. (b) Static decoupling relation for the three-body interaction effect due to the impurity on the two-body propagator. To distinguish the impurity (which has different mass) from the rest, it is depicted by a bulls eye.

only makes sense up to terms linear in $\mathcal{A}_{1,1}$. After combinatorial manipulations [similar to the derivation of (1.277) – see section 1.5.3] one gets

$$Z'^{(N)}_{0,-}(\beta) = Z^{(N)}_{0,-}(\beta) + \sum_{n=1}^{N}(-1)^{n+1}\frac{\tilde{\mathcal{A}}_{1,1}(n\beta)}{n\tilde{Z}^{(1)}_{0}(n\beta)}Z^{(N-n)}_{0,-}(\beta) + \mathcal{O}\Big(\tilde{\mathcal{A}}^{2}_{1,1}\Big) \quad (1.230)$$

for the N decoupled dressed fermions, which is *not* coinciding with the overall first-order approximation (1.228) if one takes the limit of static impurity. The reason is the following. Although in (1.230) the dressing of single-particle propagators was restricted to only one at a time by expanding up to linear order in $\tilde{\mathcal{A}}_{1,1}$, this restriction is made *after* reduction of n-body cycles to single-particle partition functions (1-cycles) by means of the semigroup property. This means that, implicitly, the dressing has happened for all particles involved in a cluster simultaneously, which cannot be captured by overall first-order truncation. In contrast to overall first order (1.228), the truncation to linear order (1.230) only restricts the dressing to *one whole cluster* at a time but *all* constituents thereof. In a sense first-order QCE in the dynamical impurity setup is by construction working already on a "decoupled" level because it only considers the effect of interaction due to a dressing of single fermions. But due to its further truncation to only one dressing at a time it induces again an artificial coupling. The artificial coupling thereby enters through the conditional nature of the dressing which is a joint concept that is not separable into individual particles. The true decoupling of the identical fermions in the limit of static impurity should rather be a property of higher-order cluster contributions. Using the static impurity decoupling as a fact, the argument can be used reversely to provide relations for higher-order cluster diagrams. This is nicely illustrated on the example of a two-cycle with additional impurity (see Fig. 1.25). Following the above line of thought one demands that the full QCE of this cycle structure (see Fig. 1.25a) becomes a pure dressing (see Fig. 1.25b). This gives a static decoupling relation of one specific three-cluster (see Fig. 1.25c), which one can, *e.g.*, use as a consistency check if one derives such a three-cluster from first principles. Another static decoupling relation is deduced from the $(1)(2)(3)$ cycle structure (see Fig. 1.25d). Or one can even identify such a relation on the level of propagators (see Fig. 1.24b) assuming the static decoupling for the dynamics as well.

It remains to be investigated in detail by future work, whether and how one can use these insights on the nature of the first-order cluster expansion and the static decoupling relations to further improve accuracy and physically addressed content of the descriptions within QCE. In fully interacting models like the Lieb-Liniger model one might think of effective dressing of particles by all other

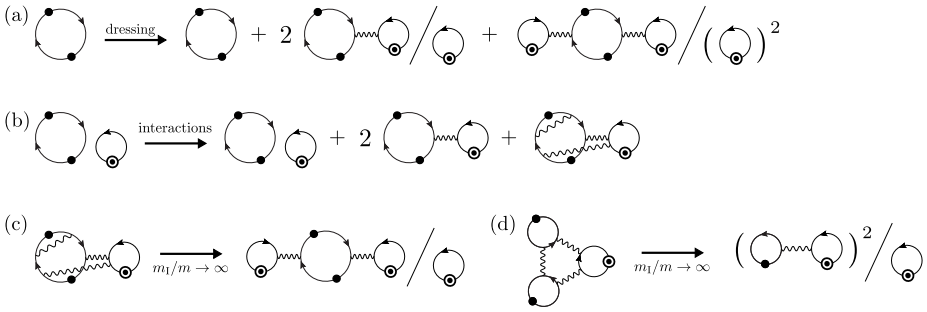

Fig. 1.25: Dressing of cycles with the impurity interaction and corresponding static decoupling relations. (a) Dressing of a two-cycle. (b) Full QCE expansion of the two-cycle with present impurity. (c) Static decoupling relation for the three-cluster with two-cycle deduced from a and b. (d) Static decoupling relation for the three-cluster with one-cycles. To distinguish the impurity (which has different mass) from the rest, it is depicted by a bulls eye.

particles, which could then again be organized by clusters hierarchically. This way there is the hope that one could come up with an effectively non-interacting theory in a mean-field sense plus residual interactions. Although this roughly reminds on the renormalization using dressed Feynman diagrams in quantum field theories, there is an essential difference originating from the finiteness of particles involved. An effective dressing of all particles simultaneously over-counts mutual interactions. There are for example contributions corresponding to a separation of all particles into N two-clusters in expressions like (1.230), where each particle interacts with an additional one chosen from the whole system. The actual presence of such a contribution in the whole expansion would falsely demand the existence of $2N$ particles. The correction of such over-counting may be within the scope of QCE and could then lead to special residual interactions emanating from the determination of a finite number of particles. This is special about the first-quantized canonical description where no virtual particles can be excited in contrast to second quantized or quantum field descriptions.

1.5 Extensions II: Methods

1.5.1 Discreteness effects – Splitting off lowest states

In this section non-universal system-specific features will be addressed. As observed in the example of the Lieb-Liniger model (see Fig. 1.17 and discussion) those may show up at ultra-low temperatures, where the specific behavior of the lowest discrete eigenstates of the system matters.

In the extreme limit of low temperatures the thermodynamics are determined by the ground state energy E_0 and the lowest energy gap $E_1 - E_0$ corresponding to the truncation

$$Z_{\text{ex}} \approx g_0 \mathrm{e}^{-\beta E_0} + g_1 \mathrm{e}^{-\beta E_1} \tag{1.231}$$

with degeneracies g_0 and g_1. While the high-temperature physics are determined by the QCE in form of a (finite) polynomial in the (thermally scaled) volume

$$\tilde{v} \coloneqq \frac{V_{\text{eff}}}{\lambda_{\text{T}}^d}\,, \tag{1.232}$$

the low-temperature asymptotics (1.231) are non-analytic at $T = 0$, displaying an essential singularity involving arbitrarily negative powers of T. Thus, the low-temperature behavior cannot be reproduced by a polynomial in $\tilde{v}$, as it involves only positive powers of T. A modification of the QCE intended to account for the ultra-low-temperature physics must necessarily break the purely polynomial form.

In order to account for both, the universal physics (at "high" temperatures) and the non-universal features (at ultra-low temperatures) related to discreteness effects, I apply here a variant of the Padé approximant method developed in [180]. There are, however, a few major differences.

First of all, the method in [180] was developed for a single particle. The author argues that in principle it might be applicable to interacting systems with smooth interaction potentials as well, using Wigner-Kirkwood expansions [181, 182] in the full configuration space. Strong objections to this statement considering the present context are that gradient expansions of the Wigner-Kirkwood type [107] are: *i)* in general very complicated to calculate to high orders, which would be needed here to fully account for the universal behavior down to quantum degeneracy, *ii)* not applicable to singular potentials, mostly considered here in form of Dirac delta interactions, and *iii)* not specifically amenable to account for symmetrization of identical particles and hence apply for Boltzmann statistics only.

Furthermore, the proposal in [180] – realizing that the coefficients of $\tilde{v}^l$ in Z would become functions of the temperature T – is to expand these coefficients in T to end up with an overall power series then used for asymptotics. Contrasting this approach, by virtue of the generic scaling of the QCE (see section 1.2.5), the nontrivial dependence on T in the "high"-temperature regime can be separated uniquely into two parameters: the thermally scaled volume $\tilde{v}$ (determining the crossover from the classical regime to quantum degeneracy) and the thermal coupling strength $s = \beta\alpha$ (representing the influence of interaction). This allows to exploit the polynomial structure in $\tilde{v}$ of the QCE for considerations on the low- and "high"-temperature asymptotics while keeping the full *non-perturbative*

nature of the interaction effects, making the approach simpler and more accurate at the same time.

While the use of Padé approximants as in [180] is capable to correctly reproduce the two opposite asymptotics $T \to 0, \infty$, they may suffer from singularities at finite temperatures in between. These have to be ruled out explicitly for any system under consideration. Indeed, in the presented context of indistinguishable interacting particles, such singularities – in the form of poles in T – are present. Therefore a simplified version, explicitly constructed in the following, which conceptually excludes the possibility of poles is used here.

Matching the low-temperature limit

To guarantee the correct asymptotics in both limits one can then split off the ground state explicitly and account for the lowest energy gap by the ansatz

$$\tilde{Z} = g_0 \mathrm{e}^{-\beta E_0} + \mathrm{e}^{-\beta E_1} Y(\tilde{v})\,, \tag{1.233}$$

with the analytic finite universal part Y accounting for the behavior at large volume (or temperatures) $\tilde{v}$. As we will see in the following, under some general assumptions, the universal part can be chosen as finite expansion in powers of $\tilde{v}$ similar to the QCE of Z.

To make this explicit the generic dimensional scaling of eigenvalues E_n is analyzed in the following. Performing a dimensional analysis similar to section 1.2.5 one finds for homogeneous external potentials that

$$\beta E_n = \frac{1}{4\pi} \tilde{v}^{-\frac{2}{d}} \tilde{E}_n(\zeta) \tag{1.234}$$

with the dimensionless scaled energies $\tilde{E}_n(\zeta)$ fully determined by a single dimensionless parameter

$$\zeta = 4\pi \tilde{v}^{\frac{2}{d}} \beta\alpha\,, \tag{1.235}$$

where α is the interaction parameter of dimension energy. The corresponding scaled Schrödinger equation in generic form reads

$$\left[-\sum_{j=1}^{N} \frac{\partial^2}{\partial \tilde{q}_i^2} + \zeta u_{\mathrm{int}}(\sqrt{\zeta}\tilde{\mathbf{q}}) + u_{\mathrm{ext}}(\tilde{\mathbf{q}}) \right] \psi_n(\tilde{\mathbf{q}}) = \tilde{E}_n \psi_n(\tilde{\mathbf{q}}) \tag{1.236}$$

in the scaled coordinates $\tilde{\mathbf{q}} = V_{\mathrm{eff}}^{-1/d} \mathbf{q}$ with dimensionless functions u_{int} and u_{ext} for the interaction- and external potentials, respectively [compare to (1.123)]. Once again the case of quantum billiards with finite domains Ω of volume V_D are included as the case of infinite degree of homogeneity ($d \mapsto D$ and $V_{\mathrm{eff}} \mapsto V_D$).

Assume that the scaled energies can be expanded as power series

$$\tilde{E}_n(\zeta) = \sum_{k=0}^{\infty} e_n^{(k)} \zeta^{\nu k} \tag{1.237}$$

with some coefficients $e_n^{(k)}$ and a fixed exponent ν. If the interaction potential itself is also homogeneous of degree μ_{int}, this assumption becomes a fact, evident by virtue of perturbation theory with the specific exponent $\nu = 1 + \mu_{\mathrm{int}}/2$. The case of Dirac delta interactions which is most relevant to this work falls under

this category with $\nu = \frac{1}{2}$. In the specific homogeneous one-dimensional case $d = D = 1$ this implies together with (1.234) the perturbative expansions

$$\beta E_n = \underbrace{a_n^{(2)} \times \tilde{v}^{-2} + a_n^{(1)} \times (\beta\alpha)^{\frac{1}{2}} \tilde{v}^{-1} + a_n^{(0)} \times (\beta\alpha)\tilde{v}^0}_{=:\beta E_n^{\mathrm{trunc}}} + \mathcal{O}\left((\beta\alpha)^{\frac{3}{2}}\tilde{v}\right) . \quad (1.238)$$

This expansion can be understood as both, an expansion around weak (thermal) coupling strengths $\beta\alpha$ and an expansion around low temperatures $\tilde{v} \to 0$ (or better small volumes). Thus, to use it in order to reproduce the correct ultracold physics (1.231) within the split-off ansatz (1.233) it suffices to truncate it at $\mathcal{O}(\tilde{v})$ if the coupling strengths are not too large.

For applications in the strong-coupling regime, the "anti-delta" potential together with fermionic antisymmetry (see section 1.4.1 on the boson-fermion duality) has to be considered. This is a bit more problematic, since the explicit form of this interaction potential [174] does not show obvious homogeneity, which invalidates the perturbation argument. Nevertheless, due to the duality the energies are the same as in the bosonic delta-interacting case, which apparently admits an asymptotic power expansion[15] at infinity yielding

$$\beta E_n = \bar{a}_n^{(2)} \times \tilde{v}^{-2} + \bar{a}_n^{(3)} \times (\beta\alpha)^{-\frac{1}{2}} \tilde{v}^{-3} + \mathcal{O}\left((\beta\alpha)^{-1}\tilde{v}^{-4}\right) . \quad (1.239)$$

A second problem with the expansion of discrete energies around strong thermal couplings $\beta\alpha$ is that, due to (1.235), it comes at the same time as an expansion around high temperatures. This narrows the range of its applicability. While for very strong interactions close to the fermionization limit it may be valid to use (1.239), with any truncation there will always be a regime of extremely low temperatures (or small volumes) where it becomes invalid. Therefore, I state here the principle possibility of the strong-coupling split-off for completeness and leave explicit investigations in this direction to future work. Not least because this regime in the Lieb-Liniger model is dominated by repulsion over effective attraction due to Bose bunching in the ring, which is why non-universality plays a sub-dominant role there anyway.

Matching the high-temperature limit

While the ansatz (1.233) can be used in more general setups (using expansions (1.237) and (1.234)) I stick here to the demonstration in the one-dimensional contact-interacting case without external potential (1.238) (and (1.239)). This makes the matching of Y especially simple because only integer powers of $\tilde{v}$ are involved. Then the correct asymptotics at high temperatures (or equivalently large volumes), which is given by the universal QCE (1.134), can be matched using a polynomial[16]

$$Y(\tilde{v}) = \sum_{l=0}^{N} y_l \tilde{v}^l \quad (1.240)$$

with coefficient functions $y_l = y_l(\beta\alpha)$ that still have to be determined. Consistently, omitting all positive powers in (1.238) is indispensable to maintain the

[15] Such an expansion cannot exist for $|\zeta| \to \infty$ with arbitrary complex phase because this would be in contradiction to the essential singularity of $\tilde{E}_n(1/x)$ at $x = 0$. But for $\zeta \in]0, \infty[$ it can be confirmed numerically for specific n and with truncation to finite orders k.

[16] Otherwise generalized but finite expansions in fractional powers of $\tilde{v}$ have to be used.

classical limit (the highest power $\tilde{v}^N$) in the full expansion of (1.233), dictated by the leading naive volume (or Thomas-Fermi) term (1.60). The coefficients could be matched by expanding the Boltzmann factors in the RHS of (1.233) and identification with the LHS in all non-negative powers of $\tilde{v}$. Alternatively one can use a more direct matching which is similar (but not exactly equivalent) that circumvents the inversion of linear systems. Rearranging (1.233) gives

$$Y(\tilde{v}) = (Z(\tilde{v}) - g_0)\mathrm{e}^{\beta E_1^{\mathrm{trunc}}} + \mathcal{O}(\tilde{v}^{-1})\,, \tag{1.241}$$

where the universal power expansion of Z in $\tilde{v}$ given by QCE (1.134) can be used to directly obtain the coefficients $y_0, \ldots, y_N$, whereas negative powers are not matched. The matching in terms of coefficients $a_n^{(k)}$ of the low-temperature expansion (1.238) and $z_l + \Delta z_l(\beta\alpha)$ of the QCE (1.134) reads

$$\begin{aligned} y_l(\beta\alpha) &= \sum_{n=0}^{N-l} \bar{z}_{l+n} \sum_{k=\lceil \frac{n}{2} \rceil}^{n} \frac{\left(a_1^{(1)}\right)^{2k-n} \left(a_1^{(2)}\right)^{n-k}}{(2k-n)!(n-k)!} (\beta\alpha)^{k-\frac{n}{2}}\,, \\ \bar{z}_l &:= \begin{cases} z_l + \Delta z_l(\beta\alpha) & : l \geq 1 \\ -g_0 & : l = 0 \end{cases}, \end{aligned} \tag{1.242}$$

where the expansion (1.238) of βE_1 was truncated further by considering only the terms of order $\mathcal{O}(\tilde{v}^{-2})$ and $\mathcal{O}(\tilde{v}^{-1})$. In principle there is no problem including the $\mathcal{O}(\tilde{v}^0)$ term but a direct comparison with numerics shows the sufficiency of omitting it.

The full range result

By this method one obtains again a finite explicit expression for the partition function and hence the pressure (1.79) as a function of the volume $\tilde{v}$ in units of the thermal de Broglie wavelength and the thermal coupling strength $s = \beta\alpha$. One should put emphasis on the fact that within this approach, all non-universality is reflected by just the ground state energy and the lowest gap. Even the weak-coupling perturbative estimations thereof suffice as ingredients in the all-over analytic result. This minimum information about the exact low-lying spectrum in combination with the universal cluster expansion to first order is enough to reproduce the system-specific low-temperature behavior in the Lieb-Liniger model as shown in Fig. 1.26. The non-trivial physics of sudden collapse (see Fig. 1.17 and discussion) is reflected by non-monotonicity that originates from the competition between repulsion and Bose-bunching enhanced to strong effective attraction by periodic boundary conditions. In the case of $N = 3$ bosons, we find an accurate description in the whole range covering arbitrary system sizes (non-universal and universal) up to repulsive interaction strong enough to fully prevent any collapse. Although the non-monotonous behavior reminds on the isotherms of the Van-der-Waals gas the elementary physics leading to attraction is here very different. In the Lieb-Liniger model it is a finite-size manifestation of Bose-Einstein condensation whereas the attractive Van-der-Waals force is electromagnetically mediated. The latter has its nature in the internal charge polarizations of molecules and does not distinguish between different quantum statistics. Furthermore, the usual Maxwell construction [183] of replacing the non-monotonicity by a horizontal line with equivalent work balance does not apply here because of the strictly few particle system. In

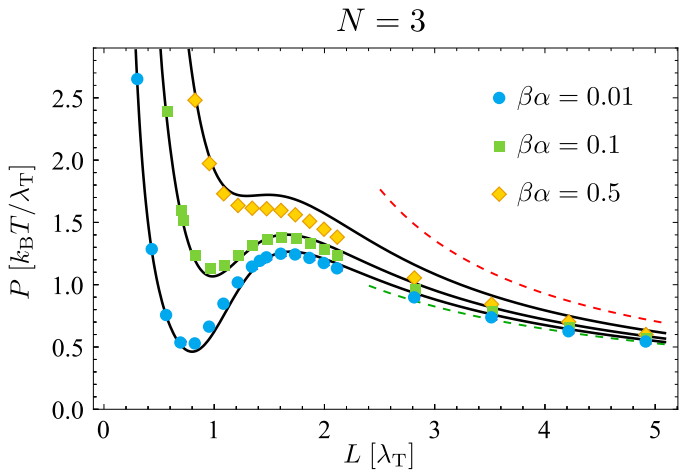

Fig. 1.26: Mechanical equation of state in the repulsive Lieb-Liniger model with $N = 3$ bosons for three different couplings $\beta\alpha = 0.01, 0.1, 0.5$. Numerical evaluation of the analytic transcendental solutions (1.179) (dots) yields non-monotonous behavior if the coupling is small enough. The prediction of this sudden collapse under compression is accurately reproduced by the combined description of universality and non-universality within the split-off method used on first-order QCE (solid). The non-interacting ($\alpha = 0$, green dashed) and the fully fermionized case ($\alpha \to \infty$, red dashed) are shown in their purely universal predictions.

the Van-der-Waals gas, this construction accounts for density and energy fluctuations all over a macroscopic gas, so that different local regions can trade a surmount of work produced by molecules that locally collapse to the liquid phase with other regions allowing them to climb the repulsive barrier. Such processes have then to be included by hand because the derivation of the Van-der-Waals equation of state treats separated pairs of particles as independent. Therefore there the non-monotonicity can be regarded as an unphysical artifact reflecting the deficiency in truncating higher-order terms in the corresponding *classical* cluster expansion. In contrast to that, taking the numerical eigenenergies of the Lieb-Liniger model (of few bosons) fully accounts for such fluctuation and must not be corrected (as long as the system is in a true thermal equilibrium). Moreover the effective mutual attraction as a manifestation of Bose-Einstein condensation is a collective effect that is not truncated to a pairwise level even in the first-order approximation of the QCE, since symmetry is accounted for in all orders.

One crucial ingredient necessary to the split-off method is that the variables can be separated into thermally scaled volume $\tilde{v} = V_{\text{eff}}/\lambda_{\text{T}}^d$ and the thermal coupling strength $s = \beta\alpha$ by virtue of the generic dimensional analysis. It allows to consider the coupling s fixed while uniquely matching the coefficients in the expansion for large volumes, which are then coefficient functions $y_n(s)$ of the thermal coupling strength. The other important ingredient making the process of matching a finite analytic algorithm (1.242) is the natural form of the QCE as polynomial in the volume. The general possibility of separately considering the dependence on two different energy scales – one given by the volume and the other by the coupling strength – together with the polynomial

structure in one of the scales opens yet another methodical advance if we move to the spectral representation in the next section.

1.5.2 The energy shifting method – Covering arbitrary interaction strengths

The general idea

In this section a systematic method will be developed to make approximations to the full QCE expansions in a different representation than truncation to a specific number of interaction events as opposed to the first-order truncation of QCE. The inspiration goes back to observations made on the counting functions of non-interacting quantum billiards in combination with the full fermionization in one-dimensional bosonic systems with contact-interaction. If the coupling strength of mutually delta-interacting bosons is increased to infinity one obtains the non-interacting fermionic spectrum (as least as far as concerns the universal or smooth part). Furthermore, in Fig. 1.7 an observation was that the sub-leading terms of non-interacting fermionic counting functions or DOS add up to small oscillations that can be considered as effectively zero-valued functions up to the ground state energy. Neglecting those artificial oscillations the main effect of alternating signs in the fermionic coefficients could be considered as shifting all energies to larger values compared to the ideal bosonic case. Also when including physical boundary effects in a two-dimensional quantum billiard (see Fig. 1.8 and discussion) we observed that the main effect from physical surface correction (and also the missing curvature correction) could be seen as a shifting of all energies.

The general idea is now to express the effect of interactions on the counting function of a system as shift in all energies (see Fig. 1.27a). The general ansatz is to express the approximate smooth counting function

$$\mathcal{N}_\alpha(E) = \mathcal{N}_0(E - \Delta E_\alpha) \tag{1.243}$$

corresponding to a coupling α in terms of a shifting of the non-interacting one. The energy shifts ΔE_α are so far completely unspecified but will be pointed out step-by-step as having a systematic form.

Already at this general level there are three reasons why this ansatz might exhibit advantages over the standard form (1.141) of the QCE. First, thinking of the effect of interactions in terms of shifting energies is closer to the effect they have on actual discrete spectra, where every single energy level gets shifted by a specific amount determined by the coupling. Degenerate levels thereby are addressed individually and can be subject to different shifts, breaking the degeneracy. In particular the general ansatz (1.243) is fulfilled exactly by the discrete staircase counting functions of exact spectra. The second reason is connected to the first one. Exact counting functions are contrasted with the first-order QCE, which may produce approximations that cannot be expressed as a shift (1.243) in the regime where it breaks down, because of artificial negativity in the predicted smooth counting functions. Thus, such enormous failure is prevented by principle with the ansatz (1.243). The third reason elaborates a bit more on this argument. In the standard polynomial form (1.75) of the non-interacting fermionic QCE with constant coefficients, the development of small oscillations involves large cancellations of all sub-dominant cycle-contributions.

The precise knowledge of all terms is needed to add up to the correct description at low energies. When this fact is transferred to the cluster contributions in the interacting case it is therefore unavoidable that any truncation of the QCE (especially to first order) will produce large defects because they lack the sensible balance between all different orders of clustering.

In the following the systematic form the shifts ΔE_α must have is revealed step-by-step. To start with, consider the shifts found in the hard-core limit of fully fermionized one-dimensional bosonic systems.

The full shifts – Infinite coupling

The limit $\alpha \to \infty$ of infinitely strong coupling of one-dimensional bosonic systems with contact interaction is equivalent to ideal fermionic systems (see section 1.4.1) on the universal level. This subsection investigates the nature of the corresponding shifts $\Delta E_\infty = \lim_{\alpha\to\infty} \Delta E_\alpha$ and their implementation in terms of non-interacting QCE. For the purpose of this whole section I write the non-interacting smooth counting function in simplified notation as

$$\mathcal{N}_0(\tilde{E}) = \sum_{l=1}^{N} c_l \tilde{E}^{ld/2} = c_N \tilde{E}^{Nd/2} + c_{N-1}\tilde{E}^{(N-1)d/2} + \dots , \tag{1.244}$$

with the scaled total energy

$$\tilde{E} = \rho_0^{\text{eff}} E , \tag{1.245}$$

measured in units of the energy scale (1.76) related to the (effective) system size. The coefficients used here related to (1.75) by

$$c_l = \frac{z_l}{\Gamma\left(\frac{ld}{2}+1\right)} . \tag{1.246}$$

The shifted counting function in the leading order terms reads

$$\begin{aligned}\mathcal{N}_0(E-\Delta E_\infty) &= c_N \tilde{E}^{\frac{dN}{2}} \left(1 - E^{-1}\Delta E_\infty\right)^{\frac{dN}{2}} + c_{N-1}\tilde{E}^{\frac{d}{2}(N-1)} + \dots \\ &= c_N \tilde{E}^{\frac{dN}{2}} - \frac{dN}{2} c_N \tilde{E}^{\frac{dN}{2}-1}(\rho_0^{\text{eff}}\Delta E_\infty) + c_{N-1}\tilde{E}^{\frac{d}{2}(N-1)} + \dots .\end{aligned} \tag{1.247}$$

From the approximate equivalence with the non-interacting fermionic function

$$\mathcal{N}_\infty(E) \overset{!}{\approx} c_N \tilde{E}^{Nd/2} - c_{N-1}\tilde{E}^{(N-1)d/2} + \dots , \tag{1.248}$$

we know that the second term in the expansion (1.247) should contribute to the term of order $\mathcal{O}(\tilde{E}^{\frac{d}{2}(N-1)})$ to correct its sign. Here we find the case $d = 2$ to be of special simplicity, because it corresponds to a full shift that is a constant. From comparison one finds in this case easily

$$\Delta E_\infty = \frac{2c_{N-1}}{Nc_N}(\rho_0^{\text{eff}})^{-1} = \frac{1}{2}N(N-1)(\rho_0^{\text{eff}})^{-1} , \quad d = 2 , \tag{1.249}$$

which is remarkably accurate when applied to the one-dimensional harmonic oscillator (for which $d = 2$), where the exact spectrum of bosons and fermions are related by the exact constant shift predicted from the universal estimations.

For arbitrary effective dimensionality the matching (1.248) demands that the full shifts asymptotically behave as

$$\rho_0^{\text{eff}} \Delta E_\infty \sim \text{const.} \times \tilde{E}^{1-\frac{d}{2}} \quad \text{as} \quad \tilde{E} \to \infty \,. \tag{1.250}$$

By comparing ideal bosonic and fermionic smooth counting functions for several different values of the effective dimension d and numbers of particles N one finds that the prescription

$$\rho_0^{\text{eff}} \Delta E_\infty = \text{const.} \times [\mathcal{N}(E)]^{(\frac{2}{d}-1)\frac{1}{N}} \tag{1.251}$$

is way more favorable than an energy-dependent prescription like (1.250). It effectively (in a smooth way) expresses the full fermionization shift of each level as a function of its quantum number rather than its (fermionized) energy. While exhibiting the same correct asymptotics for large $\tilde{E}$ the $\mathcal{N}$-dependent prescription (1.251) quite accurately produces the fully fermionized limit on all energy scales. So far (1.251) is heuristic (if $d \neq 2$) but it can be justified by consistency *w.r.t.* "interaction flow" (see the subsection after the next). From the interaction flow argument it is necessary to use the fully shifted counting function $\mathcal{N} = \mathcal{N}_\infty$ instead of the non-interacting one. In the dominant term (1.250) this does not make a difference, allowing for a direct comparison of the next-to-leading order terms in (1.247) and (1.248), which yields the explicit full shift

$$\rho_0^{\text{eff}} \Delta E_\infty = \frac{4}{Nd} c_{N-1} c_N^{-1-(\frac{2}{d}-1)\frac{1}{N}} [\mathcal{N}(E)]^{(\frac{2}{d}-1)\frac{1}{N}} \,. \tag{1.252}$$

The partial shifts – Arbitrary coupling strength

In the last subsection we have seen that the full shifts must be functions of the energy in terms of the energy scale given by the system size to match the fully fermionized QCE. The reason was the demand that the energy shifting dominantly impacts by contributing to the next-to-leading order term in the full expansion. The next step in extending the shifts to arbitrary interaction strength crucially relies on the generic scaling (1.141) of the QCE. Since the effect of arbitrary α is a correction of coefficients by coefficient functions $g_l^{(N)}$ of the energy E/α in units of the coupling parameter, one must apply the same separation in the two distinct energy scales to the shifts. The corresponding ansatz reads

$$\Delta E_\alpha = \chi\left(\frac{E}{\alpha}\right) \Delta E_\infty \,, \tag{1.253}$$

where the partial shift as fraction $\chi(E/\alpha)$ of the full shift is determined by energy in terms of the coupling strength only. The system size must not have a direct influence on this fraction.

To illuminate the physical meaning of this separation of energy scales and the prescription (1.251) a bit more, consider the shift of a single exact many-body level. Say, we talk about the n-th excited state $E_n(\alpha)$, start from its non-interacting energy $E_n(0)$ and adiabatically switch on interactions. The full shift (1.251) is expressed by the counting function which simply becomes the quantum number n. It does not change during the process of turning on interactions. The ansatz (1.253) then suggests that the ratio $E_n(\alpha)/\alpha$ of the actual interacting energy of this level and the energy-like coupling parameter

is in unique relation to how far this level has moved from the non-interacting $E_n(0)$ to the fully fermionized counter-part $E_n(\infty)$.

From the analytical point of view the ansatz (1.253) allows a matching in the next-to-leading order term of the expansion in $\tilde{E}$. The separation into two different energy scales is here crucial. Matching coefficients in a power expansion in $\tilde{E}$ (or similarly an expansion in powers of the (effective) volume), E/α is considered as a different variable kept constant. This way of separating combines the high amount of analytical control one has over power series expansions with the high value of a non-perturbative description in the interaction.

Matching by this prescription the next-to-leading order contribution from the ansatz (1.253) in (1.243) with the QCE expansion (1.141) results in

$$\chi\left(\frac{E}{\alpha}\right) = -\frac{1}{2c_{N-1}} g_{N-1}^{(N)}\left(\frac{E}{\alpha}\right) . \tag{1.254}$$

Because for delta interactions in one dimension one has the exact fermionization property

$$g_{N-1}^{(N)}\left(\frac{E}{\alpha}\right) \xrightarrow[\alpha\to\infty]{} -2c_{N-1} , \tag{1.255}$$

one reobtains the correct full shifts as $\lim_{\alpha\to\infty} \chi(E/\alpha) = \chi(0) = 1$. The analytic matching (1.252) together with the full shifts (1.252) makes the ansatz (1.243) a fully determined equation for the shifts ΔE_α, which has then to be solved. It is crucial to use the unknown shifted $\mathcal{N}(E)$ for the full shifts in this equation, which is demanded by an "interaction flow consistency" argument (see next subsection). The solution must therefore be done in a self-consistent manner. The most practical way to formulate the corresponding equation is by solving for E with a given quantum number $\mathcal{N}$ instead of the other way around. The process of solving can be thought of as starting with a non-interacting level and pushing its energy until the requirement given by the matching is fulfilled. Thereby its quantum number does not change, $\mathcal{N}_\alpha(E) = \mathcal{N}_0(E_0)$. When fixing a starting value E_0 the corresponding shift $\Delta E_\alpha(E_0, \alpha)$ is determined by

$$\rho_0^{\text{eff}} \Delta E_\alpha(E_0, \alpha) = \text{const.} \times [\mathcal{N}_0(E_0)]^{(\frac{2}{d}-1)\frac{1}{N}} \chi\left(\frac{E_0 + \Delta E_\alpha(E_0, \alpha)}{\alpha}\right) , \tag{1.256}$$

where the constant and fraction function are given in (1.252) and (1.254) by analytical matching. The root of (1.256) for given a E_0 and α can then easily be searched for numerically.

Before showing an application of this method I want to stress two important points here. The first one being generality. Although the method was deduced here starting from infinite shifts from fermionization – which is very special about delta-interactions in one dimension – the matching of the ansatz (1.253) together with the prescription (1.251) that results in (1.254) does not rely on this fact. Therefore I strongly propose the validity of this method also for different types of interaction and dimensionality. The term "full shifts" should then not be taken literally, whereas the full result should still be working. Especially for interactions that do not have a finite converging $\alpha \to \infty$ limit the shifts diverge at infinite interaction, reflected by $\lim_{\epsilon\to 0} \chi(\epsilon) = \infty$.

The second point to emphasize here is the full determination of the shifts by the first-order QCE. Only the information of a single two-body cluster is

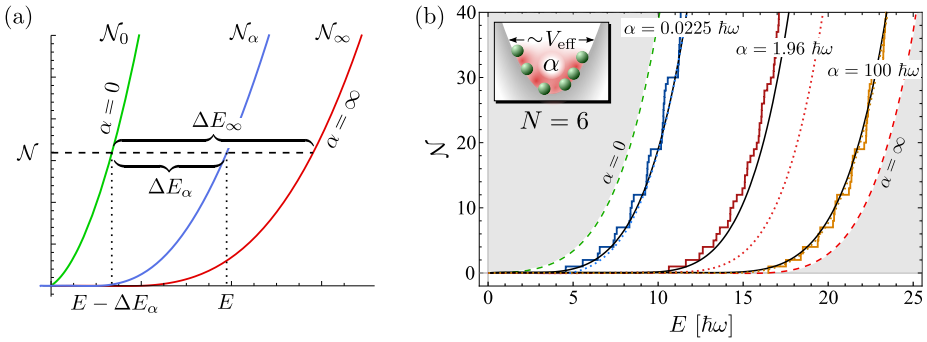

Fig. 1.27: (a)Schematic method of energy shifting. (b)Excitation spectrum of the interacting Bose gas ($N = 6$) in a harmonic trap for the three values of interaction strength $\alpha = 0.0225\hbar\omega, 1.96\hbar\omega$, and $100\hbar\omega$. Shown is the counting function obtain from numerically converged exact diagonalization (staircase) with the effective interaction potential approach (see Fig. 1.21 and discussion), its analytical predictions given by the direct first-order QCE (1.216) (dotted) as (from left to right) weak-, strong-, and strong-coupling expansion, respectively, and the prediction based on the energy-shifting method (black solid) (1.243).

needed to specify the energy shift (1.254). Up to this clustering, the first-order truncation of QCE coincides with the full expansion, which makes it exact at the universal level. This especially opens the door of applying the method to all kinds of different interaction potentials, since it reduces to the solution of a two-body problem. One may regard the energy shifting method as a way to gain the maximum knowledge on the universal properties of a few-body system out of the information on the interaction effect on an isolated pair of particles. In this sense one might consider it as a quantum few-body analog of the leading-order virial expansion of classical macroscopic systems (that, *e.g.*, leads to the Van-der-Waals equation). Both incorporate interaction effects in a way that they only depend on the two-body problem and both are on an equal footing because restricted to describing universal features. The difference being that the former describes canonical ensembles of indistinguishable particles down to the regime of quantum degeneracy while the latter is constructed to apply for classical grand canonical ensembles of typically macroscopic numbers of particles.

Figure 1.27b shows, as exemplary application, a gas of $N = 6$ bosons in an one-dimensional harmonic trap. Since this system is non-integrable, the exact solution involves exhaustive numerical exact diagonalization, which was here performed again on the basis of effective truncated interaction potentials (see Fig. 1.21 and discussion) to get fast convergence of calculated levels with the cut-off in the truncation of the single-particle basis. The shifting method still reproduces accurately the predictions of first-order QCE in the extreme regimes of weak and strong coupling, where the latter is applicable. Moreover, it provides very good agreement with the numerical simulation in the intermediate coupling regime, where both, the weak- and strong-coupling expansions to first-order all break down. It also corrects the deviations for weak couplings that occur for very low energies visible at the lowest states of the spectrum for $\alpha = 0.0225\hbar\omega$. With the given resources the solution of this system was already at the edge of numerical tractability. It therefore serves as the final confirmation that the

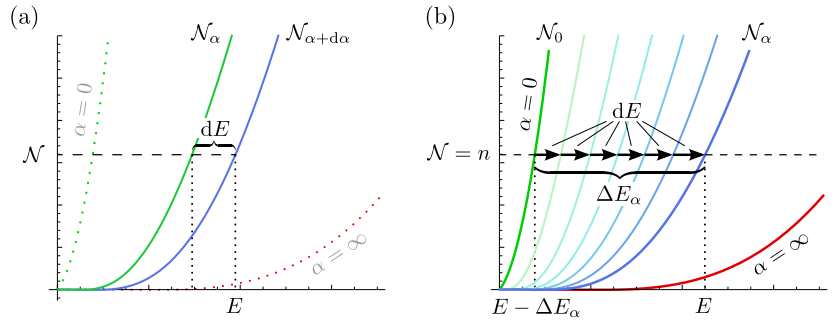

Fig. 1.28: (a) Scheme of an infinitesimal energy shifting, where $\mathcal{N}_\alpha$ is the initial point (green). (b) Sketch of integrated infinitesimal shifts $\mathrm{d}E$ (along $\mathcal{N} = \text{const.}$), reproducing the finite shift ΔE_α.

QCE develops into a predictive tools when supplied with the shifting method, applicable in regimes where numerical calculations are too exhaustive to be performed in realistic computation times.

Interaction flow consistency – A justification of the $\mathcal{N}$-prescription

In this subsection an analytical argument is presented clarifying why the $\mathcal{N}$-dependent prescription (1.251) is favorable to an energy dependent one (1.250). The argument is based on an infinitesimal version of the shifting method. Instead of applying the shifting to non-interacting counting functions $\mathcal{N}_0$ (1.244), or equivalently individual many-body levels, in order to approximately reproduce the interacting case, the starting point is here the case of finite arbitrary coupling strength α. One could think of the situation with the coupling set to α as an unperturbed system, while an infinitesimal increase $\mathrm{d}\alpha$ in the interaction can be regarded as a small perturbation. The attempt is then to implement this perturbation as an infinitesimal version of the energy shifting method applied to $\mathcal{N}_\alpha$, expressed by

$$\mathcal{N}_{\alpha+\mathrm{d}\alpha}(E) = \mathcal{N}_\alpha(E - \mathrm{d}E)\,. \tag{1.257}$$

Similar to the direct finite shift (1.253) the ansatz for the infinitesimal shift is

$$\mathrm{d}E = \underbrace{\text{const.} \times \mathcal{N}^{(\frac{2}{d}-1)\frac{1}{N}}}_{=\Delta E_\infty}\mathrm{d}\chi \sim \tilde{E}^{1-\frac{d}{2}}\mathrm{d}\chi\,, \tag{1.258}$$

where

$$\mathcal{N} = \mathcal{N}_{\alpha+\mathrm{d}\alpha}(E) = \mathcal{N}_\alpha(E - \mathrm{d}E) \tag{1.259}$$

can be regarded as the quantum number of a level to be shifted. The situation is sketched in Fig. 1.28a. The function $\mathrm{d}\chi$ is here assumed to depend on the ratio $E/\mathrm{d}\alpha$ of energy and the (here infinitesimal *additional*) coupling $\mathrm{d}\alpha$[17]. Again a separation into different energy scales is crucial. As in the previous subsection, the shift $\mathrm{d}E$ gets then determined by matching (1.257) term by term in an expansion in the energy scale $\tilde{E}$ associated with the volume. This is

[17] An additional dependence on E/α, which introduces a dependence on $\tilde{E}$ (see discussion after (1.261)) is here not strictly excluded but instead allowed as long as it is of *dominance-reducing* type, so that it *cannot* elevate $\mathrm{d}E$ to $\mathcal{O}(\tilde{E}^\nu)$ with $\nu > 1 - d/2$.

here demonstrated as a first-order shift involving only the matching of terms of next-to-leading order $\mathcal{O}(\tilde{E}^{(N-1)d/2})$. Up to this order, and expanded linearly in infinitesimal quantities, the shifted counting function, according to QCE, reads

$$\begin{aligned}\mathcal{N}_\alpha(E-\mathrm{d}E) &= c_N\tilde{E}^{N\frac{d}{2}} \\ &+\left[c_{N-1}+g\left(\frac{E}{\alpha}\right)-2c_{N-1}\mathrm{d}\chi-\underbrace{\frac{4}{Nd}c_{N-1}c_N^{-1}\frac{E}{\alpha}g'\left(\frac{E}{\alpha}\right)\tilde{E}^{-\frac{d}{2}}\mathrm{d}\chi}_{\text{subdominant}}\right]\tilde{E}^{(N-1)\frac{d}{2}} \\ &+\dots\,,\end{aligned} \tag{1.260}$$

which has to be matched with the QCE prediction

$$\mathcal{N}_{\alpha+\mathrm{d}\alpha}(E)=c_N\tilde{E}^{N\frac{d}{2}}+\left[c_{N-1}+g\left(\frac{E}{\alpha}\right)-g'\left(\frac{E}{\alpha}\right)\frac{E}{\alpha^2}\mathrm{d}\alpha\right]\tilde{E}^{(N-1)\frac{d}{2}}+\dots\,, \tag{1.261}$$

where $g(E/\alpha)$ is short hand for $g^{(N)}_{N-1}(E/\alpha)$. There is a subtle issue in identifying the order of terms in $\tilde{E}$. Since in the infinitesimal shift the energy scale regarded distinctly from $\tilde{E}$ should be $E/\mathrm{d}\alpha$ instead of E/α, the latter should be associated with the volume scale by $E/\alpha=\tilde{E}/\tilde{\alpha}$ with a scaled parameter $\tilde{\alpha}=\rho_0^{\mathrm{eff}}\alpha$. However, the corresponding terms in (1.260) and (1.261) can only be shifted to less dominant, *higher order* (if one considers, for simplicity, interactions that vanish for $\alpha\to 0$). Ignoring the possible subdominance does no harm as long as it does not interfere with the matching of dominant terms. Similarly, I keep here the clearly subdominant term in (1.260), anticipating that the same term is found in (1.261): Recognizing that

$$\frac{\mathrm{d}}{\mathrm{d}\alpha}g\left(\frac{E}{\alpha}\right)=g'\left(\frac{E}{\alpha}\right)\left(-\frac{E}{\alpha^2}+\frac{1}{\alpha}\frac{\mathrm{d}E}{\mathrm{d}\alpha}\right)\,, \tag{1.262}$$

and using (1.258) allows to refine

$$\frac{E}{\alpha^2}g'\left(\frac{E}{\alpha}\right)\mathrm{d}\alpha=-\mathrm{d}g\left(\frac{E}{\alpha}\right)+\underbrace{\frac{4}{Nd}c_{N-1}c_N^{-1}\frac{E}{\alpha}g'\left(\frac{E}{\alpha}\right)\tilde{E}^{-\frac{d}{2}}\mathrm{d}\chi}_{\text{subdominant}}+\dots\,. \tag{1.263}$$

The matching then directly leads to the infinitesimal shift

$$\frac{\mathrm{d}\chi}{\mathrm{d}\alpha}=-\frac{1}{2c_{N-1}}\frac{\mathrm{d}}{\mathrm{d}\alpha}g\left(\frac{E}{\alpha}\right)\,, \tag{1.264}$$

implying a flow equation for $E(\alpha)$ that depends on the particular choice of ΔE_∞ in (1.258).

Now comes the point where the $\mathcal{N}$-prescription becomes crucial. While for matters of matching it does not differ from an energy-dependent prescription, the situation changes when one wants to integrate infinitesimal shifts (see sketch in Fig. 1.28b) to obtain the finite shift

$$\Delta E=\int_0^\alpha \mathrm{d}\alpha'\,\frac{\mathrm{d}E(\alpha')}{\mathrm{d}\alpha'}\,. \tag{1.265}$$

While the energy $E(\alpha)$ of a point on the counting function, or equivalently of an individual many-body level $E_n(\alpha)$, naturally changes during the integration, its excitation index $\mathcal{N} = n$ remains constant. Thus, combining (1.258) with (1.264), the integrated shift becomes[18]

$$\Delta E = -\underbrace{\frac{1}{2c_{N-1}}\Delta E_\infty}_{\text{const.}} \times \left(g\left(\frac{E}{\alpha}\right) - \underbrace{\lim_{\epsilon\to\infty} g(\epsilon)}_{=0} \right) , \tag{1.266}$$

which exactly coincides with the direct finite shift (1.253) with (1.254). This feature is here referred to as interaction flow consistency: The direct, finite version of the shifting with $\mathcal{N}$-prescription is consistent with the integrated flow when applied as infinitesimal version at all steps in between, a very special feature that is, *e.g.*, not inherent in an energy-dependent prescription.

Extendability to higher orders

This subsection is intended to resolve all potential doubts about the shifting method as a systematic controlled approximation. So far, the ansatz may still seem heuristic. But in principle there is no complication in extending it in a way that one can see it as a leading order truncation of a systematic approach that narrows down the full QCE when taken to higher order. This is done in a way that admits taking into account also higher order cluster contributions. So far all the matching was performed on the level of the next-to-leading order $\mathcal{O}(\tilde{E}^{d/2(N-1)})$ in the energy scaled with the system-size. A positive side effect of the $\mathcal{N}(E)$-dependent prescription (1.251) for the full shifts is that they only contribute in the powers of $\tilde{E}$ that are immanent to the non-interacting case anyway (when neglecting negative powers). This implies that the next-to-leading order effect of the energy shift prescribed in the previous subsection has an effect on the order $\mathcal{O}(\tilde{E}^{d/2(N-2)})$ corresponding to the next higher clusterings (two two-body clusters or one three-body cluster). Assuming the knowledge of these terms within the full QCE reflected by the appropriate coefficient function $f^{(N)}_{N-2}(E/\alpha)$ in (1.141) this term can be corrected by the extended ansatz

$$\Delta E_\alpha = \Delta E^{(1)}_\alpha + \Delta E^{(2)}_\alpha , \tag{1.267}$$

where

$$\begin{aligned} \Delta E^{(m)}_\alpha &= \chi^{(m)}\left(\frac{E}{\alpha}\right) \Delta E^{(m)}_\infty , \\ \rho_0^{\text{eff}} \Delta E^{(m)}_\infty &= \text{const.} \times [\mathcal{N}(E)]^{(\frac{2}{d}-m)\frac{1}{N}} = \sum_{k=m}^{\infty} \tilde{e}^{(m)}_k \tilde{E}^{1-\frac{d}{2}k} , \end{aligned} \tag{1.268}$$

which only makes a difference in the order $\mathcal{O}(\tilde{E}^{d/2(N-2)})$ of three-clusters (and pairs of two-clusters). The coefficients $\tilde{e}^{(m)}_k$ are in general functions of E/α only so they do not interfere between different orders of $\tilde{E}$. The extended ansatz (1.267) can even be further extended to include a maximally relevant number of terms

$$\Delta E_\alpha = \sum_{m=1}^{N-1} \Delta E^{(m)}_\alpha , \tag{1.269}$$

[18] For simplicity, the interaction is assumed here to vanish for $\alpha \to 0$.

using the same definitions (1.268), which results in the general form of the partial shifts

$$\rho_0^{\text{eff}} \Delta E_\alpha = \sum_{k=1}^{\infty} \bar{\chi}_k \left(\frac{E}{\alpha} \right) \tilde{E}^{1-\frac{d}{2}k} \tag{1.270}$$

within the extended ansatz. The general form (1.270) then does not change the exponents of $\tilde{E}$ in the QCE but has an impact on the coefficients:

$$\mathcal{N}_0(E - \Delta E_\alpha) = \sum_{l=1}^{N} h_l \left(\frac{E}{\alpha} \right) \tilde{E}^{\frac{ld}{2}} + \mathcal{O}(\tilde{E}^0) \tag{1.271}$$

with coefficient functions h_l determined by the $\chi^{(m)}$ in (1.268). If one regards all resulting non-positive powers of $\tilde{E}$ as negligible artifacts, one obtains the same polynomial structure as in the direct QCE (1.216). Thus, in principle, if one knew all the higher-order contributions in the full QCE one could reproduce it (up to artificial non-positive powers of $\tilde{E}$) by extending the shifting method according to (1.269) and successively matching all $N-1$ shifting fractions $\chi^{(m)}$ to the $N-1$ interacting coefficient functions of the QCE.

Any term beyond the truncation to $m = N-1$ in (1.269) would dominantly contribute only in order $\tilde{E}^0$ or less in the whole shifted counting function (1.243). They are therefore only producing artifacts of non-essential order and may be neglected. Alternatively one might think of extending this truncation in order to cancel the existing negative powers in $\tilde{E}$ from the more dominant contributions. Most probably the power series expansions involved render this approach an asymptotic series, where the actual truncation of m has to be decided by the criterion of best convergence. Nevertheless this procedure provides a systematic way of extending the shifting method to further improve results at least in the same sense as an asymptotic series in general provides a systematic way of approximation. If one truncates to the maximum level $m \leq N-1$ (or beyond, see above), one gets an alternative formal representation of the full QCE (up to artifacts) which carries the exact same amount of information. The point is that the representation as energy shifts apparently presents the best way of incorporating the information one supplies due to low-order cluster contributions, where the direct QCE is rather in-efficient in doing that.

An application of a second order energy shifting will be given after derivation of second order QCE contributions in section 1.5.3.

Effective volume reduction

To close the section I would like to stress a very intuitive interpretation of the energy shifting method. It is an alternative to the implementation as a shift in the energy and separation into the energy scale given by the volume and the interaction, respectively. Instead, one could think of it as altering directly the volume

$$V_{\text{eff}} \mapsto V_{\text{eff}} + \Delta V(E, \alpha)\,, \tag{1.272}$$

so that

$$\mathcal{N}_\alpha(E, V_{\text{eff}}) = \mathcal{N}_0(E, V_{\text{eff}} + \Delta V(E, \alpha))\,. \tag{1.273}$$

Dimensional analysis together with the requirement to result in corrections of the coefficient functions in order to maintain the general structure of QCE would

then imply the structure

$$\Delta V(E,\alpha) \sim V_{\text{eff}}(\rho_0^{\text{eff}} E)^{-\frac{d}{2}} \omega\left(\frac{E}{\alpha}\right) \quad \text{as} \quad V_{\text{eff}} \to \infty\,, \tag{1.274}$$

which again is satisfied by a description

$$\Delta V(E,\alpha) = V_{\text{eff}}(c_N^{-1}\mathcal{N})^{-\frac{1}{N}} \omega\left(\frac{E}{\alpha}\right) \tag{1.275}$$

depending on the quantum number $\mathcal{N}$ instead of the energy directly. An expansion $\mathcal{N}^{-1/N} = \mathcal{O}(V_{\text{eff}}^{-1})$ in powers of the volume shows that the volume correction (1.275) is of order $\mathcal{O}(V_{\text{eff}}^0) = \mathcal{O}(1)$, where the function ω, similar to the fractions χ in the energy shifting, are not depending on the system size (or the associated energy scale).

To first order, the ansatz (1.275) is again easily matched to the analytic knowledge of the $\mathcal{O}(V_{\text{eff}}^{N-1})$ term in the QCE by

$$\omega(\epsilon) = (N-1)!\,\Gamma(Nd/2+1) g_{N-1}^{(N)}(\epsilon)\,. \tag{1.276}$$

In the case of repulsive interactions, (1.276) becomes negative, so that one gains a nice interpretation of the coefficient functions $g_{N-1}^{(N)}$ as an effective reduction of the overall available volume that depends on the ratio of total energy E and coupling parameter α. This interpretation underlines once more the understanding of the energy shifting as a quantum (few-body) version of the Van-der-Waals gas, where also in the latter repulsive interaction between two molecules leads to an effective reduction of the overall volume.

Analogous to the case of shifting energies, the ansatz of altered (or in particular reduced) volumes can be taken to higher order by including corrections of order $\mathcal{O}(V_{\text{eff}}^{-m})$ to the volume alteration (1.275) within a quantum number prescription.

One major potential advantage in interpreting the energy shifting method as volume alteration is that it opens the door to adapt it to thermodynamics, where the thermal coupling strength $s = \beta\alpha$ would then determine the effective volume reduction instead of the energy. This proposal has so far not been investigated within the scope of this work and remains as outlook. One issue that would have to be clarified carefully is how the thermal analogue of a quantum-number-dependent prescription would have to look like to yield consistency *w.r.t.* interaction flow.

Finally, one should stress that there is another potentially useful, slightly modified application of the energy shifting method that especially fits to the picture of effectively altered volumes. If one considers confinement of interacting particles by imposing boundary conditions, *e.g.*, of Dirichlet or Neumann (or mixed) type, the full QCE can again strongly be expected to be constrained to the form of a finite power series in the total energy $\tilde{E}$ (related to the volume) with coefficients that depend on the interaction-related energy scale[19] E/α. As in the corresponding non-interacting confined case (1.55), the two different energy

[19] Note that besides the general expectation, there is further evidence to this statement. As a matter of fact, it is verified by explicit calculation of the QCE in the case of two bosons on a line confined by hard-wall boundary conditions [168].

scales introduced by the volume and surface can be boiled down to a single scale. The mutual ratio is then absorbed into a dimensionless geometrical parameter γ (1.56). This allows for an implementation of physical boundary effects in terms of an energy shifting, which was already indicated as an appropriate description in the context of emergent ground-state energies for trapped ideal fermions (see Fig. 1.8 and discussion[20]).

For *unconfined* but *interacting* particles the second energy scale E/α was considered as an independent variable, allowing for the term-by-term matching crucial to the method. Similarly, in the case of *confined* but *non-interacting* particles, this role is taken by the independent parameter γ. If both, boundary and interaction effects, have to be combined, the most promising proposal seems to be the application of two subsequent energy shifts. This is especially advisable in two- or three-dimensional systems, because then two different increments in the powers of $\tilde{E}$ are involved.

1.5.3 Higher-order interaction terms – Connection to the thermodynamic solution of the Lieb-Liniger model

The philosophy behind universality – Solving unsolvable systems

Many aspects of the QCE addressed so far have general analytical value that is not specific about a particular dimensionality or interaction potential, *e.g.*, the combinatorial properties or generic dimensional scaling. Despite this general value explicit calculations have only been performed where at most two particles feel mutual interaction at a time. In the restricted case of contact interaction in one-dimensional systems the interacting two-body information has been successfully used on solvable systems (Lieb-Liniger model, Gaudin-Yang model, dynamical impurity model of equal masses) as well as on unsolvable models (harmonically trapped Bose gas, dynamical impurity model of unequal masses). I have already argued that it is the restriction to universal properties that allows to extract analytical information about systems that are not analytically solvable. For the reader there might still be insecurity about this statement: What if this form of effective solvability arises because of the restriction to two-body interaction effects rather than universality? So far we have not seen an explicit QCE calculation accounting for true three-body interaction processes and typically the unsolvable models considered are rendered solvable when restricting to the two-body case, *e.g.*, two contact-interacting bosons in a harmonic trap [177]. In the end, the two-body information as well had to be obtained from the explicit solution of a two-body problem, namely two particles on an infinite line with contact-interaction. So, how could it be possible to account for three-body (and higher-order) interaction effects in an unsolvable model without solving the corresponding three-body (or higher-order) problem? Although this point might have already become clear on a general level, this section aims for settling this question once and for all by explicit application.

Still consider the Dirac delta interaction potential among particles. One

[20] To be more specific, the applied heuristic rigid shift (1.65) by a constant energy in order to reproduce curvature corrections can retrospectively be identified as a proper energy shifting. This is due to the fact that the leading curvature correction, compared to the dominant naive volume term, comes with an increment of unity in the power of $\tilde{E}$, which, similar to the standard shifting method for $d = 2$, implies a *constant* shift $\Delta E_\infty \sim \mathcal{N}^0$ [compare to (1.251)].

possible route that one can take is to exploit the exact solution (1.179) of the (few-body) Lieb-Liniger model. The input one needs for the QCE is the interacting propagator of a number of particles mutually interacting but otherwise placed in free space, consistent with short-time dynamics. Alternatively these interacting short-time propagators can be obtained by taking the formal limit of large system sizes $L \to \infty$ in the solution (1.177), (1.174), and (1.179) of the Lieb-Liniger model, which renders the periodic boundary condition non-essential. This road has been taken to obtain the correct short-time two-body propagator [168] and also to successfully obtain the full short-time three-body propagator [184]. Thus after exploiting the insensibility of the universal properties (at large system size) *w.r.t.* integrability or solvability, one is free to transfer the three-body information extracted from a solvable model to unsolvable ones (*e.g.*, harmonic trapping).

Despite the possibility of deriving the fully interacting many-boson propagators with contact interaction as explicit integral expressions I will not show the details here. They will be addressed in future publications. Instead, an alternative approach is presented in the following to obtain the traces of propagation amplitudes directly. This way, by omitting the information on the spatial distribution from the beginning, the final results for the irreducible cluster diagrams $\mathcal{A}_n$ of size n can be obtained in a comparatively simple form. The approach makes explicit the connection of the canonical formalism with the grand canonical one, reviewed in the next subsection.

Irreducible diagrams as building blocks

In the following I focus on general relations between partition functions and other thermodynamic objects within the assumptions of QCE. Based on purely combinatorial considerations, the findings presented here are, in their generality, known for (interacting) homogeneous systems (see, *e.g.*, [155]). However, it is worthwhile to have a look on these relations in the outfit of the QCE, especially because they give insight to a connection between the QCE assumptions and homogeneity considerations in general thermodynamics. Furthermore, the possibility of applying external potentials in terms of the LPA (see section 1.4.2) puts the restrictive role of homogeneity into perspective.

As a core property, one finds that the (symmetry-weighted) sums $\mathcal{A}_n$ of irreducible diagrams of size n given by (1.111) and (1.212) are the central objects characterizing a specific system.

Based on the general form of the canonical partition function (1.110) within the QCE framework – also valid in the presence of external potentials in terms of the LPA – one finds the recurrence relation for fully interacting canonical partition functions

$$Z_{\pm}^{(N)} = \frac{1}{N}\sum_{n=1}^{N}(\pm 1)^{n-1}\mathcal{A}_n Z_{\pm}^{(N-n)}\,, \quad Z^{(0)} \coloneqq 1\,, \tag{1.277}$$

which is a purely combinatorial identity based on the fact that $Z^{(N)}$ comes as a sum over all possible partitions where the addends are products of objects related to the sizes of all parts. An equivalent, purely combinatorial, useful

general recurrence relation is given by

$$Z_{\pm}^{(N)} = (\pm 1)^{N-1}\frac{\mathcal{A}_N}{N} + \sum_{\substack{\mathfrak{N}\vdash N \\ |\mathfrak{N}|\geq 2}} \frac{(-1)^{|\mathfrak{N}|}(|\mathfrak{N}|-1)!}{\prod_{n=1}^{\infty} m_{\mathfrak{N}}(n)!} \prod_{n\in\mathfrak{N}} Z_{\pm}^{(n)} \tag{1.278}$$

which uses only the largest irreducible clusters and (fully interacting) partition functions of all smaller particle numbers.

The relation (1.277) is based on splitting off one part of (varying) size n from the partition of N, leaving the rest as all possible partitions of $N-n$. To see (1.277) more explicitly one can write the sum over integer partitions as a sum over ordered partitions

$$\sum_{\mathfrak{N}\vdash N} \frac{1}{\prod_{n=1}^{N} m_{\mathfrak{N}}(n)!}(\cdots) = \sum_{l=1}^{N}\frac{1}{l!}\sum_{\substack{\mathbf{n}\in\mathbb{N}^l \\ ||\mathbf{n}||=N}}(\cdots) \tag{1.279}$$

for all partition functions on the RHS of (1.277), where $||\mathbf{n}|| = ||\mathbf{n}||_1 = \sum_k n_k$ is defined as the one-norm. After splitting off the case $n = N$, swapping the sums over n and l one shifts the index l that characterizes the number of parts in the $Z^{(N-n)}$, by naming $l' = l+1$, so that l' specifies the total number of parts when regarding the whole expression as a single decomposition into partitions. After that one can again absorb the $n = N$ contribution into the sum over l as the case $l = 1$, yielding for the RHS

$$\sum_{l'=1}^{N}\frac{(\pm 1)^{N-l'}}{N(l'-1)!}\sum_{\substack{\mathbf{n}\in\mathbb{N}^{l'} \\ ||\mathbf{n}||=N}}\left(n_1\prod_{k=1}^{l'}\frac{\mathcal{A}_{n_k}}{n_k}\right) = \sum_{l'=1}^{N}\frac{(\pm 1)^{N-l'}}{l'!}\sum_{\substack{\mathbf{n}\in\mathbb{N}^{l'} \\ ||\mathbf{n}||=N}}\left(\prod_{k=1}^{l'}\frac{\mathcal{A}_{n_k}}{n_k}\right) = Z^{(N)}\,, \tag{1.280}$$

where the symmetry between all n_k in the sum over ordered partitions has been used to replace $n_1 = \sum_k n_k/l' = N/l'$ under the sum.

The QCE partition function is connected to the grand canonical description by the elementary identification with the grand canonical partition function

$$\begin{aligned} Z_{\mathrm{G}}(z) = &\left(\sum_{m_{\mathfrak{N}}(1)=0}^{\infty}\frac{(\pm 1)^{(1-1)m_{\mathfrak{N}}(1)}}{m_{\mathfrak{N}}(1)!}(\mathcal{A}_1/1)^{m_{\mathfrak{N}}(1)}z^{m_{\mathfrak{N}}(1)}\right) \\ &\times\left(\sum_{m_{\mathfrak{N}}(2)=0}^{\infty}\frac{(\pm 1)^{(2-1)m_{\mathfrak{N}}(2)}}{m_{\mathfrak{N}}(2)!}(\mathcal{A}_2/2)^{m_{\mathfrak{N}}(2)}z^{2m_{\mathfrak{N}}(2)}\right) \\ &\times\cdots \\ = &\prod_{n=1}^{\infty}\left[\sum_{m=0}^{\infty}\frac{1}{m!}\left(\pm(\pm z)^n\mathcal{A}_n/n\right)^m\right] \\ = &\exp\left[\pm\sum_{n=1}^{\infty}(\pm z)^n\mathcal{A}_n/n\right] \end{aligned} \tag{1.281}$$

as generating function of the canonical partition function

$$Z^{(N)} = \frac{1}{N!}\partial^N/\partial z^N Z_{\mathrm{G}}(z)|_{z=0}\,, \tag{1.282}$$

which is again an identity motivated purely combinatorially. Thus we identify the grand potential

$$\Phi_{\mathrm{G}} = \mp\frac{1}{\beta}\sum_{n=1}^{\infty}(\pm z)^n \mathcal{A}_n/n \tag{1.283}$$

by the basic relation $Z_{\mathrm{G}} = \exp(-k_{\mathrm{B}}T\Phi_{\mathrm{G}})$.

Under the assumptions of QCE the system size is large compared to the thermal de Broglie wavelength and to the range of the interactions, and hence each irreducible diagram is linear in the volume V_D [see discussion before (1.110) and (A.255)] or the effective volume V_{eff} associated to confining external potentials [see (1.212)]. Consider, for the moment, the homogeneous "unconfined" case $V_{\mathrm{eff}} = V_D$, for which one may write

$$\mathcal{A}_n = V_D c_n(\beta,\alpha)\,, \tag{1.284}$$

directly implying

$$\Phi_{\mathrm{G}} = -\underbrace{\left[\pm\frac{1}{\beta}\sum_{n=1}^{\infty}(\pm z)^n c_n(\beta,\alpha)/n\right]}_{=:P(\beta,\alpha,z)} V_D\,. \tag{1.285}$$

Thus one finds the thermodynamic Euler equation

$$\Phi_{\mathrm{G}} = -PV_D \tag{1.286}$$

for the grand potential, which is generally known to be true for systems that are homogeneous in the following sense [139]. The assumption is that all variables separate into intensive and extensive quantities, which correspond to variables of homogeneity degree 0 and 1, respectively, so that, *e.g.*, volume V_D and particle number N are in linear relationship with thermodynamic potentials like internal energy U, free energy F and grand potential Φ_{G}.

In the case of small systems or long-range interactions this assumption and hence the thermodynamic Euler equation (1.286) become invalid [139], which is exactly the same deal-breaker as for the QCE approach. Out of this circumstance it is not surprise that the general form (1.110) of QCE neglecting physical boundary effects maps to (1.286).

Usually one understands the system property of homogeneity as a type of scale-invariance of the system which asserts that the set of micro states in a realization of the system with volume λV_D (and λN particles) is the same as the one of λ coexisting realizations of volume V_D (and N particles). This fits to the assumption of flat or zero external potential in the *unconfined* QCE. However, in LPA smooth confining external potentials are incorporated into the framework (see section 1.4.2) in a way that is equivalent at the combinatorial level and in the functional dependence on the parameter V_{eff}, specifying effectively the volume of the system. This extends the applicability of (1.286) to systems that are not strictly scale-invariant in the above sense by virtue of the considerations within the cluster expansion. Moreover, commonly one assumes (1.286) to be restricted to macroscopic systems close to the thermodynamic limit. The connection to the QCE together with its applicability for few-body systems (see section 1.1.6)

proves this assumption wrong to some extent[21]. Furthermore, besides the usual form [139]

$$\Phi_{\mathrm{G}} = V_D(a_1 z + a_2 z^2 + a_3 z^3 + \ldots)\,, \tag{1.287}$$

the connection with QCE makes the meaning of the coefficients in the fugacity expansion explicit. They correspond to the internal amplitudes of irreducible cluster propagations.

The connection to the thermodynamic limit – Borrowing small clusters from the macroscopic solution

The crucial requirement for the connection (1.284) and (1.285) of the canonical QCE to the grand canonical descriptions is homogeneity in the latter. On the grand canonical side this in particular demands a large (average) number of particles and at the same time a large system size. One typically finds the homogeneous physics (dropping finite-size effects) by taking the thermodynamic limit of constant particle density $\langle N\rangle/V_D = \text{const.}$ while taking $\langle N\rangle \to \infty$ and $V_D \to \infty$. The homogeneity of the system described grand canonically in the thermodynamic limit then is equivalent to neglecting the finiteness of the system size in the local short-time dynamics used in the QCE (see also section 1.1.2). We see in this context universality and homogeneity as two facets of the same physical premise. As we have seen, under homogeneity the pressure is a purely intensive quantity that admits an expansion in the fugacity $z = \mathrm{e}^{\beta\mu}$ with chemical potential μ independent of the system size V_D (there is no other extensive quantity to compensate for V_D). If the coefficients c_n of the fugacity expansion

$$P(\beta,\alpha,z) = \pm\frac{1}{\beta}\sum_{n=1}^{\infty}(\pm z)^n\frac{1}{n}c_n(\beta,\alpha) \tag{1.288}$$

in the grand canonical description of a homogeneous system (usually in the thermodynamic limit) are known, the unique connection (1.285) guarantees that the summed-up irreducible cluster diagrams of size n are given as damping factors (1.136) by

$$a_n(\beta\alpha) = \lambda_{\mathrm{T}}^D n^{\frac{D}{2}} c_n(\beta,\alpha)\,. \tag{1.289}$$

In the following it will be shown how this connection can be used to obtain the higher-order damping factors $a_{\geq 3}(\beta\alpha)$ for delta interaction by exploiting the solvability of the Lieb-Liniger model. Once those are obtained, they are quantities specific for delta interaction in one dimension but do not depend on the overall number of particles, the particular boundary conditions or whether external potentials are applied or not. Therefore their information can then be transfered to non-solvable systems and especially few-particle systems for which a canonical description is essential (see section 1.1.6).

The exact analytical solution (1.179) of Lieb and Liniger was shown to be applicable to the thermodynamic limit by Yang and Yang [172]. The main idea is to transform the discrete distribution of quantum numbers (1.180) and corresponding pseudomomenta k into continuous distribution *functions* by scaling

[21] Applicability of (1.286) is meant here in the weak sense that it applies to systems that explicitly allow for particle exchange. The invalidity of grand canonical descriptions for closed systems of only few constituents is a different subject not touched here (see section 1.1.6 on a discussion on that point).

them with the system size to be infinitesimally narrow. This way Yang and Yang showed how one can obtain integral equations that represent the thermal equilibrium of the Lieb-Liniger solution in the thermodynamic limit. This procedure involves a maximization of the contribution to the partition function under variation of the density of pseudomomenta under the constraint of given (average) particle density $\langle N\rangle/L$ which introduces the chemical potential μ as a Lagrange parameter. It is therefore naturally given in grand canonical description (which is equivalent to the canonical description because of the thermodynamic limit). This procedure (and the equivalent in other systems that are solvable by Bethe ansatz) is commonly referred to as the *thermodynamic Bethe ansatz*. They give the solution for the pressure

$$P = \frac{k_{\mathrm{B}}T}{2\pi}\int_{-\infty}^{\infty}\mathrm{d}k\ \log\left(1+\mathrm{e}^{-\beta\epsilon(k)}\right) \tag{1.290}$$

in terms of $\mathrm{e}^{\beta\epsilon(k)} = \varrho_{\mathrm{h}}(k)/\varrho(k)$, representing the density $\varrho_{\mathrm{h}}(k)$ of "holes" relative to the "occupied" pseudomomenta k (given by $\varrho(k)$). It is determined as the unique solution of the non-linear integral equation

$$\mathrm{e}^{-\beta\epsilon(k)} = z\mathrm{e}^{-\beta k^2}\exp\left[\int_{-\infty}^{\infty}\mathrm{d}q\ \frac{c/\pi}{c^2+(k-q)^2}\log\left(1+\mathrm{e}^{-\beta\epsilon(q)}\right)\right], \tag{1.291}$$

where the coupling parameter $c>0$ is taken from the scaled Lieb-Liniger Hamiltonian (1.170) and gets identified as

$$c = \sqrt{2\alpha} \tag{1.292}$$

when introducing proper units. As shown in a proceeding paper [173], the integral equation (1.291) admits a solution by iteration employing the power series ansatz

$$\mathrm{e}^{-\beta\epsilon(k)} = \sum_{n=1}^{\infty} b_n(k) z^n\,. \tag{1.293}$$

By this ansatz one finds the coefficient functions $b_n(k)$ [not to be confused with $b_j^{(l)}$ in (1.161) and (1.162)] to be recursively defined by all lower ones $b_{<n}(k)$ involving multiple application of the integral operator $\int_{-\infty}^{\infty}\mathrm{d}q\ \frac{c/\pi}{c^2+(k-q)^2}$ with Lorentzian kernel[22] of width c. The dependence of the coefficients b_n on k, β and c reduces to $b_n = b_n(\sqrt{\beta}k, \beta\alpha)$ with the identification (1.292). The expansion of (1.290) in powers of the fugacity leads then to the identification of irreducible cluster diagrams (1.289). Expressed by the energy-like interaction parameter α (as premised in (1.145)) one finds the summed-up damping factors of irreducible clusters of size n to be

$$a_n(\beta\alpha) = \frac{1}{\sqrt{\pi}}n^{\frac{3}{2}}\sum_{\mathfrak{N}\vdash n}\frac{(-1)^{|\mathfrak{N}|-1}(|\mathfrak{N}|-1)!}{\prod_{m=1}^{\infty}m_{\mathfrak{N}}(m)!}\int_{-\infty}^{\infty}\mathrm{d}(\sqrt{\beta}k)\ \prod_{m\in\mathfrak{N}}b_m(\sqrt{b}k,\beta\alpha)\,. \tag{1.294}$$

[22] Note that for $c\to 0$ the kernel becomes $\delta(k-q)$ so that the integral operator becomes the identity, allowing for a direct solution of (1.291) yielding the known non-interacting grand canonical description (1.88).

For $n = 1, 2$ the application of (1.294) reproduces the results from first order QCE

$$\begin{aligned} a_1 &= 1\,, \\ a_2 &= \underbrace{1}_{\text{non-int.}} + \underbrace{2a_{1,1}(\beta\alpha)}_{\text{intra + inter}} = -1 + 2\mathrm{e}^{\beta\alpha}\,\mathrm{erfc}(\beta\alpha) \end{aligned} \tag{1.295}$$

as expected, which confirms the correctness of the identification with the grand canonical solution in the thermodynamic limit. note that sum of all irreducible clusters of size n always the non-interacting n-cycle contributing unity to the corresponding a_n.

The full three-body system

The application to the sum of irreducible three-clusters reveals that the multiple integrals involved can be reduced to

$$a_3(\beta\alpha) = 1 + \frac{9}{\sqrt{\pi}}\left(-F_{\frac{1}{\sqrt{3}}}(\beta\alpha) - F_{\sqrt{3}}(\beta\alpha) + \frac{\sqrt{\pi}}{2}\mathrm{e}^{4\beta\alpha}\,\mathrm{erfc}(\sqrt{4\beta\alpha})\right), \tag{1.296}$$

expressed in terms of the integral function (1.159) already found in the context of first-order clusters. This gives directly the interaction effect on the coefficient function $\Delta z_1^{(3)}(\beta\alpha) = 3^{-\frac{d}{2}-1}(a_3(\beta\alpha) - 1)$, which is now valid for arbitrary homogeneous external potential with effective dimension d. Correspondingly, *e.g.*, by use of the recursion (1.278) one obtains the (universal part of the) canonical partition function

$$Z^{(3)} = Z^{(1)}Z^{(2)} - \frac{1}{3}(Z^{(1)})^3 + \left(\frac{V_{\text{eff}}}{\lambda_{\text{T}}^d}\right)3^{-\frac{d}{2}-1}a_3(\beta\alpha) \tag{1.297}$$

of the fully interacting three-body system in one dimension with homogeneous potential in LPA (see section 1.4.2). The corresponding spectral counting function (1.216) is given by the coefficient function

$$g_1^{(3)}(\epsilon) = 3^{1-\frac{d}{2}}\frac{1}{2}\left(-b_3^{(d)}(\epsilon)\Big|_{\bar{\nu}=\frac{1}{\sqrt{3}}} - b_3^{(d)}(\epsilon)\Big|_{\bar{\nu}=\sqrt{3}} - \frac{\sqrt{\pi}}{4}\epsilon^{\frac{1}{2}}b_2^{(d+1)}\left(\frac{\epsilon}{4}\right)\Big|_{\bar{\nu}=1}\right) \tag{1.298}$$

in terms of the functions $b_j^{(l)}$ found for first-order contributions (see section 1.3.2). For integer effective dimension those are expressed in terms of elementary functions. Here, j indexes the four different terms, while $\bar{\nu}$ is put explicitly. To check consistency, the analytic limits $\epsilon \to 0, \infty$ of (1.297) and (1.298) reproduce the exact non-interacting bosonic and fermionic counting functions.

For comparison, I chose again the experimentally relevant case of harmonic confinement $d = 2$, which makes the system of three contact-interacting bosons truly non-solvable. The corresponding counting function of three bosons is shown in Fig. 1.29. We observe perfect agreement with the (average) exact numerical calculation in the full range from the ideal Bose gas to the fully fermionized limit of the Tonks-Girardeau gas (see section 1.4.1) on all energy scales.

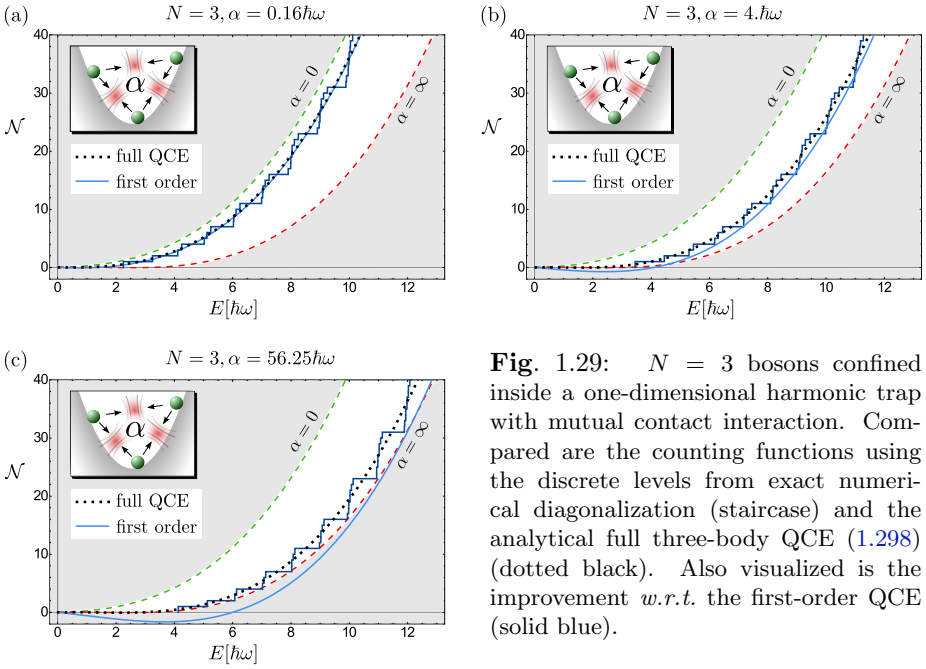

Fig. 1.29: $N = 3$ bosons confined inside a one-dimensional harmonic trap with mutual contact interaction. Compared are the counting functions using the discrete levels from exact numerical diagonalization (staircase) and the analytical full three-body QCE (1.298) (dotted black). Also visualized is the improvement *w.r.t.* the first-order QCE (solid blue).

The N-body system in second order

One way to make heavy use of the gained analytical knowledge about the irreducible three-body clusters beyond a three-particle system is to employ it for second-order energy shifting (see section 1.5.2). This is possible since the latter demands analytical matching of the next-to-leading (NL) and next-to-next-to-leading order (NNL) terms in the expansion of the counting function in powers of $\rho_0^{\text{eff}} E$ or similarly in powers of the system size V_{eff}. This involves the interaction coefficient functions $g_{N-1}^{(N)}(E/\alpha)$ and $g_{N-2}^{(N)}(E/\alpha)$, respectively. The first one corresponds to the power V_{eff}^{N-1}, related to a partition into $N-1$ clusters. This implies a clustering of two particles while all the others are unclustered, and therefore is fully determined by the first-order QCE (resulting in the first-order energy shifting). The second function, as coefficient of V_{eff}^{N-2} analogously represents partitions into $N-2$ clusters. This includes two possibilities, the clustering of two (independent) pairs of particles or the clustering of three particles at once. The two-clusters are again given by (1.295) already found within the first-order QCE. In addition to that the connection to the thermodynamic limit equips us with the analytical knowledge of the three-body clusters (1.296). The NNL order term in the full QCE of N particles is

$$\begin{aligned} g_{N-2}^{(N)}(\epsilon) =& \frac{2^{-d-3}(N-3)}{(N-3)!}\epsilon^{-\frac{(N-2)d}{2}}\,\mathscr{L}_{\text{s}}^{-1}\left[s^{-\frac{(N-2)d}{2}-1}\left((a_2(s))^2-1\right)\right](\epsilon) \\ &+ \frac{3^{-\frac{d}{2}-1}}{(N-3)!}\epsilon^{-\frac{(N-2)d}{2}}\,\mathscr{L}_{\text{s}}^{-1}\left[s^{-\frac{(N-2)d}{2}-1}\left(a_3(s)-1\right)\right](\epsilon)\,. \end{aligned} \tag{1.299}$$

Figure 1.30 shows the application of the second order energy shifting method (see section 1.5.2) to the Lieb-Liniger model. The parameters in the $(N = 6)$-particle case Fig. 1.30a are the same as in Fig. 1.19f, where the breakdown of

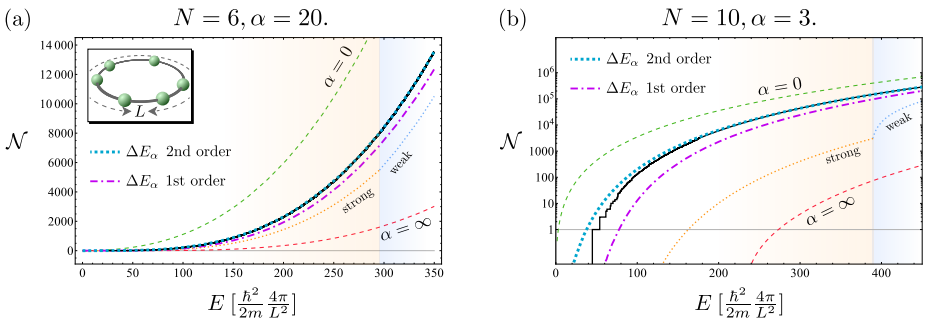

Fig. 1.30: Counting functions in the Lieb-Liniger model. Exact numerics (black staircase) as benchmark for the first-order (purple dash-dotted) and second-order (blue thick dotted) energy shifting method. Also shown is the breakdown of direct first-order QCE (weak: blue thin dotted, strong: orange thin dotted) in the regime of intermediate interaction in the case of $N = 6$ (a) and due to larger particle number $N = 10$ in (b), where a logarithmic plot is chosen to compress the strongly growing function into a good visualization of all relevant features. Coupling strengths α are given in units of $\rho_0^{-1} = \frac{\hbar^2}{2m}\frac{L^2}{4\pi}$.

first-order QCE for intermediate interactions was observed within the shown range of energies. Whereas the first-order shift already improves heavily on the direct QCE, the correction due to second order makes the analytical approach indistinguishable from the exact numerics. Because of the solvability of the model one can even go to larger numbers of particles. In Fig. 1.30b we observe very good agreement with the (average) many-body spectrum for $N = 10$ bosons, here numerically calculated up to $\sim 3 \times 10^5$ levels, whereas the direct QCE to first order deviates by several orders of magnitude.

In total this confirms even further the universal applicability of the shifting method to arbitrary numbers of particles on all energy and interaction scales. It has here been extensively benchmarked with and without the presence of harmonic confinement up to the regimes where exact numerical calculation is already at the border of tractability.

1.6 Spatial quantities

This section issues the possibility to use the knowledge obtained so-far about the QCE in order to get a more detailed view on many-body systems by looking at spatially resolved quantities. So far only spatially traced quantities have been investigated, but since the basic ingredient that is expanded in terms of interaction events is the many-body propagator, the information we started with is a spatially resolved quantity. As special applications particle densities, many-body local DOS and non-local pair correlations will be discussed in the following subsections.

To ease notation a bit and in view of the final application to contact interacting bosons in one dimension, the quantum statistics will be fixed to bosons and $D = 1$ within the scope of this section. The general statements can be easily extended to the analogous case of fermions and arbitrary D.

1.6.1 Thermal particle density and local DOS – Examples of one-body observables

Thermal equilibrium in closed or isolated systems

For a system of a fixed number of bosons N in first-quantized description, consider a one-body observable

$$\hat{O}^{(1)} := \sum_{i=1}^{N} \hat{O}_i^{(1)}\,, \tag{1.300}$$

where the $\hat{O}_i^{(1)}$ are copies of the same single-particle observable acting on the particle with label i. In general the arbitrary single-particle observable in Dirac notation can be expressed in coordinate basis as

$$\hat{O}_i^{(1)} = \int \mathrm{d}x\mathrm{d}y\; o(x,y)\big(|x\rangle\langle y|\big)_i\,. \tag{1.301}$$

While many statements to follow hold for this general case or may be easily extended to it I am here particularly interested in the probability density

$$\hat{n}_i(x) = \delta(\hat{x}_i - x) \tag{1.302}$$

to find particle i at a point x which corresponds to the one-body observable of particle density

$$\hat{n}(x) = \sum_{i=1}^{N} \hat{n}_i(x) \tag{1.303}$$

in the many-body system. Another often-studied one-body observable would be the single-particle momentum occupation density which is commonly used to study deviations from non-interacting Bose-Einstein statistics due to interactions.

The goal is to connect such quantities to the QCE approach, the scope of which are universal (or average) properties of the system. One way to look at this restriction is that it can only provide descriptions of thermally equilibrated

systems (or short time dynamics). In thermal equilibrium of constant temperature $k_{\mathrm{B}}T = 1/\beta$ the expectation value of the particle density is given as the average in the canonical ensemble (denoted by subscript C)

$$n_{\mathrm{C}}(x,\beta) := \langle \hat{n}(x) \rangle_{\mathrm{C}} = \frac{1}{Z^{(N)}} \operatorname{tr}\left(\hat{\mathbb{1}}_{+} \mathrm{e}^{-\beta \hat{H}} \hat{n}(x) \right) , \tag{1.304}$$

where the restriction to states of correct exchange symmetry is guaranteed by the corresponding projection operator $\hat{\mathbb{1}}_{+}$ as in section 1.1.3. The density can be easily expressed in terms of the symmetrized many-body propagator with imaginary time as

$$n_{\mathrm{C}}(x,\beta) = \frac{N}{Z^{(N)}} \int \mathrm{d}^{N-1}q \; K_{+}^{(N)}((x,\mathbf{q}),(x,\mathbf{q}); t = -\mathrm{i}\hbar\beta) , \tag{1.305}$$

where the intention is now again to use the short-time dynamical information contained in the expansion in Ursell operators to obtain the universal behavior. If one is interested in the particle density in a microcanonical description of an isolated system (denoted by subscript M), expression (1.305) is easily transfered by inverse Laplace transform

$$n_{\mathrm{M}}(x,E) = \mathscr{L}_{\beta}^{-1}[n_{\mathrm{C}}(x,\beta)](E) , \tag{1.306}$$

which is closely related to the many-body local DOS

$$\bar{\rho}_{\mathrm{loc}}^{(N)}(E,x) = \frac{1}{N} \bar{\rho}^{(N)}(E) n_{\mathrm{M}}(x,E) , \tag{1.307}$$

valid in the universal regime. A general one-body observable (1.301) in thermal average similarly reads

$$\langle O^{(1)} \rangle_{\mathrm{C}} = \frac{N}{Z^{(N)}} \int \mathrm{d}x \mathrm{d}y \; o(x,y) \int \mathrm{d}^{N-1}q \; K_{+}^{(N)}((y,\mathbf{q}),(x,\mathbf{q}); t = -\mathrm{i}\hbar\beta) , \tag{1.308}$$

which identifies the partial traces

$$\begin{aligned} G_{2,\mathrm{C}}(x,y;\beta) &= N \left\langle \left(|x\rangle\langle y| \right)_1 \right\rangle_{\mathrm{C}} \\ &= \frac{N}{Z^{(N)}} \int \mathrm{d}^{N-1}q \; K_{+}^{(N)}((y,\mathbf{q}),(x,\mathbf{q}); t = -\mathrm{i}\hbar\beta) \end{aligned} \tag{1.309}$$

of symmetrized (short-time) propagators (1.25) as building blocks, which are a canonical (few-body) version of (time-ordered) two-point Green's functions

$$G_{2,\mathrm{G}}(x,y;\beta) = \left\langle T\{\hat{\psi}^{\dagger}(y,\beta)\hat{\psi}(x,0)\} \right\rangle_{\mathrm{G}} \tag{1.310}$$

in a grand canonical (denoted with subscript G) second quantized or statistical quantum field approach [21], where $\hat{\psi}^{(\dagger)}(q,\tau)$ are field operators in Heisenberg picture of imaginary time $\tau = \mathrm{i}t/\hbar$.

The partition into hierarchical interaction effects (1.103) and exchange cycles (1.36) imposes the same cluster structure (see section 1.2.3) as for the full trace [compare to (1.109)] involved in the QCE for the partition function or the many-body DOS. Expanding the symmetry projection into permutations and further into cycles gives each particle an individual label. The cluster that

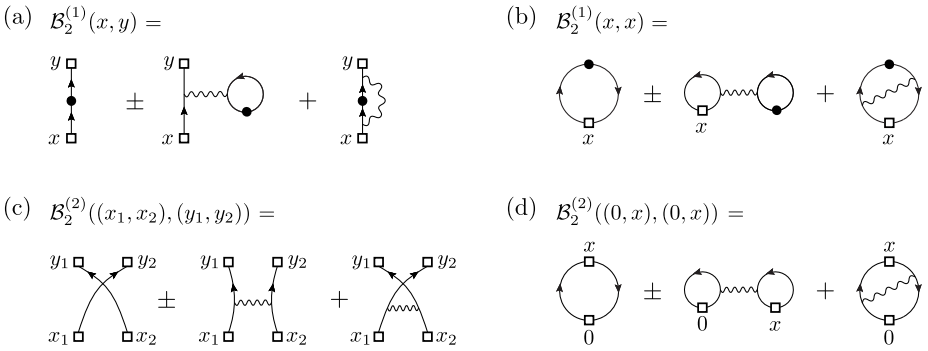

Fig. 1.31: Sums of irreducible spatial cluster diagrams of size $n = 2$ as input for one- and two-body observables. They represent the dominant effect of indistinguishability and interactions on (a) the propagator (1.312) [and (1.310)] of a particle in the gas, (b) the particle density (1.314) [and (1.317)] as its diagonal part $x = y$, (c) the (correlated) propagator (1.324) [and (1.325)] of two particles in the gas, and (d) the non-local pair correlation (1.331) as its diagonal part $\mathbf{x} = \mathbf{y}$. The diagrams of each quantity are ordered *w.r.t.* cluster structure from left to right: non-interacting symmetry effect, pure interaction effect, combination of both. The diagrams are vertically aligned so that the terms in the first line (a and b) are obtained from the second line (c and d) by tracing according to (1.323).

contains the particle (say, with label $i = 1$) with fixed initial coordinate x also contains the particle (say, with label $i = n$) with fixed final coordinate y, because they belong to the same cycle (say, $\sigma = \begin{pmatrix} 1 & 2 & \dots & n \end{pmatrix}$). Such spatial clusters contain terminal points in their diagrammatic representations, which may be depicted by squares to distinguish them from non-terminal points in the case $y = x$ (see examples in Fig. 1.31). I denote the (symmetry-weighted) sum of all such spatial clusters of size n with $\mathcal{B}_n^{(1)}(x,y)$ analogously to the fully traced clusters $\mathcal{A}_n$, which could then be obtained by the single-particle trace[23]

$$\mathcal{A}_n = \int \mathrm{d}x \; \mathcal{B}_n^{(1)}(x,x)\,. \tag{1.311}$$

These spatial cluster-sums $\mathcal{B}_2^{(1)}(x,y)$ of size $n = 2$ for one-body observables are shown in Fig. 1.31a. All combinatorial aspects are not affected by leaving out this trace besides that the irreducible objects $\mathcal{B}^{(1)}$ have to be distinguished from the cluster-sums $\mathcal{A}$. In particular one obtains the spatial analogue

$$G_{2,\mathrm{C}}(x,y,\beta) = \frac{1}{Z^{(N)}} \sum_{n=1}^{N} \mathcal{B}_n^{(1)}(x,y) Z^{(N-n)}\,, \quad Z^{(0)} \coloneqq 1 \tag{1.312}$$

of the recursive formula (1.277). A general one-body thermal average can therefore be written in the way

$$\langle O^{(1)} \rangle_{\mathrm{C}} = \frac{1}{Z^{(N)}} \sum_{n=1}^{N} \mathcal{B}_n^{(1)} Z^{(N-n)} \tag{1.313}$$

[23]The identification with the fully traced cluster-sums under tracing uniquely determines the combinatorial multiplicities for the cluster-sums $\mathcal{B}_n$ with fixed coordinates.

with $\mathcal{B}^{(1)} = \int \mathrm{d}x\mathrm{d}y\, o(x,y)\mathcal{B}^{(1)}(x,y)$. The particle density of a N-particle system becomes expressed in terms of QCE partition functions and spatial clusters as

$$n_{\mathrm{C}}(x,\beta) = \frac{1}{Z^{(N)}} \sum_{n=1}^{N} \mathcal{B}_n^{(1)}(x,x) Z^{(N-n)} \,. \tag{1.314}$$

Eq. (1.314) and in general (1.313) are the starting point to calculate universal thermal averages of one-body observables. They are given in terms of irreducible clusters (non-spatial and spatially dependent). In principle, assuming knowledge of the cluster contributions of all sizes $1,\ldots,N$, they are valid for arbitrary number of particles and should be valid down to the quantum degenerate regime of (quasi-)condensation unless system specific features and discreteness start to dominate the physics. In particular in few-body systems of very small number of particles ($N \lesssim 5$), we have observed that one can get very good approximations using the direct QCE approach by truncating to (non-perturbative) first order in the interaction, especially in the regimes of weak and strong coupling. In addition, as described in section 1.5.3, one can derive the universal fully interacting three-body propagator for delta interactions in one dimension. Thus the second-order QCE can also be calculated here even for the spatially dependent clusters[24].

But instead of using the direct canonical approach I will take here another road, which elevates the knowledge of universal spatial quantities to the application to large numbers of particles close to the thermodynamic limit.

Thermal equilibrium in open systems

In the thermal diffusive equilibrium at given temperature and chemical potential μ (or equivalently fugacity $z = \mathrm{e}^{\beta\mu}$) the description as grand canonical ensemble applies (denoted by the subscript G). In the strict thermodynamic limit of constant (average) particle density, the canonical and grand canonical descriptions are equivalent in many aspects. The general relation between the thermal averages in the two cases is

$$\langle \hat{O} \rangle_{\mathrm{G}} = \frac{1}{Z_{\mathrm{G}}} \sum_{N=1}^{\infty} z^N Z^{(N)} \langle \hat{O} \rangle_{\mathrm{C}} \,, \tag{1.315}$$

with the grand canonical partition function $Z_{\mathrm{G}} = \sum_{N=0}^{\infty} z^N Z^{(N)}$, which, in QCE, is given by (1.281). The recursive formulation (1.313) leads to the fugacity expansion

$$\langle \hat{O}^{(1)} \rangle_{\mathrm{G}} = \sum_{n=1}^{\infty} \mathcal{B}_n^{(1)} z^n \tag{1.316}$$

in terms of the irreducible spatially dependent cluster diagrams. In case of a homogeneous dilute gas far above quantum degeneracy in the sense that $\langle N \rangle / V_D \ll \lambda_{\mathrm{T}}^{-D}$ the fugacity expansion (1.316) can be inverted using

$$N = \langle \hat{N} \rangle_{\mathrm{G}} = \sum_{n=1}^{\infty} \mathcal{A}_n z^n \,. \tag{1.317}$$

[24] Note that the spatial dependence in contrast to the second-order QCE for global quantities (partition function and counting function) cannot be taken from the Yang solution (see section 1.5.3) but relies on a detailed derivation of the three-body propagator using a large system size analysis of the Lieb-Liniger solution for $N = 3$ [184].

to yield virial-type expansions (compare to section 1.1.6). The small parameter is then the thermally scaled particle density

$$\tilde{n} = n\lambda_{\mathrm{T}}^{D}\,, \tag{1.318}$$

which is the average number of particles within a cell of the size of the thermal de Broglie wavelength. The same kind of expansion would be obtained from the canonical average (1.313) by expanding the rational function in $n\lambda_{\mathrm{T}}^{d}$ with the only difference that the latter contains finite-size corrections of order N^{-1} to the constant coefficients of the clusters $\mathcal{B}_n^{(1)}$.

Because for homogeneous systems the particle density is constant and particularly uninteresting we leave the stage of one-body averages. I do not address here the work on Friedel-type oscillations in the vicinity of hard walls investigated in the non-interacting few-body sector [185] or the related influence of hard walls on two interacting bosons [168]. Further investigations in that direction, especially considering single-particle momentum occupations and particle densities for confined interacting systems are postponed to future work. Nevertheless the general considerations here serve as a good starting point to investigate two-body observables in equilibrium.

1.6.2 Non-local pair correlations as two-body observable

Thermal equilibrium in closed systems

Analogous to the considerations on one-body observables in the previous subsection one can rewrite the thermal average of two-body observables

$$\hat{O}^{(2)} = \int \mathrm{d}x_1\mathrm{d}y_1\mathrm{d}x_2\mathrm{d}y_2\; o(\mathbf{x},\mathbf{y}) \sum_{\substack{i,j=1\\ i\neq j}}^{N} \left(|x_1\rangle\langle y_1|\right)_i \otimes \left(|x_2\rangle\langle y_2|\right)_j \tag{1.319}$$

by splitting of the clusters containing the two measured particles as

$$\langle O^{(2)}\rangle_{\mathrm{C}} = \frac{1}{Z^{(N)}}\left[\sum_{n=2}^{N}\mathcal{B}_n^{(2)}Z^{(N-n)} + \sum_{n_1=1}^{N-1}\sum_{n_2=1}^{N-n_1}\mathcal{B}_{n_1}^{(1)}\mathcal{B}_{n_2}^{(1)}Z^{(N-n_1-n_2)}\right], \tag{1.320}$$

where the cluster diagrams of size n containing both observed particles at once (see Fig. 1.31) are subsumed to

$$\mathcal{B}_n^{(2)} = \int \mathrm{d}x_1\mathrm{d}y_1\mathrm{d}x_2\mathrm{d}y_2\; o(\mathbf{x},\mathbf{y})\mathcal{B}_n^{(2)}(\mathbf{x},\mathbf{y})\,, \tag{1.321}$$

while the cases of diagrams where the two measured particles belong to different clusters are subsumed to

$$\mathcal{B}_{n_1}^{(1)}\mathcal{B}_{n_2}^{(1)} = \int \mathrm{d}x_1\mathrm{d}y_1\mathrm{d}x_2\mathrm{d}y_2\; o(\mathbf{x},\mathbf{y})\mathcal{B}_{n_1}^{(1)}(x_1,y_1)\mathcal{B}_{n_2}^{(1)}(x_2,y_2)\,, \tag{1.322}$$

which has to be understood symbolically in case that the matrix elements $o(\mathbf{x},\mathbf{y})$ of the observable are not factorizing *w.r.t.* to the two particles. In the case of pair correlations considered below it factorizes literally into the product of $\mathcal{B}_{n_1}^{(1)}$ and $\mathcal{B}_{n_2}^{(1)}$.

Tracing out the two-body spatial clusters relates them to the one-body spatial clusters and fully traced clusters by (see vertically associated terms in Fig. 1.31)

$$\begin{aligned} \int \mathrm{d}q\, \mathcal{B}_n^{(2)}((x_1,q),(y_1,q)) &= (n-1)\mathcal{B}_n^{(1)}(x_1,y_1)\,, \\ \int \mathrm{d}^2x\, \mathcal{B}_n^{(2)}(\mathbf{x},\mathbf{x}) &= (n-1)\mathcal{A}_n\,. \end{aligned} \tag{1.323}$$

The building blocks of (1.320) are the canonical four point Green's functions (see Fig. 1.31c)

$$G_{4,\mathrm{C}}(\mathbf{x},\mathbf{y};\beta) = \frac{N(N-1)}{Z^{(N)}} \int \mathrm{d}^{N-2}q\; K_+^{(N)}((y_1,y_2,\mathbf{q}),(x_1,x_2,\mathbf{q});t=-\mathrm{i}\hbar\beta) \tag{1.324}$$

with second-quantized counterpart

$$G_{4,\mathrm{G}}(\mathbf{x},\mathbf{y};\beta) = \left\langle T\{\hat\psi^\dagger(y_2,\beta)\hat\psi^\dagger(y_1,\beta)\hat\psi(x_2,0)\hat\psi(x_1,0)\}\right\rangle_{\mathrm{G}}\,. \tag{1.325}$$

One commonly studied special case of particular interest is the non-local pair correlation (see, *e.g.*, [186] for a classification of regimes).

$$g_2(x) = G_{4,\mathrm{C}}((0,x),(0,x);\beta)/n^2\,, \tag{1.326}$$

not to be confused with the QCE coefficient functions $g_l(E/\alpha)$ (1.142). Here, n denotes the particle density. Assuming a homogeneous system implies invariance *w.r.t.* simultaneous translations $(\mathbf{x},\mathbf{y}) \mapsto (\mathbf{x}+\mathbf{a},\mathbf{y}+\mathbf{a})$ of measurements, so that n is constant and (1.326) reflects the probability density of finding two different particles at a spatial separation x in thermal equilibrium (of a closed system with fixed number of particles). The corresponding expression in terms of partially traced cluster diagrams (1.320) is given by

$$\mathcal{B}_n^{(1)} = \mathcal{B}_n^{(1)}(x,x) = \mathcal{B}_n^{(1)}(0,0) \quad \text{invariant } w.r.t.\ x\,, \tag{1.327}$$

$$\mathcal{B}_n^{(2)} = \mathcal{B}_n^{(2)}((0,x),(0,x))\,. \tag{1.328}$$

For small numbers of particles one could now use the representation (1.320) in terms of irreducible clusters in a direct QCE approach approximated by truncation to first order or second order in the interaction events, which should reproduce the universal behavior correctly down to quantum degenerate regime especially well for weak couplings (or strong couplings by virtue of fermionization mapping, see section 1.4.1).

Again, I will instead apply the gained knowledge about irreducible clusters to make statements about interacting homogeneous Bose gases in the thermodynamic limit in the high temperature (or equivalently dilute) regime far above quantum degeneracy.

Thermal equilibrium in open systems

By the general connection (1.315) of thermal averages in open and closed systems one can again easily obtain the fugacity expansion of equilibrium two-body observable from (1.320). It reads

$$\langle \hat O^{(2)}\rangle_{\mathrm{G}} = \sum_{n=2}^{\infty} z^n \left(\mathcal{B}_n^{(2)} + \sum_{m=1}^{n-1} \mathcal{B}_m^{(1)}\mathcal{B}_{n-m}^{(1)}\right) \tag{1.329}$$

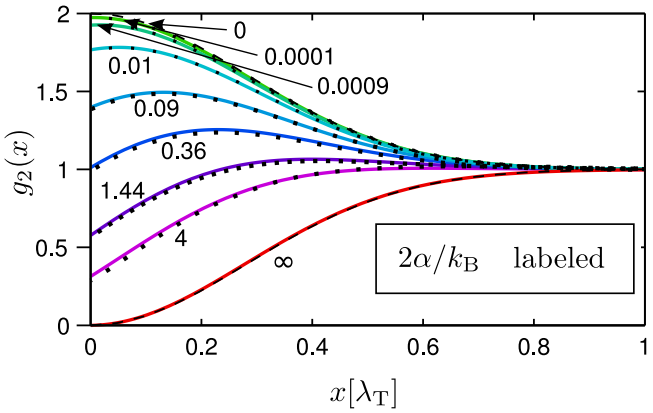

Fig. 1.32: The non-local pair correlation for repulsively short-range interacting Bose gas in the dilute high temperature regime $N\lambda_T/L = \sqrt{4\pi}/100 \approx 0.0354$. Compared are results obtained from numerical calculations taken from [187] with the dominant analytic expression (1.333) obtained from QCE. The known high-temperature asymptotics of the limits $\alpha \to 0, \infty$ (dashed) are exactly reproduced by (1.333).

in terms of the irreducible spatial clusters in general and represents the non-local pair correlation in case of (1.327)and (1.328). By fugacity inversion using (1.317) one obtains then again a virial-type expansion of g_2 in powers of the density $n\lambda_T^D$. Before applying the machinery to the case of delta interaction in one dimension one should loose a few words on the analytic structure of (1.316). The second term of measuring separate clusters factorizes in the product of two one-body expansions (1.316) which coincide with the particle density $n(x) = n$. This term therefore gives exactly the constant pair correlation of a non-interacting distinguishable gas, which is normalized to unity, hence we write

$$g_2(x) = 1 + \Delta g_2(x)\,. \tag{1.330}$$

The non-trivial pair-correlation due to exchange statistics and interactions is fully contained in the two-body cluster part (1.328). This fits consistently into the term-by-term picture of interpreting the structure of QCE. If two particles are measured that are not connected by an exchange cycle (in one particular contribution), it means they effectively behave like distinguishable particles. Moreover, if they are neither connected by interaction they can be considered non-interacting. Thus, in the sum of all such separable contributions one gets exactly the constant, non-interacting and distinguishable case $g_2 = 1$.

The fully interacting repulsive one-dimensional Bose gas in the high-temperature regime

We look into the regime of high temperatures with small average number of particles within a cell of the size of the thermal de Broglie wavelength. There, only the dominant term contributes to the pair correlation (see Fig. 1.31)

$$\Delta g_2 = n^{-2} z^2 \mathcal{B}_2^{(2)}((0,x),(0,x)) + \mathcal{O}(z^3) \tag{1.331}$$

and the average number of particles

$$\langle N\rangle_{\mathrm{G}} = \mathcal{A}_1 z = \frac{L}{\lambda_{\mathrm{T}}} z + \mathcal{O}(z^2)\,. \tag{1.332}$$

After fugacity inversion and identifying the spatial two-body clusters of size $n = 2$ as interacting two-body propagator (1.150) one directly obtains the (high temperature) dilute gas limit

$$\Delta g_2(x) \xrightarrow[N\lambda_{\mathrm{T}}\ll L]{} \mathrm{e}^{-2\pi\tilde{x}^2}\left(1 - \sqrt{4\pi s}\mathrm{e}^{(\sqrt{s}+\sqrt{2\pi}|\tilde{x}|)^2}\,\mathrm{erfc}\left(\sqrt{s}+\sqrt{2\pi}|\tilde{x}|\right)\right)\,, \tag{1.333}$$

of the repulsive Bose gas in terms of the thermal coupling strength $s = \alpha/(k_{\mathrm{B}}T)$ and the dimensionless distance $\tilde{x} = x/\lambda_{\mathrm{T}}$. As asymptotic pair-correlation in the high-temperature regime, (1.333) is valid for arbitrary interactions up to the fermionization limit $\Delta g_2(x) \xrightarrow[N\lambda_{\mathrm{T}}\ll L]{\alpha\to\infty} -\mathrm{e}^{-2\pi\tilde{x}^2}$, since all contained information (only two-clusters) is exact. One expects fermionization of pair correlations because this quantity depends on probability densities. It is only the modulus of wave functions that matters, which can be considered the same for true fermions and fermionized bosons according to (1.185).

Figure 1.32 shows a direct comparison of the obtained analytic formula (1.333) with numerics taken from [187], where they have been compared to perturbative results for $\alpha \to 0$ and $\alpha \to \infty$. Due to its non-perturbative nature, the QCE expression (1.333) is capable to accurately reproduce the crossover from perfect bunching due to Bose statistics to perfect anti-bunching due to repulsive interaction.

To the best of my knowledge, the extremely simple and useful expression (1.333) has not been found so far.

1.7 Conclusion

1.7.1 Summary

In this chapter I have shown that it is possible to develop a consistent approach to simultaneously account for interaction effects and quantum statistics in systems of a fixed number of mutually interacting indistinguishable quantum particles in a first-quantized description. It was thereby an important issue to address interactions on a genuine level that goes beyond mean-field descriptions of effectively independent particles. Another crucial non-trivial demand was to circumvent any perturbative power-expansions in coupling parameters as in the diagrammatic approach of Feynman in the context of quantum field theories.

The key simplification that makes the whole approach feasible is to focus on universal properties. The notion of universality used herein was shown to be understood as omitting exact locations of eigenergies and discreteness itself as regards the quantum mechanical spectra of the investigated systems. Equivalently, in a thermodynamic perspective, this reproduces the behavior of the system at "high" temperatures. On a dynamical level, it corresponds to the short-time behavior of the system. In these aspects, the QCE approach is a many-body analogue to the Weyl expansion in systems of a single particle.

In a first step only the non-interacting case was considered. The general geometrical aspects of the high-dimensional many-body configuration space discussed in section 1.1.3 lead to the concept of cluster zones around invariant manifolds *w.r.t.* particular permutations. Those have been identified as hierarchically organized structures where different particles collide as per partitions into clusters. The geometrical structure has been brought into contact with the single-particle Weyl expansion by identifying them as generalized high-dimensional versions of boundary elements (*e.g.*, surface, corners, edges, curvature). In one-dimensional systems, this connection was shown to be stronger (see Fig. 1.4 and discussion) than in systems of dimension $D \geq 2$, where they have no exact analogues in the Weyl formalism but have to be considered in a novel way.

The application of the method to non-interacting systems in section 1.1.4 showed that the limitations from universality are far weaker than expected. In the spectral domain, especially in the fermionic case, the observation was made (see Fig. 1.7 and Fig. 1.8) that the short-time approach of QCE is capable to accurately reproduce actual non-interacting spectra on average down to the ground state of the system, where quantum degeneracy plays an important role. Similarly, in the thermodynamic domain, the term "high temperature" has to be put into perspective. The validity of the universal approach ranges down to the quantum degenerate regime, where condensation effects are already playing a role. In section 1.1.6 this was shown to contrast grand canonical descriptions using virial expansions, that can lead to wrong physics in this regime (see Fig. 1.9).

By hierarchically decomposing exact quantum propagators of distinguishable but interacting particles into Ursell operators (see section 1.2.1) one can then get a consistent way of incorporating interaction effects. In section 1.2.2 I discussed how the geometrical organization into cluster zones, met in the context of symmetry corrections, are exactly the structures that these interaction effects can be associated to. This lead to the general way of categorizing cluster

structures in section 1.2.3, where the notion of clusters of particles connected by interaction effects and/or exchange symmetry was identified to be the key component to all calculations.

After introducing the crude truncation to first order on a general level in section 1.2.4, based on interacting two-particle propagators, the explicit analytic calculus in the case of one-dimensional Bose gases with contact interaction in section 1.3 showed its actual applicability to experimentally relevant scenarios (in this context given by cold atoms in elongated traps with tuned Feshbach resonance). By comparison to the exactly solvable Lieb-Liniger model in section 1.3.3 we observed (see Fig. 1.15 and Fig. 1.16) that in the sector of few particles and weak to moderate interactions one gains a good approximation to the spectral density. Due to a general extension to multiple species in section 1.4.3 and application to contact-interacting spin-1/2 fermions we could further verify its validity in other integrable systems (see Fig. 1.23). One key value of having a non-perturbative ansatz was immediately recognized by the finiteness of first-order QCE in the limit of infinitely repulsive bosons as expected from the known (effective) fermionization of bosons in this limit. This feature was further exploited by exact Bose-Fermi duality in section 1.4.1 to derive a version of QCE in the strong coupling regime. By general dimensional analysis in section 1.2.5 the regions of strong and weak coupling where identified as corresponding regions in the total energy. By the combined cluster expansions in the weak- and strong-coupling regimes the deficiency in the description due to first-order truncation could be bounded to a maximum in the regime of intermediate interactions (see Fig. 1.19).

Looking at the few-body thermodynamics of this model we observed agreement as long as the temperature is above the regime where quantum degeneracy becomes dominant in an extreme sense. Only when it comes to system specific features that are, *e.g.*, reflected by specific functional dependencies of the exact ground state in combination with Bose-Einstein (quasi-)condensation, the QCE description was shown to break down (see Fig. 1.17). This clarified the role of universality in one disadvantageous aspect. Such effects like the observed collapse in the Lieb-Liniger model cannot be reproduced by the direct QCE, because they strongly distinguish the system at hand from others that fall into the same category regarding universality. Recognizing that the relevant non-universal features are concentrated on the behavior of the ground state I showed in section 1.5.1 how this deficiency of the QCE can be cured by incorporating the properties of the ground state explicitly in a consistent way (see Fig. 1.26).

One advantageous aspect of universality was found in section 1.4.2 to be the possibility to easily apply homogeneous external confinement potentials in a consistent way. By this, the calculus for the solvable model could be transfered to the non-solvable and non-integrable but experimentally relevant case of harmonically confined contact-interacting bosons. Comparison with numerical calculations of low-lying states (see Fig. 1.21) proved the QCE to have comparable descriptive quality to the case without external potentials. The application to such systems emphasized a very strong benefit from universality: Solvability or non-solvability are very system-specific properties, not distinguishable from each other in their universal respects. In this sense the QCE represents a way to gain maximum knowledge about interacting, both, unsolvable and solvable systems without (approximate) calculation of individual eigenenergies and eigenstates.

This power of the canonical QCE was emphasized even further by developing the method of energy shifting in section 1.5.2, which allows accurate universal descriptions in regimes of larger numbers of particles valid for arbitrary coupling strengths in both, integrable and non-integrable systems (see Fig. 1.27). This elevated the theory from being benchmarked to a predictive tool in the regime of numerical intractability. The essence is thereby that a way was found to use the information about the lowest orders of clusters (essentially two- and three-particle clusters) in a most-efficient way to obtain virtually perfect predictions. In principle the method was demonstrated to be extensible to higher orders if the corresponding larger irreducible cluster contributions are known.

Pointing out the power of universality even further one can take the exact solution of solvable models and transfer them to the corresponding universal objects by applying the correct short-time limit (which is equivalent to the limit of large system size). After making this connection, the universal n-body propagators or clusters can again be transfered to non-integrable systems with equal dimensionality and interaction potential. I have demonstrated this procedure explicitly in section 1.5.3 by making the connection to the thermodynamic solution of the Lieb-Liniger model by Yang and Yang [172, 173]. The validity of the connection, exploiting general considerations on the equivalence of short-time dynamics and the thermodynamic limit, was demonstrated in the non-solvable case of three harmonically confined bosons (see Fig. 1.29), which was thereby fully solved in its universal aspects. The combination with the method of shifting energies in second order (relying on the full three-body cluster) was proved to yield virtually perfect predictions of smoothed spectra in an excessively stringent test in the Lieb-Liniger model of $N = 10$ bosons comparing as much as the $\sim 3 \times 10^5$ lowest levels (see Fig. 1.30).

Furthermore, to show that the approach can be used to gain more detailed information, I have demonstrated how it can be modified for the calculation of one-body and two-body (spatial) observables in thermal equilibrium in section 1.6. A special emphasis was put on the application to non-local pair correlations, which were found to be described by a simple closed analytic non-perturbative expression in the high-temperature regime of dilute gases. Since the calculation involved is, by virtue of the general structure of QCE, known to only rely on the smallest non-trivial clusters of two particles, the formula must be the exact asymptotic expression for this regime, valid for all interaction strengths ranging from perfect bunching of non-interacting bosons ($\alpha \to 0$) to perfect anti-bunching of fermionized hard-core bosons ($\alpha \to \infty$). This strong statement was proven to be correct by direct comparison (see Fig. 1.32) with numerical calculations of [187].

1.7.2 Outlook

While the potential in the fundamentals of the QCE and its extensions should be clear by now, there are several loose ends that scream for being tied up.

From few to many – The "dressed quantum liquid"

One major issue of the presented approach is the missing connection to mean-field theories of effectively non-interacting particles, valid in the many-body sector. This connection could possibly be drawn by a "dressed quantum liq-

uid" ansatz, which has a flavor of mass renormalization in second quantized and quantum field theories, and is described in the following. The idea is to approximate the partition function $Z^{(N)}$ of N interacting identical particles in full QCE by an effective non-interacting one (1.45) with modified single-particle dynamics, expressed in terms of a "dressed" (denoted by prime) single-particle partition function $Z_0'^{(1)}(\beta)$, similar to the impurity-dressing discussed in section 1.4.3. Here, each particle would have to be dressed corresponding to the mutual interaction with any arbitrary partner instead of one distinct impurity. Similar as in the case of impurity-dressing and also similar to the energy-shifting method the ansatz would allow for corrections in $Z_0'^{(1)}(\beta)$ that are of subleading power of $\tilde{v} = V_{\text{eff}}/\lambda_{\text{T}}^d$. In a first truncation this would imply the ansatz

$$Z_0'^{(1)}(\beta) = \underbrace{Z_0^{(1)}(\beta)}_{=\mathcal{O}(\tilde{v})} + \underbrace{\delta(\beta)}_{=\mathcal{O}(1)} \tag{1.334}$$

for the dressed single-particle partition function. Ordering the corresponding non-interacting expansion (1.45) in powers of $\tilde{v}$ the dressing is then fully determined by the irreducible two-clusters when analytically matched to the $\mathcal{O}(\tilde{v}^{N-1})$-term in the full QCE (1.110) and would read

$$\delta(\beta) = \pm\frac{N-1}{\tilde{v}} \times \frac{1}{2}\left(\mathcal{A}_{1,1}^{\text{intra}}(-\mathrm{i}\hbar\beta) \pm \mathcal{A}_{1,1}^{\text{inter}}(-\mathrm{i}\hbar\beta)\right) . \tag{1.335}$$

This first-order correction due to dressing is therefore to leading order proportional to the (thermally scaled) particle density (1.318), where the factor $N-1$ results from the combinatorics and expresses the number of available interaction partners. In principle one could then go on and match terms of order $\mathcal{O}(\tilde{v}^{N-2})$ (and less) as well, resulting in additional corrections to the dressing of higher order in the density $\tilde{n} = N/\tilde{v}$. While this shows that a truncation of the dressing corresponds to a focus on the dilute or high-temperature regime, it is unclear to what extent the approximation as dressed quantum liquid itself introduces deficiencies. The expectation is that the validity is limited to the many-body sector, since for few particles a significant over-counting occurs, *e.g.*, due to terms in the full dressed quantum liquid partition function $Z_0'^{(N)}(\beta)$ where each of the N particles interacts with one additional partner, which simply are not available in the true full QCE. As already discussed in section 1.4.3 in the context of dynamical impurities, a corresponding restriction of simultaneous dressings to avoid over-counting would be a joint concept, destroying the independence of particles and hence introducing a notion of residual interactions purely based on the finiteness of few-body systems. To clarify the connection of the QCE to a pure mean-field description it would be worthwhile to investigate the significance of such finite-size induced residual interactions in the dilute regime for varying particle numbers. Another expectation is that there is a competition between defects from finite size and truncation of the dressing. While relaxing the latter to higher orders in $\tilde{n}$ might in principle allow for pushing validity into the regime of quantum degeneracy (probably in terms of an asymptotic series), this procedure introduces more and more finite-size defects. To gain control over such an approximation it would therefore be necessary to explore the full range of system parameters $(N, V_{\text{eff}}, \beta, \alpha)$ addressing the question of which truncation is suited best in which regime and especially where one can locate the cross-over

from few-body physics to many-body physics. In a first attempt, the combined error introduced by the truncation (1.334) of the dressing and the overall approximation as non-interacting quantum liquid could be investigated analytically by comparing the contributions of order $\mathcal{O}(\tilde{v}^{N-2})$ with the full QCE, known from the three-cluster (see section 1.5.3). I remark here that although the matching of $\mathcal{O}(\tilde{v}^{N-1})$ terms gives the dressed quantum liquid approach the same flavor as the energy shifting method (see section 1.5.2), they are not similar in the physics they represent let alone equivalent. The latter does not correspond to effectively independent particles. This can be seen from its enhanced validity in the few-body sector, while for larger numbers of particles one needs to carry it out to higher order. In contrast, the dressed quantum liquid is expected to suffer from massive over-counting of interaction effects there.

From hot to cold – Dressing in thermal equilibrium of open systems

Another approach in the spirit of the dressed quantum liquid related to many-body physics could be taken to extend the thermal averages of one-body observables (1.316) in the grand canonical ensemble in the direction of quantum degeneracy. The ansatz would be to approximate the irreducible cluster-sums by dressed non-interacting ones:

$$\mathcal{B}_n^{(1)}(\beta) \approx \mathcal{B}_1'^{(1)}(n\beta) \tag{1.336}$$

by virtue of the semigroup property of single-particle propagators (1.40). In contrast to the canonical approach, here the dressing would have to correspond to higher orders in the fugacity, *i.e.*, a first truncated attempt would read

$$\mathcal{B}_1'^{(1)}(\beta) = \mathcal{B}_1^{(1)}(\beta) + z\Delta\mathcal{B}_1^{(1)}(\beta)\,. \tag{1.337}$$

The matching to the full expansion (1.316) in order $\mathcal{O}(z^2)$ results then in the dressing $\Delta\mathcal{B}_1^{(1)}(\beta) = \mathcal{B}_2^{(1)}(\beta) - \mathcal{B}_1^{(1)}(2\beta)$ which looks very similar (see Fig. 1.31a) to self-energy renormalization diagrams in perturbation theory, but carrying information in all orders of the coupling. Due to the additional fugacity factor the correction would only contribute to even powers of z in the full expansion approximated as effectively non-interacting system (1.336). This construction has a very nice implication in the case of contact-interacting bosons when one specifies the average number of particles (1.317) as observable. The limit of infinitely strong couplings then is correctly predicted to show full fermionization, where the dressing corrections effectively switch the sign of all even powers in the fugacity expansion:

$$\langle\hat{N}\rangle_{\mathrm{G},+} \xrightarrow[\alpha\to\infty]{\text{dressed}} -\sum_{n=1}^{\infty}\mathcal{A}_1(n\beta)(-z)^n = \langle\hat{N}\rangle_{\mathrm{G},-}^{\text{non-int.}}\,. \tag{1.338}$$

Thus, the correct free fermionic case is obtained by the first-order truncated dressing at least as regards the global observable of number of particles. It is then an important question if one also gets the correct spatially dependent observables of the Tonks-Girardeau gas in this limit, which are in general *not* identical to the ideal Fermi gas. Preliminary, one can say that this road looks promising to provide non-perturbative results on observables like momentum

distributions and also the effect of interactions on (quasi-)Bose-Einstein condensation. Moreover, analogous approximations for two-body observables (see section 1.6.2) seem to be in reach when matching to spatial three-clusters, which are for contact-interactions deducible as large size asymptotics from the Lieb-Liniger solution (see section 1.5.3). I remark that one important point to clarify here is to what extent such approximations overlap with what is apparently known as "Dyson-Ursell" series (see [155] and references therein).

Few-body systems in thermal equilibrium – The "independent pairing approximation"

Furthermore, a complementary extension in the few-body regime could be considered in order to improve the thermal equilibrium description within direct QCE. While the energy shifting already gives satisfactory results in the energy domain in this regime, it seems so far analytically cumbersome or intractable to be transferred to the temperature domain. There, one could relax the first-order truncation of QCE to approximate the full partition functions within an "independent pairing approximation", described in the following. In first-order QCE interaction effects are taken into account only between two particles at a time. An easily accessible extension would be to allow for simultaneous interaction effects in independent clusters but keeping the restriction to a single pair of particles *within each* cluster. This way, all the information needed is already available, since each sum of irreducible clusters $\mathcal{A}_n$ is given by the first-order QCE (1.118). These approximations to the full cluster sums could then be used as ingredient in the general expression for interacting partition functions (1.277). An indication for the quality of this truncation of QCE is given by the excellent agreement of the direct first-order QCE with the exact numerics in the three-particle Lieb-Liniger model (see Fig. 1.15) and the dynamical impurity model (see Fig. 1.23) as compared to Lieb-Liniger with more than three bosons (see Fig. 1.16). The reason is that in these systems, the truncation to first order exactly coincides with the independent pairing approximation because they do not allow for more than one interacting cluster simultaneously, while higher-order interaction effects *within* one cluster would be there in principle but are cut-out in both, the first-order truncation and the independent pairing approximation. Note that while the energy-shifting method is hard to be transferred to the thermal description the independent pairing would in turn be hard to be analytically transferred to the energy domain. The intention would be to obtain two approximative methods that are capable to describe the genuine few-body character in small systems and that complement each other in the thermal and spectral domain.

Discretization of smooth spectra

One obvious deficiency of the whole QCE approach is the lacking resolution of individual energies. A "requantization" of the smooth counting function of the form

$$\mathcal{N}(E_n^{(N)}) \approx n + \frac{1}{2} \quad , n = 0, 1, \ldots \tag{1.339}$$

cannot be a sufficient prescription, since the corresponding levels are maximally "repelled". Thus, in an unfolded version of the spectrum they would correspond to equidistant levels, not able to reproduce the correct universal level

statistics predicted by RMT or periodic orbit theory. On the other hand, one can apply the energy-shifting method (see section 1.5.2) on a level-by-level basis, shifting individual non-interacting levels[25]. It is thereby crucial that the shifts are founded on the average smooth counting functions, so that one can expect these shifted levels to maintain the level statistics of the non-interacting system. This can also not provide a sufficient approximation of discrete spectra, since a generic non-interacting system exhibits the Poissonian statistics of integrable systems, even when the underlying single-particle system is non-integrable. This can be seen as originating in the superimposition of individual spectra. In contrast to requantized spectra using (1.339), integrable systems with Poissonian statistics do not exhibit level repulsion at all. Thus, both approaches on their own are not satisfactory, they already fail on the level of universal properties. They might however provide a tool to approximately describe discrete spectra when combined together. Since they represent two opposite extremes regarding level statistics, an ansatz would be to interpolate between the two. While such an ansatz can only be heuristic, its solution could in principle be supplemented with external physical information. Suppose the exact (in general mixed) level statistics for a specific coupling strength are known from either RMT considerations, periodic orbit theory or any other source. The information on the actual amount of level repulsion in the system could then serve to fix the mix ratio in a blending between pure requantization and level-by-level shifting. Points to clarify in this context are *i)* how much influence has the freedom in choice of a specific blending function, *ii)* are there ways to externally obtain the level statistics in an energy-dependent manner (without full calculation or measurement of spectra), where different parts of the spectrum are allowed to exhibit different amounts of level repulsion, and *iii)* to what extent is it possible to "simulate" the full correlations of energy levels beyond a specification of level repulsion as a single parameter.

Application to different systems

Since many relevant features of the QCE are fundamentally general regarding spatial dimensionality and the type of interactions, it is mainly a matter of calculus to relax the restriction to the specific model of repulsive contact interactions in one dimension.

A first generalization is to extend interactions to *attractive* contact interactions. This extension is easily incorporated on the level of the two-body propagator [168], where an additional term $\sim \mathrm{e}^{-\kappa(|\Delta q^{\mathrm{f}}|+|\Delta q^{\mathrm{i}}|)}$ with $\kappa \sim \sqrt{|\alpha|}$ accounts for bound states. In a two-boson system on a line this extension was shown to introduce sufficient information within the framework of direct QCE to fully reproduce the mean spectrum [168]. This includes the regime of negative energies, dominated by center-of-mass excitations of a single composed particle. The bound-state dominated regime thereby differs qualitatively from the regime of positive energies, where scattering states in the relative coordinate rapidly take over. However, it is not necessary to include the bound-state regime "by hand". Rather, the direct application of QCE takes care of it "automatically" when using the correct two-body propagator, accurately describing the two regimes and the discontinuous transition between the two. For systems

[25] Also degenerate levels are shifted individually, which can break the degeneracy due to interaction.

with more attractive bosons it is however insufficient to use the first-order truncation of QCE since the lower end of the spectrum is then dominated by bound states involving all particles [188], which is not correctly described by exclusive two-particle interactions at a time. On the contrary, in the low-energy regime one can expect the largest clusters involving all particles simultaneously to be at least equally important to partitions into smaller clusters. This intuition is based on a similarity between clusters and the formation of large "strings" of complex quasimomenta in the exact solution via Bethe ansatz [189, 190]. Moreover, these many-body bound states are responsible for one of the most interesting features in the attractive Bose gas, which is a QPT between a massive bunching of bosons with spontaneously broken symmetry and a state of uniform density (see also chapter 2 on this subject). However, in the repulsive case, the method of energy shifting has proved to accurately "simulate" the effects of higher-order clusterings from the information on the smallest clusters. Its potential capability to describe the non-trivial low-energy physics of bound-state formations is therefore not ruled out, albeit questionable and remains to be investigated explicitly.

Another motivation to address attractive contact-interactions in one dimension are the physical features in the corresponding Gaudin-Yang model of two-component fermions, where one observes a BCS-BEC-like crossover (see [160] and references therein) from loosely bound pairs to the formation of larger "molecules". Since the BCS regime is governed by two-particle interactions, where apparently the interaction between different bound pairs is suppressed due to Pauli exclusion, its correct description within first-order energy shifting (or possibly also the independent pairing approximation described above) is to be expected. Similarly to the case of attractive bosons it remains then to be seen if an inclusion of three-clusters is enough to push validity into the BEC regime.

Because of the implication of discontinuous features at low energies, attractive delta interactions can be regarded to pose a stringent test for the extrapolating power from small clusters to higher-order clusterings within the method of energy shifting.

In order to answer the question to what extent the QCE and its methodical extensions are limited to interactions of short range, one could focus on other solvable continuum model systems with finite-range interactions. As a first approach, one could consider the application to a class of one-dimensional continuous models with interaction potentials given by

$$i) \qquad U_{\mathrm{int}}(q) = \frac{g}{q^2}\,, \tag{1.340}$$

$$ii) \qquad U_{\mathrm{int}}(q) = \frac{g}{\sin^2(q\pi/L)}\,, \tag{1.341}$$

$$iii) \qquad U_{\mathrm{int}}(q) = \frac{g}{\sinh^2(q\pi/L)}\,, \tag{1.342}$$

which are *asymptotically* solvable by a Bethe ansatz [191]. While the asymptotic Bethe ansatz in these models again treats the interactions effectively as short-range, they differ from pure delta interactions in the scattering phase-shifts

during two-body collisions[26].

There would then be two opposite ways to implement these models within QCE following two distinct purposes.

First, one could implement the asymptotic solutions as the propagation kernels in QCE. Because the interactions would then be treated on equal footing in both frameworks, one gains certainty about the equivalence of the two approaches, posing another benchmark to test the QCE in the short-range regime. Following this scheme opens the possibility to extract higher-order clusters from the asymptotic Bethe ansatz solution and to transfer them to non-solvable models by introducing external potentials, as already shown for delta interactions (see section 1.5.3). The drawback is that the question of finite-range validity would most likely remain untouched.

The second purpose would be to test the validity of QCE in the presence of genuine finite-range interactions and the corresponding effect of *diffraction* – which is absent from the asymptotic treatment – on properties related to the mean DOS. Because of non-solvability, the direct implementation of the finite interaction potentials (1.340), (1.341), and (1.342) can at most happen at the two-body level. Provided that this can be achieved, a direct comparison of the two different implementations – as finite-range and effective short-range interaction – within first-order QCE or first-order energy shifting could then possibly shed new light on their equivalence, similarities or differences especially in the few-body regime.

Other extensions include to relax the restriction to one-dimensional systems, where, *e.g.*, the two-particle propagators for (regularized) contact interaction are as well known analytically [158, 196].

To push generality to an extreme, in the long term one can also think of parametrizing arbitrary interactions by, *e.g.*, the two-body scattering phase shifts[27] At least on the level of first-order QCE, first-order energy shifting and promisingly the independent pairing approximation and first order dressing approaches the analytical information on two-body scattering would be in principle sufficient to produce approximate results.

Closing remark

To close this chapter, one could say that one road has been opened to analytically describe and predict universal features of interacting quantum gases. By consistent extensions, it can be even taken into the regime where system specific properties dominate the physics.

The whole approach is thereby especially suitable in the case of few particles $N \sim \mathcal{O}(10)$ where the restriction in this direction is only a soft bound that

[26] Interestingly, the periodic model based on the interaction (1.342) includes the (classically solvable) Toda lattice [192] as a limiting case, which has lead to the approximate quantization of the latter using the asymptotic Bethe ansatz [191]. While its validity in the classical thermodynamic limit could be verified, the effective short-range treatment in the few-body sector far away from the classical limit – where comparisons with an exact treatment of the quantum lattice by Gutzwiller [193] are in principle available – is apparently not fully clarified and has been subject to some controversy [194, 195].

[27] As an appetizer, for applications in the high-temperature regime and assuming central-force scattering between particles and Boltzmann statistics, the second virial coefficient was generally expressed in terms of the partial wave solutions of the elastic two-particle scattering process [197].

mainly originates from two aspects. First, the larger the number of particles, the higher the order of cluster contributions one has to take into account. However, the efficiency in relying only on the lowest orders was thereby pushed to a high degree. In combination with the principle ability to calculate higher-order clusters taken from integrable systems this puts the limitation of N into perspective.

The second reason is that the explicit expressions are given as (multiple) sums that grow with the number of particles, which might pose a problem of numeric evaluation of the formulas when large cancellations play a role (as in the free fermionic case for ultra-low energies or correspondingly strongly repulsive bosons). Again, this problem could be mostly dismissed by the energy shifting, which represents itself in a way that does not involve large cancellations also in the fermionic case or fermionization limit. Moreover, one should stress that the number of terms only grows polynomially with N in contrast to the exponential growth of computation times when performing exact numeric diagonalization.

As discussed, one major potential of the QCE approach can be seen in describing universal features of interacting few-body systems. In the basic concepts it is on equal footing as the Weyl expansion in single-particle systems. It can therefore be considered a semiclassical approach to average or smooth quantities. This has to been seen as opposed to semiclassical approaches to non-universal, fluctuating properties, which are based on the theory of periodic orbits. These two sides of semiclassics can be considered as complements that may be added up to give a full picture of the physics in particular systems.

The following chapter focuses on a subject that is on the one hand very similar to the one presented here and on the other hand complementary to it and therefore very different in many aspects, regarding both, the methodical approach and contained physics. The system under consideration will be again the one-dimensional Bose gas with contact interactions. The first difference being that now the interactions will be attractive, leading to non-trivial physics related to QPTs that are highly non-universal in the above sense. Second, on the methodical level, it focuses on the application of semiclassical periodic orbit theory to resolve these non-universal features. Third, an overall description within the formalism of second quantization will be applied. Fourth, the periodic orbit theory on the stage of second quantization naturally leads to enhanced validity for large numbers of particles instead of few-body systems, which perfectly fits the requirements to address finite-size precursors of a QPT. Thus, despite the physical system to describe is almost the same, the upcoming analysis will shine light on it from a completely complementary perspective.

Chapter 2

Classical-to-quantum criticality in the many-particle regime – A semiclassical treatise on the attractive Lieb-Liniger model

2.1 EBK quantization of integrable systems

The major semiclassical tool that will be utilized in the upcoming chapter is, in contrast to the first part of the thesis, not centered around describing smooth properties like the smooth DOS. Instead it focuses on the approximate description of discrete quantized energy levels (and corresponding wave functions) that are in the end able to give an understanding of a finite-size precursor of a QPT, an ESQPT and related features inherent in the investigated model. Since the interest still is in the integrable Lieb-Liniger model, the well-understood tool of choice is the traditional semiclassical method of torus quantization, which also goes under the name Einstein-Brillouin-Keller (EBK) quantization and is mainly a result of work by Bohr, Sommerfeld, Einstein, Brillouin, Keller and Maslov (for a historical overview see [48, 50, 198]). In this section I will give a short general introduction to the method roughly following [199]. For more detailed information about the general method, see sections 6.1–6.3, 7.1–7.3 therein.

Let us start with defining the problem as solving the stationary Schrödinger equation

$$H(\hat{\mathbf{p}}, \hat{\mathbf{q}})|\psi\rangle = E|\psi\rangle \tag{2.1}$$

for the eigenfunctions of an autonomous system with conjugate generalized coordinates and momenta, represented by the observables $\hat{\mathbf{q}}$ and $\hat{\mathbf{p}}$, respectively, which obey commutation relations

$$\begin{aligned} [\hat{q}_i, \hat{q}_j] &= [\hat{p}_i, \hat{p}_j] = 0\,, \\ [\hat{q}_i, \hat{p}_j] &= \mathrm{i}\hbar\delta_{ij}\,. \end{aligned} \tag{2.2}$$

The possibility of decomposing a complex number into its modulus and a phase

allows for writing the ansatz

$$\langle \mathbf{q}|\psi\rangle = A(\mathbf{q}) \exp\left[\frac{\mathrm{i}}{\hbar}\sigma(\mathbf{q})\right] \tag{2.3}$$

for the eigenfunctions in coordinate representation with real valued amplitude function A and phase function σ. Introducing this ansatz into (2.1) results, after applying basic quantum mechanic algebraic manipulations, in the stationary Hamilton-Jacobi equation (for an overview on the symplectic geometry aspects of classical mechanics see [198])

$$H\left(\frac{\partial\sigma}{\partial\mathbf{q}}, \mathbf{q}\right) = E\,, \tag{2.4}$$

which gets solved by action integrals $\sigma(\mathbf{q}) = S(\mathbf{q}, E)$, defined by

$$S(\mathbf{q}, E) = \int_{\mathbf{q_0}}^{\mathbf{q}} \mathrm{d}\mathbf{q}' \cdot \mathbf{p}(\mathbf{q}')\,, \tag{2.5}$$

where the integration path in phase space has to be embedded in an invariant (under Hamiltonian flow) Lagrangian surface for which

$$\oint \mathrm{d}\mathbf{q} \cdot \mathbf{p} = 0 \tag{2.6}$$

for any reducible loop, *i.e.*, a map from S^1 to the Lagrangian manifold that is null-homotopic. An equivalent statement in differential form is that the symplectic form

$$\mathrm{d}\mathbf{x} \wedge \mathrm{d}\mathbf{x}' = 0 \tag{2.7}$$

vanishes for any pair of phase space vectors tangent to the Lagrangian manifold. Here, $\mathbf{x}$ represents a point in phase space by subsuming $\mathbf{q}$ and $\mathbf{p}$. While such manifolds are absent from fully ergodic chaotic systems, they build up the whole phase space of integrable systems in a well-understood manner. The property of integrability of a classical autonomous system in D dimensions is defined as the existence of D constants of motion $F_l(\mathbf{p}, \mathbf{q})$. They are demanded to be *independent*, *i.e.*, the D vectors $\partial F_l/\partial\mathbf{x}$ have to be linearly independent at each point $\mathbf{x}$. In addition, the constants of motion have to be in mutual *involution*, meaning that the Poisson brackets

$$\{F_i, F_j\}_{\mathbf{q},\mathbf{q}} = 0 \tag{2.8}$$

vanish, which are in general defined for any two functions $f(\mathbf{q}, \mathbf{p})$, $g(\mathbf{q}, \mathbf{p})$ as

$$\{f, g\}_{\mathbf{q},\mathbf{p}} := \sum_k \left(\frac{\partial f}{\partial q_k}\frac{\partial g}{\partial p_k} - \frac{\partial g}{\partial q_k}\frac{\partial f}{\partial p_k}\right)\,. \tag{2.9}$$

The involution implies that the D flows produced by the constants of motion F_l, defined by

$$\dot{\mathbf{x}} = \{\mathbf{x}, F_l\}_{\mathbf{q},\mathbf{q}}\,, \tag{2.10}$$

are commutative. If the integrable system in addition is bound in the sense that the volume of all accessible phase space is finite, the Poincaré recurrence theorem applies individually to those D flows, which implies the existence of D independent irreducible loops γ_l, forming the fundamental group of the Lagrangian

manifold associated to the values of the F_l. From this analysis it becomes then evident that the invariant Lagrangian surfaces are D-tori characterized by D independent action variables

$$I_l = \frac{1}{2\pi} \oint_{\gamma_l} \mathrm{d}\mathbf{q} \cdot \mathbf{p} \,, \tag{2.11}$$

associated to the fundamental loops γ_l. The I_l are one specific choice of constants of motion F_l. So one can now be more specific about the action integral (2.5) and write

$$S(\mathbf{q}, E) = S(\mathbf{q}, \mathbf{I}) = \int_{\mathbf{q}_0}^{\mathbf{q}} \mathrm{d}\mathbf{q}' \cdot \mathbf{p}_\mathbf{I}(\mathbf{q}') \tag{2.12}$$

with the implicit definition of the momenta $\mathbf{p}_\mathbf{I}$ by

$$\mathbf{I}(\mathbf{q}, \mathbf{p}_\mathbf{I}(\mathbf{q})) = \mathbf{I} = \text{const.} \,, \tag{2.13}$$

which in general allows for multiple but discrete solutions. To make this obvious consider for instance an one-dimensional nonlinear oscillator $H = p^2/m + V(q)$, where

$$p = p_E(q) = \pm\sqrt{2m(E - V(q))} \tag{2.14}$$

has two discrete solutions. Therefore one gets a discrete set of action integrals $S_j(\mathbf{q}, \mathbf{I})$, each fulfilling the stationary Hamilton-Jacobi equation

$$H\left(\frac{\partial S_j(\mathbf{q}, \mathbf{I})}{\partial \mathbf{q}}, \mathbf{q}\right) = E(\mathbf{I}) \tag{2.15}$$

and – as a generating function – implicitly invoking a canonical transformation $(\mathbf{q}, \mathbf{p}) \mapsto (\boldsymbol{\phi}, \mathbf{I})$ by

$$\begin{aligned} \frac{\partial S_j}{\partial \mathbf{q}} &= \mathbf{p} \,, \\ \frac{\partial S_j}{\partial \mathbf{I}} &= \boldsymbol{\phi} \,, \end{aligned} \tag{2.16}$$

where the $\phi_l \in [0, 2\pi[$ are the periodically defined angle coordinates winding around the D circular directions of the torus. The canonical transformation defines quantum observables $\hat{\mathbf{I}}$ and $\hat{\boldsymbol{\phi}}$ (see [200] for the controversy of this point in general and [201] for its resolution in the context of semiclassics) with commutation relations

$$\begin{aligned} [\hat{I}_k, \hat{I}_l] &= [\hat{\phi}_k, \hat{\phi}_l] = 0 \,, \\ [\hat{\phi}_k, \hat{I}_l] &= \mathrm{i}\hbar\delta_{kl} \,. \end{aligned} \tag{2.17}$$

A state $|\psi_\mathbf{I}\rangle$ for which the $\mathbf{I}$ are well-defined should therefore – as plane wave in the $\boldsymbol{\phi}$ – have constant amplitude in ϕ-representation. This consideration allows to derive the semiclassical amplitude in $\mathbf{q}$-representation from the conservation of (infinitesimal) probability

$$\underbrace{|\langle \boldsymbol{\phi} | \psi_\mathbf{I} \rangle|^2}_{\text{const.}} \mathrm{d}^D\phi = |\langle \boldsymbol{q} | \psi_\mathbf{I} \rangle|^2 \, \mathrm{d}^D q \tag{2.18}$$

as

$$A^2(\mathbf{q}) = \text{const.} \times \left| \det \frac{\partial^2 S_j}{\partial \mathbf{q} \partial \mathbf{I}} \right| . \tag{2.19}$$

The multi-valuedness of the action integrals together with the amplitudes (2.19) leads to the semiclassical wave function

$$\langle \mathbf{q} | \psi_{\mathbf{I}} \rangle = \text{const.} \times \sum_j \left| \det \frac{\partial^2 S_j}{\partial \mathbf{q} \partial \mathbf{I}} \right|^{\frac{1}{2}} \exp \left[\frac{\mathrm{i}}{\hbar} S_j(\mathbf{q}, \mathbf{I}) + \mathrm{i}\alpha_j \right] \tag{2.20}$$

for the eigenfunctions as a superposition of individual solutions to (2.15) within the ansatz (2.3). The wave function (2.20) is divergent at the boundaries of the torus layers, *i.e.*, the boundaries of the supports of $S_j(\mathbf{q})$, outside of which the action as a function of $\mathbf{q}$ usually would become imaginary. In one dimension those points correspond to classical turning points whereas for $D > 1$ the boundaries in $\mathbf{q}$-space joining the different branches S_j together correspond to caustics of the projection of the torus onto $\mathbf{q}$-space. They coincide with foldings of the invariant Lagrangian manifold in the most generic case, producing caustics of dimension $D - 1$ (denoted as codimension one). In general, for an arbitrary number of degrees of freedom, there are also singularities of codimension larger than one. All possible such generic singularities have been categorized [198, 202] and in general they correspond to the coincidence of different singularities of smaller codimension, *e.g.*, a point-like *cusp* (codimension two) in $D = 2$ corresponds to the encounter of two smooth folds (codimension one). Therefore, folds could be considered the most generic type of caustics and indeed for the purpose of energy quantization there is no need to specify the behavior at higher singularities. The reason is that all involved quantities, which are functions of closed paths on the torus, show up to be topological invariants, so that one can choose or deform paths in a way they do not accidentally hit singularities of higher codimension. For this reason I may use the two terms folds and caustics synonymously and sufficiently consider those and the corresponding divergence of (2.20) exclusively. There, the semiclassical wave function (2.20) is still normalizable and the divergence can be resolved by switching to a momentum representation $\langle \mathbf{p} | \psi_{\mathbf{I}} \rangle$ in the vicinity of the caustics (known as *Maslov's method*). The coordinate and momentum representations can be shown to be asymptotically equivalent in the regions on the torus that are well-separated (in units of wave-lengths) from such boundaries (either in $\mathbf{q}$ or $\mathbf{p}$) by means of a stationary phase approximation to the Fourier integral mediating between the two representations. For this reason one can stick to the approximate solution (2.20) away from caustics and replace it by the Fourier transform of the wave function in $\mathbf{p}$-representation close to a caustic. There, $\mathbf{q}(\mathbf{p})$ can usually be locally approximated to be quadratic in $\mathbf{p}$ in the direction that moves across the folding of the Lagrangian manifold. This consideration is exactly equivalent to the one-dimensional method of approximating wave functions in q-representation in the vicinity of turning points by a linearization of the potential $V(q)$, which leads to Airy functions as local solutions. In the case $D > 1$, the local problem can effectively be reduced to a one-dimensional one by stationary phase approximation to the integration of momenta transverse to the caustic. The corresponding local solution in perpendicular direction q for a fold of the form

$$q = q_\mathrm{c} + a(p - p_\mathrm{c})^2 , \tag{2.21}$$

where q_c is the coordinate of the caustic and can here be considered as the parameter indexing the family of tori, reads

$$\psi_\perp(q) = \text{const.} \times \mathrm{e}^{\frac{\mathrm{i}}{\hbar} p_c q} \, \mathrm{Ai}\Big[-\operatorname{sgn}(a) \hbar^{-\frac{2}{3}} |a|^{-\frac{1}{3}} |q - q_c|) \Big] \,, \tag{2.22}$$

which regularizes the divergence at the caustic to a finite peak that smoothly connects to the exponentially damped behavior outside the classically allowed region. An asymptotic analysis of (2.22) deep in the classically allowed region $(q - q_c) \to \operatorname{sgn}(a)\infty$ reveals the equivalence to the approximate semiclassical wave function (2.20) exactly if the so far undetermined phases $\alpha_\pm$ have a difference of

$$\alpha_+ - \alpha_- = -\frac{\pi}{2} \,. \tag{2.23}$$

The essence of such phase jumps between branches of actions $S(\mathbf{q})$ when crossing a caustic is captured by the notion of the *Maslov index* ν, a quantity associated to an arbitrary closed path on the Lagrangian manifold. It counts the number of times $\partial q/\partial p$ becomes positive at a caustic minus the times it becomes negative and has been shown to be a topological invariant, so that it does not change under smooth deformations of the closed curve, allowing to circumvent touching any higher caustic beyond folds.

The only ingredient that is missing to finally arrive at the EBK-quantization conditions is uniqueness of the wave function. This uniqueness has to be fulfilled when one counts all phase jumps accumulated along a closed loop, because then one ends up in the same branch S_j one started with. When a closed curve involves a series of n successive different branches, one has to tune the n different α_j so that the phase differences match (2.23). One real free parameter gets absorbed by an undetermined global constant phase, so that only at $n-1$ of these connections the match (2.23) can be fulfilled in general. To close the circle, also the last phase difference has to match, which imposes then a condition on the action integrals S_j. As a result, the total phase accumulated when going around a closed curve γ, consisting of the full action integral $\hbar^{-1} \oint_\gamma \mathrm{d}\mathbf{q} \cdot \mathbf{p}$ in units of $\hbar$ and the phase jumps of $\pm\pi/2$ when crossing caustics, has to be a multiple of 2π. Since this is true for any closed curve on the torus and since there are D independent closed loops γ_l, one gets D quantization conditions

$$S_{\gamma_l} := \oint_{\gamma_l} \mathrm{d}\mathbf{q} \cdot \mathbf{p} = 2\pi\hbar \left(m_l + \frac{\nu_l}{4} \right) \,, \qquad l = 1, \ldots, D \,, \tag{2.24}$$

or equivalently for the action variables

$$I_l = \hbar \left(m_l + \frac{\nu_l}{4} \right) \,, \qquad l = 1, \ldots, D \,, \tag{2.25}$$

where $m_l \in \mathbb{N}_0$ are D independent quantum numbers.

Equipped with (2.24), (2.25) we can now turn to the actual system under consideration, given as an integrable model.

2.2 The truncated Lieb-Liniger model

In the previous chapter the repulsive Lieb-Liniger model and related interacting systems were treated within the formalism of first quantization where the main simplification to make the problem analytically tractable was to neglect the discreteness of the quantum mechanical spectrum.

In this chapter I will make use of an alternative approach in order to semiclassically investigate the physics of the Lieb-Liniger model [33, 34] with attractive coupling between bosons. This attractive one-dimensional Bose gas – in contrast to the repulsive case – admits a QPT and also an ESQPT, which both become sharp in the limit of large numbers of particles $N \to \infty$ (see [203, 204] for reviews on the general subject and, *e.g.*, [22] for the particular case of the attractive one-dimensional Bose gas). Although these physical features (especially the ESQPT, see, *e.g.*, [205]) may also have signatures in the mean DOS, their essential physics is governed by specific properties of single quantum states. This makes it necessary to describe single states rather than smooth properties.

On the one hand, there have been vast investigations of this system in terms of *i)* mean field theory and Bogoliubov approximation, which leads to analytical results valid in the extreme $N \to \infty$ limit [28, 206, 207] and *ii)* numerical direct diagonalization in truncated Hilbert spaces, which are applied to finite numbers of particles (see, *e.g.*, [189, 208, 209]). On the other hand, almost no analytical results for finite N are available except the exact solution by Lieb and Liniger [33] in terms of a Bethe ansatz, which has been applied by several authors [189, 210, 211] for smaller numbers of bosons ($N \lesssim 20$). The method involves the solution of N coupled transcendental equations in N unknown quasi-momenta k_j. In contrast to the repulsive case (see section 1.3.3), the attractive case does not admit an ordering of solutions in terms of quantum numbers. The numerical solution for arbitrarily excited sets of eigenenergies is then way less efficient and under control, because each search for a single solution (as for example in the Newton scheme) depends on the initial conditions for the k_j in a way that is hard to predict. Thus one may narrow down the same unique solution multiple times while others might be overlooked completely. Furthermore, for attractive interaction the roots of the equations for the quasi-momenta k_j have to be found in the complex plane instead of the real axis. These two circumstances complicate the numerical search substantially compared to the repulsive case, pushing larger numbers of particles out of reach when excited states are considered as well as the ground state.

The intention here is to capture the interesting physics of the finite-size QPT, ESQPT and related features using semiclassical methods which become exact for infinitely many particles and give approximate but analytical results for finite N. Besides the ability to give analytical expressions for, *e.g.*, energy gaps at the transition point, characteristic energy spacings of level-bunches and associated time scales, the resemblance between quantum and classical dynamics will open the possibility of defining a sharp point of transition even for finite N, where all quantum signatures are smeared out to a cross-over. The reason is that a discontinuous feature related to the transition will show up to be inherent in the semiclassical treatment for arbitrary finite size.

The starting point is the Hamiltonian for bosons on a ring with attractive

contact interaction formulated in second quantization [207]

$$\hat{H} = \int_0^{2\pi} \mathrm{d}\theta \left[-\hat{\psi}^\dagger(\theta) \frac{\partial^2}{\partial\theta^2} \hat{\psi}(\theta) + \frac{g}{2} \hat{\psi}^\dagger(\theta)\hat{\psi}(\theta)\hat{\psi}^\dagger(\theta)\hat{\psi}(\theta) \right] \quad (g \leq 0)\,, \tag{2.26}$$

where the field operators $\hat{\psi}^\dagger(\theta)$ and $\hat{\psi}(\theta)$ are creation and annihilation operators of bosons at position θ with periodic identification $\hat{\psi}(\theta+2\pi) = \hat{\psi}(\theta)$ and obeying the bosonic commutation relations

$$\begin{aligned} [\hat{\psi}(\theta), \hat{\psi}(\theta')] = [\hat{\psi}^\dagger(\theta), \hat{\psi}^\dagger(\theta')] = 0\,, \\ [\hat{\psi}(\theta), \hat{\psi}^\dagger(\theta')] = \delta(\theta - \theta')\,, \end{aligned} \tag{2.27}$$

making use of the restriction of θ to one specific interval of length 2π. The form (2.26) corresponds to the Lieb-Liniger model when setting units by $\frac{\hbar^2}{2m} = 1$ and $L = 2\pi$. In other words, energy will be given in units of

$$[E] = \frac{4\pi^2\hbar^2}{2mL^2}\,, \tag{2.28}$$

where L is the length of the system. Similarly the coupling parameter is related to the two-body scattering length (1.146) (which is negative for attractive interactions considered here) by

$$g = \frac{2m}{\pi\hbar} L a_s \omega_\perp < 0\,, \tag{2.29}$$

when applied to realistic Bose gases with transversal harmonic confinement of frequency $\omega_\perp$ (see section 1.3).

Besides the fact that the second quantized form (2.26) allows for arbitrary particle numbers and also for superpositions of states of different particle numbers, it is equivalent to the first quantized form by one-to-one correspondence when one restricts the Hilbert space to the N particle sector defined by

$$\mathcal{H}_N = \left\{ |\varphi\rangle \in \mathcal{H} \;\middle|\; \hat{N}\,|\varphi\rangle = N\,|\varphi\rangle \right\} \tag{2.30}$$

with the particle number operator

$$\hat{N} = \int_0^{2\pi} \mathrm{d}\theta\, \hat{\psi}^\dagger(\theta)\hat{\psi}(\theta)\,. \tag{2.31}$$

The connection to the Lieb-Liniger model formulated in first quantization (1.170) is established by the relation

$$g = \frac{L}{\pi} c\,. \tag{2.32}$$

By Fourier decomposition of the field operators into momentum modes

$$\hat{\psi}(\theta) = \frac{1}{\sqrt{2\pi}} \sum_{k\in\mathbb{Z}} \mathrm{e}^{ik\theta} \hat{a}_k\,, \tag{2.33}$$

where the annihilation and creation operators in the momentum modes fulfill

$$\begin{aligned} [\hat{a}_k, \hat{a}_l] = [\hat{a}_k^\dagger, \hat{a}_l^\dagger] = 0\,, \\ [\hat{a}_k, \hat{a}_l^\dagger] = \delta_{kl}\,, \end{aligned} \tag{2.34}$$

the Hamiltonian (2.26) reads

$$\hat{H} = \sum_{k\in\mathbb{Z}} k^2 \hat{a}_k^\dagger \hat{a}_k - \frac{\tilde{\alpha}}{4} \sum_{k,l,m,n\in\mathbb{Z}} \delta_{k+l-m-n} \hat{a}_k^\dagger \hat{a}_l^\dagger \hat{a}_m \hat{a}_n \,, \tag{2.35}$$

where I introduced the coupling parameter

$$\tilde{\alpha} = -\frac{g}{\pi} \,, \tag{2.36}$$

not to be confused with the energy-like coupling parameter α in the QCE treatment of the repulsive case in the last chapter. It has been shown [189, 208, 209] based on exact calculations of low-lying spectra for small numbers of particles ($N \leq 20$) that most of the relevant physics are inherited if one truncates the Hilbert space to the three lowest single particle momentum modes $k = -1, 0, 1$:

$$\hat{H}_3 = \sum_{k\in\{-1,0,1\}} k^2 \hat{a}_k^\dagger \hat{a}_k - \frac{\tilde{\alpha}}{4} \sum_{k,l,m,n\in\{-1,0,1\}} \delta_{k+l-m-n} \hat{a}_k^\dagger \hat{a}_l^\dagger \hat{a}_m \hat{a}_n \,, \tag{2.37}$$

as long as the coupling strength stays at moderate values. The validity of this truncation thereby goes far beyond a perturbative expansion in powers of $\tilde{\alpha}$. One can easily show that

$$\begin{aligned} [\hat{H}_3, \hat{N}] &= 0 \,, \\ [\hat{H}_3, \hat{L}] &= 0 \,, \end{aligned} \tag{2.38}$$

with the total number of particles and momentum operator

$$\begin{aligned} \hat{N} &= \sum_{k\in\{-1,0,1\}} \hat{a}_k^\dagger \hat{a}_k \\ \hat{L} &= \sum_{k\in\{-1,0,1\}} k \hat{a}_k^\dagger \hat{a}_k = \hat{a}_1^\dagger \hat{a}_1 - \hat{a}_{-1}^\dagger \hat{a}_{-1} \,. \end{aligned} \tag{2.39}$$

When a specific quantum state is considered, an indicator for the defect introduced due to the truncation (2.37)is the depopulation of the single-particle ground state $k = 0$. If an eigenstate of (2.37) in the truncated Hilbert space is merely slightly populated in the modes $k = \pm 1$, one can assume that the occupation of all truncated modes $|k| > 1$ in the corresponding exact eigenstate of the full Hamiltonian (2.35) is even smaller and hence neglectable. Later, when it comes to discussing the QPT, the ESQPT and related physical scenarios, it will become clear that by increasing the number of particles, the depletion of the condensate can be made arbitrarily small. In the case of the ESQPT this involves the freedom of choosing an appropriately small coupling strength when N is large.

2.3 The classical limit

In order to obtain the classical counterpart of the truncated quantum system, one has to replace the creation and annihilation operators by complex valued classical variables

$$\begin{aligned} \hat{a}_k \mapsto \phi_k =: \frac{1}{\sqrt{2}}(q_k + \mathrm{i}p_k)\,, \\ \hat{a}_k^\dagger \mapsto \phi_k^* =: \frac{1}{\sqrt{2}}(q_k - \mathrm{i}p_k)\,, \end{aligned} \tag{2.40}$$

with the new classical coordinates q_k and canonically conjugated momenta p_k that take real values. In addition special care has to be taken considering the ordering of operators. The correct prescription [212] thereby is to replace symmetrically ordered products of operators

$$\left\{\hat{a}_{k_1}\cdots\hat{a}_{k_m}\hat{a}_{l_1}^\dagger\cdots\hat{a}_{l_n}^\dagger\right\}_{\mathrm{sym}} \mapsto \phi_{k_1}\cdots\phi_{k_m}\phi_{l_1}^*\cdots\phi_{l_n}^*\,, \tag{2.41}$$

where the symmetric ordering is defined by the sum of all possible orderings divided by their number

$$\{\hat{c}_1\cdots\hat{c}_n\}_{\mathrm{sym}} := \frac{1}{n!}\sum_{\sigma\in S_n}\hat{c}_{\sigma(1)}\cdots\hat{c}_{\sigma(n)}\,, \tag{2.42}$$

where the c_j can be any creation and/or annihilation operators. Ordering the operators in (2.37) using (2.34) and performing the prescription (2.41) yields the classical Hamiltonian for the truncated Lieb-Liniger model

$$H_{\mathrm{cl}} = \sum_k\left(k^2+\frac{3\tilde{\alpha}}{2}\right)|\phi_k|^2 - \frac{\tilde{\alpha}}{4}\sum_{k,l,m,n}\delta_{k+l-m-n}\phi_k^*\phi_l^*\phi_m\phi_n - \frac{9\tilde{\alpha}}{8} - 1\,, \tag{2.43}$$

where I have omitted the specification of the index sets in the sums in order to ease notation.

The canonical transformation

$$\begin{aligned} \frac{1}{\sqrt{2}}(q_k + \mathrm{i}p_k) \mapsto \sqrt{n_k}\mathrm{e}^{-i\theta_k} \\ n_k \in \mathbb{R}^+\,, \theta_k \in [0, 2\pi]\,, \end{aligned} \tag{2.44}$$

obeys the Poisson commutation relations

$$\begin{aligned} \{\theta_k, \theta_l\}_{\mathbf{q},\mathbf{p}} = \{n_k, n_l\}_{\mathbf{q},\mathbf{p}} = 0\,, \\ \{\theta_k, n_l\}_{\mathbf{q},\mathbf{p}} = \delta_{kl}\,, \end{aligned} \tag{2.45}$$

with Poisson brackets defined in (2.9), so that θ_k are the new coordinates and n_k the conjugated momenta. Note for later that this transformation becomes singular at the axes $n_k = 0$ so that in the context of global objects (as contrasted to local quantities), *e.g.*, orbits that run around the axes, one has to take special care. Topologically speaking, the transformation into polar coordinates introduces a punctuation of the (q_k, p_k)-planes, so that orbits or paths

cannot continuously be deformed across these singularities. As expected, this will become especially important for the calculation of Maslov indexes later.

The transformation brings the Hamiltonian into the form

$$H_{\mathrm{cl}} = \sum_k \left(k^2 + \frac{3\tilde{\alpha}}{2}\right) n_k - \frac{9\tilde{\alpha}}{8} - 1 - \frac{\tilde{\alpha}}{4}\left[n_0^2 + n_1^2 + n_{-1}^2 + 4(n_0 n_1 + n_0 n_{-1} + n_1 n_{-1}) + 4n_0\sqrt{n_1 n_{-1}}\cos(2\theta_0 - \theta_1 - \theta_{-1})\right] . \tag{2.46}$$

In addition to energy conservation $\frac{\mathrm{d}}{\mathrm{d}t}H_{\mathrm{cl}} = \frac{\partial}{\partial t}H_{\mathrm{cl}} = 0$ there exist two constants of motion

$$\begin{aligned} \tilde{N} &= n_0 + n_{-1} + n_1 \,, \\ \tilde{L} &= n_1 - n_{-1} \,, \end{aligned} \tag{2.47}$$

$$\{\tilde{N}, H_{\mathrm{cl}}\} = \{\tilde{L}, H_{\mathrm{cl}}\} = 0 \,, \tag{2.48}$$

closely related to the total number of particles N and the total momentum L as eigenvalues of (2.39). This means that the classical system at hand is integrable and can therefore be semiclassically quantized using the EBK quantization rule (2.24).

Before investigating the classical torus-structure, one further canonical transformation is applied to make two of the three momenta constant. The transformation takes the phase space variables $(\theta_0, \theta_{-1}, \theta_1, n_0, n_{-1}, n_1)$ into $(\varphi_0, \varphi_N, \varphi_L, n_0, \tilde{N}, \tilde{L})$ given by

$$\begin{aligned} \varphi_0 &= \theta_0 - \frac{1}{2}(\theta_1 + \theta_{-1}) \,, \\ \varphi_N &= \frac{1}{2}(\theta_1 + \theta_{-1}) \,, \\ \varphi_L &= \frac{1}{2}(\theta_1 - \theta_{-1}) \,, \end{aligned} \tag{2.49}$$

which is a point transformation and leaves us with the expression

$$H_{\mathrm{cl}} = (\tilde{N} - n_0) + \frac{3\tilde{\alpha}}{2}\tilde{N} - \frac{9\tilde{\alpha}}{8} - 1 - \frac{\tilde{\alpha}}{4}\left[\frac{3}{2}\tilde{N}^2 - \frac{3}{2}n_0^2 + n_0\tilde{N} - \frac{1}{2}\tilde{L}^2 + 2n_0\sqrt{(\tilde{N} - n_0)^2 - \tilde{L}^2}(2\cos^2\varphi_0 - 1)\right] . \tag{2.50}$$

For later use I further ease notation by scaling according to

$$\begin{aligned} \tilde{\epsilon} &:= \frac{H_{\mathrm{cl}}}{\tilde{N}} \,, \\ z &:= \frac{n_0}{\tilde{N}} \,, \\ l &:= \frac{\tilde{L}}{\tilde{N}} \,, \\ \bar{\alpha} &:= \tilde{\alpha}\tilde{N} \,, \end{aligned} \tag{2.51}$$

where z is then closely related to the classical version of the condensate fraction and l is closely related to the average angular momentum per particle. These

two relations will show up to become exact in the limit $N \to \infty$. Therefore, I will simply refer to the two quantities as the mentioned notions, keeping in mind that they are not exactly correct for finite N. In these scaled variables the energy (per particle) transformed from (2.50) reads

$$\begin{aligned}\tilde{\epsilon} = 1 - z - \frac{1}{\tilde{N}} + \frac{3\bar{\alpha}}{2}\frac{1}{\tilde{N}} - \frac{9\bar{\alpha}}{8}\frac{1}{\tilde{N}^2} \\ - \frac{\bar{\alpha}}{4}\left[\frac{3}{2} - \frac{3}{2}z^2 + z - \frac{1}{2}l^2 + 2z\sqrt{(1-z)^2 - l^2}(2\cos^2\varphi_0 - 1)\right] .\end{aligned} \tag{2.52}$$

or

$$\tilde{\omega} = 1 - z - \frac{\bar{\alpha}}{4}\left[\frac{1}{2} + z - \frac{3}{2}z^2 - \frac{1}{2}l^2 - 2z\sqrt{(1-z)^2 - l^2}(1 - 2\cos^2\varphi_0)\right] , \tag{2.53}$$

after subtraction

$$\tilde{\omega} := \tilde{\epsilon} - \tilde{\epsilon}_0 , \tag{2.54}$$

of the constant energy shift

$$\tilde{\epsilon}_0 = -\frac{\bar{\alpha}}{4} - \frac{1}{\tilde{N}} + \frac{3\bar{\alpha}}{2}\frac{1}{\tilde{N}} - \frac{9\bar{\alpha}}{8}\frac{1}{\tilde{N}^2} , \tag{2.55}$$

which corresponds to the mean-field ground state energy per particle $\frac{gN}{4\pi} \approx -\frac{\bar{\alpha}}{4}$ up to $\mathcal{O}(N^{-1})$-corrections one gets in the sub-critical regime when solving the Gross-Pitaevskii-equation [206, 207] corresponding to the continuous model (2.26).

The scaled version (2.53) does not depend on $\tilde{N}$ anymore. The scaled variables (2.51) can therefore be considered the natural variables characterizing the physics. This means *i)* that the coupling strength $\bar{\alpha}$ and *ii)* the angular momentum per particle l are the correctly scaled properties characterizing the physical situation, and *iii)* that the condensate fraction z, its conjugated coordinate φ_0 and their dynamics are classically determined by only those two constants $\bar{\alpha}$ and l and do not depend on the number of bosons N explicitly. The explicit influence of N on the physics then takes place purely on the quantum level through its role as an effective quantum of action, which is the subject of the next section.

2.4 Effective quantum of action

The relations (2.40) between creation and annihilation operators in the single particle momentum modes and the quadratures are on the quantum level given by

$$\begin{aligned} \hat{q}_k &= \frac{1}{\sqrt{2}} \left(\hat{a}_k + \hat{a}_k^\dagger \right) , \\ \hat{p}_k &= \frac{1}{\sqrt{2}\mathrm{i}} \left(\hat{a}_k - \hat{a}_k^\dagger \right) . \end{aligned} \tag{2.56}$$

They imply, using (2.34), the commutation relations

$$\begin{aligned} [\hat{q}_k, \hat{q}_l] &= [\hat{p}_k, \hat{p}_l] = 0 \,, \\ [\hat{q}_k, \hat{p}_l] &= \mathrm{i}\delta_{kl} =: \mathrm{i}\hbar_{\mathrm{eff}}^{(q,p)} \delta_{kl} \,, \end{aligned} \tag{2.57}$$

which are canonical up to a constant factor. Therefore $\hat{\mathbf{q}}$ and $\hat{\mathbf{p}}$ can be considered a set of canonically conjugated coordinate and momentum observables with an effective quantum of action

$$\hbar_{\mathrm{eff}}^{(q,p)} = 1 \,. \tag{2.58}$$

Furthermore, the transformation to polar coordinates (2.44) is canonical as can be seen in their Poisson bracket relations (2.45). The same is true for the transformation given by (2.47) and (2.49). The corresponding effective quantum of action is therefore the same as for the quadratures and I express this fact by writing

$$\hbar_{\mathrm{eff}}^{(\theta,n)} = \hbar_{\mathrm{eff}}^{(\varphi,n)} = 1 \,. \tag{2.59}$$

By convention I will use the quadratures or their canonically transformed variants as conjugate phase space variables which defines action integrals as

$$S = \int \mathrm{d}\mathbf{q} \cdot \mathbf{p} \tag{2.60}$$

and makes (2.58) and (2.59) the effective quantum of action par excellence. In other words, since the latter is unity, (2.60) defines the action in units of the actual physical constant $\hbar$.

To understand the meaning or quality of semiclassical approximations, neither the absolute value of $\hbar$ nor the value of an effective quantum of action $\hbar_{\mathrm{eff}}$ alone are decisive. What counts is the ratio of *typical* classical actions to $\hbar$. Therefore it is educational to have an additional look at the scaled variables (2.51) with the dynamically non-trivial pair of coordinates φ_0 and z with

$$\hbar_{\mathrm{eff}}^{(\varphi_0,z)} = \{\varphi_0, z\}_{\mathbf{q},\mathbf{p}} \cdot \hbar_{\mathrm{eff}}^{(q,p)} = \frac{1}{\tilde{N}} \,. \tag{2.61}$$

We saw that the energy landscape is naturally represented as (2.53) in those scaled variables, giving off any explicit dependence on N in the dynamics and hence in the typical (scaled) actions defined in those scaled variables. This fact together with (2.61) clarifies the very important basic point that semiclassical methods in the given context of application to second quantized bosonic many-body systems become asymptotically exact for $N \to \infty$ and should result in

good approximations if the number of bosons is not extremely small. The only prerequisite to this statement in the given system is that $\bar{\alpha}$ and l are considered fixed constants that do not scale with N, which is true for almost all upcoming discussions in this thesis. There is only one exception to be anticipated here. In section 2.8.4, we will find and discuss a situation where this requirement is not fulfilled. There, further improvement beyond the semiclassical EBK quantization will be needed for an asymptotically exact description.

2.5 Phase space structure

2.5.1 Reduction of phase space

Since $\tilde{N}$ and $\tilde{L}$ are constants of motion

$$\dot{\tilde{N}} = \dot{\tilde{L}} = 0\,, \tag{2.62}$$

it suffices to investigate the energy landscape and classical orbits in the dimensionally reduced phase space (φ_0, n_0) with fixed values of $\tilde{N}$ and $\tilde{L}$ while keeping in mind that φ_N and φ_L may still be free variables especially when it comes to the investigation of classical tori. First of all, the relevant phase space is restricted by the non-negativity of the n_k:

$$\begin{aligned} \tilde{N} - |\tilde{L}| - n_0 = n_1 + n_{-1} - |n_1 - n_{-1}| \geq 0\,, \\ \Rightarrow \quad n_0 \in [0, \tilde{N} - |\tilde{L}|]\,. \end{aligned} \tag{2.63}$$

Furthermore, (2.50) exhibits a φ_0-periodicity of π, which indicates some phase space doubling. The identification of equivalent phase space points is given by the simultaneous shift

$$\begin{aligned} \varphi_0 &\mapsto \varphi_0 + \pi\,, \\ \varphi_{\tilde{N}} &\mapsto \varphi_{\tilde{N}} + \pi\,, \\ \varphi_{\tilde{L}} &\mapsto \varphi_{\tilde{L}} + \pi\,, \end{aligned} \tag{2.64}$$

which, after transforming back, leads to

$$\begin{aligned} \theta_0 &\mapsto \theta_0 + 2\pi\,, \\ \theta_1 &\mapsto \theta_1 + 2\pi\,, \\ \theta_{-1} &\mapsto \theta_{-1}\,, \end{aligned} \tag{2.65}$$

being identical to the original unshifted point, since all θ_k are defined modulo 2π. This identification allows to reduce the unique φ_j-space to, *e.g.*,

$$\begin{aligned} \varphi_0 &\in [-\frac{\pi}{2}, \frac{\pi}{2}]\,, \\ \varphi_N &\in [0, 2\pi]\,, \\ \varphi_L &\in [0, 2\pi]\,. \end{aligned} \tag{2.66}$$

Note that no more identifications are possible, as it is easily argued by comparison of the available coordinate space volume in the old and new coordinates

$$\begin{aligned} \prod_j \int \mathrm{d}\varphi_j &= \frac{1}{2}(2\pi)^3\,, \\ \prod_k \int \mathrm{d}\theta_k &= (2\pi)^3\,, \end{aligned} \tag{2.67}$$

where the relative factor corresponds to the Jacobian $\left|\left|\left(\frac{\partial\varphi_j}{\partial\theta_k}\right)_{jk}\right|\right| = \frac{1}{2}$ of the point transformation. I also want to stress that the phase space is not simply π-periodic in φ_0, but the simultaneous π-shift in φ_N and φ_L is rather essential especially for topological issues like the construction of elementary loops on the tori of the system.

2.5.2 Torus structure for zero interaction

It is instructive to consider first the non-interacting case $\bar{\alpha} = 0$ where the solutions of constant energy are given by flat lines $n_0(\varphi_0) = \text{const.}$ in the (φ_0, n_0) surface of section. The corresponding tori are, *e.g.*, parametrized by

$$\begin{aligned} (n_0, \tilde{N}, \tilde{L}) &= \text{const.}\,, \\ (\varphi_0, \varphi_N, \varphi_L) &= (-\frac{\pi}{2} + \pi\tau_0, 2\pi\tau_N, 2\pi\tau_L)\,, \\ \tau_j &\in [0,1]\,. \end{aligned} \tag{2.68}$$

In the old coordinates this corresponds to

$$\begin{aligned} n_k &= \text{const.}\,, \\ \theta_k &= 2\pi\tau_k\,, \\ \tau_k &\in [0,1]\,, \end{aligned} \tag{2.69}$$

which is the most natural parametrization of a three-torus without any non-trivial identifications. The elementary loops are given by the trivial loops in the old coordinates

$$\begin{aligned} C_0: &\quad (\mathbf{n}, \boldsymbol{\theta})(\tau) = (\mathbf{n}(0), 2\pi\tau, \theta_1(0), \theta_{-1}(0))\,, \\ C_1: &\quad (\mathbf{n}, \boldsymbol{\theta})(\tau) = (\mathbf{n}(0), \theta_0(0), 2\pi\tau, \theta_{-1}(0))\,, \\ C_{-1}: &\quad (\mathbf{n}, \boldsymbol{\theta})(\tau) = (\mathbf{n}(0), \theta_0(0), \theta_1(0), 2\pi\tau)\,, \end{aligned} \tag{2.70}$$

with τ running from 0 to 1.

The easiest way to address the Maslov indexes of the three elementary loops $C_{0,1,-1}$ is to go back to $(\mathbf{p}, \mathbf{q})$-coordinates, where each of them traverses a circle in one of the (p_k, q_k)-planes. The direction of the loops thereby coincides with simple one-dimensional harmonic oscillators. Therefore the Maslov indexes are given by the number of turning points, which is $\nu_{0,1,-1} = 2$ for each loop. It has to be stressed that the loops considered in $(\mathbf{n}, \boldsymbol{\theta})$-loops would falsely lead to indexes of 0. This apparent contradiction is a consequence of the singularity of the canonical transformation (2.44) between the two spaces.

The corresponding action integrals are

$$S_{C_k} = \int_{C_k} \mathrm{d}\mathbf{q} \cdot \mathbf{p} = \int_0^{2\pi} \mathrm{d}\theta_k\, n_k = 2\pi n_k\,, \tag{2.71}$$

so that EBK quantization (2.24) gives

$$n_k = m_k + \frac{1}{4}\nu_k = m_k + \frac{1}{2}\,, \quad m_k \in \mathbb{N}_0\,. \tag{2.72}$$

Physically, the m_k are occupation numbers of the corresponding momentum modes, which can be seen when applying (2.72) to the classical analogues of occupation number operators

$$\hat{n}_k = \hat{a}_k^\dagger \hat{a}_k = \{\hat{a}_k^\dagger \hat{a}_k\}_{sym} - \frac{1}{2} \mapsto n_k - \frac{1}{2} = m_k\,. \tag{2.73}$$

This is a special relation that only holds for the non-interacting case. Nevertheless it allows the proper interpretation of $\tilde{N}$ and $\tilde{L}$ as

$$\begin{aligned} \tilde{N} &= n_0 + n_1 + n_{-1} = m_0 + m_1 + m_{-1} + \frac{3}{2} = N + \frac{3}{2}\,, \\ \tilde{L} &= n_1 - n_{-1} = m_1 - m_{-1} = L\,, \end{aligned} \tag{2.74}$$

in terms of the total number of particles N and the total (angular) momentum L of the system. This relation expresses a purely kinematic property, so that it holds also for the interacting case.

2.5.3 Phase space structure for $L = 0$

In order to investigate the physics of the QPT one can restrict oneself to the case of zero total momentum $L = 0$, since the ground state falls into this class. Also the physics involving excited states can be studied restricting oneself to $L = 0$. The states of different non-zero total angular momenta introduce only limited qualities on top of the $L = 0$-states. As has been studied numerically [208, 209], on either side of the transition, *i.e.*, for rather strong or rather weak couplings, they form bunches of levels each of which is quasi-degenerate with one ($L = 0$)-state and therefore share their quality with the latter to some extent. The main feature of those states is that they change the specific ($L = 0$)-state they are associated to during the cross-over around the QPT [208, 209]. However, in the regimes of quasi-degenerate bunches fixing the total angular momentum to zero can be viewed as a representative for all non-vanishing L in one way or another. The question if different L-branches could be related also in the regime of the transition, *e.g.*, by moving to rotating frames of reference is not addressed here. I leave it open for future discussion. The calculations in this subsection will focus on $L = 0$ while some more qualitative statements may also hold for arbitrary L. The general case $L \neq 0$ will be discussed in the subsequent subsection.

For $L = 0$ the Hamiltonian in the scaled version (2.53) simplifies to

$$\tilde{\omega} = 1 - z - \frac{\bar{\alpha}}{8}(1-z)^2 - \bar{\alpha} z (1-z)\cos^2\varphi_0 \,. \tag{2.75}$$

There are several regions of the coupling strength $\bar{\alpha}$ for which the structure of the relevant phase space behaves qualitatively different. One property that they have in common though is that the boundaries $z = 1$ and $z = 0$ of the relevant phase space are solutions of constant energy:

$$\begin{aligned} \tilde{\omega}(z = 1, \varphi_0) &= 0 =: \tilde{\omega}^{(1)} \,, \\ \tilde{\omega}(z = 0, \varphi_0) &= 1 - \frac{\bar{\alpha}}{8} =: \tilde{\omega}^{(2)} \,, \end{aligned} \tag{2.76}$$

and correspondingly $E^{(1,2)} := \tilde{N}(\tilde{\omega}^{(1,2)} + \tilde{\epsilon}_0)$.

The subcritical region $0 < \bar{\alpha} < 1$

For sufficiently small coupling $0 < \bar{\alpha} < 1$ all of the relevant phase space and its tori inside are just smooth continuous deformations of their non-interacting counterparts regarding topological aspects. In this region the energy $\tilde{\omega}$ is a monotonously decreasing function of z (in $0 < z < 1$) for all values of φ_0. This means there can be no "turning points" in the (n_0, φ_0)-plane. All orbits traverse the full φ_0-range and they do it in a monotonous manner. Another implication is that the ground state of the system will be concentrated at the large n_0 end ($n_0 \to \tilde{N}$ or $z \to 1$) of the relevant phase space and smeared over all φ_0. Figure 2.1 shows an example with slightly deformed constant-energy solutions. Such deformed flat solutions passing through the full φ_0-range will be referred to as, in analogy to the pendulum, *librations*.

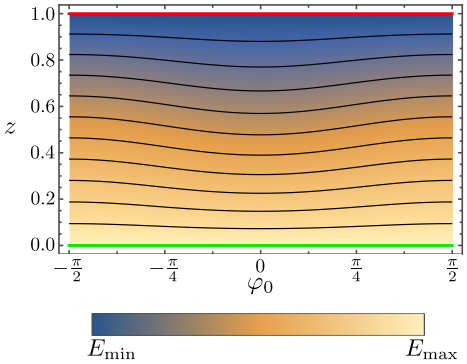

Fig. 2.1: Phase space portrait for zero angular momentum $L = 0$ and small coupling $\bar{\alpha} = 0.3$. The color code represents the value of the energy with the minimum energy in the relevant phase space labeled as $E_{\min}$ and its maximum labeled as $E_{\max}$. The orbits, which are solutions of constant energy, are drawn as lines, where the flat red and green orbits correspond to the boundaries $z = 1$ and $z = 0$, respectively, and black orbits are librations in-between.

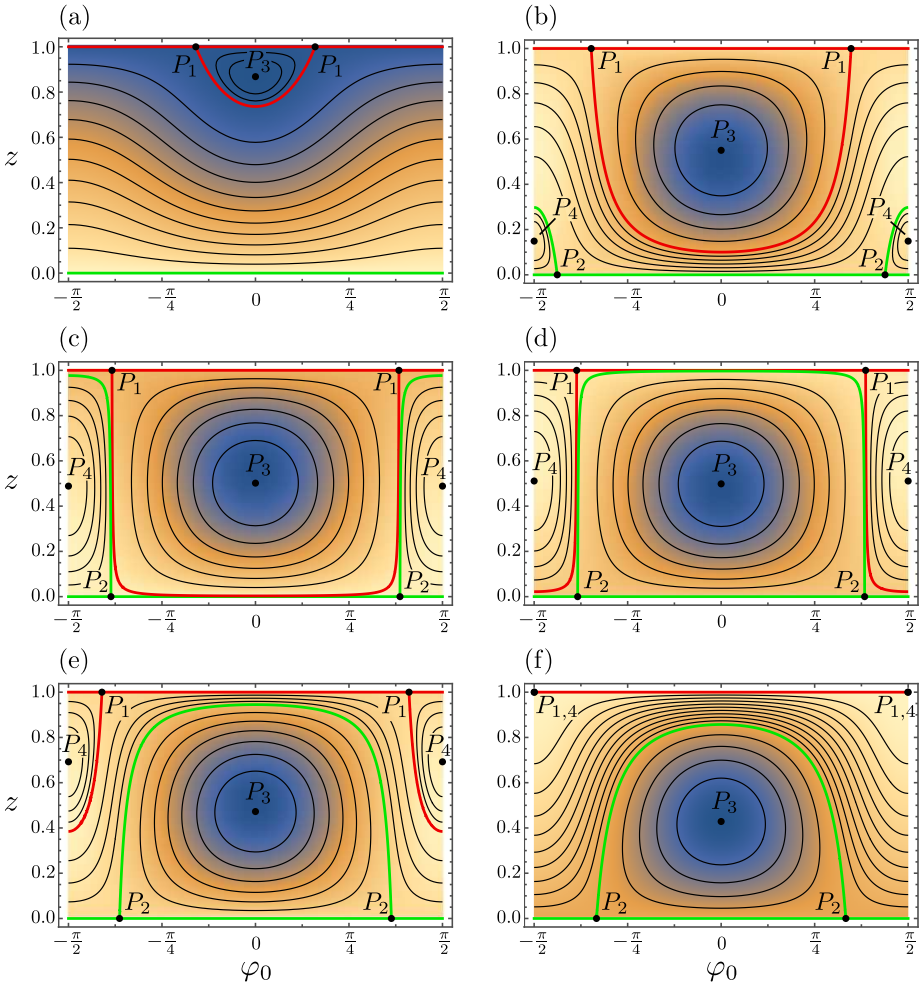

Fig. 2.2: Phase space portraits for zero angular momentum $L = 0$ and different couplings $\bar{\alpha} = 1.3$(a), 4.7(b), 7.82(c), 8.18(d), 13(e), ∞(f). The color code represents the value of the energy (see Fig. 2.1). The orbits, which are solutions of constant energy are drawn as lines, where the red and green orbits correspond to the boundaries and separatrices with energy $\tilde{\omega} = \tilde{\omega}^{(1)}$ and $\tilde{\omega} = \tilde{\omega}^{(2)}$, respectively and black curves show librations in-between or vibrations inside the separated islands.

The supercritical region $1 < \bar{\alpha} < 4$

When $\bar{\alpha}$ passes through the critical value $\bar{\alpha}_1 := 1$, a second solution to $\tilde{\omega}(z, \varphi_0) = \tilde{\omega}^{(1)}$ penetrates the phase space. It intersects the $z = 1$ solution in the two symmetrically lying points P_1 at $\cos^2 \varphi_0 = \frac{1}{\bar{\alpha}}$, which are saddle points of the energy landscape. This solution will be referred to as

$$z^{(1)}(\varphi_0) = \frac{8 - \bar{\alpha}}{\bar{\alpha}(8\cos^2 \varphi_0 - 1)} \,. \tag{2.77}$$

Together with the solution $z = 1$, they play the role of mutually crossing separatrices that break up into individual pieces at their intersections P_1. Between the two an island builds up that is energetically well separated from the outside (see Fig. 2.2a). Outside of this island the energy is still a monotonous function of z for arbitrary φ_0 so that all orbits in this regime are still librations. Whereas inside the island a global energy minimum appears at the point P_3 lying on the symmetry line $\varphi_0 = 0$ exactly half-way between $z = 1$ and the separatrix $z = z^{(1)}(0) = \frac{1}{7}(\frac{8}{\bar{\alpha}} - 1)$ with the energy

$$\tilde{\omega}_{\min} = -\frac{2}{7}\bar{\alpha}\left(1 - \frac{1}{\bar{\alpha}}\right)^2 \,. \tag{2.78}$$

Since no orbit inside the island can cross the separatrix, all of them are circulating around the minimum P_3. Those orbits do not traverse through all values of φ_0 but correspond to two-fold solutions

$$z_\pm(\varphi_0) = \frac{4}{8\cos^2 \varphi_0 - 1}\left(\cos^2 \varphi_0 - \frac{1}{\bar{\alpha}} \pm \sqrt{\left(\cos^2 \varphi_0 - \frac{1}{\bar{\alpha}}\right)^2 + \frac{\tilde{\omega}}{2\bar{\alpha}}(8\cos^2 \varphi_0 - 1)}\right) , \tag{2.79}$$

that exist in finite φ_0-intervals and become single-solutions at the boundaries of the respective intervals (where the square-root in (2.79) vanishes). Such orbits will be referred to as *vibrations*. Figure 2.2a shows an example of the coexistence of librations and vibrations. It is this change from purely librating orbits to vibrations that will give rise to the existence of a QPT in the semiclassical sense. For $\bar{\alpha}$ exceeding some critical value, the ground state will be concentrated on the inside of the separated low-energy island.

Extreme couplings $\bar{\alpha} > 4$ – breakdown and irrelevance

When $\bar{\alpha}$ exceeds the value of $\bar{\alpha}_2 := 4$, additional separatrices enter the allowed phase space. This is an artifact that originates from the truncation to the lowest three momentum modes and can be considered unphysical. It starts to qualitatively alter the structure of the classical phase space in the region of full depletion of the condensate ($z = 0$), where the truncated model cannot be trusted to decently reproduce the physics of the continuous model. As long as the focus is on the physics related to large condensate fractions, these artifacts can be ignored. Furthermore, as will be seen in the discussion of QPTs, the perspective of large numbers of particles renders such large values of $\bar{\alpha}$ physically irrelevant. The rich and non-trivial features related to phase transitions take

place at values around $\bar{\alpha} \approx 1$, far away from the regime where depletion of the condensate starts to introduce strong deficiencies. This renders also additional artifacts irrelevant that appear for even larger values $\bar{\alpha} = 8$.

For completeness, representative phase space portraits of all qualitatively different regions are shown in Fig. 2.2 and interesting albeit for physical situations non-relevant details can be found in appendix D.1.

2.5.4 Phase space structure for $L \neq 0$

From the non-interacting case the meanings of $\tilde{N}$ and L are clear (see (2.74)). From the quantum system one knows which values they can take since the spectra of the conserved operators $\hat{N}$ and $\hat{L}$ are trivial. Nevertheless, when turning towards a semiclassical quantization of the system, one cannot fix the classical variables $\tilde{N}$ and L to those eigenvalues, because it is not clear from the beginning that the full three-torus quantization procedure will reproduce them exactly. The only way that would allow to fully reduce the degrees of freedom to one would be by fully expressing the quantum Hamiltonian (2.37) by the operators $\hat{N}, \hat{L}$ and $\hat{n}_0$ and subsequently restricting to a subspectra by fixing the eigenvalues of $\hat{N}$ and $\hat{L}$. Unfortunately, such a simplification, that would leave a single degree of freedom already on the quantum level, is not possible. Therefore, the semiclassical quantization procedure in general will be performed with all three dimensions being dynamical variables. For this reason, one needs to extend the knowledge about the classical phase space structure to the $L \neq 0$ case at least on a qualitative level. This level could be as superficial as it suffices to know that also for $L \neq 0$, the orbits in relevant phase space come in the two classes of librations and vibrations but nothing else. This statement is indeed a fact. Figure 2.3 shows examples of phase portraits for $L = 0.05\tilde{N}$.

The case $L \neq 0$ also admits constant solutions at the upper and lower boundary of reduced phase space with the energies per particle (2.53)

$$\tilde{\omega}^{(1)} = \tilde{\omega}(z = 1 - |l|, \varphi_0) = |l| \left(1 - \frac{\bar{\alpha}}{2}(1 - |l|)\right) , \tag{2.80}$$

$$\tilde{\omega}^{(2)} = \tilde{\omega}(z = 0, \varphi_0) = 1 - \frac{\bar{\alpha}}{8}(1 - l^2) , \tag{2.81}$$

and correspondingly $E^{(1,2)} := \tilde{N}(\tilde{\omega}^{(1,2)} + \tilde{\epsilon}_0)$, respectively.

Upper separatrix and minimum energy island

The major difference to $L = 0$ is that the counterparts of the upper separatrix $z^{(1)}$ and the corresponding island of minimal energy (global energy minimum at P_3) already exist for arbitrarily small $\bar{\alpha}$ (this will be expressed by setting $\bar{\alpha}_1 = 0$. For small couplings, though, the island is squeezed very tightly to the upper boundary of relevant phase space. Apart from this qualitative difference the phase space structure behaves similar to the $L = 0$ case when changing the coupling $\bar{\alpha}$. The separatrix intersects the upper boundary $n_0 = \tilde{N} - |L|$ (or equivalently $z = 1 - |l|$)at constant points P_1 at $\varphi_0 = \pm\frac{\pi}{4}$, which cannot be called saddle points in the strict sense because of the non-analyticity of the energy landscape at this boundary.

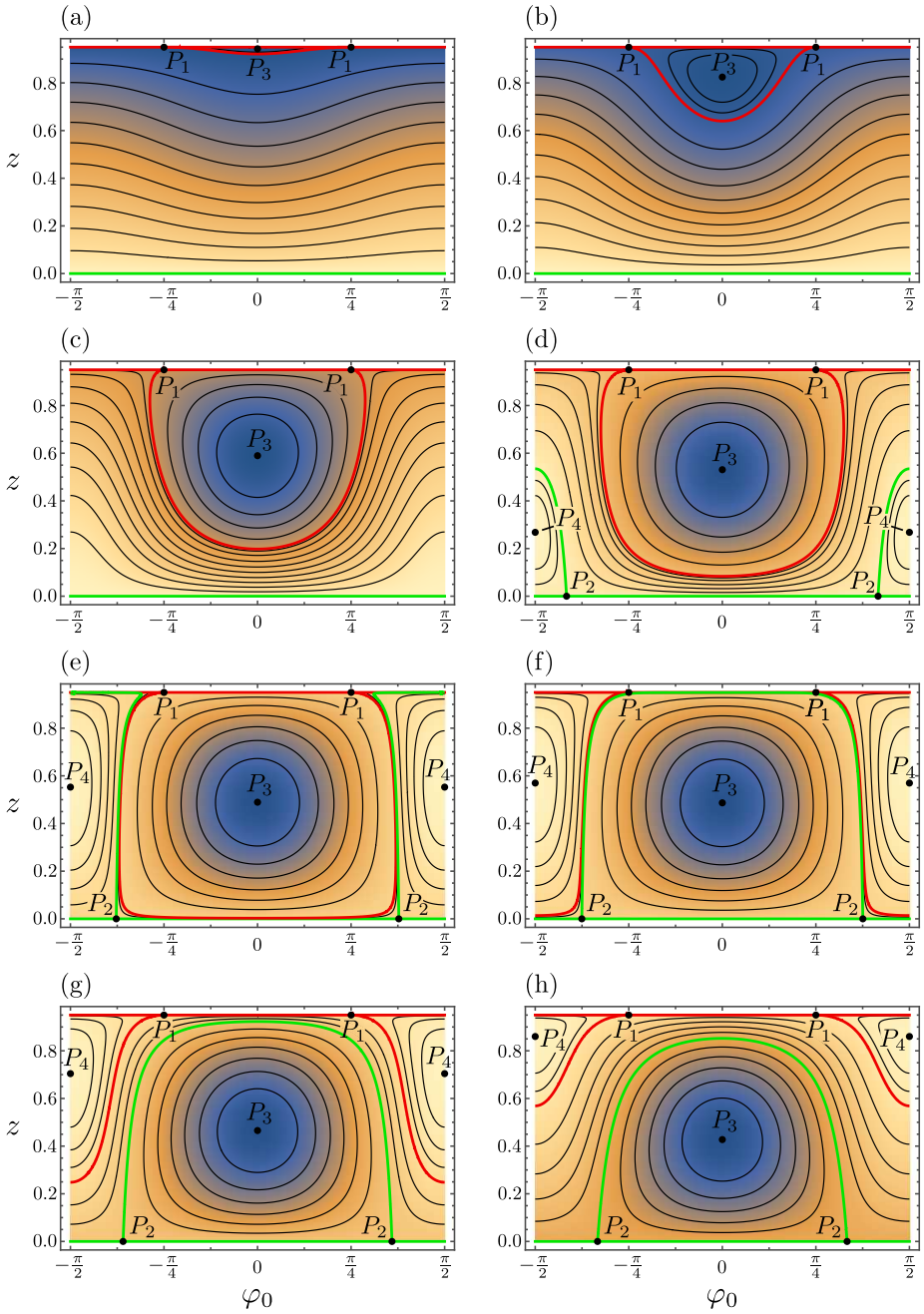

Fig. 2.3: Phase space portraits for angular momentum $L = 0.05\tilde{N}$ and different couplings $\bar{\alpha} = 0.7$(a), 1.4(b), 3.5(c), 5.5(d), 9.2(e), 9.6(f), 15(g), ∞(h).

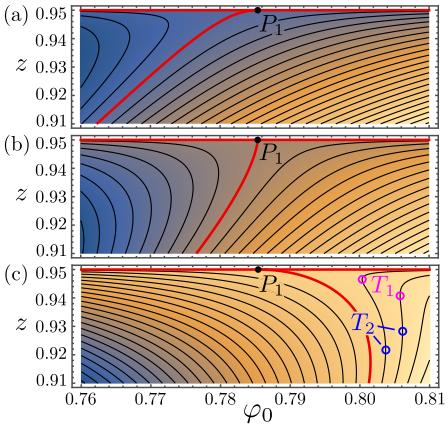

Fig. 2.4: Phase space portraits for $l = 0.05$ in the vicinity of P_1 at $\varphi_0 = \frac{\pi}{4}$ for different couplings:
(a) $\bar{\alpha} = 0.95\bar{\alpha}_{\rm bf}$, bell-shaped upper separatrix that adapts to the upper boundary with zero slope;
(b) $\bar{\alpha} = \bar{\alpha}_{\rm bf}$, perpendicular crossing of the separatrix and the boundary;
(c) $\bar{\alpha} = 1.1\bar{\alpha}_{\rm bf}$, back-folded separatrix. Two of the shown orbits are folded librations with the subsequent turning points $T_{1,2}$ marked with empty circles (blue: counter-clockwise, purple: clockwise rotational direction).

Backfolding

An expansion around the points P_1 reveals that the separatrix $z^{(1)}$ veers away from the boundary quadratically with $\delta\varphi_0$, according to

$$\delta z \approx -\frac{2|l|(1-|l|)^2}{(\bar{\alpha}_{\rm bf}^{-1} - \bar{\alpha}^{-1})^2}\delta\varphi_0^2\,, \tag{2.82}$$

meaning that it connects to the boundary with zero slope. Thereby the direction in which $z^{(1)}$ takes off is either towards the center $\varphi_0 = 0$ for $\bar{\alpha} < \bar{\alpha}_{\rm bf}$ or towards larger absolute values of φ_0 for $\bar{\alpha} > \bar{\alpha}_{\rm bf}$. This shows that the separatrix is bell-shaped for smaller couplings (see Fig. 2.3a,b and Fig. 2.4a) whereas a *back-folding* occurs for larger couplings (see Fig. 2.3c–e). Right at the back-folding point $\bar{\alpha} = \bar{\alpha}_{\rm bf}$ the separatrix hits the boundary perpendicularly (see Fig. 2.4b) and turns towards $\varphi_0 = 0$ according to

$$\delta z \approx -\left(\frac{8}{3}\sqrt{2|l|}(1-|l|)\right)^{\frac{2}{3}}(\mp\delta\varphi_0)^{\frac{2}{3}} \tag{2.83}$$

in the vicinity of P_1, where $\mp$ corresponds to $\varphi_0 = \pm\frac{\pi}{4}$, respectively.

A consequence of the back-folding of the upper separatrix is that librating orbits in its vicinity may have an additional *folding* where two subsequent turning points T_1 and T_2 of opposite rotational direction in the (φ_0, n_0)-plane create a small intermediate situation of triple-valuedness in $n_0(E, \tilde{N}, L, \varphi_0)$ instead of unique determination (see Fig. 2.4c). I enumerate the three solutions by the notation $n_0^{(j)}(E, \tilde{N}, L, \varphi_0), j = 1, 2, 3$, where the lowest superscript corresponds to the branch of lowest value in the relevant interval $n_0 \in [0, \tilde{N} - |L|]$. The position of the turning points will be denoted $\varphi_0^{(T_{1,2})} \in [0, \frac{\pi}{2}]$ and $-\varphi_0^{(T_{1,2})}$.

Since such a folding is a smooth deformation of a flat torus or unfolded libration, it is equivalent from the topological point of view and will only find minor need of special treatment in the next section. The corresponding orbits will be referred to as *folded librations*.

For $|l| \geq \frac{2}{3}$, $\bar{\alpha}_{\rm bf}$ becomes negative and no back-folding occurs (see Fig. D.21b in appendix D.2).

As in the case of vanishing angular momentum, unphysical and irrelevant artifacts from truncation for depleted condensates appear when the coupling is

increased to large values. For $L \neq 0$ they occur at even larger couplings

$$\bar{\alpha}_2 := \frac{4}{2\sqrt{1-l^2}-1}\,, \tag{2.84}$$

as compared to the case $L = 0$. For completeness the corresponding phase space portraits are shown in Fig. 2.3. For the interesting albeit physically irrelevant details see appendix D.2.

2.6 EBK quantization of the truncated model

2.6.1 Quantization of librations

The quantization of librating orbits is based on the quantization of the non-interacting case since the torus-structure of librations is topologically equivalent to the flat non-interacting tori. For this reason the elementary loops of librations can be found starting with the loops $C_{0,1,-1}$ of the non-interacting case and taking the continuous deformation due to interaction into account. Because of $\tilde{N}$ and L being constants of motion, the following analysis is best been performed in the new coordinates $\xi = (n_0, \tilde{N}, L, \varphi_0, \varphi_N\varphi_L)$ using the transformation (2.49).

Unfolded librations

Since, due to energy conservation, n_0 on any *unfolded* librating orbit is uniquely determined by $\boldsymbol{\varphi}$ and the constants $E, \tilde{N}$ and L, the loops are sufficiently described as curves in coordinate space $\boldsymbol{\varphi}$. The deformed analogues of (2.70) are given by

$$\begin{aligned} C_0' : &\quad \boldsymbol{\varphi}(\tau) = (2\pi\tau, \varphi_N(0), \varphi_L(0))\,, \\ C_1' : &\quad \boldsymbol{\varphi}(\tau) = (\varphi_0(0) - \pi\tau, \varphi_N(0) + \pi\tau, \varphi_L(0) + \pi\tau)\,, \\ C_{-1}' : &\quad \boldsymbol{\varphi}(\tau) = (\varphi_0(0) - \pi\tau, \varphi_N(0) + \pi\tau, \varphi_L(0) - \pi\tau)\,, \end{aligned} \tag{2.85}$$

while $\tilde{N}, L$ and E – not n_0 – are kept constant. The given expression for C_0' can also be mapped into the reduced φ-space (2.66) by the identification (2.64) so that

$$C_0' : \boldsymbol{\varphi}(\tau) = \begin{cases} (2\pi\tau, \varphi_N(0), \varphi_L(0)) & : \tau \in [0, \frac{1}{2}]\,, \\ (2\pi\tau - \pi, \varphi_N(0) - \pi, \varphi_L(0) - \pi) & : \tau \in [\frac{1}{2}, 1]\,. \end{cases} \tag{2.86}$$

One can then continuously deform the $C_{0,1,-1}'$ into series of partial paths $\gamma_{0,N,L}$

$$\begin{aligned} \gamma_0 : &\quad \varphi_0(\tau) = \varphi_0(0) + \pi\tau\,, \\ \gamma_N : &\quad \varphi_N(\tau) = \varphi_N(0) + \pi\tau\,, \\ \gamma_L : &\quad \varphi_L(\tau) = \varphi_L(0) + \pi\tau\,, \end{aligned} \tag{2.87}$$

which involve only one φ-coordinate at a time while the other φ-coordinates, $\tilde{N}$ and L are kept constant and $n_0 = n_0(E, \tilde{N}, L, \varphi_0)$ is uniquely determined for a given energy E of the orbit. Then the loops are given as the compositions

$$\begin{aligned} C_0' &= \gamma_0 \circ \gamma_0\,, \\ C_1' &= \gamma_0^- \circ \gamma_N \circ \gamma_L\,, \\ C_{-1}' &= \gamma_0^- \circ \gamma_N \circ \gamma_L^-\,, \end{aligned} \tag{2.88}$$

where $\cdot\circ\cdot$ means path-composition (the $\varphi_j(0)$ are thereby matched to the points of connection), γ_j^- is the inversion of γ_j and the equal signs are meant as equivalence up to path-homotopy. The action integrals $S_{\gamma_j} = \int_{\gamma_j} \mathrm{d}\mathbf{q} \cdot \mathbf{p}$ of the partial

paths are given by

$$\begin{aligned} S_{\gamma_0} &= \int_{-\frac{\pi}{2}}^{\frac{\pi}{2}} \mathrm{d}\varphi_0 \, n_0(E, \tilde{N}, L, \varphi_0) \,, \\ S_{\gamma_N} &= \int_0^{\pi} \mathrm{d}\varphi_N \, \tilde{N} = \pi \tilde{N} \,, \\ S_{\gamma_L} &= \int_0^{\pi} \mathrm{d}\varphi_L \, L = \pi L \,, \end{aligned} \tag{2.89}$$

so that the full action integrals of the elementary loops (which are homotopy invariant) are given by

$$\begin{aligned} S_{C'_0} &= 2S_{\gamma_0} \,, \\ S_{C'_1} &= -S_{\gamma_0} + \pi\tilde{N} + \pi L \,, \\ S_{C'_{-1}} &= -S_{\gamma_0} + \pi\tilde{N} - \pi L \,. \end{aligned} \tag{2.90}$$

Since the used loops are smooth deformations of the non-interacting loops $C_{0,1,-1}$, their Maslov indexes (which express a topological property) are again $\nu_k = 2$. According to EBK quantization (2.24) the action integrals are then quantized to

$$\frac{1}{2\pi} S_{C'_k} = m_k + \frac{1}{4}\nu_k = m_k + \frac{1}{2} \,, \quad m_k \in \mathbb{N}_0 \,, \tag{2.91}$$

which yields

$$\tilde{N} = m_0 + m_1 + m_{-1} + \frac{3}{2} \,, \tag{2.92}$$

$$L = m_1 - m_{-1} \,, \tag{2.93}$$

$$\frac{1}{\pi} S_{\gamma_0} = m_0 + \frac{1}{2} \tag{2.94}$$

by linear combination. Thus finally (2.92) and (2.93) show that the semiclassical EBK quantization of librating orbits indeed leads to the correct spectra of $N = \tilde{N} - \frac{3}{2}$ and L. Despite the striking resemblance of (2.92), (2.93) to the noninteracting case (2.74), where m_k had the meaning of occupation numbers, the latter is not true for the interacting case, since occupation numbers are non-conserved quantities. Nevertheless, because of the similarity in the equations and the equivalence in the limit $\bar{\alpha} \to 0$ I will call the quantum numbers m_k *pseudo-occupation numbers* of the three modes, which, in a fuzzy way, still represent a notion of the average occupation numbers in a corresponding quantum state.

In practice, I will choose a specific $N \in \mathbb{N}$ and $L \in -N, \ldots, N$ (based on (2.92) and (2.93)) understood as parameters of the system which leaves a single quantum number m_0 for the corresponding energy (sub-)spectra that can be semiclassically obtained using (2.94). Thereby this quantum number is restricted to $m_0 \leq N - |L|$, which purely results from the positiveness of all three quantum numbers m_k. Another way to express this boundary is to say that the librating orbit should live in the interior of the relevant phase space, which can be seen using (2.94) to obtain

$$S_{\gamma_0} \leq \pi(\tilde{N} - |L|) - \pi \,. \tag{2.95}$$

Thus the constant upper boundary solution $n_0 = \tilde{N} - |L|$ cannot get quantized. This is especially interesting for $L = 0$, since then this solution is an actual libration as long as $\bar{\alpha} < 1$ so that it is not broken up into pieces of separatrices. This restriction is crucial for the physics in this region, since it would correspond to the state of lowest energy.

Folded librations

In the case of *folded* librations n_0 is piece-wise not uniquely defined so that one has to alter the definitions of the paths $C'_{0,1,-1}$ to make the triple-valuedness explicit. Alternatively one can split the partial γ_0 curve into the different branches according to

$$\gamma_0 \mapsto \gamma_0^{(02)} \circ \gamma_0^{(21)} \circ \gamma_0^{(11)} \circ \gamma_0^{(12)} \circ \gamma_0^{(20)} , \tag{2.96}$$

where

$$\begin{aligned}
\gamma_0^{(02)} : \quad & n_0 = n_0^{(3)} , \\
& \varphi_0 = -\frac{\pi}{2} + (\frac{\pi}{2} - \varphi_0^{(T_2)})\tau , \\
\gamma_0^{(21)} : \quad & n_0 = n_0^{(2)} , \\
& \varphi_0 = -\varphi_0^{(T_2)} + (\varphi_0^{(T_2)} - \varphi_0^{(T_1)})\tau , \\
\gamma_0^{(11)} : \quad & n_0 = n_0^{(1)} , \\
& \varphi_0 = -\varphi_0^{(T_1)} + 2\varphi_0^{(T_1)}\tau , \\
\gamma_0^{(12)} : \quad & n_0 = n_0^{(2)} , \\
& \varphi_0 = -\varphi_0^{(T_1)} + (\varphi_0^{(T_2)} - \varphi_0^{(T_1)})\tau , \\
\gamma_0^{(20)} : \quad & n_0 = n_0^{(3)} , \\
& \varphi_0 = \varphi_0^{(T_2)} + (\frac{\pi}{2} - \varphi_0^{(T_2)})\tau ,
\end{aligned} \tag{2.97}$$

while $\varphi_{N,L}$, $\tilde{N}$ and L are kept constant. In the regions where there is only a single solution $n_0(E, \tilde{N}, L, \varphi_0) \in [0, \tilde{N} - |L|]$ the superscript of n_0 may simply be ignored. With this change to γ_0 and $\gamma_{N,L}$ unchanged (2.87), one choice of deformed version of the elementary loops $C'_{0,1,-1}$ is again given by the composition (2.88), which leaves (2.90) unchanged. Only the value of S_{γ_0} has to be altered to

$$\begin{aligned}
S_{\gamma_0} \mapsto 2 \Bigg[& \int_0^{\varphi_0^{(T_1)}} \mathrm{d}\varphi_0 \, n_0^{(1)}(E, \tilde{N}, L, \varphi_0) - \int_{\varphi_0^{(T_2)}}^{\varphi_0^{(T_1)}} \mathrm{d}\varphi_0 \, n_0^{(2)}(E, \tilde{N}, L, \varphi_0) \\
& + \int_{\varphi_0^{(T_2)}}^{\frac{\pi}{2}} \mathrm{d}\varphi_0 \, n_0^{(3)}(E, \tilde{N}, L, \varphi_0) \Bigg] ,
\end{aligned} \tag{2.98}$$

or alternatively

$$S_{\gamma_0} \mapsto \pi n_0\Big(E, \tilde{N}, L, \varphi_0 = \frac{\pi}{2}\Big) - 2 \int_{n_0(E,\tilde{N},L,\varphi_0=0)}^{n_0(E,\tilde{N},L,\varphi_0=\frac{\pi}{2})} \mathrm{d}n_0 \, \varphi_0(E, \tilde{N}, L, n_0) , \tag{2.99}$$

which might be more efficient for calculations (also for unfolded librations in the case $L \neq 0$), since this way the integrand does not involve the solution to a quartic equation but only the limits of integration do. $\varphi_0(E, \tilde{N}, L, n_0) \in [0, \pi/2]$ thereby is the unique positive solution to $H_{\mathrm{cl}}(\tilde{N}, L, n_0, \varphi_0) = E$.

Folded librations share the Maslov index $\nu = 2$ with the unfolded ones, since turning points of opposite direction give a contribution of opposite sign. Thus the quantization conditions (2.92)–(2.94) remain the same for folded librations with the sole difference that the correct action (2.98) or (2.99) has to be used.

2.6.2 Quantization of vibrations

In contrast to librations, the (φ_0, n_0)-sections of vibrating orbits are not smooth deformations of the flat non-interacting orbits. Hence, one cannot use the elementary loops $C_{0,1,-1}$ of the non-interacting case or smooth deformations thereof to get the fundamental loops of the corresponding three-torus as directly as for librations. A signature of this statement can be seen in the parametrizations $\boldsymbol{\varphi}(\tau)$ (2.85) corresponding to the non-interacting loops, where in all three curves, φ_0 traverses an interval that covers at least a range of π, whereas the available φ_0 of vibrating orbits are restricted to smaller intervals.

Similar to the quantization of librations I define (now closed) paths

$$\begin{aligned}
&\eta_N: \quad n_0 = n_0(0)\,, \quad \varphi_N = 2\pi\tau\,, \quad \varphi_{0,L} = \varphi_{0,L}(0)\,,\\
&\eta_L: \quad n_0 = n_0(0)\,, \quad \varphi_L = 2\pi\tau\,, \quad \varphi_{0,N} = \varphi_{0,N}(0)\,,\\
&\eta_0 = \eta_0^{(1)} \circ \eta_0^{(2)}
\end{aligned}$$

with

$$\begin{aligned}
&\eta_0^{(1)}: \quad n_0 = n_0^{(1)}\,, \quad \varphi_0 = \varphi_0^{(T_\mathrm{v})}(1-2\tau)\,, \quad \varphi_{N,L} = \varphi_{N,L}(0)\,,\\
&\eta_0^{(2)}: \quad n_0 = n_0^{(2)}\,, \quad \varphi_0 = \varphi_0^{(T_\mathrm{v})}(-1+2\tau)\,, \quad \varphi_{N,L} = \varphi_{N,L}(0)\,,
\end{aligned} \tag{2.100}$$

where $n_0^{(1,2)} = n_0^{(1,2)}(E, \tilde{N}, L, \varphi_0)$ correspond to the solutions of smaller and greater value, respectively, and $\varphi_0^{(T_\mathrm{v})} \in [0, \frac{\pi}{2}]$ denotes the location of the right turning point. Eq. (2.100) actually is specific about the choice of vibrations in the minimum-energy island. In the case of maximum-energy vibrations centered around $\varphi_0 = \pm\frac{\pi}{2}$ one correspondingly has to shift all φ_0 by $\frac{\pi}{2}$. The sense in choosing those paths is again that the corresponding line-integrals yield the natural actions

$$\begin{aligned}
S_{\eta_N} &= \int_0^{2\pi} \mathrm{d}\varphi_N\, \tilde{N} = 2\pi\tilde{N}\,,\\
S_{\eta_L} &= \int_0^{2\pi} \mathrm{d}\varphi_L\, L = 2\pi L\,,\\
S_{\eta_0} &= \int_{-\varphi_0^{(T_\mathrm{v})}}^{\varphi_0^{(T_\mathrm{v})}} \mathrm{d}\varphi_0 \left[n_0^{(2)}(E, \tilde{N}, L, \varphi_0) - n_0^{(1)}(E, \tilde{N}, L, \varphi_0)\right]\,,
\end{aligned} \tag{2.101}$$

of the system. One main difference to the analysis of librations is that the contours for $\eta_{N,L}$ traverse a range of 2π instead of π in the case of librations.

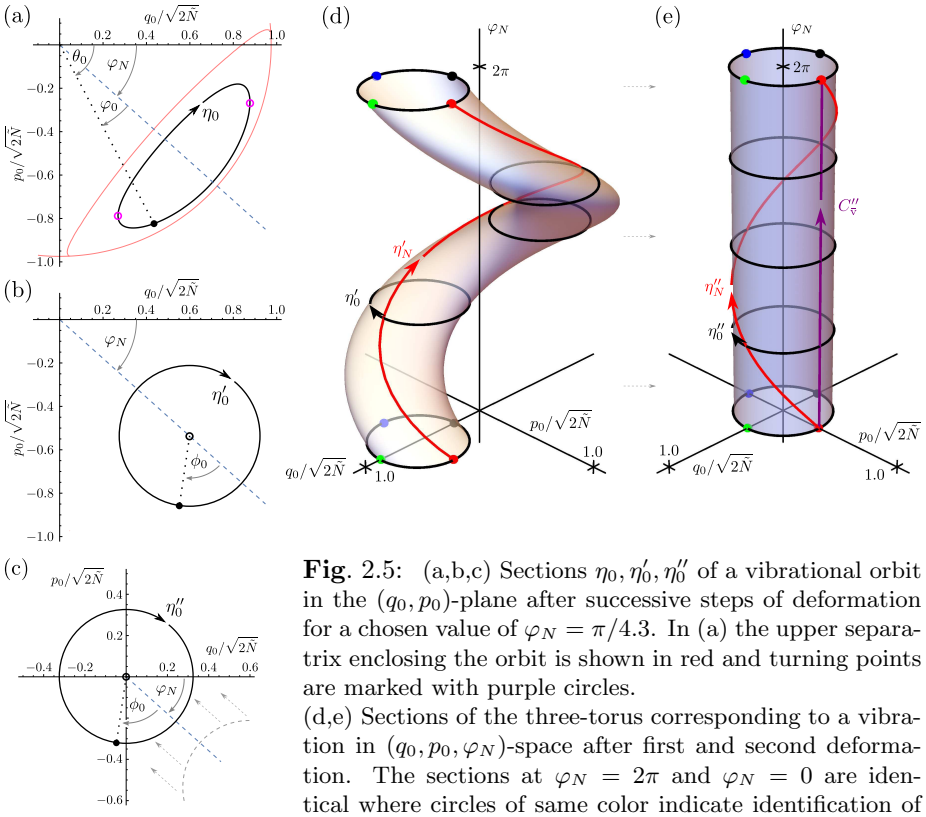

Fig. 2.5: (a,b,c) Sections $\eta_0, \eta_0', \eta_0''$ of a vibrational orbit in the (q_0, p_0)-plane after successive steps of deformation for a chosen value of $\varphi_N = \pi/4.3$. In (a) the upper separatrix enclosing the orbit is shown in red and turning points are marked with purple circles.
(d,e) Sections of the three-torus corresponding to a vibration in (q_0, p_0, φ_N)-space after first and second deformation. The sections at $\varphi_N = 2\pi$ and $\varphi_N = 0$ are identical where circles of same color indicate identification of points. The loops η_0', η_0'' for the values $\varphi_N = 0, \frac{\pi}{2}, \pi, \frac{3\pi}{2}, 2\pi$ are shown in black. The loops η_N', η_N'' (2.102) for a chosen value of $\phi_0 = -\frac{\pi}{2}$ are shown as red curves. The elementary loop $C_{\bar{\nu}}''$ (2.104) is shown in purple.

The reason is that on a vibrational torus to make a path closed, it can never contain an odd number of γ_N or γ_L, since there is no smooth connection of two points that differ by $\Delta\varphi_0 = \pi$ while fixing the other angles. This is the crucial point that makes an extra analysis of vibrations necessary.

The next step is to find the elementary loops. In order to examine topological aspects of the three-tori of vibrations I focus on their section in the (q_0, p_0)-plane. For any fixed value of $\tilde{N}, L$ and E and any value of φ_N those sections are homotopic to S^1 and do not encircle the origin $q_0 = p_0 = 0$. Figure 2.5a shows such a section for a vibration centered at $\varphi_0 = 0$ with the path η_0 indicated. Changing φ_N, the section gets rotated by φ_N according to $\theta_0 = \varphi_N + \varphi_0$ (2.49) whereas φ_L has no influence on the section. We deform the section at any value of $\varphi_{N,L}$ to a circle of fixed radius and denote the angle describing the circle out of the φ_N-rotation by ϕ_0. The corresponding deformed versions of the loops $\eta_{0,N,L}$ are homotopic to the loops

$$\begin{aligned}
\eta_0' &: \quad \phi_0 = 2\pi\tau\,, \quad \varphi_{N,L} = \varphi_{N,L}(0)\,, \\
\eta_N' &: \quad \varphi_N = 2\pi\tau\,, \quad \phi_0 = \phi_0(0)\,, \quad \varphi_L = \varphi_L(0)\,, \\
\eta_L' &: \quad \varphi_L = 2\pi\tau\,, \quad \phi_0 = \phi_0(0)\,, \quad \varphi_N = \varphi_N(0)\,.
\end{aligned} \tag{2.102}$$

Figures 2.5b,d show the corresponding deformed section and the twisted torus when the φ_N-dependence is added as third dimension. To bring the torus into a standard form it can further be deformed by shifting the circular (q_0, p_0)-sections without rotating them into the origin for any value of $\varphi_{N,L}$ (see Fig. 2.5c,e). The shifting naturally induces the definition of $\phi_0, \varphi_{N,L}$ as coordinates on the (now regularly shaped) deformed torus, which leaves the parametrization (2.102) of the loops after the second deformation (then called $\eta''_{0,N,L}$) as they are. With

$$\theta_0 = \varphi_N + \phi_0 \,, \tag{2.103}$$

θ_0, φ_N and φ_L are not only uniquely describing a point on the corresponding untwisted torus but they are also the natural orthogonal coordinates on it. Therefore the elementary loops are given by

$$\begin{aligned}
C''_{\mathrm{v}} = \eta''_0 : &\quad \theta_0 = 2\pi\tau + \theta_0(0)\,, \quad \varphi_{N,L} = \varphi_{N,L}(0)\,, \\
C''_{\bar{\mathrm{v}}} = \eta''_N \circ \eta''^{-}_0 : &\quad \theta_0 = \theta_0(0)\,, \quad \varphi_N = 2\pi\tau + \varphi_N(0)\,, \quad \varphi_L = \varphi_L(0)\,, \\
C''_L = \begin{cases} \eta''_L \\ \eta''^{-}_L \end{cases} : &\quad \theta_0 = \theta_0(0)\,, \quad \varphi_N = \varphi_N(0)\,, \quad \varphi_L = \begin{cases} 2\pi\tau+\varphi_L(0) & :L\geq 0 \\ -2\pi\tau+\varphi_L(0) & :L<0 \end{cases},
\end{aligned} \tag{2.104}$$

where the choice of direction in C''_L corresponds to the choice of positive action integral along the contour.

The identification of the elementary loops in (2.104) as compositions of the loops $\eta''_{0,N,L}$ can directly be adopted to describe the elementary loops in the original, undeformed torus by corresponding compositions of $\eta_{0,N,L}$:

$$\begin{aligned}
C_{\mathrm{v}} &= \eta_0 \,, \\
C_{\bar{\mathrm{v}}} &= \eta_N \circ \eta_0^{-} \,, \\
C_L &= \begin{cases} \eta_L & :L\geq 0 \\ \eta_L^{-} & :L<0 \end{cases} .
\end{aligned} \tag{2.105}$$

This recipe works independently of the details of the diffeomorphism that maps between the original three-torus, described by the loops $\eta_{0,N,L}$, and its regular-shaped counterpart. This is true because elementary loops are invariant concepts under *i)* homotopy on a given manifold and *ii)* diffeomorphism between two manifolds.

In order to prescribe the appropriate quantization rule, it remains to determine the Maslov-indexes of the loops $C_{\mathrm{v},\bar{\mathrm{v}},L}$ or equivalently $\eta_{0,N,L}$ and their subsequent composition. Again, it is easiest to analyze the Maslov-indexes in the original phase space coordinates q_k, p_k.

First, considering η_0, one counts two turning points (clockwise) in the (q_0, p_0)-plane (see Fig. 2.5a). On the contrary, the projections to the $(q_{\pm1}, p_{\pm1})$-planes are degenerate closed paths on straight lines, since $\theta_{\pm1} = \varphi_N \pm \varphi_L = \text{const.}$, $n_{\pm1} = \frac{1}{2}(\tilde{N} - n_0 \pm L)$. This means they do not contribute to the Maslov index. One gets $\nu_0 = 2$.

Second, the loop η_N corresponds to $n_{0,\pm1} = \text{const.}$ and $\theta_{0,\pm1} = 2\pi\tau + \text{const.}$, thus one gets two turning points (clockwise) for each coordinate, resulting in a Maslov index of $\nu_N = 6$.

Third, the η_L-projections also have constant radii $n_{0,\pm1} = \text{const.}$ and $\theta_0 = \text{const.}, \theta_{\pm1} = \pm 2\pi\tau + \text{const.}$, meaning a counting of two pairs of turning points

of opposite rotational direction, which cancel each other, leading to a vanishing Maslov index $\nu_L = 0$.

Since composition and inversion of loops translates to addition and sign inversion of Maslov indexes, the elementary loops $C_{\mathrm{v},\bar{\mathrm{v}},L}$ are assigned to the indexes $\nu_{\mathrm{v}} = \nu_0 = 2$, $\nu_{\bar{\mathrm{v}}} = \nu_N - \nu_0 = 4$, $\nu_L = 0$. The EBK quantization prescription (2.24) then is

$$\begin{aligned} \frac{1}{2\pi}\left(S_{\eta_N} - S_{\eta_0}\right) &= k_{\bar{\mathrm{v}}} + 1\,, \\ \frac{1}{2\pi} S_{\eta_0} &= k_{\mathrm{v}} + \frac{1}{2}\,, \\ \frac{1}{2\pi} S_{\eta_L} &= k_L\,, \end{aligned} \tag{2.106}$$

with $k_{\mathrm{v}}, k_{\bar{\mathrm{v}}} \in \mathbb{N}_0$ and $k_L \in \mathbb{Z}$, where $|k_L|$ is the actual non-negative quantum number corresponding to the loop C_L. After linear combination and using (2.101) one gets

$$\begin{aligned} \tilde{N} &= k_{\bar{\mathrm{v}}} + k_{\mathrm{v}} + \frac{3}{2}\,, \\ L &= k_L\,, \\ \frac{1}{2\pi} S_{\eta_0} &= k_{\mathrm{v}} + \frac{1}{2}\,, \end{aligned} \tag{2.107}$$

where again the two first equations give the (trivial) spectra of N and L and the quantization of S_{η_0} implicitly defines the semiclassical quantization of energy levels. The physical meaning of $k_{\mathrm{v},\bar{\mathrm{v}},L}$ and the appropriate bounds become clear after renaming according to the prescription

$$\begin{aligned} m_0 &:= k_{\bar{\mathrm{v}}} - |k_L| - k_{\mathrm{v}}\,, \\ m_1 &:= \begin{cases} |k_L| + k_{\mathrm{v}} & : L \geq 0 \\ k_{\mathrm{v}} & : L < 0 \end{cases}\,, \\ m_{-1} &:= \begin{cases} k_{\mathrm{v}} & : L \geq 0 \\ |k_L| + k_{\mathrm{v}} & : L < 0 \end{cases}\,, \end{aligned} \tag{2.108}$$

which yields again the natural representation

$$N = m_0 + m_1 + m_{-1}\,, \tag{2.109}$$

$$L = m_1 - m_{-1}\,, \tag{2.110}$$

$$\frac{1}{2\pi} S_{\eta_0} = \min\{m_{\pm 1}\} + \frac{1}{2}\,, \tag{2.111}$$

which already suggests the interpretation $m_{0,1,-1}$ as pseudo-occupation numbers as in the case of libration-quantization. though the connection to average occupation numbers is weakened compared to the librational case. Nevertheless, the naming is useful as it corresponds to a natural choice of common quantum numbers for libration and vibration. This point will be considered in more detail in the next subsection.

For now, it remains to show that the pseudo-occupation numbers are properly bounded. While the bounds for $m_{\pm 1} \geq 0$ are trivial, the bound for m_0 expresses the finiteness of the relevant phase space. The total area of relevant

phase-space (in the (φ_0, n_0)-plane) is the upper bound for the area enclosed by the vibrational orbit

$$S_{\eta_0} \leq \pi(\tilde{N} - |L|)\,, \tag{2.112}$$

and hence

$$2\min\{m_{\pm1}\} + 1 \leq m_0 + m_1 + m_{-1} - \max\{m_{\pm1}\} + \min\{m_{\pm1}\} + \frac{3}{2}\,, \tag{2.113}$$

or equivalently

$$m_0 \geq -\frac{1}{2} \Rightarrow m_0 \in \mathbb{N}_0\,. \tag{2.114}$$

Thus there simply is no vibrational orbit large enough to get quantized with $m_0 < 0$.

2.6.3 Common quantum numbers

Fixing N and L as given parameters one can again reduce to a single quantum number and use

$$\begin{aligned} m_0 &= N - |L| - 2\min\{m_{\pm1}\}\,, \\ \max\{m_{\pm1}\} &= |L| + \min\{m_{\pm1}\}\,, \end{aligned} \tag{2.115}$$

which is purely a consequence of (2.92) and (2.93) or (2.109) and (2.110), to relate the others. This gives the alternative form

$$\frac{1}{2\pi}\bar{S}_{\gamma_0} = \min\{m_{\pm1}\} + \frac{1}{2} \tag{2.116}$$

as a quantization rule for librations, where the barred version $\bar{S}$ of an action integral S is defined as its complement

$$\bar{S} := \pi(\tilde{N} - |L|) - S\,. \tag{2.117}$$

Moderate coupling strengths

I focus on the regime $\bar{\alpha} < \bar{\alpha_2}$, which is physically most interesting, since for very large couplings $\bar{\alpha} \gg 1$ the truncation to the three lowest single-particle modes becomes a poor approximation to the actual continuous system. This insufficiency has been shown by comparing exact solutions of the Lieb-Liniger model with numerical spectra of the three-site-model [189] and is indicated by the rather large condensate depletions $1 - z$ involved.

As will become clear in the following a natural choice of quantum number in this region is

$$m := \min\{m_{\pm1}\}\,. \tag{2.118}$$

Since this region implies $\bar{\alpha} < \bar{\alpha}_{\mathrm{S}}$, so that no swapping has occurred, the action integral for libration is a monotonously decreasing function of the energy E. Therefore the energies quantized using (2.117) are a monotonously growing sequence $\frac{\partial E}{\partial m} > 0$, which has sense when compared to the non-interacting case, where m counts the depopulation of the $k = 0$ mode for fixed N, L, with $m = 0$ corresponding to the state of maximum m_0.

If $\bar{\alpha} > \bar{\alpha}_1$, the quantum number m for librations is bound from below, since $\bar{S}_{\gamma_0} \leq S^{(1)}_{\rm sep}$, where

$$S^{(1)}_{\rm sep} = \lim_{E \to E^{(1)-}} S^{(1)}_{\eta_0}(E) = \lim_{E \to E^{(1)+}} \bar{S}_{\gamma_0}(E) \tag{2.119}$$

is the action integral of the island enclosed by the upper separatrix. At the same time, the quantum number $\min\{m_{\pm 1}\}$ in (2.111) for vibrations in the upper island is bound from above by the same value and $\frac{\partial E}{\partial \min\{m_{\pm 1}\}} > 0$ for these vibrations, since $\frac{\partial S^{(1)}_{\eta_0}}{\partial E} > 0$. This situation implies that one can use $m = \min\{m_{\pm 1}\}$ as a common quantum number and write the quantization condition for all states as

$$\begin{aligned} \frac{1}{2\pi} S^{(1)}_{\eta_0} &= m + \frac{1}{2}\,, \quad && m \in \{0, 1, \ldots, M^{(1)}_{\rm vib}\}\,, \\ \frac{1}{2\pi} \bar{S}_{\gamma_0} &= m + \frac{1}{2}\,, \quad && m \in \{M^{(1)}_{\rm vib} + 1, \ldots, M\}\,, \end{aligned} \tag{2.120}$$

where the superscript (1) indicates vibration in the *upper* island. The maximum quantum number for vibrations is given as

$$M^{(1)}_{\rm vib} = \left\lfloor \frac{1}{2\pi} S^{(1)}_{\rm sep} - \frac{1}{2} \right\rfloor\,, \tag{2.121}$$

and the maximum overall quantum number is

$$M = \left\lfloor \frac{N - |L|}{2} \right\rfloor\,, \tag{2.122}$$

corresponding to the restriction $S_{\gamma_0} \geq 0$, so that the total number $M + 1$ of semiclassically quantized states coincides with the dimension of the Hilbert space in the sector $\hat{N} = N, \hat{L} = L$. Eq. (2.120) has two appropriate implications. First, the quantized energies E_m monotonously grow with m. Second, the sequence $\{E_m\}$ is a continuous function of the coupling $\bar{\alpha}$. With increasing coupling, $S^{(1)}_{\rm sep}$ gets larger. Every time $M^{(1)}_{\rm vib}$ increases by one, the lowest librational state becomes the highest vibrational state with its energy changing continuously, taking the value $E = E^{(1)}$ right at the transition.

This "jumping" of a quantized orbit from outside the separatrix to its interior is the essential signature of the finite-size QPT. It is not only the ground state that experiences this transition but instead there is a whole sequence of critical couplings $\bar{\alpha}^{\rm cr}_m$ at which successively more and more excited states jump from libration to vibration. Therefore one could categorize the physical situation as a finite-size ESQPT related to a separatrix crossing – a similar situation to what has been already discussed in the literature in other cases (see, *e.g.*, [213]). Figure 2.6 shows the transition of orbits for $m = 0, 1$.

Larger couplings

In the region $\bar{\alpha} > \bar{\alpha}_2$ the artificial and unphysical additional features lead to additional transitions of librations to vibrations. This affects only the upper end of the semiclassically quantized spectrum. These highly excited levels suffer from discontinuities *w.r.t.* sweeping the coupling strength due to these artifacts.

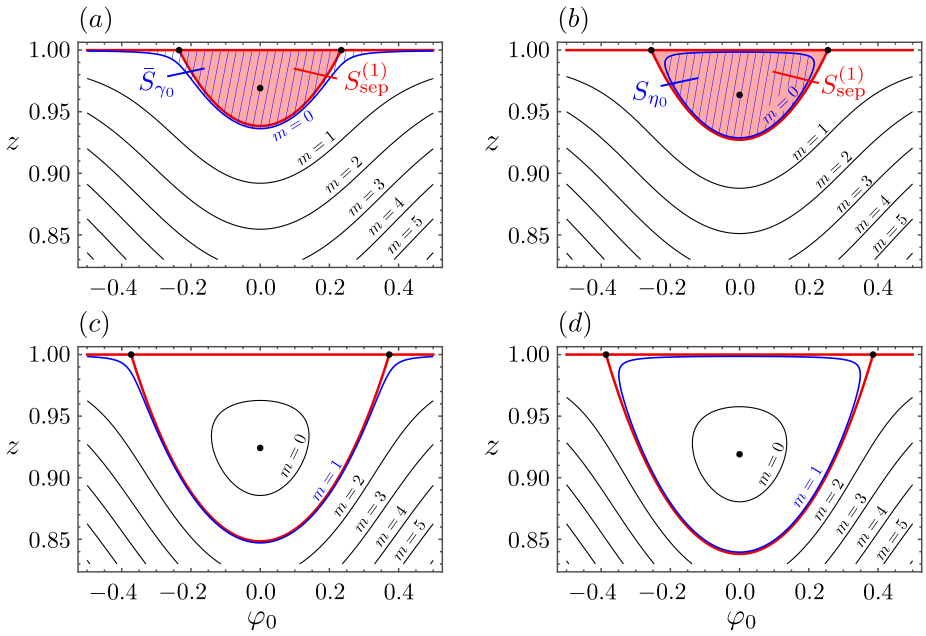

Fig. 2.6: (a,b) Transition of the orbit quantized as the ground state $m = 0$ (blue) for $N = 100$, $L = 0$ as the coupling changes from $\bar{\alpha} = 1.057 < \bar{\alpha}_0^{\rm cr}$ to $\bar{\alpha} = 1.068 > \bar{\alpha}_0^{\rm cr}$. The areas corresponding to the action integrals $S^{(1)}_{\rm sep}$ of the island and $\bar{S}_{\gamma_0}$ and S_{η_0} of the quantized orbits for $m = 0$ are shown with light red solid filling and blue hatched filling respectively. At the transition $\bar{\alpha} = \bar{\alpha}_0^{\rm cr}$ all three areas become equal.
(c,d) Transition of the orbit corresponding to the first excited state for the same setup (blue). The couplings are $\bar{\alpha} = 1.153 < \bar{\alpha}_1^{\rm cr}$ and $\bar{\alpha} = 1.165 > \bar{\alpha}_1^{\rm cr}$.

Nevertheless, one can give the quantization rules involving a common quantum number yielding a monotonously increasing sequence of energies in this regime, which – for completeness – is given in appendix D.3. There, a careful analysis is given that shows that for an arbitrary setup $N, L, \bar{\alpha}$ at least the lowest $\sim 47.8\%$ of all semiclassically quantized energies are well behaved and do not suffer from any unphysical discontinuities.

2.7 Semiclassical spectra for $L = 0$

Since, as discussed in section 2.5.3, the case $L = 0$ is of special interest here, the remaining part of this study will focus on zero total angular momentum. Furthermore, we restrict ourselves here to moderate coupling strengths $\bar{\alpha} < \bar{\alpha}_2 = 4$ since almost no additional physics is contained in the original untruncated system (2.26), (2.35) for larger couplings whereas the appearance of artifacts like the maximum energy islands and separatrix swapping (see section 2.5.3) indicate a breakdown of the approximation due to truncation of single particle momentum modes (2.37). While there is no problem in carrying the semiclassical calculations to $\bar{\alpha} > 4$, this restriction will ease notation and allow us to drop unnecessary ballast.

2.7.1 Ground state energy

Because the system is known to undergo a QPT, the first property to look at – using the full semiclassical description developed in section 2.6 – is the dependence of the ground state energy on the coupling $\bar{\alpha}$ and the total number of particles N. For now, the full semiclassical action integrals (2.101) and (2.89) will be used for determining the semiclassical approximations $\tilde{\omega}_n$ to the energy levels obtained from the quantization conditions (2.120).

Elementary manipulations give the explicit quantization rule for librations and vibrations in terms of the substituted variables

$$\begin{aligned} \zeta &= 1 - z\,, \\ x &= \cos^2\varphi_0 \end{aligned} \tag{2.123}$$

as

$$\begin{aligned} \frac{1}{\tilde{N}}\bar{S}_{\gamma_0} &= \int_0^1 \mathrm{d}x \frac{\zeta_+(\tilde{\omega}_m, x)}{\sqrt{x(1-x)}} = \frac{2\pi}{\tilde{N}}\left(m + \frac{1}{2}\right) \quad (\tilde{\omega}_m > 0)\,, \\ \frac{1}{\tilde{N}}S_{\eta_0} &= \int_{x^{(T_\mathrm{v})}}^1 \mathrm{d}x \frac{\Delta\zeta(\tilde{\omega}_m, x)}{\sqrt{x(1-x)}} = \frac{2\pi}{\tilde{N}}\left(m + \frac{1}{2}\right) \quad (\tilde{\omega}_\mathrm{min} < \tilde{\omega}_m < 0)\,, \end{aligned} \tag{2.124}$$

where

$$\begin{aligned} \zeta_+(\tilde{\omega}, x) &:= \frac{1}{2\left(x - \frac{1}{8}\right)}\left(x - \frac{1}{\bar{\alpha}} + \sqrt{D(\tilde{\omega}, x)}\right)\,, \\ \Delta\zeta(\tilde{\omega}, x) &:= \frac{1}{\left|x - \frac{1}{8}\right|}\sqrt{D(\tilde{\omega}, x)}\,, \\ D(\tilde{\omega}, x) &:= \left(x - \frac{1}{\bar{\alpha}}\right)^2 + \frac{4\tilde{\omega}}{\bar{\alpha}}\left(x - \frac{1}{8}\right)\,. \end{aligned} \tag{2.125}$$

The turning point for vibrations is given by

$$x^{(T_\mathrm{v})} = \frac{1}{\bar{\alpha}}\left(1 - 2\tilde{\omega} + 2\sqrt{\tilde{\omega}\left(\tilde{\omega} - 1 + \frac{\bar{\alpha}}{8}\right)}\right)\,. \tag{2.126}$$

Note that $x = \frac{1}{8}$ is a removable discontinuity of $\zeta_+(\tilde{\omega}, x)$ and does not affect the integral $\bar{S}_{\gamma_0}$ as it has zero measure.

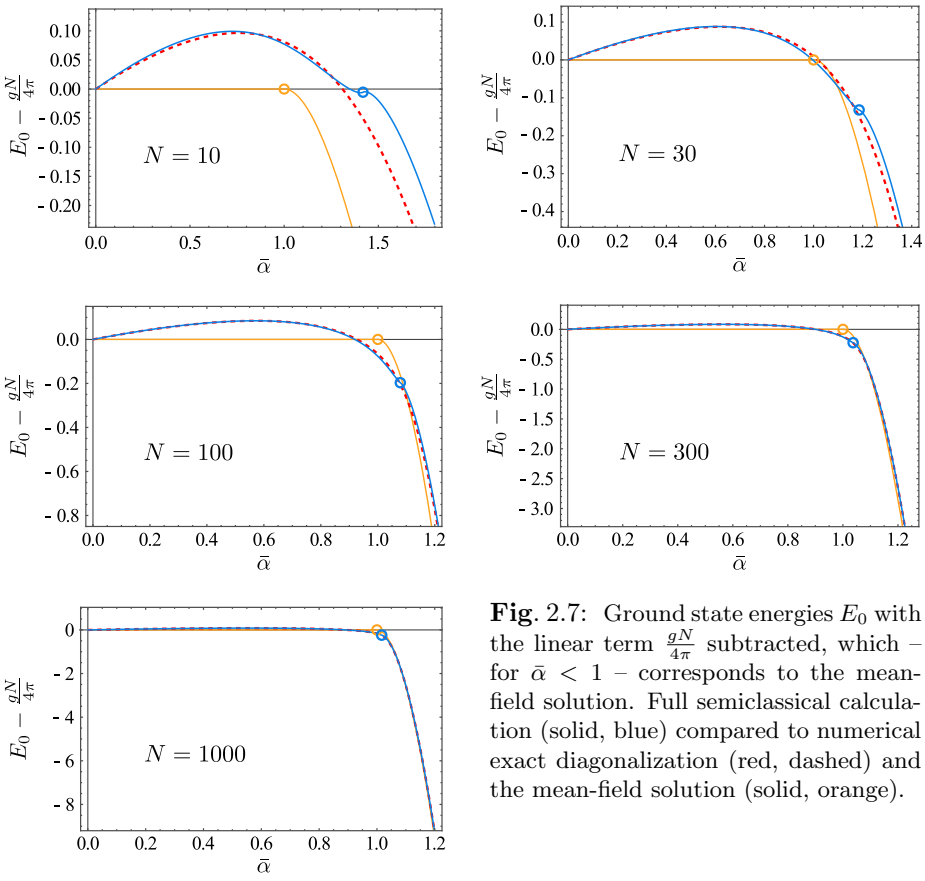

Fig. 2.7: Ground state energies E_0 with the linear term $\frac{gN}{4\pi}$ subtracted, which – for $\bar{\alpha} < 1$ – corresponds to the mean-field solution. Full semiclassical calculation (solid, blue) compared to numerical exact diagonalization (red, dashed) and the mean-field solution (solid, orange).

For now (2.124) gets evaluated by numerical integration while further analytical approximations will be given later. The semiclassical calculations are compared to numerical results obtained by exact diagonalization of the truncated model with corresponding number of particles N. Comparison of the ground state energy can be seen as a stringent test for the semiclassical approximation in this system since, in general, semiclassics is known for its increasing validity when one moves to higher excitations.

Figure 2.7 shows the dependence of the calculated ground state energies as a function of the coupling strength for various numbers of particles. To allow for better comparison with the numerical data, the linear term

$$E_<^{\mathrm{mf}}(\bar{\alpha}) = \frac{gN}{4\pi} = -\frac{\bar{\alpha}N}{4}\frac{1}{1+\frac{3}{2N}} \tag{2.127}$$

has been subtracted. For $\bar{\alpha} < 1$ this term corresponds to the lowest mean-field energy when solving the Gross-Pitaevski equation of the continuous system. Therefore, the mean-field curves shown coincide with the axis of abscissas in this region. At $\bar{\alpha} = 1$ the mean-field energy changes qualitatively (discontinuity in second derivative). This is the point of the QPT for $N \to \infty$ and is marked with a circle. For $\bar{\alpha} > 1$ the mean-field curves are taken from the global energy

minimum of the classical phase space

$$E^{\mathrm{mf}}_{>}(\bar{\alpha}) = E^{\mathrm{mf}}_{<}(\bar{\alpha}) + \frac{2}{7\pi} gN \left(1 - \frac{1}{\bar{\alpha}}\right)^2 = E^{\mathrm{mf}}_{<}(\bar{\alpha}) + \frac{N^2}{N + \frac{3}{2}} \tilde{\omega}_{\min}(\bar{\alpha}) \,, \quad (2.128)$$

because they correspond to the actual approximation of truncated modes rather than the mean-field energies of the continuous system. One should mention that there is an ambiguity in defining the mean-field energy by the classical global energy minimum. This ambiguity comes from interchanging N with $\tilde{N}$ and has no physical meaning, since it only makes a relative difference of order $\mathcal{O}(N^{-1})$ while mean-field-solutions in general only make sense for large N, where the ambiguity tends to zero.

In the subcritical regime the semiclassical result agrees rather good with numerics already for small N. When the quantized orbits cross from libration to vibration (see Fig. 2.6) the energies have an inflexion point (marked by circles) that results in a bump in the graph. This bump is an artifact from the semiclassical approximation. The reason for this deviation lies in the fact that very close to a separatrix, a quantized orbit always lives either on one side of the separatrix or the other, whereas the corresponding exact quantum state can be considered as smeared out because of finite $\hbar_{\mathrm{eff}}$ and thus depending on the combined properties of phase space on both sides. This effect could be taken into account by allowing for a real-valued (instead of integer-valued) effective Maslov index that changes smoothly very close to the transition. Such modifications have been investigated (see, *e.g.*, [214], [215] and references therein) within the framework of uniform approximations and related methods and lead, *e.g.*, to the well known Langer modification of radial Schrödinger equations. For increasing N this artifact vanishes, as this can be seen as a decrease in the effective quantum of action (see section 2.4). Therefore I postpone further improvement in this direction to future work. As expected, for large N the semiclassical prediction converges very fast to the numerical values. Further increasing N shows how the smooth cross-over of the finite system approaches the transition of the mean-field solution. The inflexion point of the semiclassical energy thereby approaches the point of the QPT for $N \to \infty$. This observation together with the qualitative change of classical dynamics, *i.e.*, a *discontinuous* deformation of a quantized torus, allows for *defining* the crossing of the separatrix as the point of the (finite-size) QPT. It is educational to emphasize here that the semiclassical picture allows to uniquely define this point as a *transition* rather than a cross-over although N is finite, because of this classical discontinuous feature. In contrast, all properties obtained quantum mechanically are smooth functions of $\bar{\alpha}$ for finite N, which makes the definition of a (finite-size) transition point ambiguous.

2.7.2 Low-lying spectra

Figure 2.8 shows the low-lying excitation spectra obtained by the full semiclassical calculation (2.120), (2.89), (2.117), and (2.101) in comparison with the spectra obtained from exact numerical diagonalization for $N = 200$ and $N = 1000$. For all curves, the ground state energy that is numerically calculated serves as reference, which underlines the agreement of absolute energies on top of energy differences.

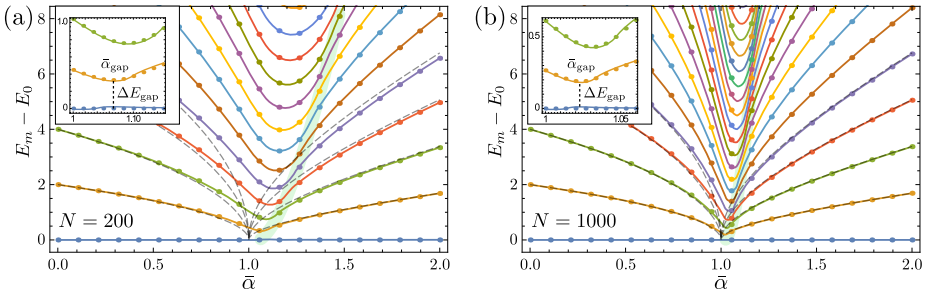

Fig. 2.8: Low-lying excitation spectra as function of the coupling strength $\bar{\alpha}$ for (a) $N = 200$ and (b) $N = 1000$. Compared are the full semiclassical result (solid) and the spectra obtained from numerical exact diagonalization (dots). Also shown are the four lowest Bogoliubov-like excitations (dashed) that break down around $\bar{\alpha} \approx 1$. The inset show blow-ups of the region around the minimal lowest energy gap. The light green shaded flank is centered around the separatrix (excitation-)energy as a guide to the eye, where the levels bunch together.

More important than the good agreement are the obvious finite-size features, which are *i)* the finite excitation energy gaps and *ii)* the enhanced DOS along the line of separatrix energy, where the spectra remind of successive avoided crossings. In addition, Bogoliubov-like excitation spectra (see next section, Eq. (2.134) and (2.136)) are shown to break down close to the critical point.

Now that the validity of the full semiclassical calculation is evident, the purpose of the next section is to take the calculus to the asymptotic regime of large numbers of bosons N in order to obtain explicit and simple to handle expressions and scaling laws which are capable to describe the observed finite-size features on a qualitative as well as quantitative level.

2.8 Large-N asymtotics

2.8.1 Critical couplings

The action integral

$$S_{\text{sep}}^{(1)} = \tilde{N} \int_{-\arccos\frac{1}{\sqrt{\bar{\alpha}}}}^{\arccos\frac{1}{\sqrt{\bar{\alpha}}}} \mathrm{d}\varphi_0 \, \left(1 - z^{(1)}(\varphi_0)\right) \tag{2.129}$$

of the separatrix (2.77) can be analytically evaluated and yields the condition

$$\arccos\frac{1}{\sqrt{\bar{\alpha}_m^{\text{cr}}}} - \frac{1}{\sqrt{7}}\left(\frac{8}{\bar{\alpha}_m^{\text{cr}}} - 1\right) \operatorname{artanh}\left(\sqrt{\frac{\bar{\alpha}_m^{\text{cr}} - 1}{7}}\right) = \frac{\pi}{\tilde{N}}\left(m + \frac{1}{2}\right), \quad m \in \mathbb{N}_0 \tag{2.130}$$

for the critical values $\bar{\alpha}_m^{\text{cr}}$ where the m-th quantized orbit crosses the separatrix.

For large N and fixed quantum number m the critical value of the coupling strength tends to the mean-field critical coupling $\bar{\alpha}_{\text{mf}}^{\text{cr}} = 1$ so that there the separatrix involves only small φ_0 and can therefore be approximated by a parabola. The corresponding action integral becomes

$$S_{\text{sep}}^{(1)} \overset{\bar{\alpha}-1 \ll 1}{\approx} \frac{32}{21}\tilde{N}(\bar{\alpha}-1)^{\frac{3}{2}} + \tilde{N}\mathcal{O}\Big((\bar{\alpha}-1)^{\frac{5}{2}}\Big) \,. \tag{2.131}$$

Using this result with the quantization condition (2.120) yields the asymptotic expression

$$\bar{\alpha}_m^{\text{cr}} = 1 + \left(\frac{21\pi}{16}\right)^{\frac{2}{3}} \left(m + \frac{1}{2}\right)^{\frac{2}{3}} \tilde{N}^{-\frac{2}{3}} + \mathcal{O}\Big(\tilde{N}^{-\frac{4}{3}}\Big) \tag{2.132}$$

for the critical coupling strengths.

2.8.2 Low-lying excitations for $\bar{\alpha} < 1$

In the subcritical regime for a fixed coupling $\bar{\alpha} < 1$ and fixed quantum number m the quantized orbits approach the upper boundary $z = 1$ of the phase space when $N \to \infty$. Therefore one can approximate the actual form of the librations by linearizing the energy landscape $\tilde{\omega}(z, \varphi_0)$ in z at $z = 1$.

$$\begin{aligned} \left.\frac{\partial\tilde{\omega}}{\partial z}\right|_{z=1} &= \bar{\alpha}\cos^2\varphi_0 - 1 \,, \\ \frac{1}{\tilde{N}}\bar{S}_{\gamma_0} &\approx 2\int_0^{\frac{\pi}{2}} \mathrm{d}\varphi_0 \, \frac{\tilde{\omega}}{1 - \bar{\alpha}\cos^2\varphi_0} = \frac{\pi\tilde{\omega}}{\sqrt{1-\bar{\alpha}}} \,. \end{aligned} \tag{2.133}$$

This gives the asymptotic energy levels

$$\tilde{\omega}_m \approx \frac{1}{\tilde{N}}\sqrt{1-\bar{\alpha}}(2m+1) \,, \quad m \in \mathbb{N}_0 \,, (\bar{\alpha} < 1, N \gg 1) \,, \tag{2.134}$$

which reproduces exactly the excitation energies of the continuous system within Bogoliubov approximation [22] corresponding to the angular momenta ± 1, which are the only non-vanishing modes allowed in the truncated model. For any finite number of particles the linear approximation (2.133) as well as Bogoliubov

approximation break down when $\bar{\alpha}$ approaches 1. The former becomes a bad approximation because the linear term in z vanishes at $\varphi_0 = 0$ for $\bar{\alpha} \to 1$, resulting in a local quadratic dependence, which pushes the orbit further away from $z = 1$ or equivalently from $n_0 = \tilde{N}$. This in turn can be interpreted as an enhanced depopulation of the single-particle zero-momentum mode. The reason for the Bogoliubov approximation to break down is also the depletion of the condensate [22], which is considered negligible within its ansatz. This shows the similarity and even indicates an equivalence of Bogoliubov approximation and lowest order expansion of classical energy landscapes around mean-field solutions (*i.e.*, global energy minima) in general. The approximate energy (2.134) becomes complex in the supercritical regime $\bar{\alpha} > 1$ due to the imaginary quantity $\mathrm{i}\lambda = \sqrt{1-\bar{\alpha}}$. One can therefore interpret this breakdown as the occurrence of an instability. Indeed, this interpretation becomes more explicit in a mean-field treatment of the continuous problem (2.26), which has to be understood as a purely classical version. It can be shown (see, *e.g.*, [22]) that the uniform solution of the corresponding NLSE, which is the solution with lowest energy in the subcritical regime, becomes dynamically unstable when $\bar{\alpha} > 1$. There, the non-uniform bright soliton solution takes over the role of the classical state of lowest energy. The correspondence of this transition in the classical phase space of truncated momenta considered here is the disappearance of the upper-boundary solution $z = 1$ as a classical state in favor of the classical fix point solution at the appearing global energy minimum $\tilde{\omega}_{\min}$ (2.78). The imaginary part λ can then be interpreted as a dynamical stability exponent characterizing the degree of instability. Later considerations will make this connection an exact identity (2.170). Moreover, the instability λ will be interpreted as a (local) Lyapunov exponent rendering the actually regular system apparently chaotic in some respects of physical interest (see section 2.8.5 and section 2.9).

2.8.3 Low lying excitations for $\bar{\alpha} > 1$

For fixed coupling $\bar{\alpha} > 1$, fixed quantum number m and $N \to \infty$ the corresponding quantized orbits are beyond their transition across the separatrix and approach the global energy minimum inside the separated island. The corresponding approximation is to expand the energy landscape $\tilde{\omega}(z, \varphi_0)$ up to second order in z and φ_0 around its minimum which gives

$$\tilde{\omega} \approx \tilde{\omega}_{\min} + \frac{4}{49\bar{\alpha}}(\bar{\alpha}-1)(4+3\bar{\alpha})\varphi_0^2 + \frac{1}{8}(8-\bar{\alpha})\delta z^2\,, \tag{2.135}$$

which, after solving for δz and integrating results in the asymptotic energy levels

$$\tilde{\omega}_m \approx \tilde{\omega}_{\min} + \frac{1}{\tilde{N}}\sqrt{\frac{2}{7}}\sqrt{(4+3\bar{\alpha})}\sqrt{\bar{\alpha}-1}\left(m+\frac{1}{2}\right)\,. \tag{2.136}$$

Again, this approximation breaks down for finite N when one approaches $\bar{\alpha} = 1$ from above.

Thus, for any finite number of particles, both Bogoliubov-like approximations (2.134) and (2.136) are rough estimations that work only at some distance from the QPT or corresponding transition of the m-th excited state. In order to make more sophisticated estimates for the energy gap behavior during the QPT and in the ESQPT, better ways of approximating semiclassical energy levels around criticality will be given in the following subsections.

2.8.4 The finite-size ground state energy gap

As shown in the preceding subsections, linearization (respectively quadratic expansion) of $\tilde{\omega}(z, \varphi_0)$ break down at the transition at $\bar{\alpha} \approx 1$. In this section, in order to make analytic estimates for the energy gap between the ground state and the first excited state, I will make use of a specific asymptotic scaling property. It can be stated as follows and will be given more rigor afterwards.

For different N, equivalent physical situations – *i.e.*, transition of the ground state ($\bar{\alpha} = \bar{\alpha}_0^{\mathrm{cr}}$), first excited state ($\bar{\alpha} = \bar{\alpha}_1^{\mathrm{cr}}$) or the system sitting at the minimum excitation energy – correspond to relevant phase-space structures that are asymptotically ($N \to \infty$) related by a similarity relation. In other words, the separatrix, ground state vibration and first excited libration at the transition look *the same* for different (but large) N. They are just scaled versions of each other.

Analytically this scaling is revealed by applying a small-angle approximation in φ_0, which is justified for large N close to the QPT, where the separatrix and vibrational orbits live at small $|\varphi_0|$, and also the relevant contributions to the action integral of librations originate from this region. In general this has to be distinguished from the expansions (2.133) and (2.135) of $\tilde{\omega}(z, \varphi_0)$, as the program here is to take the exact solutions $z(\varphi_0)$ of orbits and do small-angle replacements wherever it makes sense. This leads to results that are way more accurate than the Bogoliubov-like excitations (2.134) and (2.136), and – in contrast to the latter – they are able to describe the energy gap directly at the (finite-size) QPT.

Librations in small angle approximation

The exact orbit for a libration ($\tilde{\omega} > 0$) is given by (see (2.125))

$$z_+(\tilde{\omega}, \varphi_0) = 1 - \zeta_+(\tilde{\omega}, \cos^2 \varphi_0)\,. \tag{2.137}$$

To perform a reasonable small angle approximation one needs to realize that $\cos^2 \varphi_0$ should be approximated by $1 - \varphi_0^2$ when it is compared to $\frac{1}{\bar{\alpha}}$, because this takes into account the correct behavior around the saddle points P_1, whereas it may be approximated by 1 when it is compared to numerical constants. Taking into account the φ_0^2 or higher order terms in the latter would only result in higher order corrections in $(\bar{\alpha} - 1)$.

Thus the small-angle approximation to librations reads

$$z_+^{\mathrm{sa}}(\tilde{\omega}, \varphi_0) = 1 - \frac{4}{7}\left[\left(1 - \frac{1}{\bar{\alpha}}\right) - \varphi_0^2 + \sqrt{\left(1 - \frac{1}{\bar{\alpha}} - \varphi_0^2\right)^2 + \frac{7\tilde{\omega}}{2\bar{\alpha}}}\right], \tag{2.138}$$

which becomes the parabolic small-angle approximation to the separatrix $z^{(1)}$ for $\tilde{\omega} \to 0$. This approximation allows for a major simplification of the problem

by applying a scaling of variables [with $\tilde{\omega}_{\min}$ given by (2.78)]:

$$\begin{aligned} \tilde{z} &:= \frac{7}{4A} z \,, \\ \phi &:= \frac{1}{\sqrt{A}} \varphi_0 \,, \\ \eta &:= \frac{\tilde{\omega}}{|\tilde{\omega}_{\min}|} \,, \\ A &:= 1 - \frac{1}{\tilde{\alpha}} \,. \end{aligned} \tag{2.139}$$

The (scaled) distance of the libration to the separatrix within this approximation is given by

$$\delta \tilde{z}^{\mathrm{sa}}_{\mathrm{lib}}(\eta, \phi) = \sqrt{(1-\phi^2)^2 + \eta} - |1 - \phi^2| \,. \tag{2.140}$$

The simple form of (2.140) expresses the asymptotic scaling behavior mentioned before.

I define also a scaled version of all action integrals by

$$I := \frac{7}{8} \frac{1}{\tilde{N}} A^{-\frac{3}{2}} S \,. \tag{2.141}$$

With this, the action between a low lying libration and the separatrix close to criticality is asymptotically given by

$$\delta I_{\mathrm{lib}}(\eta) = \int_0^\infty \mathrm{d}\phi \, \left(\sqrt{(1-\phi^2)^2 + \eta} - |1 - \phi^2| \right) \,. \tag{2.142}$$

Note that extending the upper integration limit to infinity does neither contradict with the finiteness of φ_0 nor with the small angle approximation, since the integrand (2.140) has a converging $\mathcal{O}(\phi^{-2})$-tail.

Vibrations in small angle approximation

Doing the same small-angle replacements for vibrational orbits as above results in

$$\delta \tilde{z}^{\mathrm{sa}}_{\mathrm{vib}}(\eta, \phi) = 2\sqrt{(1-\phi^2)^2 + \eta} \,, \tag{2.143}$$

describing the distance between the upper and lower half-cycle of the vibration. Note that $\eta < 0$ for vibrations since they live inside the minimum energy island, where energy is smaller compared to the separatrix energy. The corresponding scaled action integral reads

$$I_{\mathrm{vib}}(\eta) = 2 \int_0^{\sqrt{1-\sqrt{-\eta}}} \mathrm{d}\phi \, \sqrt{(1-\phi^2)^2 + \eta} \,. \tag{2.144}$$

The scaled version of the separatrix action is easily calculated from (2.144) by taking $\eta \to 0$ as

$$I_{\mathrm{sep}} = \frac{4}{3} \,, \tag{2.145}$$

which gives again the action of a parabolic separatrix (2.131) already used before.

Quantization

Now one can apply the semiclassical quantization rule (2.120) to the scaled actions (2.142) and (2.144). Because of the asymptotic scaling these quantization conditions can be formulated with just one free (dimensionless) parameter q instead of the two free parameters $\tilde{N}$ and $\bar{\alpha}$, which had independent influence in the first place. This parameter should determine the physical situation, meaning it should reflect where exactly the system is between the two separatrix-transitions of the ground state and the first excited state. A convenient choice is to define q as the area fraction of the vibrational orbit compared to the separatrix. With this choice the quantization conditions read

$$\begin{aligned} I_{\mathrm{vib}}(\eta_{\mathrm{vib}}) &= \frac{4}{3}q\,, \\ \delta I_{\mathrm{lib}}(\eta_{\mathrm{lib}}) &= 4q - \frac{4}{3}\,. \end{aligned} \tag{2.146}$$

The explicit relation between $\bar{\alpha}$, $\tilde{N}$ and q is given by

$$A = 1 - \frac{1}{\bar{\alpha}} = \left(\frac{21\pi}{32}\frac{1}{q\tilde{N}}\right)^{\frac{2}{3}}\,, \tag{2.147}$$

which can be easily seen from quantizing the vibration $S_{\mathrm{vib}} = \pi$ using (2.146) and (2.141). The relation (2.147) describes how $\bar{\alpha}$ asymptotically scales with $\tilde{N}$ when the position within the cross-over as a physical quality – reflected by q – is fixed. Thus, without further calculation, one is already able to give analytical substantiation for the scaling $\bar{\alpha}_{\mathrm{gap}} - 1 \sim N^{-\frac{2}{3}}$ of the location of the lowest gap observed in numerical calculations (see, *e.g.*, [22] and Fig. 2.9). The meaningful values of q vary between $\frac{1}{3}$ and 1, corresponding to the transition of the libration ($\bar{\alpha} = \bar{\alpha}_1^{\mathrm{cr}}$) and the vibration ($\bar{\alpha} = \bar{\alpha}_0^{\mathrm{cr}}$), respectively. Inverting (2.146) after the explicit use of (2.142) and (2.144) yields then two functions $\eta_{\mathrm{lib}}(q)$ and $\eta_{\mathrm{vib}}(q)$ that are independent of any system parameter. The gap energy (per particle) is

$$\begin{aligned} \Delta\tilde{\omega}(q) &= |\tilde{\omega}_{\mathrm{min}}(q)|\,\Delta\eta(q)\,, \qquad \text{with} \\ \Delta\eta(q) &= \eta_{\mathrm{lib}}(q) - \eta_{\mathrm{vib}}(q)\,. \end{aligned} \tag{2.148}$$

Actually there is still an additional explicit $\tilde{N}$-dependence in $\tilde{\omega}_{\mathrm{min}}(q)$, but it factorizes out in the regime of asymptotic scaling as

$$|\tilde{\omega}_{\mathrm{min}}(q)| = \frac{2}{7}\frac{A^2}{1-A} \approx \frac{2}{7}A^2 \propto \tilde{N}^{-\frac{4}{3}}\,. \tag{2.149}$$

This enables the eventual universal determination of the energy-gap and its location in the regime of asymptotic scaling. The condition $\frac{\mathrm{d}}{\mathrm{d}q}\log\Delta\tilde{\omega}(q) = 0$ at the gap translates to

$$\frac{\mathrm{d}}{\mathrm{d}q}\log\Delta\eta(q) = -\frac{\mathrm{d}}{\mathrm{d}q}\log|\tilde{\omega}_{\mathrm{min}}(q)| \approx \frac{4}{3q}\,, \tag{2.150}$$

where in the last step the asymptotic expression in (2.149) has been used. Solving (2.150) for q once and for all determines the universal numerical constants

$$\begin{aligned} q_{\mathrm{gap}}^{\mathrm{scl}} &= 0.525916\ldots\,, \\ \Delta\eta_{\mathrm{gap}}^{\mathrm{scl}} &= 0.953599\ldots\,, \end{aligned} \tag{2.151}$$

characterizing the finite-size QPT in the asymptotic limit $\tilde{N} \to \infty$ by semiclassical analysis. The energy-gap and its location are semiclassically estimated to be

$$\Delta E^{\mathrm{scl}}_{\mathrm{gap}} = \tilde{N}\Delta\tilde{\omega}^{\mathrm{scl}}_{\mathrm{gap}} = \frac{2}{7}\left(\frac{21\pi}{32q_{\mathrm{gap}}}\right)^{\frac{4}{3}} \Delta\eta_{\mathrm{gap}}\tilde{N}^{-\frac{1}{3}} \approx 1.6841\ldots \times N^{-\frac{1}{3}}\,, \quad (2.152)$$

$$\bar{\alpha}^{\mathrm{scl}}_{\mathrm{gap}} = 1 + \left(\frac{21\pi}{32q_{\mathrm{gap}}}\right)^{\frac{2}{3}} \tilde{N}^{-\frac{2}{3}} \approx 1 + 2.4862\ldots \times N^{-\frac{2}{3}}\,. \quad (2.153)$$

Comparison with numerics

To check the validity of the asymptotic semiclassical scalings (2.152) and (2.153) I compare to full semiclassics on the one hand to check the asymptotic analysis and to numerical calculations obtained from exact diagonalization on the other hand. Figure Fig. 2.9 shows these comparisons for the gap energy ΔE_{gap} and the gap location $\bar{\alpha}_{\mathrm{gap}} - 1$. While the deviation of the asymptotics from full semiclassics tends to zero for $N \to \infty$ as expected, a relative error of the asymptotics compared to numerics seems to be persistent in this limit. The relative error in the gap energy saturates at about 10% whereas the estimate for the finite-size correction to the coupling strength seems to be more accurate, but still saturates at a non-zero relative error of about 1%. So the question is, where this discrepancy is coming from. Since the effective quantum of action for the natural coordinates φ_0 and z is given by $\hbar^{(\varphi_0,z)}_{\mathrm{eff}} = 1/\tilde{N}$ (see section 2.4) one may expect the asymptotics to become exact in this limit. The problem is that this expectation is only true for fixed $\bar{\alpha}$, but here the coupling is scaled with the number of particles. First consider the first excitation energy very close to the critical coupling compared to numerics for two exemplary large numbers of particles shown in Fig. 2.10. In the region of the QPT a clear deviation from semiclassics can be seen. But what is more important is that the similarity in the two plots comes close to identity and is not a coincidence but a consequence of the asymptotic scaling behavior. The scaling happens in a way that typical actions characterizing the scale on which the (involved) classical phase space is varying changes similarly to the quantum of action $\hbar_{\mathrm{eff}}$. To make this obvious, take the separatrix action (taking z and φ_0 as conjugate pair) as such a typical action, which according to (2.141) and (2.145) scales like $S_{\mathrm{sep}}/\tilde{N} \propto A^{3/2}$ and hence $S_{\mathrm{sep}}/\tilde{N} \propto 1/\tilde{N}$ when staying at the gap according to (2.153). One could say that this is the dark side of the asymptotic scaling behavior discussed above while it enabled the asymptotic analysis in the first place. It makes the QPT to contain a constant persistent portion of "quantumness", no matter how small one makes $\hbar^{(\varphi_0,z)}_{\mathrm{eff}}$. In order to overcome this problem while still exploiting the scaling property I will show how to apply a requantization technique in the next section after the semiclassical analysis for the ESQPT is given.

2.8.5 The finite-size ESQPT

Before showing a way to account for the deep "quantumness" in the QPT in the next section, an asymptotic semiclassical analysis of energy scalings around the ESQPT is given. Here the coupling $\bar{\alpha} > 1$ is considered fixed, looking at the asymptotic spectrum around the separatrix energy in the limit $N \to \infty$.

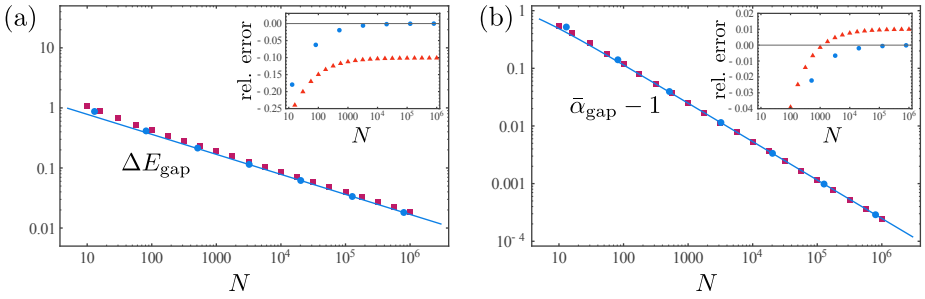

Fig. 2.9: (a) Gap energy $\Delta E_{\rm gap}$ and (b) correction $\bar{\alpha}_{\rm gap} - 1$ to the gap location as a function of the number of particles. Asymptotic semiclassical results (2.152) and (2.153) (solid blue), underlined by data obtained from the full semiclassical calculations (blue circles) and compared to numerical results obtained from exact diagonalization of the truncated model (purple squares). Insets: relative errors in the corresponding quantities of semiclassical asymptotics compared to full semiclassics (blue dots) and numerics (red triangles).

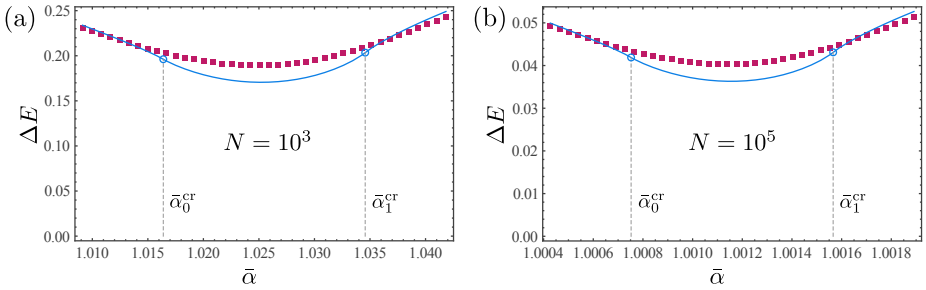

Fig. 2.10: The lowest excitation energy in full semiclassical calculation (solid blue) compared to numerical exact diagonalization (purple squares) for (a) $N = 10^3$ particles and (b) $N = 10^5$ particles. The transitions of the two involved orbits at $\bar{\alpha}_0^{\rm cr}$ and $\bar{\alpha}_1^{\rm cr}$ are marked with blue circles. The rannge of $\bar{\alpha}$ is scaled according to the critical couplings. The similarity of (a) and (b) is a consequence of the asymptotic scaling behavior.

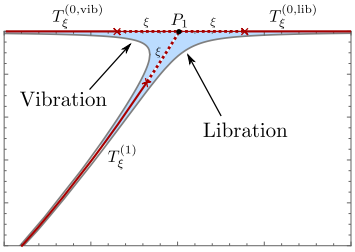

Fig. 2.11: Two orbits very close to the separatrix in energy. The corresponding orbit actions are dominated by the region around the saddle point (areas shown in light blue). Subdominant non-local contributions are given by on-separatrix traversal times $T_\xi^{(0,\mathrm{lib})}, T_\xi^{(0,\mathrm{vib})}$ and $T_\xi^{(1)}$ cutoff at distances ξ from P_1. The same cut-offs are applied on the other end of each segment, corresponding to the left P_1.

Therefore here the semiclassical analysis is not expected to suffer from the scaling behavior as in the QPT. In the limit $N \to \infty$ the quantized energy-levels close to $\tilde{\omega} = 0$ get arbitrarily small. This allows for considering local expansions of $\tilde{\omega}(z, \varphi_0)$ around the separatrix for the corresponding orbits. In contrast to the simple expansions used for the rough Bogoliubov-like approximations in section 2.8.2 and section 2.8.3, one can neither purely linearize $\tilde{\omega}$ at the upper boundary $z = 1$ nor use a quadratic expansion around the global energy minimum in this context. Instead one has to realize that $\tilde{\omega}$ is quadratic at the saddle-points P_1 while it behaves only linearly on other parts of the separatrix. Thus, the corresponding action integrals should be split into local parts close to the saddle points using a quadratic expansion there and non-local parts using linearization around the separatrix. A consequence of the splitting is that the dominant contribution to orbit actions (relative to the separatrix) originates from the regions around the saddle-points as illustrated in Fig. 2.11.

Universal separatrix quantization

A general semiclassical analysis based on quadratic expansion around saddle points in combination of a linearization around separatrices whenever separatrix-crossings are involved reveals that the quantized levels close to $\tilde{\omega} = 0$ depend only on properties of the saddle point and the separatrix itself.

Without giving a derivation here, the general formulas for semiclassical separatrix quantization read

$$\bar{\varrho}(\omega) = -\frac{1}{2\pi\hbar}\frac{1}{\lambda_\sigma}\log\frac{|\omega|}{\Omega} + \frac{t_\sigma}{2\pi\hbar} + (\mu_< - \mu_>)\delta(\omega) + \mathcal{O}(\omega)\,, \tag{2.154}$$

for the mean DOS and correspondingly

$$\omega_k \approx \frac{-2\pi\hbar\lambda_\sigma(\mu_\sigma + k)}{\mathcal{W}_{-1}(-2\pi\hbar\lambda_\sigma\Omega^{-1}\mathrm{e}^{-1-\lambda_\sigma t_\sigma}|\mu_\sigma + k|)}\,, \quad k \in \mathbb{Z}\,, \tag{2.155}$$

for the energy levels around the ESQPT. The dominant term $\sim \log|\omega|$ determined locally by solely the saddle point has been found before (see [205] for a classification in low dimensions) by counting the reduction of classical phase space volumes due to energy maxima. In contrast, the subdominant terms are non-locally determined by properties of the whole separatrix and are apparently original. In (2.154) and (2.155), $\mathcal{W}_{-1}$ is the lower branch of the Lambert-$\mathcal{W}$ function, which is the solution to $\mathcal{W}(x)\mathrm{e}^{\mathcal{W}(x)} = x$ with $x \in [-\mathrm{e}^{-1}, 0[$ and $\mathcal{W}_{-1}(x) \leq -1$. The inverse total stability exponent $\lambda^{-1} = \sum_j 1/\lambda^{(j)}$ is the sum of reciprocal stability exponents of all saddle points j involved. The energy ω

is measured with respect to the separatrix energy – set to $\omega = 0$ – and gets compared to an arbitrary unit of energy Ω, on which the expressions (2.154) and (2.155) finally do not depend. The time constant t contains non-local contributions from the separatrix given by

$$t = T^{\text{conv}} - \sum_j \frac{1}{\lambda^{(j)}} \log\left(\frac{\Omega}{2}\left(\frac{1}{\lambda_+^{(j)}} + \frac{1}{|\lambda_+^{(j)}|}\right)\right) , \tag{2.156}$$

where $\lambda_\pm^{(j)}$ are the positive and negative eigenvalues of the Hessian when expanding the Hamiltonian around the saddle point j and

$$T^{\text{conv}} := \lim_{\xi\to 0}\left(T_\xi + \frac{2}{\lambda}\log\xi\right) \tag{2.157}$$

is the convergent part of the separatrix traversal time, with T_ξ the sum of on-separatrix traversal times cut-off at (phase-space-) distances ξ from all involved saddle-points. To calculate the non-local constant t in a specific system one has to give meaning to $\lambda_\pm$ and phase space distance ξ, which are actually ill-defined objects because in general a phase space in Hamiltonian mechanics does not have a metric but rather a simplectic form (Note that in contrast, λ is well defined). To do the calculation one has to define arbitrary units q_0 of length and p_0 of momentum to get a dimensionless phase-space. The meaning of $\lambda_\pm$ and ξ are then defined in that space (using Euclidean norm) with the outcome t not depending on the particular choice of q_0 and p_0. The constant index shifts $\mu_\sigma \in [0, 1[$ are related to the Maslov index and separatrix action. The index

$$\sigma = \begin{cases} < : \ \omega < 0 \\ > : \ \omega > 0 \end{cases} = \begin{cases} < : \ k < 0 \\ > : \ k \geq 0 \end{cases} \tag{2.158}$$

was introduced to indicate on which side of the separatrix the corresponding orbit lives, which may in principle involve different saddle-points and separatrix-segments, hence the distinction in λ, t and μ. If $\mu_< = \mu_> =: \mu$ I will call the quantized orbits *"smoothly connected"* through the transition. If in addition the separatrix fully encloses one of the two regions, say $\omega < 0$, so that orbits inside this island are quantized by the condition

$$S = 2\pi\hbar\left(n + \frac{\nu}{4}\right) , \quad n \in \mathbb{N}_0 , \tag{2.159}$$

with the Maslov index ν, then the index shift is

$$\mu = \left(\frac{\nu}{4} - \frac{S_0}{2\pi\hbar}\right) \bmod 1 , \tag{2.160}$$

where S_0 is the action integral of the full island enclosed by the separatrix.

Considering the formal semiclassical limit $\hbar \to 0$ in (2.154) and (2.155), the (local) contribution of saddle points is dominant, resulting in a universal scaling law

$$\omega_k \sim 2\pi\hbar\lambda_\sigma \left(\log\frac{s_0}{\hbar}\right)^{-1} (\mu_\sigma + k) \times \left(1 + \mathcal{O}\left(\frac{\log\log\frac{s_0}{\hbar}}{\log\frac{s_0}{\hbar}}\right)\right) \tag{2.161}$$

of asymptotically equidistant energy levels where the level spacing depends only on the stability exponents associated with involved saddle-points. Here s_0 is an

arbitrarily chosen but classically defined (typical) action of the system. This action is just introduced to be consistent with units but its explicit value is not important for the asymptotics since it is subdominant.

If $\lambda_< = \lambda_> =: \lambda$ the asymptotic level spacing (2.161) induces a single time-scale

$$\tau \sim \frac{1}{\lambda} \log \frac{s_0}{\hbar} \tag{2.162}$$

for quantum mechanical processes that dominantly involve the states in the band of high DOS around the separatrix energy $\omega = 0$. This enables for example an analytic estimation for the asymptotic scrambling time or quantum-break-time in the attractive Lieb-Liniger model. Remarkably, the characteristic time-scale (2.162) reminds of the Ehrenfest time in chaotic systems [216], which also goes logarithmically with $\hbar$ instead of algebraically like the Heisenberg time (see, *e.g.*, [107]), the time-scale associated to the mean DOS, provided the latter is not singular.

The correspondence of (2.162) to the Ehrenfest-time becomes precise when the stability exponent λ takes the role of a Lyapunov exponent. This shows an intriguing duality between the quantum behavior of classically chaotic systems on the one hand and close-to-instability behavior of classically integrable systems on the other hand. Because of this resemblance (2.162) can be interpreted as a *local* Ehrenfest time associated to specific (local) unstable fixed points instead of (global) Lyapunov exponents.

Range of validity

There is, however, a subtlety involved in the asymptotic expressions (2.161) and (2.162). The quantum number k was here assumed to be fixed during the limiting process. Stated differently, the number of states around the separatrix energy following the asymptotic law increases with decreasing $\hbar$. For a physical process as considered in the last subsection the number of dominantly involved states also grows with $s_0/\hbar$. To get a bound for the scaling of this number, for which (2.162) applies, consider the average level-spacing

$$\langle \Delta\omega \rangle_K = \frac{\Delta\Omega}{K} \tag{2.163}$$

over an energy range $\Delta\Omega$ bordering the separatrix energy and corresponding to a number of states K, both of which are regarded as $\hbar$-dependent since the relevant number of states should scale in some way with the system size (characterized by $s_0/\hbar$). I assume that $\lim_{\hbar\to 0} \hbar K(\hbar) = 0$, since otherwise macroscopic distance from the separatrix forbids the usage of the asymptotics given in (2.154). The latter implies $\Delta\Omega \log \Delta\Omega \approx -2\pi\hbar\lambda K$, which translates to

$$\langle \Delta\omega \rangle_K \approx -\frac{2\pi\hbar\lambda}{\log \Delta\Omega(\hbar)} \,. \tag{2.164}$$

Since $\Delta\Omega$ is assumed small, its dependence on K is given by the asymptotics of (2.155) as

$$\Delta\Omega \sim -\frac{\hbar K(\hbar)}{\log(\hbar K(\hbar))} \times \text{const.}\,, \tag{2.165}$$

which implies

$$\langle \Delta\omega \rangle_K \approx -\frac{2\pi\hbar\lambda}{\log\frac{\hbar}{s_0} + \log K(\hbar)}\,. \tag{2.166}$$

Now two cases of scalings have to be distinguished. First, if the number of involved states grows algebraically with $\hbar$,

$$\langle \Delta\omega \rangle_K \approx \frac{2\pi\hbar\lambda}{\log\frac{s_0}{\hbar}}(1-\nu)^{-1} \quad \text{for} \quad K(\hbar) \sim \left(\frac{s_0}{\hbar}\right)^{\nu} \quad \text{with} \quad 0<\nu<1\,, \tag{2.167}$$

which produces an additional constant factor $(1-\nu)$ in the characteristic time compared to (2.162). Second, if the number of involved states is sub-algebraic in $\hbar$,

$$\langle \Delta\omega \rangle_K \approx \frac{2\pi\hbar\lambda}{\log\frac{s_0}{\hbar}} \quad \text{for} \quad (\forall \nu>0)\left(\lim_{\hbar\to 0}\left(\frac{\hbar}{s_0}\right)^{\nu} K(\hbar) = 0\right)\,, \tag{2.168}$$

producing exactly the time scaling (2.162) given before. The fact that the universal scalings (2.167) and (2.168) do not change when multiplying $K(\hbar)$ with an arbitrary constant shows indeed that one can consider the (relevant local) spectrum as effectively equidistant for small $\hbar$. This is especially true for a sub-algebraic number of states where the level spacing does not depend on any details of the scaling of K at all.

Application to the model

To apply the general separatrix quantization formulas to the three-mode model I use the scaled phase-space variables (z, φ_0) which fortunately are already dimensionless, thus no extra care has to be taken there. The corresponding effective quantum of action is $\hbar_{\text{eff}} = 1/\tilde{N}$. Because of parity symmetry *w.r.t.* φ_0 it is sufficient to analyze one of the two saddle points P_1. I choose the one located at positive φ_0. The Hessian of $\tilde{\omega}(z, \varphi_0)$ in P_1 is easily calculated to be

$$\mathcal{H} = \begin{pmatrix} 0 & -2\sqrt{\bar{\alpha}-1} \\ -2\sqrt{\bar{\alpha}-1} & 2-\frac{\bar{\alpha}}{4} \end{pmatrix}\,, \tag{2.169}$$

which gives the stability exponent $\lambda^{(j)} = \sqrt{-\det\mathcal{H}} = 2\sqrt{\bar{\alpha}-1}$ for each of the two saddle-points and therefore the total exponent

$$\lambda = \sqrt{\bar{\alpha}-1}\,, \tag{2.170}$$

which is – as the local contribution – all one needs to know to get the asymptotic level-scaling.

For the non-local contributions, the eigenvalues of $\mathcal{H}$ give

$$\frac{1}{2}\left(\frac{1}{\lambda_+^{(j)}} + \frac{1}{|\lambda_-^{(j)}|}\right) = \frac{\sqrt{\left(1-\frac{\bar{\alpha}}{8}\right)^2 + 4(\bar{\alpha}-1)}}{4(\bar{\alpha}-1)}\,. \tag{2.171}$$

For the separatrix traversal times the separatrix can be split into three segments, defining the traversal times *i)* $T_\xi^{(0,\text{lib})}$ for the outer upper boundary at $\cos^2\varphi_0 < 1/\bar{\alpha}$ for librations, *ii)* $T_\xi^{(0,\text{vib})}$ for the inner upper boundary at $\cos^2\varphi_0 > 1/\bar{\alpha}$

for vibrations and *iii)* $T_\xi^{(1)}$ for the curved separatrix segment between the two saddle points separating librations and vibrations and therefore involving both (see Fig. 2.11). In general the traversal times

$$T_\gamma = \int_{\mathcal{C}_\gamma} \mathrm{d}\varphi_0 \left|\frac{\partial\tilde{\omega}}{\partial z}\right|^{-1}_{\mathcal{C}_\gamma} \tag{2.172}$$

are here calculated in φ_0-representation along the corresponding segment $\mathcal{C}_\gamma$. The cut-off traversal time of the first segment (which connects the two P_1 by going over $\varphi_0 = \pi/2 \equiv -\pi/2 \mod \pi$) is given by

$$T_\xi^{(0,\mathrm{lib})} = 2\int_{\arccos\frac{1}{\sqrt{\bar{\alpha}}}+\xi}^{\frac{\pi}{2}} \mathrm{d}\varphi_0 \left(1-\bar{\alpha}\cos^2\varphi_0\right)^{-1}, \tag{2.173}$$

which can be elementarily integrated to yield

$$T_\xi^{(0,\mathrm{lib})} = -\frac{1}{\sqrt{\bar{\alpha}-1}}\log\xi + \frac{1}{\sqrt{\bar{\alpha}-1}}\log\left(\frac{2}{\bar{\alpha}}\sqrt{\bar{\alpha}-1}\right) + \mathcal{O}(\xi), \tag{2.174}$$

containing the convergent part

$$T_{\mathrm{conv}}^{(0,\mathrm{lib})} = \frac{1}{\sqrt{\bar{\alpha}-1}}\log\left(\frac{2}{\bar{\alpha}}\sqrt{\bar{\alpha}-1}\right). \tag{2.175}$$

An analogous calculation gives the same for the vibration-related boundary segment

$$\begin{aligned} T_\xi^{(0,\mathrm{vib})} &= T_\xi^{(0,\mathrm{lib})}, \\ T_{\mathrm{conv}}^{(0,\mathrm{vib})} &= T_{\mathrm{conv}}^{(0,\mathrm{lib})}. \end{aligned} \tag{2.176}$$

The linearized energy $\frac{\partial\tilde{\omega}}{\partial z}$ takes the same form on the curved segment as for the upper boundary, thus again, for this segment one gets a similar integral

$$T_\xi^{(1)} = 2\int_0^{\arccos\frac{1}{\sqrt{\bar{\alpha}}}-\Delta\varphi_\xi} \mathrm{d}\varphi_0 \left(\bar{\alpha}\cos^2\varphi_0 - 1\right)^{-1}, \tag{2.177}$$

but this time the cut-off in φ_0, denoted by $\Delta\varphi_\xi$ has to be related to the Euclidean phase-space distance ξ from P_1 by

$$\Delta\varphi_\xi = \left(1+\left(\frac{\mathrm{d}z^{(1)}}{\mathrm{d}\varphi_0}\Big|_{P_1}\right)^2\right)^{-\frac{1}{2}}\xi = \frac{1-\frac{\bar{\alpha}}{8}}{\sqrt{(1-\frac{\bar{\alpha}}{8})^2+4(\bar{\alpha}-1)}}\xi. \tag{2.178}$$

The traversal time is then given by

$$T_\xi^{(1)} = -\frac{1}{\sqrt{\bar{\alpha}-1}}\log\xi + T_{\mathrm{conv}}^{(1)} + \mathcal{O}(\xi), \tag{2.179}$$

with its convergent part

$$T_{\mathrm{conv}}^{(1)} = \frac{1}{\sqrt{\bar{\alpha}-1}}\log\left(\frac{2}{\bar{\alpha}}\sqrt{\bar{\alpha}-1}\right) + \frac{1}{\sqrt{\bar{\alpha}-1}}\log\left(\frac{\sqrt{(1-\frac{\bar{\alpha}}{8})^2+4(\bar{\alpha}-1)}}{1-\frac{\bar{\alpha}}{8}}\right). \tag{2.180}$$

The cumbersome looking second term in (2.180) seems to be a manifestation of the specific choice of phase space units, which also enters (2.171) in a way that they compensate each other almost perfectly – an indication that the definitions (2.156) and (2.157) using intermediately chosen phase-space units (and induced Euclidean norm) may be circumstantial. Obviously the physically meaningful objects that are independent on a specific choice are the constants (2.156) as some kind of convergent part of (diverging) separatrix traversal times. I leave the issue of a more direct definition of the cutoff points (here given as distance ξ) in terms of physically more meaningful quantities open.

In total one gets the non-local time-constant

$$t = \frac{1}{\sqrt{\bar{\alpha}-1}} \log\left(\frac{128(\bar{\alpha}-1)^2}{\bar{\alpha}^2(8-\bar{\alpha})}\right) \tag{2.181}$$

on both sides of the transition. The index shift $\mu = \mu(\tilde{N}, \bar{\alpha})$ of the smoothly connected transition is given by (2.160) together with $\nu = 2$ and the separatrix action $S_0/\hbar = S_{\text{sep}}^{(1)}$ in units of $\hbar$ given explicitly by $2\tilde{N}$ times the LHS of (2.130) with $\bar{\alpha}_m^{\text{cr}}$ replaced by $\bar{\alpha}$. Note that here the full expression has to be used instead of the small angle approximation (2.131), since the ESQPT occurs at arbitrary fixed $\bar{\alpha} > 1$.

Altogether, the asymptotic DOS $\bar{\varrho}(E) = \frac{1}{\tilde{N}}\tilde{\varrho}(\tilde{\omega})$ close to the ESQPT reads

$$\bar{\varrho}(E) = -\frac{1}{2\pi\sqrt{\bar{\alpha}-1}} \log\left(\frac{\left|E-E^{(1)}\right|\bar{\alpha}^2(8-\bar{\alpha})}{128\tilde{N}(\bar{\alpha}-1)^2}\right) + \mathcal{O}(N^{-2}) \tag{2.182}$$

with the separatrix energy $E^{(1)} = \tilde{N}\tilde{\epsilon}_0$ (see (2.55)). Furthermore, according to (2.168) the asymptotically universal constant level spacing is

$$\Delta E \approx \frac{2\pi\sqrt{\bar{\alpha}-1}}{\log \tilde{N}} \tag{2.183}$$

for a number of states that scales sub-algebraically with N.

Comparison with numerics

The asymptotic expression (2.182) is checked against numerics for a 200-boson system in Fig. 2.12. The ESQPT is clearly visible as a divergent feature along the separatrix energy $\tilde{\omega} = 0$ (or equivalently $E = E^{(1)}$). The logarithmic divergence predicted in the DOS quantitatively fits extremely well to the actual level spacings well beyond the QPT, meaning at coupling strengths well above the (finite-size) critical coupling, *i.e.*, $\bar{\alpha} - 1 \gg \bar{\alpha}_0^{\text{cr}} - 1 = 0.0489\ldots$ for $N = 200$. In Fig. 2.12c an exemplary section at $\bar{\alpha} = 2$ is shown. In the supercritical regime the divergence around the ESQPT obviously is a dominant feature of the whole spectrum. Note that for larger couplings approaching $\bar{\alpha}_2 = 4$ an additional feature appears at the upper end of the spectrum, its precursor being visible in Fig. 2.12a as an increase of the DOS in the upper right corner. The latter is an artifact from truncation to three single-particle modes produced by the lower separatrix closing in to penetrate the phase space at the high energy end, finally creating another logarithmic divergence for $\bar{\alpha} > 4$ (not shown here).

It might seem contradictory that one can assign a single energy- and corresponding time scale to the level spacings at the ESQPT despite the divergence

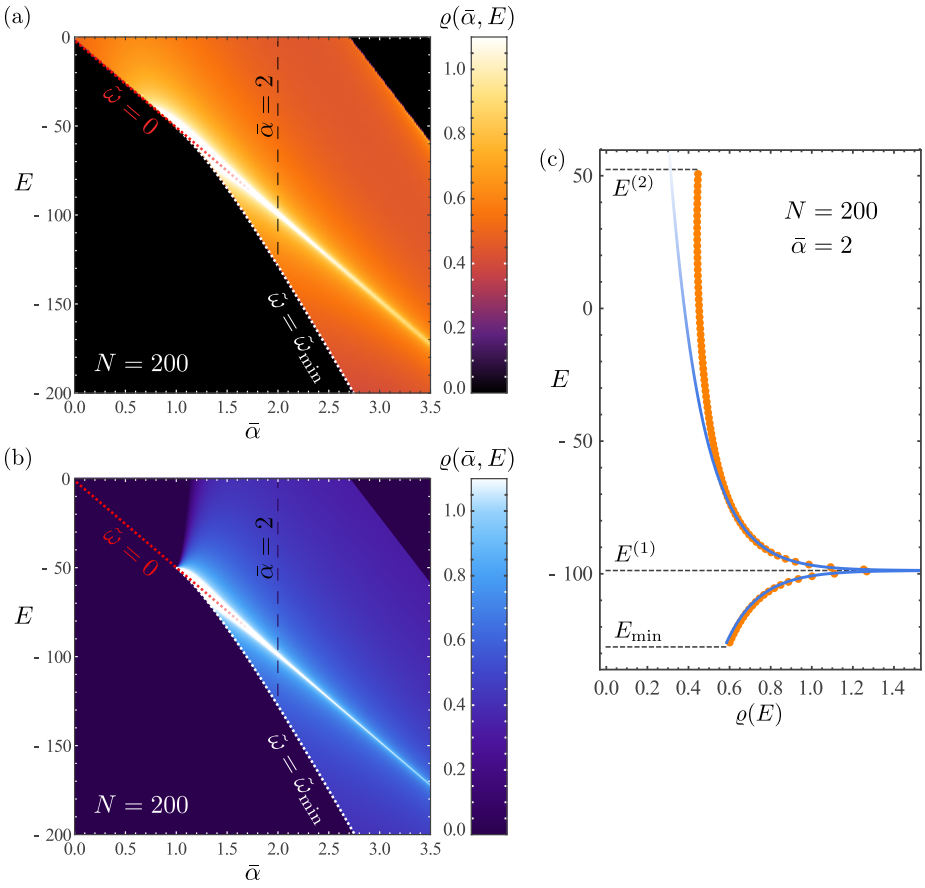

Fig. 2.12: DOS for $N = 200$ as a function of $\bar{\alpha}$ and E based on (a) numerical exact diagonalization and (b) the asymptotic expression (2.182) for separatrix quantization. A direct comparison for a section at $\bar{\alpha} = 2$ over the full spectrum is shown in (c) where orange dots correspond to inverse level spacings between two adjacent eigenstates each and the asymptotic prediction is shown in solid blue.

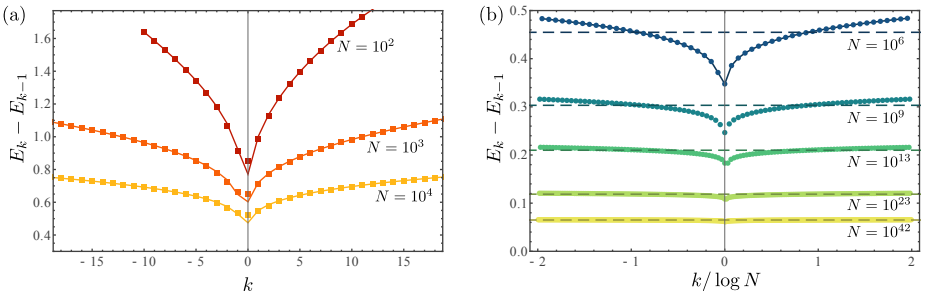

Fig. 2.13: Level spacings $E_k - E_{k-1}$ around the separatrix where $k = 0$ corresponds to the lowest quantized energy larger than the separatrix energy.
(a) Numerically calculated gaps (symbols) compared to full semiclassical prediction (solid) for $N = 10^2, 10^3, 10^4$ (from top/dark red to bottom/yellow).
(b) Gaps taken from the asymptotic expression (2.155) containing non-local contributions (symbols) compared to the universal constant spacing (2.183) (dashed) for $N = 10^6, 10^9, 10^{13}, 10^{23}, 10^{42}$ (from top/dark blue to bottom/yellow) with the number of considered levels scaling with $\log N$. For $N = 10^6$ the full semiclassical gaps are added (solid) to verify the validity of the asymptotics (2.155).

in the large N regime. This fact is due to the logarithmic nature of the singularity. When increasing N, the levels around it become indeed asymptotically equidistant according to (2.161) albeit much more slowly (in a logarithmic fashion) compared to any other regular point of the spectrum. In order to underline this statement level spacings around the separatrix are examined in Fig. 2.13. On the one hand this involves a validation of the applicability of the semiclassical method close to the separatrix by comparing to exact diagonalization in a regime of N that is still numerically tractable. On the other hand the asymptotic level-spacings (2.155) and (2.161) are verified by comparing to full semiclassical calculations in the regime of large N. The first plot shows excellent agreement of the full semiclassical calculation with numerics up to the energy difference between the closest two levels around the separatrix already for 100 particles. The slight deviation at $k = 0$ originates from the failure of the semiclassical approximation due to wave packet smearing across the separatrix already observed in the context of ground state energy calculations (see section 2.7.1).

2.9 Scrambling time

A neat application of the universal scaling (2.183) found for the ESQPT is the particular quantum break time $\tau_{\rm br}$ for the non-interacting ground state in the interacting Lieb-Liniger model, which is a characteristic time scale for the production of inter-particle correlations, representing the breakdown of classical descriptions. Besides the general interest, this quantity has formerly been discussed to model the time scale of information scrambling $\tau_{\rm scr}$ in black holes [217], where the latter are considered as self-sustaining condensates of soft gravitons stuck at criticality. The characteristic time for the development of inter-particle correlations (or, similarly, the scrambling of information among particles) is measured using the von Neumann entropy

$$S(t) = -\operatorname{tr}\left(\rho(t)\log\rho(t)\right) \tag{2.184}$$

of the time-dependent reduced one-body density matrix (ROBDM)

$$\rho_{kl}(t) = \frac{1}{N}\left\langle\phi(t)\right|\hat{a}_k^\dagger\hat{a}_l\left|\phi(t)\right\rangle \tag{2.185}$$

of the pure state $|\phi(t)\rangle$ initialized as the homogeneous ground state

$$|\phi(0)\rangle = |0,N,0,\rangle_{\rm FS} \tag{2.186}$$

of the non-interacting system here represented in the Fock basis

$$|m_{-1},m_0,m_1\rangle_{\rm FS} := \frac{1}{\sqrt{m_{-1}!}}\left(\hat{a}_{-1}^\dagger\right)^{m_{-1}}\frac{1}{\sqrt{m_0!}}\left(\hat{a}_0^\dagger\right)^{m_0}\frac{1}{\sqrt{m_1!}}\left(\hat{a}_1^\dagger\right)^{m_1}|0\rangle\ , \tag{2.187}$$

where $|0\rangle$ denotes the vacuum of $N=0$ particles. Because of total momentum conservation $[\hat{L},\hat{H}]=0$, the ROBDM takes a very simple form. Taking $L=0,\bar{\alpha}>1$ the time-evolved state in Fock basis (for simplicity consider N even) becomes

$$|\phi(t)\rangle = \sum_{m=0}^{\frac{N}{2}}\alpha_m(t)\,|m,N-2m,m\rangle_{\rm FS}\ . \tag{2.188}$$

The matrix element of $\hat{a}_k^\dagger\hat{a}_l$ in Fock basis is restricted to

$${}_{\rm FS}\langle n,N-2n,n|\hat{a}_k^\dagger\hat{a}_l\,|m,N-2m,m\rangle_{\rm FS} \propto \delta_{nm}\delta_{kl}\,, \tag{2.189}$$

because the operator cannot change three occupation numbers simultaneously. This results in the diagonal form

$$\rho(t) = \frac{1}{N}\begin{pmatrix}\langle m_{\pm1}\rangle_t & 0 & 0\\ 0 & N-2\langle m_{\pm1}\rangle_t & 0\\ 0 & 0 & \langle m_{\pm1}\rangle_t\end{pmatrix}\,, \tag{2.190}$$

depending only on the expectation value

$$\langle m_{\pm1}\rangle_t = \sum_m |\alpha_m(t)|^2\,m \tag{2.191}$$

of the $k=\pm1$ momentum mode occupation.

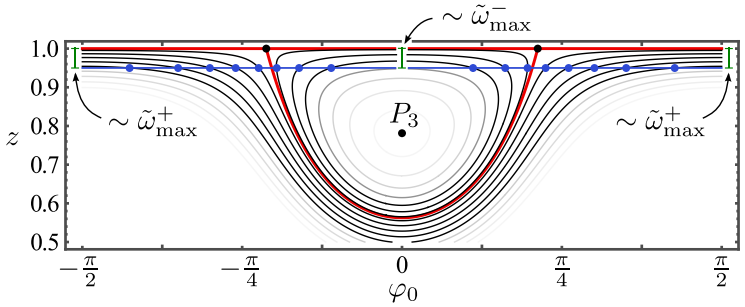

Fig. 2.14: Vibrations and librations (black) in the vicinity of the separatrix are intersecting (blue dots) the horizontal line corresponding to the non-interacting ground state (blue solid). The overlaps of the latter with eigenstates corresponding to non-intersecting orbits are exponentially suppressed (grayed out). The criterion for intersection depends on the peak value of z located at $\varphi_0 = \pm\frac{\pi}{2}$ (lib.) or $\varphi_0 = 0$ (vib.), where $\tilde{\omega}(z, \varphi_0)$ can be linearized in z and therefore $1 - z_{\max} \sim \tilde{\omega}_{\max}$.

When represented in the energy eigenbasis $\{|n\rangle\}$ of the interacting system, the ROBDM reads

$$\rho_{kl}(t) = \frac{1}{N} \sum_{n,m} \beta_n^* \beta_m \langle n| \hat{a}_k^\dagger \hat{a}_l |m\rangle \, \mathrm{e}^{-\mathrm{i}(E_m - E_n)t} \,, \tag{2.192}$$

where

$$|\phi(0)\rangle = \sum_n \beta_n |n\rangle \,. \tag{2.193}$$

States in the vicinity of the ESQPT are dominantly involved in the process, because $|\phi(0)\rangle$ corresponds to the classical orbit given by the horizontal line $z = z_\phi = 1 - 1/(2\tilde{N})$, very close to the upper boundary of the phase space, which serves as a separatrix in the interacting system. A semiclassical estimate of the number of states dominantly involved around the separatrix is given by the criterion that the corresponding orbits intersect this horizontal line. For quantized orbits (corresponding to the state $|n\rangle$) beyond intersection, the coefficients β_n typically drop of exponentially. This is completely analogous to the exponential decay of any eigenstate wave function in the classically forbidden region beyond a turning point, assuming a sufficiently smooth potential. With increasing energy difference $|\tilde{\omega}|$ from the separatrix, librational orbits approach the lower boundary $z = 0$ (assuming $\bar{\alpha} < 4$) and vibrational orbits approach the global minimum P_3, which both lie below the horizontal line $z = z_\phi$ for sufficiently large N. Therefore the number of contributing librational and vibrational states can be estimated by a linearization of $\tilde{\omega}(z, \varphi_0)$ at $(z, \varphi_0) = (0, \pi/2)$ and $(z, \varphi_0) = (0, 0)$, respectively – being well separated from the saddle points – as depicted in Fig. 2.14. The bounds $-\tilde{\omega}^-_{\max} < \tilde{\omega} < \tilde{\omega}^+_{\max}$ are easily calculated to be

$$\begin{aligned} \tilde{\omega}^-_{\max} &= \frac{\bar{\alpha} - 1}{\tilde{N}} \,, \\ \tilde{\omega}^+_{\max} &= \frac{1}{\tilde{N}} \,, \end{aligned} \tag{2.194}$$

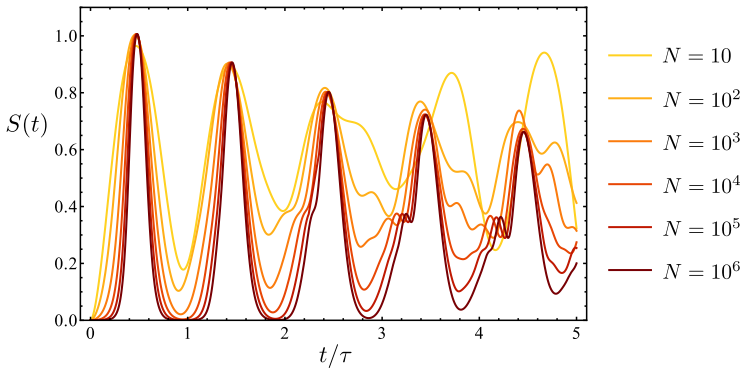

Fig. 2.15: Evolution of the von Neumann entropy (2.184) of the ROBDM (2.184) initialized in the non-interacting ground state numerically calculated for $\bar{\alpha} = 2$ and $N = 10^n$ with $n = 1, 2, 3, 4, 5, 6$. The increasing quality of periodicity with growing N is in particular reflected in the improvement of revivals $S(\tau\mathbb{N}) \approx 0$. The time is scaled with the (pseudo-)period τ (2.200) associated with the estimate for the average involved level-spacing.

so that in both cases the bound scales as

$$\tilde{\omega}_{\max} \sim \frac{1}{\tilde{N}}\,, \tag{2.195}$$

which, corresponding to (2.161), yields the scaling

$$K \sim \tilde{\omega}_{\max}\tilde{N}\log\tilde{N} \sim \log N \tag{2.196}$$

for the number of dominantly contributing states. The sub-algebraic scaling (2.196) then justifies using (2.161) in the first place and furthermore, according to (2.168), produces the asymptotically equidistant level spacing (2.183) for the involved states. For exactly equidistant energies

$$E_m - E_n = \Delta E(m-n) \tag{2.197}$$

the ROBDM (2.192) becomes periodic in time since

$$\rho_{kl}\Big(t + \frac{2\pi}{\Delta E}\Big) = \rho_{kl}(t)\,. \tag{2.198}$$

While (2.198) should hold asymptotically, for finite N this periodicity is flawed, resulting in only partial recurrence, because neither is the spectrum exactly equidistant for dominantly contributing states, nor can states with larger $|\tilde{\omega}| > |\tilde{\omega}^{\pm}_{\max}|$ be fully ignored. When increasing N the periodicity should slowly become more and more perfect. This tendency is demonstrated in figure Fig. 2.15. As an estimate for the finite-size characteristic time-scale one can give meaning to the average inverse level-spacing of involved states by calculating

$$\langle\Delta\tilde{\omega}^{-1}\rangle \approx \langle\Delta\tilde{\omega}\rangle^{-1} = \frac{1}{\tilde{\omega}^{+}_{\max} - \tilde{\omega}^{-}_{\max}}\int_{\tilde{\omega}^{+}_{\max}}^{\tilde{\omega}^{-}_{\max}} \mathrm{d}\tilde{\omega}\;\bar{\rho}(\tilde{\omega}) \tag{2.199}$$

with the DOS given by (2.154) and (2.182) and the energy-bounds (2.194), which results in the estimated time-scale

$$\tau = \frac{1}{\sqrt{\bar{\alpha}-1}}\left[\log N + 1 + \log\left(\frac{128(\bar{\alpha}-1)^2}{\bar{\alpha}^2(8-\bar{\alpha})}\right) - \frac{\bar{\alpha}-1}{\bar{\alpha}}\log(\bar{\alpha}-1)\right]\,, \tag{2.200}$$

which, in the limit $N \to \infty$, converges to the asymptotic period associated with the universal constant level spacing (2.183) and in addition includes finite-size corrections. One should mention that the rather rough approximations involved in this estimate only affect those finite-size corrections so that the asymptotic limit is untouched.

Although periodicity is flawed for finite N, the (pseudo-)period (2.200) still serves as a characteristic time scale τ_{br} for the evolution of $S(t)$, usually determined by the condition

$$S(\tau_{\mathrm{br}}) = S_{\mathrm{th}}\,, \tag{2.201}$$

with some arbitrary chosen, small valued threshold S_{th}. Thus, the asymptotic scrambling time or break time for large N is given by

$$\tau_{\mathrm{scr}} = \tau_{\mathrm{br}} = \text{const.} \times \frac{2\pi}{\Delta E} = \text{const.} \times \frac{1}{\sqrt{\bar{\alpha} - 1}} \log N\,, \tag{2.202}$$

where the undetermined constant prefactor related to the choice of S_{th} is of minor importance while the major interest lies in the scaling with the parameters N and $\bar{\alpha}$. The sub-algebraic dependence of (2.202) on N is usually referred to as *fast scrambling*, because even for macroscopic systems it can be conceivably fast. This is a property black holes are known to exhibit [218, 219], which indicates the validity of the model in the given context. In addition to the general attribute of fast scrambling it now can clearly be related to the existence of a classical instability close to a saddle point, including the analytic dependence on the coupling strength via the (total) stability exponent (2.170). While the logarithmic scaling with N has been numerically observed and the general connection to an instability has been suspected before [217], the semiclassical treatment provides sufficient analytical ground for supplying those statements with explicit expressions and thorough derivation. Finally Fig. 2.16, 2.17 show numerical confirmation of (2.202).

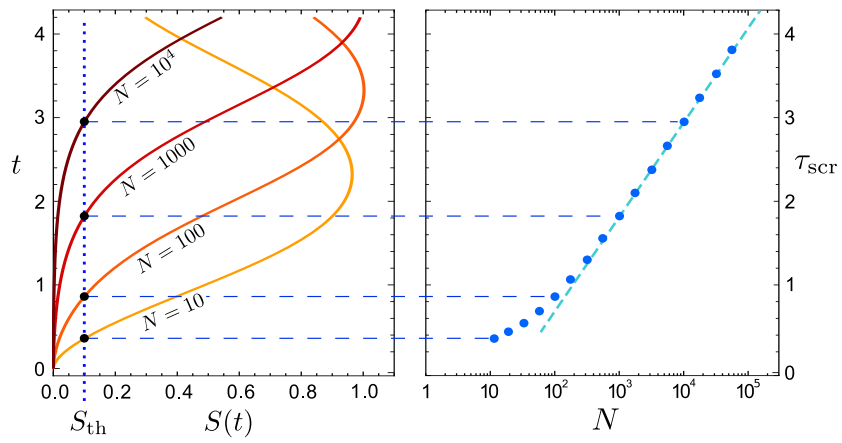

Fig. 2.16: Scrambling times $\tau_{\rm scr}$ for $\bar{\alpha} = 2$ determined by setting $S_{\rm th} = 0.1$ in (2.201) for the numerically evolved entropies $S(t)$ (2.184) for several numbers of particles (left). Plotting those against $\log N$ (right) shows agreement with the dominant logarithmic scaling (2.202) in form of saturation to a linear curve for $N \gtrsim 100$ (dashed). The missing additive constant is attributed to finite-size corrections of which an approximate estimate is given by (2.200).

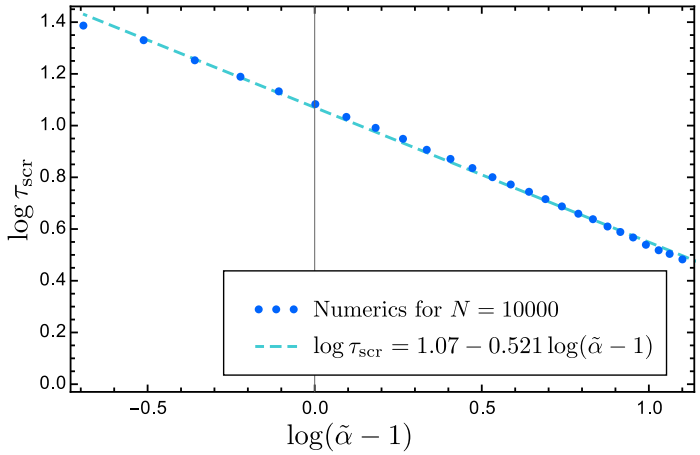

Fig. 2.17: Numerically calculated scrambling times for $N = 10^4$ as a function of $\bar{\alpha}$. A linear fit to the doubly logarithmic data supports the predicted dominant scaling with $\sqrt{\bar{\alpha} - 1}$ (2.202). Deviations thereof (small mismatch in the exponent 0.521 from the prediction 0.5 and additional functional dependence on $\bar{\alpha}$) are attributed to finite-size effects expected to vanish asymptotically.

2.10 Requantization: Improving the description at criticality

In the last section concerning the truncated attractive Lieb-Liniger model I put the focus back to the regime of asymptotic scaling around criticality. As a reminder, this means that the coupling strength $\bar{\alpha}$ is not considered as a fixed constant parameter but rather involves a scaling with the number of bosons N to ensure that one stays in the vicinity of the finite-size analogue of the quantum critical point. This subject was investigated in section 2.8.4 using semiclassical methods. There an asymptotic scaling property was found saying that the classical phase space feels a change of N only as a rescaling of φ_0, z and $\tilde{\omega}$ when the N-dependence of $\bar{\alpha}$ fixes criticality. This allowed to analytically extract the exact exponents for the energy gap $\Delta E_{\mathrm{gap}} \sim N^{-1/3}$ (2.152) and its location $\bar{\alpha}-1 \sim N^{-2/3}$ (2.153). It also enabled the semiclassical prediction of the corresponding coefficients while the latter quantitatively suffer (see Fig. 2.9 and subsequent discussion) from the asymptotic scaling property since it prevents the system to become more classical when increasing N. To overcome this problem in this section deep quantum effects are reintroduced by performing a requantization of the system after exploiting the asymptotic scaling on the classical level. While this may look cumbersome at first glance, the intermediate step of going into the classical analogue of the original quantum system is crucial. The reason is that formalizing the system in a way that it obeys the scaling law requires to neglect terms that can be quite easily identified as being subdominant in the semiclassical picture, where it becomes clear that orbit action integrals are dominantly covered by the region around the separatrix island.

Hamiltonian in scaling regime

In order to requantize the system I use the scaled variables $\phi = \varphi_0/\sqrt{A}$, $\eta = \tilde{\omega}/|\tilde{\omega}_{\mathrm{min}}|$ defined in (2.139) and similarly the scaled depletion of the condensate

$$x = \frac{7}{4A}(1-z)\,. \tag{2.203}$$

The dominance of the separatrix region then is expressed by

$$\begin{aligned} \phi &= \mathcal{O}(1)\,, \\ x &= \mathcal{O}(1)\,, \\ \eta &= \mathcal{O}(1)\,, \\ A &= \mathcal{O}(N^{-\frac{2}{3}}) \end{aligned} \tag{2.204}$$

in the relevant region of phase space under the scaling $\bar{\alpha} - 1 \sim N^{-2/3}$. The energy then reads

$$\eta = x^2 - 2x(1-\phi^2) + \mathcal{O}(A)\,, \tag{2.205}$$

where the dominant $\mathcal{O}(1)$ part does not depend on parameters and hence expresses the asymptotic scaling.

Poisson brackets and effective $\hbar$

After neglecting $\mathcal{O}(A)$-terms the dependence on the actual choice of the coupling $\bar{\alpha}$ enters only via the effective quantum of action

$$\hbar_{\text{eff}}^{(x,\phi)} = \frac{7}{4NA^{\frac{3}{2}}}\hbar_{\text{eff}}^{(q,p)} =: g\,, \tag{2.206}$$

obtained from (2.58) and the Poisson bracket

$$\{x,\phi\}_{\mathbf{q},\mathbf{p}} = \frac{7}{4NA^{\frac{3}{2}}} \times \left(1+\mathcal{O}(N^{-1})\right)\,. \tag{2.207}$$

For better comparison with the semiclassical discussion (see section 2.8.4), note that (2.206) also implies the relation

$$q = \frac{3\pi}{8}g \tag{2.208}$$

to the area fraction q (2.146) of the separatrix area that the lowest quantized vibrational orbit encloses.

Requantization philosophy

The general philosophy behind the requantization technique followed here is to ignore the origin of the coordinates x and ϕ, which were occupation numbers restricted to integers and angles that cannot be treated as standard quantum observables [200] in the first place. Instead the effective classical system is taken with continuous conjugate coordinates, and deep quantum corrections – missed by the semiclassical method – are introduced by replacing the coordinates by operators and solving the resulting Schrödinger-like equations for the eigenvalues η_n. Conditions like the minimization of the lowest gap $\Delta\eta = \eta_1 - \eta_0$ then correspond to specific numerical values of g. So, already at this stage considering the requantized system confirms the exact asymptotic exponents in (2.152) and (2.153) on a quantum level, since

$$\begin{aligned}
\Delta E_{\text{gap}} &= \tilde{N}\Delta\tilde{\omega} = \underbrace{\frac{2}{7}\left(\frac{7}{4g}\right)^{\frac{4}{3}}\Delta\eta}_{\text{const.}}\, N^{-\frac{1}{3}} \times \left(1+\mathcal{O}(N^{-1})\right)\,,\\
\bar{\alpha}_{\text{gap}} - 1 &= A \times \left(1+\mathcal{O}(N^{-1})\right) = \underbrace{\left(\frac{7}{4g}\right)^{\frac{2}{3}}}_{\text{const.}}\, N^{-\frac{2}{3}} \times \left(1+\mathcal{O}(N^{-1})\right)\,.
\end{aligned} \tag{2.209}$$

Justification for ignoring the conceptually problematic origin of x and ϕ [200, 201] is given by the following two considerations. First, the restriction to integer occupations is expressed as $\Delta n_0 = \mathcal{O}(1)$ so that the support of x values obeys the discretization $\Delta x = \mathcal{O}(A^{-1}N^{-1}) = \mathcal{O}(N^{\frac{-1}{3}}) \to 0$, meaning that one can asymptotically consider x as an observable $\hat{x}$ with continuous spectrum. Second, the periodicity of φ_0 in π corresponds to a periodicity of ϕ in $\pi/\sqrt{A} = \mathcal{O}(N^{\frac{1}{3}}) \to \infty$, so that one may neglect periodicity at all in order to define a corresponding observable $\hat{\phi}$.

Schrödinger equation in ϕ-representation

Instead of applying the prescription of replacing $x\phi^2$ in (2.205) by a symmetrized product of operators one can equivalently prefix a "gauging"

$$\bar{x} := x - (1-\phi^2)^2\,, \tag{2.210}$$

which sets $\bar{x} = 0$ to the η-minimum for fixed ϕ. Then the scaled energy

$$\eta = \bar{x}^2 - (1-\phi^2)^2 \tag{2.211}$$

becomes an especially simple Hamiltonian of the standard form $H = p^2 + V(q)$ with an inverted double-well potential. The Poisson bracket (2.209), which also holds for $\bar{x}$, then suggests the replacement

$$\bar{x} \mapsto \hat{\bar{x}} = \mathrm{i}g\partial_\phi \tag{2.212}$$

in ϕ-representation which yields the Schrödinger equation

$$-g^2\partial_\phi^2\psi - (1-\phi^2)^2\psi - \eta\psi = 0 \tag{2.213}$$

for stationary wave functions

$$\psi(\phi) = \langle\phi|\psi\rangle\,. \tag{2.214}$$

Unfortunately, the intriguingly simple form of the Schrödinger equation in ϕ-representation (2.213) is overshadowed by several major problems.

First, the classical values of $\bar{x}$ are restricted by a lower bound that depends on ϕ, which poses a non-trivial constraint to the Fourier modes of ψ. For example, in the outer region of the inverted double well, $|\phi| > 1$ implies $\bar{x} > 0$, so that only "left-moving" waves are allowed. One side effect of this is that some of the usual tunneling and backscattering processes between inner and outer region are suppressed *kinematically*. Although this circumstance might even have helped to improve the semiclassical description (where tunneling was not accounted for), in the quantum context it poses a major problem, because standard solution techniques cannot be applied.

Second, the inverted double well is a system without lower bound, since $V(\phi) \xrightarrow[|\phi|\to\infty]{} -\infty$. A continuum of solutions seems to be prevented by the restrictions to $\bar{x}$, which, as sort of boundary condition, in principle has the capability to constrain the quantization to a set of discrete solutions, but in a rather non-trivial way.

There are potential ways to circumvent these issues. I will superficially discuss two such possibilities in the following. The restrictions to $\bar{x}$ are strongest outside the centering well and become stronger and stronger for increasing $|\phi|$, which lies outside the classically dominant region and could be considered non-crucial for the physics. Neglecting the $\bar{x}$-constraint in the inner region leads to the possibility of interpreting it in the outer region as a condition for resonance. While this approach can only be an approximation it opens the possibility to use standard techniques and would result in discrete solutions for η. An additional simplification could be to replace the potential in the outer region by a flat one

$$V(\phi) \mapsto V_{\text{eff}}(\phi) = \begin{cases} -(1-\phi^2)^2 & : |\phi| \le 1 \\ 0 & : |\phi| > 1 \end{cases}\,, \tag{2.215}$$

so that at least a number of low-lying states (with $\eta < 0$) could be represented by bound states. Nevertheless, for the situation of minimized lowest gap, already the first excited state would correspond to a resonance again (since $\eta > 0$), but maybe one that is easier to handle than in the full potential. However, the interpretation as resonance condition can only be an approximation and furthermore the numerical search for resonances is harder, more time consuming and less stable than the search for bound states.

Those techniques were, to some extent, successfully applied, improving the semiclassical coefficients in (2.152) and (2.153). However, I will leave this approach without detailed discussion here, and instead conclude that the ϕ-representation is contraindicated to treat this problem asymptotically exactly and move on to express the problem in x-representation.

Schrödinger equation in x-representation

From the Poisson commutation relation (2.209) one infers the x-representation of the operator for the angle variable as

$$\phi \mapsto \hat{\phi} = -\mathrm{i}g\partial_x \,. \tag{2.216}$$

Two basic commutators are given by

$$\begin{aligned} [\hat{\phi}, \hat{x}] &= -\mathrm{i}g \,, \\ [\hat{\phi}^2, \hat{x}] &= -2\mathrm{i}g\phi \,. \end{aligned} \tag{2.217}$$

The correct requantization of the (dominant part of the) Hamiltonian (2.205) requires to be consistent with the process of taking the classical limit (2.50) in the first place. Following the prescription of using symmetrized operator products (2.42) to replace classical products is therefore the most reasonable way of reversing the classical limit after the manipulations on the classical level involving the small angle approximation and scaling. Applying this rule and using (2.217) gives the replacement

$$x\phi^2 \mapsto \{\hat{x}\hat{\phi}\hat{\phi}\}_{\mathrm{sym}} = \hat{x}\hat{\phi}^2 - \mathrm{i}g\hat{\phi} \,, \tag{2.218}$$

which leads to the stationary Schrödinger equation in x-representation

$$\underbrace{-2g^2\partial_x^2\psi - 2g^2\frac{1}{x}\partial_x\psi}_{\text{kinetic term}} \underbrace{-\frac{\eta}{x}\psi - 2\psi + x\psi}_{\text{potential}} = 0 \tag{2.219}$$

for the eigenfunctions

$$\psi(x) = \langle x|\psi\rangle \tag{2.220}$$

with eigenenergies η. In contrast to the representation in ϕ the restriction in x is simply given by $x \geq 0$. All that remains is to determine the boundary condition for $\psi(x)$ at $x = 0$, which has to be specified to get a discrete set of solutions and eigenenergies rather than a continuum. For this purpose investigating the $x \to 0$ limit of (2.219) brings some clarification. By keeping only the dominant η-dependent Coulomb-like potential term in (2.219) and substituting

$$y := \sqrt{\frac{2|\eta|x}{g^2}} \,, \tag{2.221}$$

one arrives at Bessel's differential equation [220, 221]

$$\left[y^2\partial_y^2 + y\partial_y + \mathrm{sgn}(\eta)y^2\right]\psi \approx 0 \tag{2.222}$$

for small x, which admits the solutions

$$\psi(x) \approx \begin{cases} c_1 I_0\left(\sqrt{2|\eta|/g^2}\sqrt{x}\right) + c_2 K_0\left(\sqrt{2|\eta|/g^2}\sqrt{x}\right) & : \eta < 0 \\ c_1 J_0\left(\sqrt{2|\eta|/g^2}\sqrt{x}\right) + c_2 Y_0\left(\sqrt{2|\eta|/g^2}\sqrt{x}\right) & : \eta > 0 \end{cases} \tag{2.223}$$

for small x, where J_0, Y_0 (I_0, K_0) are (modified) Bessel functions of order 0 of the first and second kind, respectively. The Bessel functions of the second kind are divergent at $x = 0$ as $I_0(z) \sim K_0(z) \sim \log z$ but still are normalizable. Nevertheless, they are ruled out as solutions because of a semiclassical argument. Since every quantized orbit, libration or vibration, have turning points in z (or x) at finite positive values, their semiclassical wave functions are exponentially decreasing towards $x \to 0$. Although this damping behavior might actually not be developed to a noticeable level over the short distance from classical turning point to the boundary of relevant phase space, the wave function should – at least from a semiclassical perspective – be regular in the vicinity, which contradicts a logarithmic divergence. The Bessel functions of the first kind instead are well behaved at $x \to 0$ with the asymptotic behavior

$$\psi(x) = 1 - \frac{\eta}{2g^2}x + \mathcal{O}(x^2)\,. \tag{2.224}$$

There is also a closed analytical approximate solution

$$\psi(x) \approx c_1 x^{-\frac{1}{2}} M_{-\frac{i\eta}{4g},0}\left(\frac{2\mathrm{i}}{g}x\right) + c_2 x^{-\frac{1}{2}} W_{-\frac{i\eta}{4g},0}\left(\frac{2\mathrm{i}}{g}x\right) \tag{2.225}$$

in terms of Whittaker's functions M, W [220] when taking one more sub-dominant potential-term into account, where the standard form of Whittaker's differential equation can be found using the substitution $\psi(x) = x^{-1/2}\chi(x)$. While the linear independent solutions (2.225) may be more accurate in a wider range of finite values of x, they share the same asymptotics with (2.223) for $x \to 0$ and hence do not provide any more insight into the issue of boundary conditions. Furthermore, the Whittaker-solutions still form a continuum of scattering-like states instead of discrete bound states and are therefore not able to provide any approximate information about the eigenenergies. The reason is that the crucial ingredient for the system to be bound is the most sub-dominant linear potential term $x\psi$ in (2.219), which was neglected deriving (2.225).

Ruling out the logarithmically diverging solutions by setting $c_2 = 0$ in (2.223) or (2.225) implies the mixed boundary condition

$$\psi'(0) = -\frac{\eta}{2g^2}\psi(0)\,, \tag{2.226}$$

which may be used as initial condition for numerically integrating (2.219). In practice, the boundary condition has to be implemented effectively at a short but finite distance $x > 0$ for standard iterative differential solvers to be well-defined because of the singularities in the potential at $x = 0$. For this I will use the asymptotic solutions (2.223) or even (2.225) for higher numerical accuracy

compared to the linear approximation (2.224). For a given parameter g one searches then for values of η that yield (normalizable) wave functions that do not diverge at $x \to \infty$ but instead converge to $\psi(x) \to 0$. In practice, because of finite accuracy, any numerical wave function will eventually diverge if x is chosen large enough. Therefore I fix a large value of $x = x_1$ for which the wave function is demanded to obey a certain effective boundary condition reflecting the converging behavior at infinity. The two options I applied were *i)* a Dirichlet boundary condition by fixing $\psi(x_1) = 0$ and *ii)* a mixed boundary condition by fixing $\partial_x \psi/\psi|_{x=x_1}$ to the value given by the asymptotic Airy solution in the classically forbidden region by linearization of the potential. Both methods gave comparable results with the second one being – as expected – slightly more accurate. The choice of a suitable evaluation point x_1 was as well made involving a linearization of the potential $V(x) \approx (x - x_{\mathrm{cl}})\lambda$ at the classical turning point x_{cl} yielding a characteristic approximate Airy-like behavior

$$\psi(x) \overset{x>x_{\mathrm{cl}}}{\sim} \frac{1}{\sqrt{x}} \operatorname{Ai}\Bigg(\underbrace{\left(\frac{|\eta|}{2g^2}\right)^{\frac{2}{3}} \lambda^{\frac{1}{3}}(x - x_{\mathrm{cl}})}_{\overset{!}{=} a_1} \Bigg) , \tag{2.227}$$

so that a fixed value a_1 of the argument of the Airy function Ai corresponds to a fixed characteristic suppression of the wave function, corresponding to an evaluation point

$$x_1 = x_{\mathrm{cl}} + \left(\frac{2g^2}{|\eta|}\right)^{\frac{2}{3}} \lambda^{-\frac{1}{3}} a_1 \, . \tag{2.228}$$

In the numerical calculation, I took $a_1 \approx 8$, a value for which the solutions of η were well converged in the sense that they didn't change anymore within the prescribed accuracy when increasing a_1. The same holds for other numerical parameters like the initial-value of $x \gtrsim 0$ and the number of integration steps.

The minimal gap is then found by solving for

$$g \frac{\mathrm{d}}{\mathrm{d}g} \Delta\eta(g) - \frac{4}{3} \Delta\eta(g) \overset{!}{=} 0 \, , \tag{2.229}$$

which is formally completely equivalent to the semiclassical case (2.150), just expressed in terms of g rather than q.

Applying those methods results in the values

$$\begin{aligned} g_{\mathrm{gap}}^{\mathrm{req}} &= 0.45351443(1)\ldots \, , \\ \Delta\eta_{\mathrm{gap}}^{\mathrm{req}} &= 1.0807081(1)\ldots \, , \end{aligned} \tag{2.230}$$

which yield the asymptotic scaling of the lowest energy gap

$$\Delta E_{\mathrm{gap}}^{\mathrm{req}} = \frac{2}{7} \left(\frac{7}{4g_{\mathrm{gap}}^{\mathrm{req}}}\right)^{\frac{4}{3}} \Delta\eta_{\mathrm{gap}}^{\mathrm{req}} \tilde{N}^{-\frac{1}{3}} \approx 1.8688292(4)\ldots \times N^{-\frac{1}{3}} \, , \tag{2.231}$$

$$\bar{\alpha}_{\mathrm{gap}}^{\mathrm{req}} = 1 + \left(\frac{7}{4g_{\mathrm{gap}}^{\mathrm{req}}}\right)^{\frac{2}{3}} \tilde{N}^{-\frac{2}{3}} \approx 1 + 2.46016721(3)\ldots \times N^{-\frac{2}{3}} \, . \tag{2.232}$$

With these numbers, the numerical calculation of energy gaps by exact diagonalization cannot be distinguished from the asymptotics for large N anymore.

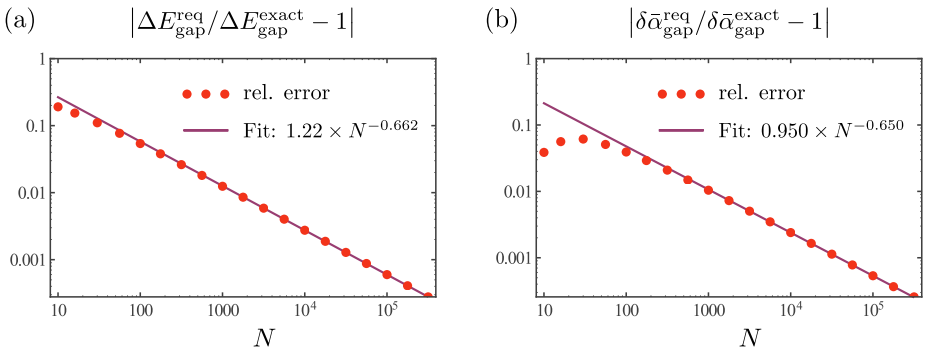

Fig. 2.18: Relative errors in the (a) gap energy $\Delta E_{\rm gap}$ and (b) correction $\bar{\alpha}_{\rm gap}-1$ to the gap location as a function of the number of particles N. It is defined as the relative deviation of the asymptotic estimates (2.231) and (2.232) by requantization compared to the corresponding quantities obtained from numerical exact diagonalization. In the investigated region of N, the relative deviation drops down without saturation. A linear fit (solid) in the doubly logarithmic plot suggests that the relative error in both cases scales as $\sim N^{-2/3}$.

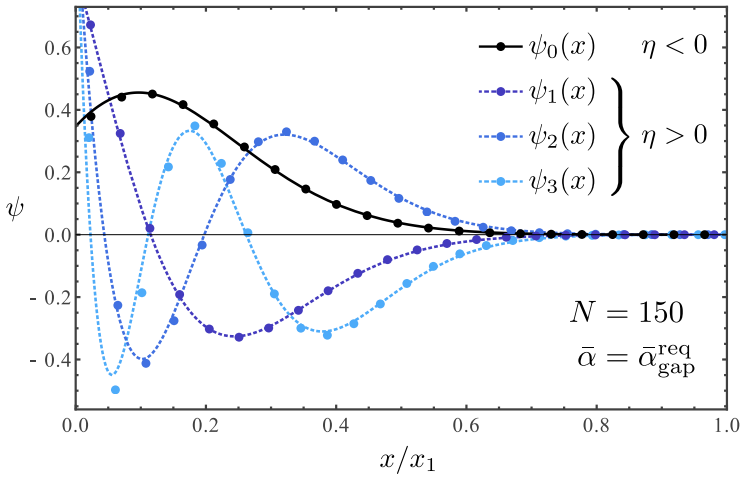

Fig. 2.19: Lowest four wave functions at the gap $\bar{\alpha}=\bar{\alpha}_{\rm gap}^{\rm req}$. Compared are the solutions of the asymptotic continuous one-dimensional Schrödinger equation (2.219) (solid for $\eta<0$ and dotted for $\eta>0$) with the discrete exact eigenvectors of the finite-dimensional Hamiltonian for $N=150$ particles (dots), normalized to $\sum_{m_0}\psi(m_0)=1$ and the corresponding continuous condition, respectively.

The excellent agreement is presented in Fig. 2.18 which shows the relative error in the asymptotics. Figure 2.19 shows the lowest wave functions using the requantization scheme compared to the discrete wave functions from exact diagonalization for $N = 150$ bosons, evaluated at the minimum gap. The excellent agreement confirms the scheme in general, and in particular that the logarithmically divergent functions have to be ruled out.

2.11 Conclusion

2.11.1 Summary

As a conclusion one can say that semiclassical methods are a successful tool to describe interacting many-body systems with a large number of constituents. Especially in predicting finite-size precursors of quantum critical behavior the EBK quantization prescription (reviewed in section 2.1) proved itself very useful. It was applied to the one-dimensional Bose gas with contact-interactions, a standard model for ultracold neutral atoms confined in quasi-one-dimensional traps, which is known for its quantum critical behavior in the thermodynamic limit in the attractive case. For more details on the experimental relevance I refer the reader to the last subsection of the introduction.

As a further approximation valid in the regime of moderate coupling strengths (including the regime of QPT) a truncation of single-particle momentum modes to the lowest three was introduced in section 2.2, which results in an integrable model, as is the untruncated, continuous model.

The integrability of the proper classical limit of the truncated model was shown in section 2.3, exhibiting three constants of motion, related to the total number of particles N, the total angular momentum L and the total energy, here all considered as continuous classical variables. An appropriately scaled version of the Hamiltonian and generalized coordinates brought up the condensate fraction z and a corresponding phase variable φ_0 as the relevant dynamical variables. In section 2.4 I discussed the relevance of an effective version of Planck's quantum of action with a special emphasis on the role of the semiclassical limit in the second-quantized context. In combination with the significance of the scaled variables z and φ_0 for the classical dynamics, the relevant parameter that characterizes "classicality" showed up as $\hbar_{\text{eff}}^{(\varphi_0,z)} = \frac{1}{N}$, clarifying that the semiclassical technique can be expected to have enhanced validity in the regime of large numbers of particles, becoming asymptotically exact in the limit $N \to \infty$, a regime where conventional numerical methods quickly become inapplicable.

A careful analysis of the classical phase space in section 2.5 revealed the restriction to a fundamental domain and the corresponding identification of boundary points that gives rise to a non-trivial topology of the six-dimensional phase space. Considering the non-interacting case by means of the EBK quantization (see section 2.5.2) clarified the relation of two of the generalized classical variables to the total number of particles N and the total angular momentum L, respectively, an identification that happens on the kinematic level and therefore directly applies to the interacting case as well. With this identification, considering N and L as fixed parameters, the phase space could be investigated in an effective one-dimensional picture, only involving z and φ_0. For vanishing total angular momentum (the case mostly considered in the literature) the classical picture of the quantum critical point (at the scaled coupling $\bar{\alpha} = 1$) was identified as the point where the classical dynamics change qualitatively. In the subcritical regime $\bar{\alpha} < 1$ the classical trajectories, called "librations", were found to be smoothly connected to the non-interacting case – indicating the adiabatic connection of the two corresponding spectra. In contrast, this is no longer true for the supercritical regime $\bar{\alpha} > 1$, which admits additional "vibra-

tions" (hallmarking the failure of perturbative expansions): a distinct class of orbits bounded by a separatrix that emerges due to a bifurcation directly at the point of QPT at $\bar{\alpha} = 1$. Furthermore, the emergence of the separatrix encloses an island of lowest energy, giving rise to a deep global energy minimum. The emergence of this classical fixed point solution – with an energy that rapidly drops off with increasing coupling – reflects the discontinuous change from a uniform gas to a bright soliton state with spontaneously broken symmetry in mean-field descriptions [22], here to be understood as *purely classical* solutions corresponding to $N \to \infty$. A generalized study of orbits for arbitrary angular momentum $L \neq 0$ (see section 2.5.4) pointed out the same qualitative behavior.

The EBK quantization technique was then first applied to the librating orbits (see section 2.6.1), which, as smooth deformations of the non-interacting case, could be understood in terms of the latter in their topological aspects. The correct restriction of the number of particles N to natural numbers and the angular momentum to $L = -N, \ldots, N$ was found as an *implication* of the EBK quantization rules rather than a presupposition. They can then be regarded as fixed parameters, leaving a single quantization rule in effective one-dimensional description similar to a WKB quantization. Furthermore, the three quantum numbers introduced could be identified as pseudo-occupation numbers in the three momentum modes, a notion that becomes increasingly fuzzed when approaching criticality (the separatrix).

After a careful geometrical analysis of the less trivial three-torus structure of vibrations in section 2.6.2 and corresponding quantization rules – again implying the expected (trivial) quantization of N and L – a single common quantum number was identified that specifies excitations for given N and L and covers both classes of quantum states, associated to librations and vibrations, respectively.

One powerful aspect of semiclassics – at a qualitative level – was found to be the identification of *finite-size* quantum criticality as *discontinuous* "jumps" of individual quantized orbits *across* the separatrix at specific critical couplings $\bar{\alpha}_j^{\mathrm{cr}} > 1$ (see Fig. 2.6), whereas these points get fuzzed to cross-over regions in direct quantum mechanical treatment.

At the quantitative level, comparisons of ground state energies with numerical calculations in section 2.7.1 confirmed the accuracy of the semiclassical method, especially for large systems $N \gtrsim 100$ (see Fig. 2.7). The comparison of the analytical low-lying spectra in section 2.7.2 gave further confirmation with an emphasis on the finite-size features in form of finite energy gaps and level bunching – a precursor of an ESQPT – of quantized orbits around the separatrix, perfectly reproduced by semiclassics, while lying out of reach of the conventional method of Bogoliubov excitations (see Fig. 2.8). This clarified one of the main strengths of semiclassical methods in the context of second-quantized many-body theories: the correct description of *finite-size* effects, corresponding to a small but finite effective quantum of action, hard to access with conventional many-body techniques like mean-field and Bogoliubov theory, which can be considered as (quasi-)classical, since they consider $N \to \infty$.

In investigating the *asymptotic* behavior for large N in section 2.8 the EBK quantization turned out to be an extremely powerful tool. This included the predicted finite-size critical couplings, Bogoliubov like low-lying excitations, the finite energy gaps around the QPT and the level spacings around the ESQPT. The power lies in the fact that the regime of large N combines *i)* the abil-

ity of extracting accurate and simple closed analytic expressions from the full semiclassical analysis with *ii)* the systematic improvement of the quality of the general method because approaching classicality, while *iii)* numerical methods become intractable. Thereby the analytical results are still finite-N properties that are beyond the reach of the more traditional $N \to \infty$ analysis using mean-field techniques [24, 25, 206, 222] and Bogoliubov approximation [26–28]. To the best of my knowledge, the correct asymptotics of the energy gap could so far not be deduced analytically in the literature.

In the case of predicting the asymptotic lowest energy gap during the QPT in section 2.8.4 the quality of the semiclassical approximation showed to have an upper bound when increasing N arbitrarily (see Fig. 2.9 and Fig. 2.10). While the scalings of the gap $\Delta E_{\mathrm{gap}}^{\mathrm{scl}} \sim N^{-1/3}$ and the associated coupling $\bar{\alpha}_{\mathrm{gap}}^{\mathrm{scl}} \sim N^{-2/3}$ could be correctly predicted, a remaining relative error in the coefficients saturated at about 10% and 1%, respectively. The reason was found to be an additional implicit scaling of the coupling strength $\bar{\alpha}$ with N, so that it cannot be considered as a constant in that situation. As a consequence, an asymptotic scaling was found that resulted in a saturation of the ratio of the typical classical actions in units of the corresponding effective $\hbar$, so that "deep quantum effects" would play a role even in the limit $N \to \infty$. In other words, the classically critical features in phase space, *i.e.*, the separatrix and the enclosed region, are scaled with N such that they are of comparable size to a single Planck cell if one stays directly at the critical point, no matter how small $\hbar_{\mathrm{eff}}^{(\varphi_0,z)}$ becomes. The energy landscape can therefore not be considered to be particularly smooth on the scale of $\hbar_{\mathrm{eff}}^{(\varphi_0,z)}$, an assumption crucial to semiclassical approximations.

To improve the description in this regime, a way of using the asymptotic scaling of the classical system was found in section 2.10 that enables to write asymptotic continuous one-dimensional Schrödinger equations by requantizing the classical phase-space variables. The intermediate step of formulating the semiclassical analogue of the original quantum system was thereby essential. Only in that picture it became explicit that the specific region of the classical phase space where the asymptotic scaling applies dominates the relevant orbit actions. After the appropriate expansion in classical observables, their subsequent requantization could be applied in a meaningful way. Furthermore, the restriction of the classical phase space due to the maximum condensate fraction $z = 1$ showed to demand special care in choosing correct boundary conditions in the effective Schrödinger equations, an issue where again semiclassical considerations helped. Direct comparison of the lowest wave functions of the effective continuous model with exact numerics in the actually discrete model showed virtually perfect agreement for $N = 150$ (see Fig. 2.19), confirming the validity of the requantization technique and the associated choice of boundary conditions. The universal dependence of the energy gap $\Delta E_{\mathrm{gap}}^{\mathrm{scl}}$ (2.231) and its location $\bar{\alpha}_{\mathrm{gap}}^{\mathrm{scl}}$ (2.232) were, by comparison to exact diagonalization, confirmed to have imperceptible error within the bounds of numerical tractability (see Fig. 2.18).

For the prediction of the asymptotics of the level bunching around the separatrix characteristic for the finite-size ESQPT, a general *universal separatrix quantization* was used in section 2.8.5. The corresponding analytical expression coincides in its dominant, logarithmically divergent term with previously known results (see, *e.g.*, [205]), while a subdominant term, related to separatrix

traversal times is non-neglectable in the finite N regime (see Fig. 2.12). To further make use of the ESQPT level bunching, an asymptotic analysis revealed that, despite the divergent DOS, the levels around the separatrix energy can be considered to be equidistant under certain circumstances. While the universal asymptotic equidistance was recognized (in other systems) before [223, 224], the necessary assumptions could here be specified and confirmed by comparison with numerics and the full semiclassical calculation (see Fig. 2.13). Moreover, the time scale associated with the (asymptotically constant) level spacing was here identified as a *local* Ehrenfest time, mimicking the Ehrenfest time of chaotic systems, where the stability exponent of the hyperbolic fixed points in this integrable system plays the role of a Lyapunov exponent. In section 2.9 this intriguing similarity of chaos and local instabilities found a striking application to information scrambling in the truncated model, which has been considered as a model for quantum black holes as condensates of soft gravitons stuck at criticality [217]. The relevant physics, determined by a quantum interaction quench of the non-interacting ground state, dominantly involve states in the vicinity of the ESQPT (see Fig. 2.14) and were here shown to meet the assumptions necessary for equidistant level spacing. A comparison with extensive numerics (see Fig. 2.15) confirmed the consequent asymptotic *periodicity* of the scrambling process and the local Ehrenfest time as its period and hence as the characteristic scrambling time (see Fig. 2.16 and Fig. 2.17). While within the bounds of numerical tractability (here $N < 10^6$) the periodicity is not yet fully developed but instead seen as a precursor, the asymptotic semiclassical analysis is not limited to any finite N. We find therefore a prediction of this feature, which crucially depends on the *finiteness* and at the same time *extreme values* of the number of particles, once again underlining the regime where second-quantized many-body semiclassical methods have their most definite potential.

2.11.2 Outlook

There are several possible directions of extending this study.

One argument for the validity of the truncation to $k = 0, \pm 1$ was the small depletion of the $k = 0$ mode. In regimes of larger couplings this depletion is still finite, thus one obvious extension would be to include the next-higher single particle momenta $k = \pm 2$ or even higher ones. Preliminary considerations have indicated that this would break integrability, resulting effectively in a partially chaotic three-dimensional system, which is not easy to treat semiclassically. Therefore it would be worth to think about effective inclusions of higher modes. When investigating effects governed by instabilities this could be to treat only the least stable direction around a fixed point or an orbit exactly while considering the other directions as effectively flattened out due to their large stability exponents [225]. This could effectively reduce again the dimensionality of the problem while the effect of higher modes would still be included.

Another way of including $|k| > 1$ would be a Born-Oppenheimer approach [226, 227], well known as adiabatic approximation in classical Hamiltonian systems, where the variables n_k, θ_k in the lower modes $k = 0, \pm$ would serve as parameters for the quantum dynamics of the higher modes, which are then solved. In a second step the quantum (or semiclassical) solution of the higher modes would then serve as an effective potential in the lower modes, altering the quantum and therefore semiclassical interactions of the truncated model.

The preliminary reason for taking this road is that the additional degrees of freedom could be considered much *faster* than the lower ones as long as the occupations in the higher modes are suppressed. Because then, their variance is expected to be small in comparison, being equivalent to narrow potential wells in those coordinates $n_{\pm 2}$, while the variance of n_0 and $n_{\pm 1}$ can be larger because of mutual transfer.

A third open question addressing the truncation and its possible extensions is whether truncations to specific cut-offs $|k| \leq k_{\max}$ could be understood within a renormalization group approach [228, 229] on a basic level. This could possibly allow to deduce renormalization group flow equations (or maybe discrete versions thereof) to relate different truncations together. Usually such approaches result in renormalizations of physical bare parameters. The hope is then to obtain a prescription how the results in the three-site-model had to be modified when increasing the cut-off to infinity.

Another modification more easy to implement would be to allow for arbitrary two-body interactions

$$\begin{aligned} \hat{U} &= \int_0^{2\pi} \mathrm{d}\theta \int_0^{2\pi} \mathrm{d}\theta' \hat{\psi}^\dagger(\theta')\hat{\psi}(\theta')\hat{\psi}^\dagger(\theta)\hat{\psi}(\theta)V(\theta'-\theta) \\ &= \sum_{klmn} \delta_{k+m,l+n}\tilde{v}_{k-l}\hat{a}_k^\dagger\hat{a}_l\hat{a}_m^\dagger\hat{a}_n \,, \end{aligned} \tag{2.233}$$

which would result in just two additional parameters (four for asymmetric potentials V) within the truncated Hilbert space. In contrast to the contact-interaction $V(\vartheta) \sim \delta(\vartheta)$, which has uniform Fourier components

$$\tilde{v}_k = \frac{1}{2\pi}\int_0^{2\pi} \mathrm{d}\vartheta V(\vartheta)\mathrm{e}^{-\mathrm{i}k\vartheta} \,, \tag{2.234}$$

characterized by a single parameter $\tilde{v}$, an arbitrary (symmetric) potential would be characterized by two additional parameters representing the deviating Fourier components $\tilde{v}_{-1} = \tilde{v}_1$ and $\tilde{v}_{-2} = \tilde{v}_2$ and would still result in an integrable model with the conservation of energy, particle number and total angular momentum untouched. While the basic properties like torus structure, elementary loops and separatrix-crossing-induced criticality are expected to stay the same on a qualitative level, this would allow to investigate the quantitative effect of finite- and long-range interactions on the quantum critical features, which has gained interest during the last years (see, *e.g.*, [230, 231]). A neat property making the study in this direction additionally tempting is that the quantitative significance of the three mode truncation increases with the range of interactions because of the duality of standard-deviations between mutual Fourier transforms.

An extension opening a relatively wide range of new questions would be to introduce non-integrability to study what happens in the presence of chaotic motion. Instead of breaking integrability by relaxing the momentum cut-off to $|k| \leq 2$ a better option to start with could be to stay in the three-site truncation but break the conservation of total angular momentum by introducing a non-uniform periodic external potential. The advantages being an effective dimensionality of two instead of three and the possibility to smoothly introducing

chaos by decreasing the homogeneity of the external potential. The question is then how the introduction of chaotic motion would affect the semiclassics on both the methodological level and also on the level of quantitative predictions. This would put special emphasis on the context of scrambling times and related local Ehrenfest times (see section 2.9), where physics is dominated by the dynamics around the separatrix and the unstable fixed points in particular. There, chaos is expected to have the strongest influence while other regions of phase space might still be governed by regular motion. In the limit of integrability the time scale is the local Ehrenfest time that is purely associated to the unstable fixed points, thus only certain specific local regions of phase space play a role. Moreover this local Ehrenfest time is at the same time the local Heisenberg time (see, *e.g.*, [107]), since it is fully determined by the smooth DOS at the separatrix energy. In contrast to that, in the opposite limit of hard chaos, the time scale is expected to be the (proper) Ehrenfest time – a non-local quantity fully determined by the Lyapunov exponent of the accessible phase space which generically differs from the Heisenberg time distinctly. It would be interesting to understand how the cross-over from a spectrally defined local quantity to a dynamically defined more global quantity takes place and if in the latter case it is still possible to establish a relation between the unstable dynamics and the level spacing.

For similar reasons as mentioned in the previous paragraph it would also be educational to study another quantity in the system, namely out-of-time-order correlators, which were first introduced by Larkin and Ovchinikov [232], revived by Kitaev [233] to study information scrambling in high energy physics, and recently received renewed interest in the many-body context [234, 235]. One version, addressable in the truncated model, would be the expectation value

$$ {}_{\mathrm{FS}}\langle 0,N,0|\left[\hat{n}_0(t),\hat{n}_0\right]^2|0,N,0\rangle_{\mathrm{FS}} \tag{2.235}$$

in the non-interacting ground state, where $\hat{n}_0 = \hat{a}_0^\dagger\hat{a}_0$ and $\hat{n}_0(t)$ is its time evolved version in the Heisenberg picture. In chaotic systems, such correlators are known to have an exponential growth [236] up to the Ehrenfest time with the characteristic time-scale also given by the Ehrenfest time associated with the Lyapunov exponent of the system. This behavior, especially in view of the saturation after the Ehrenfest time, has been observed numerically [237], suspected using analytical arguments [238] and recently could be deduced more rigorously with semiclassical methods [239] using generalized Sieber-Richter loops [73]. Similarly to the discussion of scrambling times, the physics here centers on dynamical instabilities influencing the non-interacting ground state. Therefore a behavior similar to chaos is expected in the integrable model and indeed, preliminary work confirms this [240] quite accurately with the local Ehrenfest time (2.162) showing up again.

Final conclusion

To summarize this work into a general statement, one can say that semiclassical methods have proved to provide a major tool for describing systems of interacting identical particles in situations that are hard to address otherwise.

On the one hand this includes the few-body regime, usually hard to access because many-body techniques do not apply, while the number of particles may be already too large to admit tractability in a fully quantum-mechanical treatment.

On the other hand, systems comprising large finite numbers of particles can show non-trivial effects due to their finiteness, especially in the presence of quantum criticality. There, semiclassical methods can provide physical comprehensibility, analytical feasibility and accuracy unrivaled by usual many-body techniques. This superiority is pushed to an extreme directly at quantum criticality, where treatments within mean-field approaches supported by quasi-particle excitations are doomed to break down.

These two regimes were here addressed by different approaches, providing complementary perspectives. Complete summaries of the presented work on these approaches, pointing out their strengths (and also weaknesses) and including extensive outlooks on future perspectives are given in section 1.7 and section 2.11, respectively.

The few-particle sector was covered by the quantum cluster expansion (QCE) based on first quantization with a focus on a specific kind of universality that can equivalently be understood as reducing *i)* spectra to their smooth counterparts or *ii)* quantum dynamics to their short-time behavior, creating a framework especially suitable for mutual short-range interactions. This kind of universality was shown to boil down the physics just as much to render non-soluble systems effectively solvable in these "coarse" quantities, making the two classes equally accessible.

In the many-body sector a complementary view was provided by the semiclassical method of Einstein-Brillouin-Keller (EBK) quantization within a second-quantized description. The focus of this approach on system specific properties, capable to predict individual discrete many-body levels and related effects, relies on the integrability of the underlying classical system.

While both approaches are in principle applicable to a wider set of systems, explicit calculations were performed in the case of contact interactions in one dimension, especially relevant for experiments with cold neutral atoms.

The overall conclusion is that semiclassical methods provide a bridge in systems of interacting particles. This bridge is similar to the one supplied by single-particle semiclassics, albeit different from it in a crucial point.

The semiclassical treatment of single-particle systems addresses the intermediate region between classical and quantum mechanics, parametrized by *Planck's constant* $\hbar$, assumed to be *small compared to typical classical actions*. It provides a picture of quantum effects in terms of the underlying classical dynamics and at the same time provides analytical feasibility for accurate descriptions of complex quantum systems in a certain regime: The main target are mesoscopic quantum systems that are hard to treat fully quantum mechanically because of their complexity and where (quasi-)classical descriptions are insufficient.

In the present context of interacting systems, the semiclassical approaches proved to provide this bridge in a different manner. Instead of addressing the intermediate layer between the micro- and the macroworld, reflected by the relation of $\hbar$ and typical classical actions, the major strength here lies in describing interacting systems in the regime of *intermediate numbers of particles*.

Altogether, this brings us back to the fascinating subject of reductionism, addressing the question about how simple effective descriptions of systems with macroscopically large numbers of particles emerge from an underlying fundamental theory, and especially what happens in between. Indeed, it is this intriguing zone between layers of abstraction where we find the potential of many-body semiclassics: closing the gap at the lower end, where the complexity starts to deny comprehension from the bottom layer and at the upper end, where the simple elementary mechanisms of the top layer are just not yet fully emerged.

Appendix

A Formalization of cluster structures

A.1 Symbolic classification of cluster structures

First, a *multi-cluster structure* is defined as an ordered sequence

$$\tilde{\mathfrak{C}} = c_1 \quad c_2 \quad \cdots \quad c_l \tag{A.236}$$

of (symmetry-related) *symbolic cycle structures*, which are tuples

$$c_i = \left[c_i^{(1)} \quad c_i^{(2)} \quad \cdots \quad c_i^{(n_i)} \right], \tag{A.237}$$

that correspond to cyclic propagations due to the cycles σ_i in the decomposition (1.36) of a particular permutation P, where n_i is the length of a cycle[1]. I denote the membership relation between a cycle structure and a multi-cluster structure by

$$c \in \tilde{\mathfrak{C}}\,. \tag{A.238}$$

The same cycle structure c may appear multiple times in $\tilde{\mathfrak{C}}$. These are counted multiple times whenever (A.238) appears as a specifier for sums as in

$$\sum_{c \in \tilde{\mathfrak{C}}} f(c) \coloneqq \sum_{i=1}^{l} f(c_i)\,, \tag{A.239}$$

using the specific notation (A.236). The symbolic cycle structures comprise index pairs

$$c_i^{(j)} = (u,k) \in \mathbb{N} \times \mathbb{N} \quad \forall i = 1, \ldots, l\,, \quad j = 1, \ldots, n_i\,. \tag{A.240}$$

The meaning of these index pairs is that u represents the order or size of an Ursell contribution $\Delta K^{(u)}$ (1.102) and k is an index for different Ursell contributions of the same size u. The index pairs (A.240) are further called *symbols*. The multiplicity of a particular symbol in the multi-cluster structure $\tilde{\mathfrak{C}}$ (A.236) is

$$m_{\tilde{\mathfrak{C}}}((u,k)) \coloneqq \sum_{i=1}^{l} \sum_{j=1}^{n_i} \delta_{c_i^{(j)},(u,k)}\,, \tag{A.241}$$

[1] To be precise, the permutation that is related to a multi-cluster structure is the restriction $P|_I$ of a permutation $P \in S_N$ to a subset $I \subseteq \{1, \ldots, N\}$ of particle indexes that is closed in the sense that it represents itself a permutation $P|_I \in S_{|I|}$ on the index subset. To reduce notation, I will simply write P when actually $P|_I$ is meant.

where the number of cycles l and the cycle lengths n_i are defined through (A.236) and (A.237) for a specific structure $\tilde{\mathfrak{C}}$. The Kronecker delta for symbols has to be understood as

$$\delta_{(u,k),(u',k')} = \delta_{uu'}\delta_{kk'} \,. \tag{A.242}$$

For $\tilde{\mathfrak{C}}$ to be a valid multi-cluster structure one has to demand the consistency restriction

$$m_{\tilde{\mathfrak{C}}}((u,k)) \in \{0,u\} \quad \forall (u,k) \in \mathbb{N}\times\mathbb{N}\,, \tag{A.243}$$

which simply expresses that each Ursell contribution (indexed by k) of order or size u involves exactly u particles. With this definition of multi-cluster structures an (irreducible) *cluster structure* $\mathfrak{C}$ is defined as a multi-cluster structure that is inseparable in the sense that

$$\begin{gathered} \mathfrak{C} \text{ is a valid (irreducible) cluster structure} \\ \Updownarrow \\ (\nexists \mathfrak{C}_{\text{sub}} \subset \mathfrak{C})(\mathfrak{C}_{\text{sub}} \text{ is a valid multi-cluster structure})\,, \end{gathered} \tag{A.244}$$

where the inclusion relation $\mathfrak{C}_{\text{sub}} \subset \mathfrak{C}$ is defined as set inclusion of sequences perceived as multisets with additionally prescribing that the order of elements in $\mathfrak{C}_{\text{sub}}$ is also found in $\mathfrak{C}$. The number of particles involved in a cluster-structure is the *size* of the cluster defined by the notation

$$|\mathfrak{C}| \coloneqq \sum_{c\in\mathfrak{C}} |c| = \sum_{i=1}^{l} n_i \,, \tag{A.245}$$

where $|c_i| = \left|\left[\, c_i^{(1)} \quad \cdots \quad c_i^{(n_i)} \,\right]\right| \equiv n_i$ denotes the length of a cycle c_i. I denote the number of cycles in a cluster by

$$l(\mathfrak{C}) \coloneqq l \tag{A.246}$$

in the above notation (A.236) and (A.237).

I further define an equivalence relation on cluster structures that represent the same cluster diagram. The equivalence originates in equivalence relations in a three-fold way. First, renaming the indexes k of interaction effects by

$$(u,k) \mapsto (u, f_u(k)) \tag{A.247}$$

with some bijective *symbolic renaming* $f_u : \mathbb{N} \to \mathbb{N}$ for each order u, does not change the corresponding diagram. Second, a cyclic permutation

$$\left[\, c_i^{(1)} \quad c_i^{(2)} \quad \cdots \quad c_i^{(n_i)} \,\right] \mapsto \left[\, c_i^{(2)} \quad \cdots \quad c_i^{(n_i)} \quad c_i^{(1)} \,\right] \tag{A.248}$$

of symbols in any cycle structure $c_i \in \mathfrak{C}$ does not change a diagram. Third, interchanging the order of whole cycle structures in the sequence $\mathfrak{C}$ by $c_i \leftrightarrow c_j$ does not change the corresponding diagram. Because the so-defined equivalence exactly mirrors the equivalence of cluster diagrams one may identify cluster diagrams and (equivalence classes of) symbolic cluster structures directly, so that diagrams may be denoted with the corresponding $\mathfrak{C}$.

As a notation, symbols (u,k) may be identified with the variable s and also be written in a subscript form

$$s \coloneqq u_k \coloneqq (u,k)\,. \tag{A.249}$$

According to this identification the variables u or k may sometimes be understood as unique functions $u(s)$ and $k(s)$ of s. For $u = 1$ one can also omit the index k, so that the symbol 1 is used instead of 1_k, since for particles that are propagating independently no association to specific interaction effect contributions $\Delta K^{(n)}$ is needed. Figure 1.11 shows a selection of examples of irreducible cluster diagrams together with their symbolic cluster structures.

To be able to translate cluster diagrams of a given structure $\mathfrak{C}$ to formal expressions in general I introduce one last notational ingredient. Each element $c_i^{(j)}$ of each cycle c_i in $\mathfrak{C}$ gets associated a unique particle index specified by the pair (i, j), where i indexes the position of the containing cycle structure in the cluster structure and j indexes the position of the symbol in the cycle. Thus a pair (i, j) is identified as a single-particle index. I denote the set of all particle indexes (i, j) in a cluster structure by

$$I(\mathfrak{C}) = \bigcup_{i=1}^{l(\mathfrak{C})} \bigcup_{j \in \mathbb{Z}/n_i\mathbb{Z}} \{(i, j)\} . \tag{A.250}$$

Choosing the indexation within each cycle to form the (additive) group of integers modulo n_i rather than natural numbers accounts for its cyclic nature by imposing the cyclic property

$$(i, j + n_i) = (i, j) \tag{A.251}$$

as equivalence relation (on $j \in \mathbb{Z}$), which simplifies further notation[2]. I denote the spatial location of the particle specified by the index (i, j) as

$$\mathbf{q}_{(i,j)} . \tag{A.252}$$

Each symbol $s = u_k$ appears u times in $\mathfrak{C}$ at positions denoted by

$$I_s(\mathfrak{C}) = \{(i_1^s, j_1^s), (i_2^s, j_2^s), \dots (i_u^s, j_u^s)\} . \tag{A.253}$$

With this set of notations, the amplitude from a single irreducible diagram specified by its cluster structure $\mathfrak{C}$ is given by

$$\begin{aligned} \mathcal{A}_{\mathfrak{C}}(t) = & \left[\prod_{(i,j) \in I(\mathfrak{C})} \int_\Omega \mathrm{d}^D q_{(i,j)} \right] \\ & \times \prod_{\substack{s \in \mathbb{N} \times \mathbb{N} \\ m_{\mathfrak{C}}(s) \neq 0}} \Delta K^{(u)}\big((\mathbf{q}_{(i_1^s, j_1^s + 1)}, \dots, \mathbf{q}_{(i_u^s, j_u^s + 1)}), (\mathbf{q}_{(i_1^s, j_1^s)}, \dots, \mathbf{q}_{(i_u^s, j_u^s)}); t\big) . \end{aligned} \tag{A.254}$$

The consequences of clustering under the assumption of short-time dynamics explained in section 1.2.2 allow for relaxing the domains of integration Ω to full space $\mathbb{R}^D$ in all integrals except one. This is in particular true in the absence of an external potential, where the latter one yields a factor V_D because of

[2] The case $n_i = 1$ is included as the trivial group $Z_1 = \{0\}$, where all integers $j \in \mathbb{Z}$ are identified as a single element, *i.e.*, $\dots = -2 = -1 = 0 = 1 = 2 = \dots$.

translational invariance:

$$\mathcal{A}_{\mathfrak{C}}(t) = V_D \left[\prod_{\substack{(i,j)\in I(\mathfrak{C}) \\ (i,j)\neq(1,1)}} \int_{\mathbb{R}^D} \mathrm{d}^D q_{i,j} \right] \times \prod_{\substack{s\in\mathbb{N}\times\mathbb{N} \\ m_{\mathfrak{C}}(s)\neq 0}} \Delta K^{(u)}\big((\mathbf{q}_{(i_1^s,j_1^s+1)},\dots,\mathbf{q}_{(i_u^s,j_u^s+1)}),(\mathbf{q}_{(i_1^s,j_1^s)},\dots,\mathbf{q}_{(i_u^s,j_u^s)});t\big) \,. \tag{A.255}$$

As discussed in section 1.4.2, a similar statement holds when smooth external potentials are included. The contributions $\mathcal{A}_{\mathfrak{C}}$ from a specific internal cluster structure can then be related back to the corresponding *unconfined* expression (A.255). This happens by virtue of a separation (1.206) into an *external* part (1.208) and an *internal* part (1.207), where the latter only depends on the cluster structure and is equivalent in the confined and unconfined case. Thus, the formalized value of cluster diagrams in the presence of a smooth external potential does not have be stated explicitly.

A.2 Multiplicity of irreducible clusters

In order to make the calculus applicable up to the explicit calculation of irreducible cluster diagrams by virtue of (1.110) and (1.111), the last thing that has to be clarified are the combinatorics involved due to multiplicities of equivalent cluster structures (or synonymously equivalent diagrams) appearing in (1.109). Different permutations P and partitions $\mathfrak{I}$ into interaction effects can yield equivalent diagrams $\mathcal{A}_{\mathfrak{C}}$ and therefore have to be counted with their multiplicities. These multiplicities are already partially absorbed in the combinatorial factors $c_{\mathfrak{N}}^{(N)}$ in (1.110) related to the partitioning in whole clusters. The exact definition (1.46) of the coefficients $c_{\mathfrak{N}}^{(N)}$ is inspired by the non-interacting case, where it fully accounts for the multiplicity of clusters (which are given by non-interacting n-cycles). The additional diagrams of size n including interaction effects in general have multiplicities that differ from that, which is accounted for by the purely combinatorial factor $M_{\mathfrak{C}}$ in (1.111). For specific cluster structures $\mathfrak{C}$ the multiplicities and correspondingly $M_{\mathfrak{C}}$ have to be unraveled in detail.

The first step is to clarify the role of $c_{\mathfrak{N}}^{(N)}$. Consider the partition function as a sum over all possible (separable or irreducible) multi-cluster diagrams $\tilde{\mathfrak{C}}$ of all N particles. Consider the simple case that such a diagram comprises cluster diagrams that are all mutually distinct. The sizes of the clusters correspond to an integer partition $\mathfrak{N}$ of N. The multiplicity of the full diagram is then partially given by the distribution of particle indexes $1,\dots,N$ among the individual clusters, because distinct distributions of particle labels for sure give contributions of equivalent value but must correspond to distinct choices of P and/or $\mathfrak{I}$. The number of possible distributions of indexes is then determined by the sizes $n \in \mathfrak{N}$ of the clusters. The number of ways to simultaneously assign sets $i_1,\dots,i_n$ of labels to all clusters is given by the multinomial coefficient

$$\binom{N}{\mathbf{n}} = \frac{N!}{\prod_{n\in\mathfrak{N}} n!} \,. \tag{A.256}$$

The next step is to generalize to the case that some of the individual clusters may be equivalent. Then interchanging all labels of two equivalent clusters is over-counted because it does not correspond to distinct P and/or $\mathfrak{I}$. I will refer to this as *pseudo-relabeling* or *non-essential relabeling*. To account for that one has to correct with a factor

$$\frac{1}{\prod_{\mathfrak{C}} m(\mathfrak{C})!} \tag{A.257}$$

given by the multiplicities $m(\mathfrak{C})$ of equivalent (irreducible) clusters $\mathfrak{C}$ in the full diagram. Because a stronger way to combinatorially organize all possible contributions is by the *sizes* n of the individual clusters only rather than their explicit structure $\mathfrak{C}$, one has to account for the over-counting of equivalent diagrams using the multiplicities $m_{\mathfrak{N}}(n)$ of their sizes by the factor

$$\frac{1}{\prod_{n\in\mathfrak{N}} m_{\mathfrak{N}}(n)!} \tag{A.258}$$

rather than (A.257). But then clusters of same size n but different structure would falsely identified as pseudo-relabelings. This deficiency is corrected automatically in the overall sum of all possible diagrams of N particles. The reason is that after organizing the sum by cluster sizes, for each size n one needs a sum $\mathcal{A}_n = \sum_{\mathfrak{C}}(\ldots)\mathcal{A}_{\mathfrak{C}}$ of all cluster diagrams of this size (with some at the moment unspecified coefficients). If the size n has a multiplicity $m = m_{\mathfrak{N}}(n)$ in the partition $\mathfrak{N}$, then the sum of diagrams appears with power m. A product of particular cluster structures appearing as a summand in the expanded power $\mathcal{A}_n^m$ comes with the multinomial coefficient

$$\binom{m}{\mathbf{m}} = \frac{m!}{m_1!m_2!m_3!\cdots} = \frac{m_{\mathfrak{N}}(n)!}{\prod_{\mathfrak{C}} m(\mathfrak{C})!}\,, \tag{A.259}$$

where the m_i are now multiplicities of equivalent cluster diagrams, which together with (A.258) combines to the proper correction (A.257) accounting for multiplicities of equivalent clusters. All in all one ends up with a factor

$$\frac{N!}{\prod_{n\in\mathfrak{N}} n! \prod_{n=1}^{N} m_{\mathfrak{N}}(n)!} = c_{\mathfrak{N}}^{(N)} \frac{1}{\prod_{n\in\mathfrak{N}}(n-1)!} \tag{A.260}$$

that accounts for multiplicity coming from *distributing particle labels* among clusters. What is left to unravel is the multiplicity of diagrams beyond this distribution of labels. What one has to count is the number of distinct permutations P and interaction effect partitions $\mathfrak{I}$ that lead to the same multi-cluster diagram given a fixed set of labels $\{i_1,\ldots,i_n\}$ for each n-cluster.

Since clusters are defined as the objects that are not coupled by P or $\mathfrak{I}$, the restrictions $P|_{\{i_1,\ldots,i_n\}}$ and $\mathfrak{I}|_{\{i_1,\ldots,i_n\}}$ to a particular n-cluster are themselves permutations and partitions in the set of particle indexes of the isolated cluster. Two (global) permutations P (or partitions $\mathfrak{I}$) of all N particles in a specific clustering $\mathfrak{N}$ together with distribution of particle labels among the clusters are then distinct if and only if any of their restrictions $P|_{\{i_1,\ldots,i_n\}}$ (or $\mathfrak{I}|_{\{i_1,\ldots,i_n\}}$) to the individual clusters are distinct. This allows us to determine the multiplicity cluster by cluster. Thus we proceed by considering a single cluster of size $|\mathfrak{C}| = n$. I relax notation by simply writing P and $\mathfrak{I}$ for the restrictions and set the particle indexes to $(i_1,\ldots,i_n) = (1,\ldots,n)$ without loss of generality. A crucial

point to understand the further combinatorics is to recognize that equivalent contributions in $\sum_P \sum_{\mathfrak{I}}$ regarding a single specific n-cluster diagram can only correspond to the internal relabeling of particles. Thus, one has to count the ways of internal relabelings and address the question of how many of those relabelings correspond to distinct contributions in the sense that either the associated P or $\mathfrak{I}$ (or both) are distinct. This will be called the number of *essential relabelings* $\#_{P,\mathfrak{I}}(\mathfrak{C})$ whereas relabelings that correspond to the same P and $\mathfrak{I}$ will be referred to as *non-essential* or *pseudo-relabelings*. The easiest case is a non-interacting cluster, which comprises a single cycle of length n where out of the $n!$ relabelings always n correspond to the same cyclic permutation and are therefore non-essential. Therefore the number of essential relabelings for a non-interacting cluster is $(n-1)!$. This number is already absorbed into the factor $c_{\mathfrak{N}}^{(N)}$, compensating for the second factor in (A.260). Therefore the remaining combinatorial factor in (1.111) is given by

$$M_{\mathfrak{C}} = \frac{\#_{P,\mathfrak{I}}(\mathfrak{C})}{(|\mathfrak{C}|-1)!}\,. \tag{A.261}$$

I factorize the number of essential relabelings

$$\#_{P,\mathfrak{I}}(\mathfrak{C}) = \#_P(\mathfrak{C}) \cdot \#_{\mathfrak{I}}^{(P)}(\mathfrak{C}) \tag{A.262}$$

into the number $\#_P(\mathfrak{C})$ of relabelings that yield distinct permutations P and the number $\#_{\mathfrak{I}}^{(P)}(\mathfrak{C})$ of relabelings yielding distinct interaction effect partitions $\mathfrak{I}$ under the constraint of a fixed particular permutation P.

Considering distinction of permutations only depends on the cycle lengths in the cluster structure $\mathfrak{C}$ rather than the symbol content and is, equivalently to the non-interacting case, given by

$$\#_P(\mathfrak{C}) = \frac{|\mathfrak{C}|!}{\prod_{c\in\mathfrak{C}} |c| \prod_{\nu=1}^{|\mathfrak{C}|} m_{\mathfrak{C}}(\nu)!}\,, \tag{A.263}$$

where $|c|$ is again the length of the cycle c and $m_{\mathfrak{C}}(\nu)$ denotes the multiplicity of the cycle length ν in the cluster $\mathfrak{C}$.

For the considerations on $\#_{\mathfrak{I}}^{(P)}(\mathfrak{C})$, without loss of generality, one can specify a unique particle labeling in an ordered form of the cycle decomposition of P:

$$\begin{aligned} P = {} & \big(1\big)\big(2\big)\cdots\big(m_1\big) \\ & \underbrace{\big(m_1+1 \;\; m_1+2\big)\cdots\big(\circ \;\; \circ\big)}_{m_2} \\ & \underbrace{\big(m_1+2m_2+1 \;\; m_1+2m_2+2 \;\; m_1+2m_2+3\big)\cdots\big(\circ \;\; \circ \;\; \circ\big)}_{m_3} \\ & \cdots\,. \end{aligned} \tag{A.264}$$

Now I assign the symbolic cycle structures $c_i = \big[\cdots\big]$ in $\mathfrak{C}$ to the cycles in (A.264) matching the sizes of cycles which represents a particular grouping of the specified particle indexes in (A.264) corresponding to $\mathfrak{I}$. The assignment allows for exchanges of symbolic cycle structures of same size as a whole and for cyclic permutations of symbols inside each cycle structure. Non-cyclic

permutation inside cycle structures are not allowed because they would correspond to non-equivalent clusters. As an example take the cluster structure $\mathfrak{C} = \left[3_1\right]\left[2_1\right]\left[1\ \ 3_1\right]\left[2_2\ \ 2_1\right]\left[2_2\ \ 1\ \ 3_1\right]$ with two possible assignments

$$\begin{array}{rccccc} P: & \left(1\right) & \left(2\right) & \left(3\ \ 4\right) & \left(5\ \ 6\right) & \left(7\ \ 8\ \ 9\right) \\ \text{Assignment a}: & \left[2_1\right] & \left[3_1\right] & \left[2_1\ \ 2_2\right] & \left[3_1\ \ 1\right] & \left[1\ \ 3_1\ \ 2_2\right] \\ \text{Assignment b}: & \left[3_1\right] & \left[2_1\right] & \left[2_1\ \ 2_2\right] & \left[3_1\ \ 1\right] & \left[2_2\ \ 1\ \ 3_1\right], \\ \vdots & \vdots & \vdots & \vdots & \vdots & \vdots \end{array}$$

where vertical alignment represents the assignment. By this way of assigning symbolic cycle structures one ensures to access all possible relabelings of equivalent diagrams constrained to the specified P. The question is what is the number of essential assignments in the sense that they correspond to distinct interaction partitions $\mathfrak{I}$. Since the particle labels where specified (A.264) two assignments correspond to the same partition $\mathfrak{I}$ if and only if they are pure symbolic renamings (A.247) of each other without changing the order in the whole sequence of symbols. The number of cluster relabelings $\#_{\mathfrak{I}}^{(P)}(\mathfrak{C})$ corresponding to distinct interaction effect groupings with fixed permutation P is then given as the number of distinct assignments in this sense. As an example take the cluster structure $\mathfrak{C} = \left[2_1\right]\left[2_2\right]\left[2_1\ \ 2_2\right]$ with its four possible assignments

$$\begin{array}{rccc} P: & \left(1\right) & \left(2\right) & \left(3\ \ 4\right) \\ \text{Assignment a}: & \left[2_1\right] & \left[2_2\right] & \left[2_1\ \ 2_2\right] \\ \text{Assignment b}: & \left[2_2\right] & \left[2_1\right] & \left[2_1\ \ 2_2\right] \\ \text{Assignment c} \sim \text{ b}: & \left[2_1\right] & \left[2_2\right] & \left[2_2\ \ 2_1\right] \\ \text{Assignment d} \sim \text{ a}: & \left[2_2\right] & \left[2_1\right] & \left[2_2\ \ 2_1\right], \end{array} \tag{A.265}$$

where the assignments c and d are pure symbolic renamings of the assignments b and a, respectively. Therefore the cluster of example (A.265) has a factor $\#_{\mathfrak{I}}^{(P)}(\mathfrak{C}) = 2$.

In most cases it is probably easiest to factorize this number into the number of distinct (combined) cyclic permutations in the cycle structures c_i and the number of (strongly) distinct reorderings of cycle structures of equal size. The distinction of reorderings is thereby stronger in the sense that two reorderings are understood to be equivalent if they are symbolic renamings of each other after additional arbitrary cyclic permutation in the cycle structures. I express this separation by adopting these textual definitions without further formalization:

$$\begin{aligned} \#_{\mathfrak{I}}^{(P)}(\mathfrak{C}) = {} & \#\text{distinct cyclic permutations in cycle structures} \\ & \times \#\text{strongly distinct reorderings of cycle structures}\,. \end{aligned} \tag{A.266}$$

Furthermore, in most cases the number of distinct simultaneous cyclic permutations may easiest be obtained by counting cyclic permutations for individual cycles, multiplying them and accounting for overall symbolic renamings in the cluster. Each individual symbolic cycle contributes as factor the number of its cyclic permutations that do not give the *exact* same symbolic sequence (without renaming!). This distinction that does not take into account symbolic renaming will be called *weak distinction*. To account for symbolic renamings

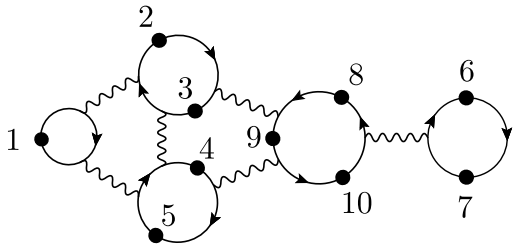

Fig. A.20: An example of an irreducible cluster comprising ten particles. Each particle is here associated with a (nonirrelevant) specific particle index to clarify the association with the symbolic cluster structure (see text).

the product gets divided by the number of renamings that yield sequences that are accessible through (combined) cyclic permutations in all cycles (but without allowing reordering). Again, I express this additional separation by adopting textual definitions:

$$\#_{\mathfrak{J}}^{(P)}(\mathfrak{C}) = \frac{\prod_{c\in\mathfrak{C}} \#\text{weakly distinct cyclic permutations in } c}{\#(\text{symbolic renamings} = \text{combined cyclic permutations})} \times \#\text{strongly distinct reorderings of cycle structures}\,. \tag{A.267}$$

By combination of (A.261), (A.262) and (A.263) one gets the expression for the multiplicity factors

$$M_{\mathfrak{C}} = \frac{|\mathfrak{C}|}{\prod_{c\in\mathfrak{C}} |c| \prod_{\nu=1}^{n} m_{\mathfrak{C}}(\nu)!} \#_{\mathfrak{J}}^{(P)}(\mathfrak{C})\,, \tag{A.268}$$

where the last term has to be taken from one of the equivalent forms (A.266) or (A.267).

All in all, one ends up with formulae (1.110) and (1.111) together with the integral expressions (A.255) for irreducible cluster diagrams and their multiplicity factors given by (A.268). The factor $(\pm 1)^{l(\mathfrak{C})-1}$ thereby accounts for the correct sign of the overall permutation $P \in S_N$, which depends only on the total number of cycles l by virtue of the identity $(-1)^P = (-1)^{N-l}$.

As an important example, the complete set of possible irreducible three-clusters including their symbolic cluster structures and the related combinatoric factors is shown in Fig. 1.12 of the main text.

A.3 An illustrative example

To further clarify the symbolics and corresponding combinatorics consider the example of a irreducible ten-particle cluster shown in Fig. A.20. The corresponding symbolic cluster $\mathfrak{C}$ together with an association to the specified (irrelevant) particle indexes and a specification of cycle-structure names c_i is

$$\begin{array}{rccccc} \text{indexes} & \left(1\right) & \left(2\ \ 3\right) & \left(4\ \ 5\right) & \left(6\ \ 7\right) & \left(8\ \ 9\ \ 10\right) \\ \mathfrak{C} = & \left[3_1\right] & \left[2_1\ \ 3_1\right] & \left[2_2\ \ 3_1\right] & \left[1\ \ 2_3\right] & \left[2_1\ \ 2_2\ \ 2_3\right] \\ \text{cycle names} & c_1 & c_2 & c_3 & c_4 & c_5\,. \end{array} \tag{A.269}$$

The number of constituents is $n = |\mathfrak{C}| = 10$, while the number of cycles is $l(\mathfrak{C}) = 5$. In the following, the multiplicity factor of this cluster is calculated

with the above recipe in detail. The cycle lengths are $|c_1|, \ldots, |c_5| = 1, 2, 2, 2, 3$ and have multiplicities $m_{\mathfrak{C}}(1) = 1$, $m_{\mathfrak{C}}(2) = 3$ and $m_{\mathfrak{C}}(3) = 1$. The formula for the number of distinct permutations (A.263) gives therefore

$$\#_P(\mathfrak{C}) = \frac{10!}{1 \times 2^3 \times 3 \times 3!}\,. \tag{A.270}$$

To calculate the number $\#_{\mathfrak{I}}^{(P)}(\mathfrak{C})$ of distinct interaction partitions under constrained permutation, I choose to evaluate using formula (A.267). In this case, for each individual cycle, every cyclic permutation of symbols yields a distinct symbolic sequence, hence

$$\begin{array}{rccccc} \text{cycle } c: & c_1 & c_2 & c_3 & c_4 & c_5 \\ \#\text{weakly distinct cyclic permutations in } c: & 1 & 2 & 2 & 2 & 3\,. \end{array} \tag{A.271}$$

To count the number of symbolic renamings, one has to consider exchanging the symbols $2_1, 2_2, 2_3$ simultaneously for the whole cluster. None of these renamings corresponds to a combined cyclic permutation of symbols in the cycles c_i. To clarify this a bit more, consider the renaming $2_1 \mapsto 2_2, 2_2 \mapsto 2_3, 2_3 \mapsto 2_1$, which produces the cluster structure $\mathfrak{C}' = \big[3_1\big]\big[2_2\ \ 3_1\big]\big[2_3\ \ 3_1\big]\big[1\ \ 2_1\big]\big[2_2\ \ 2_3\ \ 2_1\big]$. Despite the fact that this renaming yields a cyclic permutations of c_5 (and c_1) if considered as an isolated object, the same is *not* true for all cycle structures simultaneously:

$$\begin{array}{rccccc} \mathfrak{C}' = & \big[3_1\big] & \big[2_2\ \ 3_1\big] & \big[2_3\ \ 3_1\big] & \big[1\ \ 2_1\big] & \big[2_2\ \ 2_3\ \ 2_1\big] \\ & \updownarrow \text{cyc. } P & \updownarrow \text{no cyc. } P & \updownarrow \text{no cyc. } P & \updownarrow \text{no cyc. } P & \updownarrow \text{cyc. } P \\ \mathfrak{C} = & \big[3_1\big] & \big[2_1\ \ 3_1\big] & \big[2_2\ \ 3_1\big] & \big[1\ \ 2_3\big] & \big[2_1\ \ 2_2\ \ 2_3\big]\,. \end{array} \tag{A.272}$$

Therefore, one gets

$$\#(\text{symbolic renamings} = \text{combined cyclic permutations}) = 1\,. \tag{A.273}$$

The last ingredient is the number of strongly distinct reorderings of cycle structures. The only reordering that has to be checked for possibly yielding cluster structures that are not strongly distinct is the interchange of c_2 and c_3:

$$\cdots\big[2_2\ \ 3_1\big]\big[2_1\ \ 3_1\big]\cdots \mapsto \cdots\big[2_1\ \ 3_1\big]\big[2_2\ \ 3_1\big]\cdots\,. \tag{A.274}$$

To fulfill the criterion for not being counted as strongly distinct reorderings of each other, they should correspond to a symbolic renaming and subsequent cyclic permutation in the cycle structures. The renaming that would swap the two cycle structures c_2 and c_3, is $2_1 \leftrightarrow 2_2$. Since this renaming transfers the fifth cycle $c_5 \mapsto \big[2_2\ \ 2_1\ \ 2_3\big]$, which is a *non-cyclic* permutation, the criterion is not met, hence all the reorderings count distinctly and one gets

$$\#\text{strongly distinct reorderings of cycle structures} = 3!\,. \tag{A.275}$$

Combining (A.271), (A.273) and (A.275) using (A.267) gives

$$\#_{\mathfrak{I}}^{(P)}(\mathfrak{C}) = \frac{1 \times 2^3 \times 3}{1} \times 3!\,. \tag{A.276}$$

Multiplying with (A.270) yields the number of essential relabelings (A.262)

$$\#_{P,\mathfrak{I}}(\mathfrak{C}) = 10!\,. \tag{A.277}$$

The final result for the multiplicity factor using (A.261) is

$$M_{\mathfrak{C}} = 10\,. \tag{A.278}$$

B Numerically stable representation of $F_{\bar{\nu}}(s)$

The integral given in (1.159) is subject to numerical instability for large values of the thermal interaction strength s. The reason are (multiplicative) large cancellations between the exponentially growing prefactor with the remaining integral that decreases exponentially. In order to represent the function $F_{\bar{\nu}}(s)$ in a form where numerical accuracy is not an essential issue, one can partially treat the integral analytically in a way that a remaining term involving numerical integration gives only small contributions also for large values of s. To achieve this, recognize that $F_{\bar{\nu}}(s)$ can be written in terms of Owen's T-function

$$T(a,b) = \frac{1}{2\pi}\int_0^b \mathrm{d}x \frac{\mathrm{e}^{-\frac{1}{2}a^2(1+x^2)}}{1+x^2}\,. \tag{B.279}$$

The corresponding expression is

$$\begin{aligned} F_{\bar{\nu}}(s) = \frac{\sqrt{\pi}}{2}\mathrm{e}^{(1+\bar{\nu}^2)s}\Big[&\mathrm{erf}(\bar{\nu}\sqrt{s}) - \mathrm{erf}(\sqrt{(1+\bar{\nu}^2)s}) \\ &+ 4T(\bar{\nu}\sqrt{2s}, \bar{\nu}^{-1})\Big]\,, \end{aligned} \tag{B.280}$$

and by use of the general property

$$T(h,a) + T\left(ah, \frac{1}{a}\right) = \frac{1}{4}\left(1 - \mathrm{erf}\left(\frac{h}{\sqrt{2}}\right)\mathrm{erf}\left(\frac{ah}{\sqrt{2}}\right)\right) \tag{B.281}$$

it is equivalent to

$$\begin{aligned} F_{\bar{\nu}}(s) = \frac{\sqrt{\pi}}{2}\mathrm{e}^{(1+\bar{\nu}^2)s}\Big[&\mathrm{erfc}(\sqrt{(1+\bar{\nu}^2)s}) - \mathrm{erfc}(\bar{\nu}\sqrt{s})\mathrm{erfc}(\sqrt{s}) \\ &+ \mathrm{erfc}(\sqrt{s}) - 4T(\sqrt{2s}, \bar{\nu})\Big]\,. \end{aligned} \tag{B.282}$$

The terms in the first row of this equation are well behaved numerically, since the asymptotics $\mathrm{e}^{x^2}\mathrm{erfc}(x) = 1/(\sqrt{\pi}x) + \mathcal{O}(x^{-3})$ for $x \gg 1$ are very well known. The numerical problem now lies in cancellation effects between the two terms of the second row. To overcome this, one can split the Owen T function

$$4T(\sqrt{2s}, \bar{\nu}) = \frac{2}{\pi}\int_0^\infty \mathrm{d}x \frac{\mathrm{e}^{-s(1+x^2)}}{1+x^2} - \frac{2}{\pi}\int_{\bar{\nu}}^\infty \mathrm{d}x \frac{\mathrm{e}^{-s(1+x^2)}}{1+x^2}\,. \tag{B.283}$$

The first term can be evaluated to

$$\frac{2}{\pi}\int_0^\infty \mathrm{d}x \frac{\mathrm{e}^{-s(1+x^2)}}{1+x^2} = \mathrm{erfc}(\sqrt{s})\,, \tag{B.284}$$

which gets obvious after derivation with respect to s, and therefore compensates exactly the term $\mathrm{erfc}(\sqrt{s})$ in (B.282). From the remaining integral a factor can be extracted to compensate for the exponential prefactor while keeping it still bounded. In total one numerically well behaved form of the function F is

$$\begin{aligned} F_{\bar{\nu}}(s) = &\frac{\sqrt{\pi}}{2}\mathrm{e}^{(1+\bar{\nu}^2)s}\Big[\mathrm{erfc}(\sqrt{(1+\bar{\nu}^2)s}) - \mathrm{erfc}(\bar{\nu}\sqrt{s})\mathrm{erfc}(\sqrt{s})\Big] \\ &+ \frac{1}{\sqrt{\pi}}\int_{\bar{\nu}}^\infty \mathrm{d}x \frac{\mathrm{e}^{-s(x^2-\bar{\nu}^2)}}{1+x^2}\,. \end{aligned} \tag{B.285}$$

Another well-behaved alternative form is given by

$$F_{\bar{\nu}}(s) = \int_0^\infty \mathrm{d}x\, \mathrm{e}^{-x(x+2\sqrt{(1+\bar{\nu}^2)s})}\, \mathrm{erfc}(\bar{\nu}x)\,, \tag{B.286}$$

which can be easily derived from (1.159) directly. To do so, one expands the complementary error function as integral

$$\mathrm{erfc}\, z = \frac{2}{\sqrt{\pi}} \int_0^\infty \mathrm{d}t\, \mathrm{e}^{-(t+z)^2}\,, \tag{B.287}$$

so that the whole expression for $F_{\bar{\nu}}(s)$ involves two integrals with one limit being finite in each of them. Since both integration variables appear as quadratic form in the exponent, one can evaluate the outer integral to an error function, while keeping the integration introduced by (B.287) unevaluated. By this procedure the exponentially *increasing* prefactor gets absorbed into the integrand, which, after this compensation, is still exponentially *decreasing* with s.

C Calculation of spectral QCE contributions

For the explicit calculation of (1.161) it is convenient to split the cluster damping factor (1.158)

$$a_{n_1,n-n_1}(s) = a_1(s) + a_2(s) + a_3(s) + a_4(s) \tag{C.288}$$

into its four addends

$$\begin{aligned} a_1(s) &= \frac{2}{\pi}\tan^{-1}\bar{\nu} - 1 + \frac{2\bar{\nu}^2}{\sqrt{\pi(1+\bar{\nu}^2)}}\sqrt{s}\,, \\ a_2(s) &= -\frac{2}{\sqrt{\pi}}\bar{\nu}\sqrt{s}\mathrm{e}^s\,\mathrm{erfc}(\sqrt{s})\,, \\ a_3(s) &= \frac{2}{\sqrt{\pi}}F_{\bar{\nu}}(s)\,, \\ a_4(s) &= -\frac{4}{\sqrt{\pi}}\bar{\nu}^2 s F_{\bar{\nu}}(s) = -2\bar{\nu}^2 s a_3(s)\,, \end{aligned} \tag{C.289}$$

where I have omitted the dependence on n_1 and n through $\bar{\nu}$ (1.155) to ease notation. In the following the explicit expressions for the four b_j are calculated.

Calculation of $b_1^{(l)}(\epsilon)$ and $b_2^{(l)}(\epsilon)$

While the expression (1.163) for $b_1^{(l)}(\epsilon)$ is easily calculated by applying standard rules of inverse Laplace transforms of power functions, the expression (1.164) for the second term $b_2^{(l)}(\epsilon)$ can be derived following the recursive approach in [168].

Calculation of $b_3^{(l)}(\epsilon)$

First, I remove the exponential prefactor by defining

$$\tilde{F}_{\bar{\nu}}(s) := \mathrm{e}^{-(1+\bar{\nu}^2)s}F_{\bar{\nu}}(s)\,. \tag{C.290}$$

The integral in $\tilde{F}_{\bar{\nu}}(s)$ can not be evaluated to elementary expressions directly. In contrast to that its inverse Laplace transform can be related to the solvable derivative given by

$$\mathrm{e}^{(1+\bar{\nu}^2)s}\tilde{F}'_{\bar{\nu}}(s) = \frac{\bar{\nu}}{2}s^{-\frac{1}{2}}\mathrm{e}^s\,\mathrm{erfc}(\sqrt{s}) - \frac{1}{2}\sqrt{1+\bar{\nu}^2}s^{-\frac{1}{2}}\,. \tag{C.291}$$

Using this observation one can calculate

$$\begin{aligned} \mathscr{L}_{\mathrm{s}}^{-1}\left[F_{\bar{\nu}}(s)\right](\epsilon) &= \mathscr{L}_{\mathrm{s}}^{-1}\left[\tilde{F}_{\bar{\nu}}(s)\right](\epsilon + (1+\bar{\nu}^2)) \\ &= -\frac{\mathscr{L}_{\mathrm{s}}^{-1}\left[\tilde{F}'_{\bar{\nu}}(s)\right](\epsilon + (1+\bar{\nu}^2))}{\epsilon + (1+\bar{\nu}^2)} \\ &= -\frac{\mathscr{L}_{\mathrm{s}}^{-1}\left[\mathrm{e}^{(1+\bar{\nu}^2)s}\tilde{F}'_{\bar{\nu}}(s)\right](\epsilon)}{\epsilon + (1+\bar{\nu}^2)} \\ &= (\epsilon + (1+\bar{\nu}^2))^{-1}\left(\frac{\sqrt{1+\bar{\nu}^2}}{2\sqrt{\pi}}\frac{\theta(\epsilon)}{\sqrt{\epsilon}} - \frac{\bar{\nu}}{2\sqrt{\pi}}\frac{\theta(\epsilon)}{\sqrt{1+\epsilon}}\right)\,. \end{aligned} \tag{C.292}$$

From there one gets

$$\begin{aligned}\mathscr{L}_{\mathrm{s}}^{-1}\left[s^{-1}F_{\bar{\nu}}(s)\right](\epsilon) &= \int_{-\infty}^{\epsilon} \mathrm{d}x\, \mathscr{L}_{\mathrm{s}}^{-1}\left[F_{\bar{\nu}}(s)\right](x) \\ &= \frac{\theta(\epsilon)}{\sqrt{\pi}}\left[\tan^{-1}\left(\sqrt{\frac{\epsilon}{1+\bar{\nu}^2}}\right) + \tan^{-1}\left(\sqrt{\frac{\bar{\nu}^2}{1+\epsilon}}\right) - \tan^{-1}\bar{\nu}\right],\end{aligned} \tag{C.293}$$

and

$$\begin{aligned}&\mathscr{L}_{\mathrm{s}}^{-1}\left[s^{-\frac{1}{2}}F_{\bar{\nu}}(s)\right](\epsilon) \\ &\quad= \int_{-\infty}^{\infty} \mathrm{d}x\, \mathscr{L}_{\mathrm{s}}^{-1}\left[s^{-\frac{1}{2}}\right](\epsilon - x)\, \mathscr{L}_{\mathrm{s}}^{-1}\left[F_{\bar{\nu}}(s)\right](x) \\ &\quad= \frac{\theta(\epsilon)}{2\pi}\int_0^{\epsilon} \mathrm{d}x \frac{1}{\sqrt{\epsilon - x}}\left[\frac{\sqrt{1+\bar{\nu}^2}}{\sqrt{x}(x+(1+\bar{\nu}^2))}\right. \\ &\qquad\qquad \left. - \frac{\bar{\nu}}{\sqrt{1+x}(x+(1+\bar{\nu}^2))}\right] \\ &\quad= \frac{\theta(\epsilon)}{\pi}(\epsilon + (1+\bar{\nu}^2))^{-\frac{1}{2}} \tan^{-1}\left(\frac{1}{\bar{\nu}}\sqrt{1+\frac{1+\bar{\nu}^2}{\epsilon}}\right).\end{aligned} \tag{C.294}$$

I calculate $\mathscr{L}_{\mathrm{s}}^{-1}\left[s^{-n}\tilde{F}_{\bar{\nu}}(s)\right]$ for larger negative powers of s using a recursive approach, where (C.293) and (C.294) will serve as initial values. I define

$$G_n(s) := \Gamma(n) s^{-n}\tilde{F}_{\bar{\nu}}(s)\,, \tag{C.295}$$

where n may be either integer or half-integer. Taking the derivative of (C.295) with respect to s leads to

$$G_{n+1}(s) = -\frac{\partial}{\partial s}G_n(s) + \Gamma(n) s^{-n}\tilde{F}'_{\bar{\nu}}(s)\,, \tag{C.296}$$

which implies the recursion relation

$$\begin{aligned}\mathscr{L}_{\mathrm{s}}^{-1}\left[G_{n+1}(s)\right](\epsilon) &= \epsilon\, \mathscr{L}_{\mathrm{s}}^{-1}\left[G_n(s)\right](\epsilon) \\ &\quad + \Gamma(n)\, \mathscr{L}_{\mathrm{s}}^{-1}\left[s^{-n}\tilde{F}'_{\bar{\nu}}(s)\right](\epsilon)\end{aligned} \tag{C.297}$$

for the inverse Laplace transformed objects, where the initial values $\mathscr{L}_{\mathrm{s}}^{-1}\left[G_1(s)\right]$ or $\mathscr{L}_{\mathrm{s}}^{-1}\left[G_{\frac{1}{2}}(s)\right]$ are given explicitly by (C.293) and (C.294). The solution to (C.297) is either given by

$$\begin{aligned}\mathscr{L}_{\mathrm{s}}^{-1}\left[G_{n+1}(s)\right](\epsilon) &= \epsilon^n\, \mathscr{L}_{\mathrm{s}}^{-1}\left[G_1(s)\right](\epsilon) \\ &\quad + \sum_{k=1}^{n} \epsilon^{n-k}\Gamma(k)\, \mathscr{L}_{\mathrm{s}}^{-1}\left[s^{-k}\tilde{F}'_{\bar{\nu}}(s)\right](\epsilon)\end{aligned} \tag{C.298}$$

for integer indexes or by

$$\begin{aligned}\mathscr{L}_{\mathrm{s}}^{-1}\left[G_{n+\frac{1}{2}}(s)\right](\epsilon) &= \epsilon^n\, \mathscr{L}_{\mathrm{s}}^{-1}\left[G_{\frac{1}{2}}(s)\right](\epsilon) \\ &\quad + \sum_{k=0}^{n-1} \epsilon^{n-1-k}\Gamma\left(k+\frac{1}{2}\right) \mathscr{L}_{\mathrm{s}}^{-1}\left[s^{-k-\frac{1}{2}}\tilde{F}'_{\bar{\nu}}(s)\right](\epsilon)\end{aligned} \tag{C.299}$$

for half-integer indexes. In the given form, both solutions (C.298) and (C.299) are valid for $n \in \mathbb{N}_0$. After reintroducing the exponential prefactor, (C.298) and (C.299) become

$$\begin{aligned}\Gamma(n+1)\,\mathscr{L}_{\mathrm{s}}^{-1}\left[s^{-n-1}F_{\bar{\nu}}(s)\right](\epsilon) &= (\epsilon+(1+\bar{\nu}^2))^n\,\mathscr{L}_{\mathrm{s}}^{-1}\left[s^{-1}F_{\bar{\nu}}(s)\right](\epsilon)\\ &\quad+\sum_{k=1}^{n}(\epsilon+(1+\bar{\nu}^2))^{n-k}\Gamma(k)\\ &\quad\times\mathscr{L}_{\mathrm{s}}^{-1}\left[s^{-k}\mathrm{e}^{(1+\bar{\nu}^2)s}\tilde{F}'_{\bar{\nu}}(s)\right](\epsilon)\,,\end{aligned}\tag{C.300}$$

and

$$\begin{aligned}\Gamma\left(n+\frac{1}{2}\right)\mathscr{L}_{\mathrm{s}}^{-1}\left[s^{-n-\frac{1}{2}}F_{\bar{\nu}}(s)\right](\epsilon) &= \sqrt{\pi}(\epsilon+(1+\bar{\nu}^2))^n\,\mathscr{L}_{\mathrm{s}}^{-1}\left[s^{-\frac{1}{2}}F_{\bar{\nu}}(s)\right](\epsilon)\\ &\quad+\sum_{k=1}^{n}(\epsilon+(1+\bar{\nu}^2))^{n-k}\Gamma\left(k-\frac{1}{2}\right)\\ &\quad\times\mathscr{L}_{\mathrm{s}}^{-1}\left[s^{-k+\frac{1}{2}}\mathrm{e}^{(1+\bar{\nu}^2)s}\tilde{F}'_{\bar{\nu}}(s)\right](\epsilon)\,,\end{aligned}\tag{C.301}$$

where $n \in \mathbb{N}_0$. The remaining step is to calculate $\mathscr{L}_{\mathrm{s}}^{-1}\left[s^{-n}\mathrm{e}^{(1+\bar{\nu}^2)s}\tilde{F}'_{\bar{\nu}}(s)\right](\epsilon)$ for n being either integer or half-integer. Using (C.291) leads to

$$\begin{aligned}&\mathscr{L}_{\mathrm{s}}^{-1}\left[s^{-n}\mathrm{e}^{(1+\bar{\nu}^2)s}\tilde{F}'_{\bar{\nu}}(s)\right](\epsilon)\\ &\quad=\frac{\bar{\nu}}{2}\,\mathscr{L}_{\mathrm{s}}^{-1}\left[s^{-n-1}\sqrt{s}\,\mathrm{erfc}(\sqrt{s})\right](\epsilon)-\frac{1}{2}\sqrt{1+\bar{\nu}^2}\,\mathscr{L}_{\mathrm{s}}^{-1}\left[s^{-n-\frac{1}{2}}\right](\epsilon)\\ &\quad=-\frac{\sqrt{\pi}}{4}\epsilon^n b_2^{(2n)}(\epsilon)-\frac{\sqrt{1+\bar{\nu}^2}}{2\Gamma(n+\frac{1}{2})}\epsilon^{n-\frac{1}{2}}\theta(\epsilon)\,.\end{aligned}\tag{C.302}$$

For $l \geq -1$ one gets the expression (1.167) together with the definition (1.168).

Finally, as written in the main text, the fourth term $b_4^{(l)}(\epsilon)$ is related to $b_3^{(l)}(\epsilon)$ as a modified version (1.169).

D Extreme couplings in the truncated attractive Lieb-Liniger model

D.1 Phase space structure for vanishing angular momentum

The region $4 < \bar{\alpha} < 8$

When $\bar{\alpha}$ exceeds the value of $\bar{\alpha}_2 := 4$, while the low-energy island discussed above keeps on growing, another separatrix

$$z^{(2)}(\varphi_0) = \frac{\bar{\alpha}(2 - 8\cos^2\varphi_0) - 8}{\bar{\alpha}(1 - 8\cos^2\varphi_0)} \tag{D.303}$$

penetrates the phase space, but this time entering at the "lower" end $n_0 = 0$ ($z = 0$). It is symmetrically located around $\varphi_0 = \pm\frac{\pi}{2}$, shares the energy $\tilde{\omega} = \tilde{\omega}^{(2)}$ with the lower boundary, intersects with the latter in the saddle points P_2 at $\cos^2\varphi_0 = \frac{1}{4} - \frac{1}{\bar{\alpha}}$ and separates a region of *largest* energy from the outside with a global energy maximum at P_4, which lies on the symmetry line $\varphi_0 = \pm\frac{\pi}{2}$ half-way between the boundary $z = 0$ and the separatrix $z = z^{(2)}(\pi/2) = 2 - \frac{8}{\bar{\alpha}}$ with the energy

$$\tilde{\omega}_{\max} = \frac{2}{\bar{\alpha}}\,. \tag{D.304}$$

The orbits inside the high-energy island, similar to the low-energy island, are vibrations around P_4 rather than librations. Since they correspond to states of largest energy this qualitative change will not affect the low-lying spectra in the semiclassical sense. Figure 2.2b shows a phase space portrait with vibrations inside the low-energy and high-energy islands and librations in between.

The limits $\bar{\alpha} \to 8^{\pm}$

When $\bar{\alpha}$ approaches the value $\bar{\alpha}_{\mathrm{S}} := 8$ from below, the saddle points P_1 and P_2 approach $\cos^2\varphi_0 = \frac{1}{8}$ from two sides, the minimum and maximum approach the center line $z = \frac{1}{2}$ and the separatrices $z^{(1)}$ and $z^{(2)}$ become rectangles that touch each other, so that the full phase space is covered by the two islands. The energies of the two boundaries become the same $\tilde{\omega}^{(1)} = \tilde{\omega}^{(2)}$ and cross each other. At this point, (almost) no librations exist any more. Passing through $\bar{\alpha}_{\mathrm{S}} = 8$ the top and bottom boundaries swap their roles as the low-energy island gets attached to the bottom $z = 0$ while the high-energy island gets attached to the top $z = 1$. The separatrices $z^{(1,2)}$ interchange their locations in φ_0. Figure 2.2c and Fig. 2.2d show phase space portraits for values of $\bar{\alpha}$ slightly less and greater than $\bar{\alpha}_{\mathrm{S}}$.

The region $\bar{\alpha} > 8$

When the interaction strength gets further increased, the two islands drift apart again, where the high-energy island approaches more and more the upper boundary while the global minimum decreases in z and the low-energy island becomes smaller. There is again space for orbits to librate between the two islands. In this region the maximum P_4 is half-way between the upper boundary $z = 1$ and

the upper separatrix $z^{(1)}(\pi/2)$ while the minimum P_3 is half-way between the lower boundary $z = 0$ and the lower separatrix $z^{(2)}(0)$. Figure 2.2e shows the phase space portrait for large $\bar{\alpha}$.

The limit $\bar{\alpha} \to \infty$

At infinitely large attractive interaction strength, the maximum P_4 converges to $z = 1$ and the high-energy island vanishes whereas the low-energy island and the location of the global energy minimum converge to finite values

$$\begin{aligned} z^{(2)}(x) &\xrightarrow[\bar{\alpha}\to\infty]{} \frac{2 - 8\cos^2\varphi_0}{1 - 8\cos^2\varphi_0}\,, \\ P_3 = (\varphi_0^{(P_3)}, z^{(P_3)}) &\xrightarrow[\bar{\alpha}\to\infty]{} \left(0, \frac{4}{7}\right). \end{aligned} \tag{D.305}$$

This means that semiclassically the lowest energy states will remain vibrations around the global minimum for arbitrarily large couplings $\bar{\alpha}$. In the low-lying spectra, there will be no transition from vibrations back to librations. Figure 2.2f shows the phase space portrait for this limit.

D.2 Phase space structure for non-vanishing angular momentum

Lower separatrix and maximum energy island

When the coupling strength passes through the value

$$\bar{\alpha}_2 := \frac{4}{2\sqrt{1 - l^2} - 1}\,, \tag{D.306}$$

a second separatrix appears as in the case $L = 0$ that separates an island of maximum energy (global energy maximum at P_4) centered at $\varphi_0 = \pm\frac{\pi}{2}$ (see Fig. 2.3d,e). It hits the lower boundary $z = 0$ at the saddle points (the energy is analytic there) P_2 given by

$$\cos^2\varphi_0^{(P_2)} = \frac{1}{2} - \frac{4 + \bar{\alpha}}{4\bar{\alpha}\sqrt{1 - l^2}}\,. \tag{D.307}$$

If $|l| \geq \frac{\sqrt{3}}{2}$ the critical coupling $\bar{\alpha}_2$ becomes negative and the maximum island and its separatrix never appear (see Fig. D.21c).

Separatrix swapping

Analogous to the case $L = 0$ a swapping of the two separatrices appears when they touch each other and their energies

$$\begin{aligned} \tilde{\omega}^{(1)} &= |l|\left(1 - \frac{\bar{\alpha}}{2}(1 - |l|)\right), \\ \tilde{\omega}^{(2)} &= 1 - \frac{\bar{\alpha}}{8}(1 - l^2)\,, \end{aligned} \tag{D.308}$$

which are the energies of the upper and lower boundary, become equal (see Fig. 2.3e,f). The swap happens when the coupling passes through the value

$$\bar{\alpha}_\mathrm{S} = \frac{8}{1 - 3|l|}\,. \tag{D.309}$$

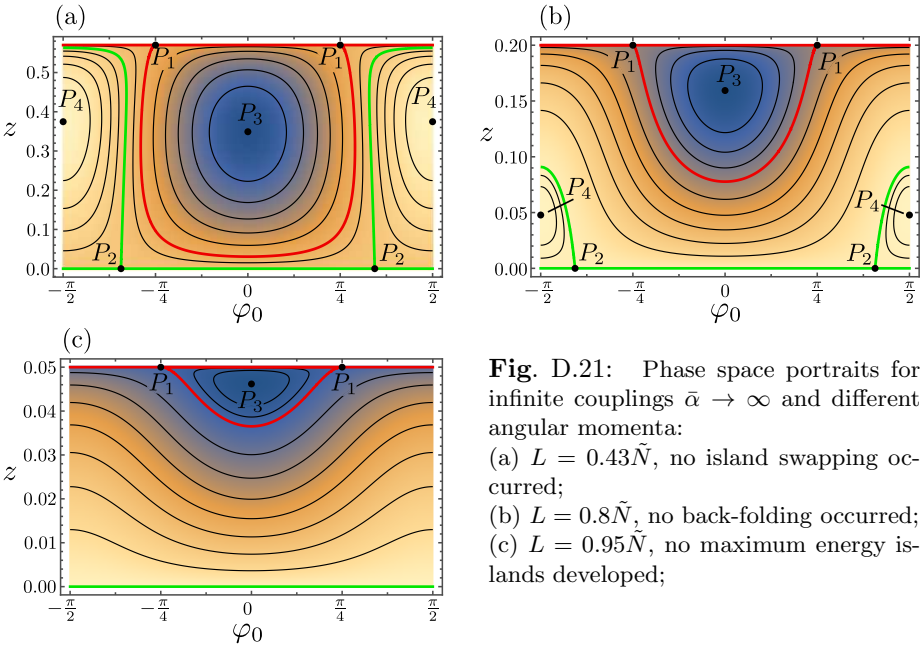

Fig. D.21: Phase space portraits for infinite couplings $\bar{\alpha} \to \infty$ and different angular momenta:
(a) $L = 0.43\tilde{N}$, no island swapping occurred;
(b) $L = 0.8\tilde{N}$, no back-folding occurred;
(c) $L = 0.95\tilde{N}$, no maximum energy islands developed;

As in the case $L = 0$, after the swap ($\bar{\alpha} > \bar{\alpha}_S$) the roles of the upper and lower separatrix are exchanged in separating the minimum or maximum energy island, respectively (see Fig. 2.3g,h). This swapping may never occur if $|l| \geq \frac{1}{3}$ (see Fig. D.21a).

Infinite coupling

Also for finite angular momentum the limit $\bar{\alpha} \to \infty$ produces a limiting energy landscape which globally scales linearly with $\bar{\alpha}$. Differing qualitatively from the case $L = 0$, the maximum energy islands never disappear but limit in a final shape (see Fig. 2.3h). The features in the final shape of the energy landscape for $\bar{\alpha} \to \infty$ depends on the value of L due to its influence on whether a maximum energy island ever occurred ($l < \frac{\sqrt{3}}{2}$), whether back-folding ever occurred ($l < \frac{2}{3}$), and whether island swapping occurred ($l < \frac{1}{3}$). Figure D.21 shows a series of final phase portraits for the different cases.

D.3 Artificial transitions of highly excited states

In the region $\bar{\alpha} > \bar{\alpha}_2$ additional transitions of librations to vibrations crossing the artificial and unphysical lower separatrix appear. This effect in general involves only highly excited states. This transition affects quantized states by an enhanced increase of the corresponding energies with $\bar{\alpha}$ in contrast to an enhanced decrease of energies for states crossing the upper separatrix. For $\bar{\alpha} > \bar{\alpha}_S$ the roles of upper and lower separatrix get swapped in this context. Furthermore, the quantized vibrations inside the lower island do not continuously connect to the quantized librations outside the lower island. This means that the high lying spectrum suffers from discontinuities at certain values of the coupling where additional quantized vibrations appear before the correspond-

ing libration disappears. Even the total number of semiclassically quantized states therefore jumps between the quantum mechanical number of states and a neighboring number. These effects can be regarded as an unphysical artifact resulting from the truncation of the Hilbert space. The lower lying spectrum is not affected by those discontinuities. This statement will be quantified later.

Nevertheless, one can give the quantization rules involving a common quantum number yielding a monotonously increasing sequence of energies in this regime. One has to distinguish the cases before and after separatrix swapping. For $\bar{\alpha}_2 < \bar{\alpha} < \bar{\alpha}_\mathrm{S}$ the quantization rules are

$$\begin{aligned}
\frac{1}{2\pi} S^{(1)}_{\eta_0} &= m + \frac{1}{2}\,, \quad m \in \{0, \ldots, M^{(1)}_\mathrm{vib}\}\,, \\
\frac{1}{2\pi} \bar{S}_{\gamma_0} &= m + \frac{1}{2}\,, \quad m \in \{M^{(1)}_\mathrm{vib} + 1, \ldots, M_\mathrm{lib}\}\,, \\
\frac{1}{2\pi} \bar{S}^{(2)}_{\eta_0} &= m + \frac{1}{2} + \Delta\,, \quad m \in \{M_\mathrm{lib} + 1, \ldots, M\}\,,
\end{aligned} \tag{D.310}$$

whereas for $\bar{\alpha} > \bar{\alpha}_\mathrm{S}$ the rules are

$$\begin{aligned}
\frac{1}{2\pi} S^{(2)}_{\eta_0} &= m + \frac{1}{2}\,, \quad m \in \{0, \ldots, M^{(2)}_\mathrm{vib}\}\,, \\
\frac{1}{2\pi} S_{\gamma_0} &= m + \frac{1}{2} + \Delta\,, \quad m \in \{M^{(2)}_\mathrm{vib} + 1, \ldots, M_\mathrm{lib}\}\,, \\
\frac{1}{2\pi} \bar{S}^{(1)}_{\eta_0} &= m + \frac{1}{2} + \Delta\,, \quad m \in \{M_\mathrm{lib} + 1, \ldots, M\}\,,
\end{aligned} \tag{D.311}$$

where the maximum quantum numbers for the different classes of orbits are given as

$$\begin{aligned}
M^{(1,2)}_\mathrm{vib} &= \left\lfloor \frac{1}{2\pi} S^{(1,2)}_\mathrm{sep} - \frac{1}{2} \right\rfloor\,, \\
M_\mathrm{lib} &= \begin{cases} \left\lfloor \frac{N-|L|}{2} - \frac{1}{2\pi} S^{(2)}_\mathrm{sep} + \frac{1}{4} \right\rfloor & : \bar{\alpha} < \bar{\alpha}_\mathrm{S}\,, \\ \frac{N-|L|}{2} - \left\lfloor \frac{1}{2\pi} S^{(2)}_\mathrm{sep} + \frac{1}{2} \right\rfloor - \frac{5}{4} - \Delta & : \bar{\alpha} > \bar{\alpha}_\mathrm{S}\,, \end{cases} \\
M &= \frac{N - |L|}{2} - \frac{1}{4} - \Delta\,,
\end{aligned} \tag{D.312}$$

and the mismatch Δ is defined as

$$\begin{aligned}
N - |L| \text{ even}: \quad \Delta &= \begin{cases} \frac{3}{4} & : \Delta S^{(2)}_\mathrm{sep} \in \left]\frac{\pi}{2}, \pi\right[\,, \\ -\frac{1}{4} & : \text{else}\,, \end{cases} \\
N - |L| \text{ odd}: \quad \Delta &= \begin{cases} -\frac{3}{4} & : \Delta S^{(2)}_\mathrm{sep} \in [\pi, \frac{3\pi}{2}]\,, \\ \frac{1}{4} & : \text{else}\,, \end{cases}
\end{aligned} \tag{D.313}$$

which depends on the 2π-remainder

$$\Delta S^{(2)}_\mathrm{sep} = S^{(2)}_\mathrm{sep} \bmod 2\pi = S^{(2)}_\mathrm{sep} - 2\pi \left\lfloor \frac{1}{2\pi} S^{(2)}_\mathrm{sep} \right\rfloor \tag{D.314}$$

of the area

$$S^{(2)}_\mathrm{sep} = \lim_{E \to E^{(2)\pm}} S^{(2)}_{\eta_0}(E) = \lim_{E \to E^{(2)\mp}} S_{\gamma_0}(E) \tag{D.315}$$

enclosed by the lower separatrix and is therefore $\bar{\alpha}$-dependent. The upper and lower sign in (D.315) indicating the direction of the one-sided limits correspond to $\bar{\alpha} < \bar{\alpha}_{\mathrm{S}}$ and $\bar{\alpha} > \bar{\alpha}_{\mathrm{S}}$, respectively.

In the following I will give an estimated bound for the number n_{cont} of low-lying states that do not suffer from discontinuities. From the quantization prescriptions (2.120), (D.310) and (D.311) this number is given by

$$n_{\mathrm{cont}} = \begin{cases} M+1 & : \bar{\alpha} < \bar{\alpha}_2 \,, \\ M_{\mathrm{lib}}+1 & : \bar{\alpha}_2 < \bar{\alpha} < \bar{\alpha}_{\mathrm{S}} \,, \\ M_{\mathrm{vib}}+1 & : \bar{\alpha}_{\mathrm{S}} < \bar{\alpha} \,. \end{cases} \tag{D.316}$$

I will consider large $N \gg 1$ and fixed l here and give the bound for the fraction $q_{\mathrm{cont}} = n_{\mathrm{cont}}/M \approx 2n_{\mathrm{cont}}/(\tilde{N}-|L|)$.

$$q_{\mathrm{cont}} \approx \begin{cases} 1 & : \bar{\alpha} < \bar{\alpha}_2 \,, \\ 1 - \frac{1}{\pi(\tilde{N}-|L|)} S^{(2)}_{\mathrm{sep}} & : \bar{\alpha}_2 < \bar{\alpha} < \bar{\alpha}_{\mathrm{S}} \,, \\ \frac{1}{\pi(\tilde{N}-|L|)} S^{(2)}_{\mathrm{sep}} & : \bar{\alpha}_{\mathrm{S}} < \bar{\alpha} \,, \end{cases} \tag{D.317}$$

which connects smoothly at $\bar{\alpha} = \bar{\alpha}_2$ and $\bar{\alpha} = \bar{\alpha}_{\mathrm{S}}$. Furthermore, q_{cont} is a monotonously decreasing function of $\bar{\alpha}$, since $S^{(2)}_{\mathrm{sep}}$ is monotonously increasing for $\bar{\alpha} < \bar{\alpha}_{\mathrm{S}}$ and decreasing for $\bar{\alpha} > \bar{\alpha}_{\mathrm{S}}$, respectively. This means the smallest number will be obtained in the limit $\bar{\alpha} \to \infty$, where I define $q_{\mathrm{cont}} \xrightarrow[\bar{\alpha}\to\infty]{} q^{\infty}_{\mathrm{cont}}(|l|)$ given by

$$q^{\infty}_{\mathrm{cont}}(|l|) := \begin{cases} \frac{2}{\pi(1-|l|)} \int_0^{z^{(2)}(0)} \mathrm{d}z \, \lim_{\bar{\alpha}\to\infty} \varphi^{(2)}_0(z) & : |l| < \frac{1}{3} \,, \\ 1 - \frac{z^{(2)}(\frac{\pi}{2})}{1-|l|} + \frac{2}{\pi(1-|l|)} \int_0^{z^{(2)}(\frac{\pi}{2})} \mathrm{d}z \, \lim_{\bar{\alpha}\to\infty} \varphi^{(2)}_0(z) & : |l| > \frac{1}{3} \,. \end{cases} \tag{D.318}$$

The function $q^{\infty}_{\mathrm{cont}}(|l|)$ grows monotonously with $|l|$ so that the worst case of a minimal fraction of well-behaved states is given when $L = l = 0, \bar{\alpha} \to \infty$. One gets the bound

$$q_{\mathrm{cont}} \geq q^{\infty}_{\mathrm{cont}}(|l|) \geq q^{\infty}_{\mathrm{cont}}(0) \approx 0.478 \,, \tag{D.319}$$

meaning for an arbitrary set-up $N, L, \bar{\alpha}$ at least the lowest 47.8% of all semi-classically quantized energies are well behaved and do not suffer from any discontinuities.

Bibliography

[1] P. W. Anderson, "More is different," Science **177**, 393 (1972).

[2] D. G. Yakovlev, P. Haensel, G. Baym, and C. Pethick, "Lev Landau and the concept of neutron stars," Phys.-Usp.+ **56**, 289 (2013).

[3] F. Özel and P. Freire, "Masses, radii, and the equation of state of neutron stars," Annu. Rev. Astron. Astr. **54**, 401 (2016).

[4] J. F. Annett, *Superconductivity, Superfluids and Condensates*, Oxford Master Series in Physics (Oxford University Press, 2004).

[5] L. N. Cooper, "Bound electron pairs in a degenerate fermi gas," Phys. Rev. **104**, 1189 (1956).

[6] H. L. Stormer, "Nobel lecture: The fractional quantum Hall effect," Rev. Mod. Phys. **71**, 875 (1999).

[7] O. Morsch and M. Oberthaler, "Dynamics of Bose-Einstein condensates in optical lattices," Rev. Mod. Phys. **78**, 179 (2006).

[8] I. Bloch, J. Dalibard, and W. Zwerger, "Many-body physics with ultracold gases," Rev. Mod. Phys. **80**, 885 (2008).

[9] M. Greiner, O. Mandel, T. Esslinger, T. W. Hänsch, and I. Bloch, "Quantum phase transition from a superfluid to a Mott insulator in a gas of ultracold atoms," Nature **415**, 39 (2002).

[10] P. M. Preiss, R. Ma, M. E. Tai, A. Lukin, M. Rispoli, P. Zupancic, Y. Lahini, R. Islam, and M. Greiner, "Strongly correlated quantum walks in optical lattices," Science **347**, 1229 (2015).

[11] M. Lewenstein, A. Sanpera, and V. Ahufinger, *Ultracold Atoms in Optical Lattices: Simulating Quantum Many-Body Systems* (Oxford University Press, 2012).

[12] R. D. Woods and D. S. Saxon, "Diffuse surface optical model for nucleon-nuclei scattering," Phys. Rev. **95**, 577 (1954).

[13] H. A. Bethe, "An attempt to calculate the number of energy levels of a heavy nucleus," Phys. Rev. **50**, 332 (1936).

[14] Q. Hummel, J. D. Urbina, and K. Richter, "The Weyl expansion for systems of independent identical particles," J. Phys. A: Math. Theor. **47**, 015101 (2014).

[15] G. H. Hardy and S. Ramanujan, "Asymptotic formulæ in combinatory analysis," P. Lond. Math. Soc. **s2-17**, 75 (1918).

[16] E. K. U. Gross and R. M. Dreizler, *Density Functional Theory*, NATO ASI series: Physics (Springer, 1995).

[17] K. Capelle, "A bird's-eye view of density-functional theory," Braz. J. Phys. **36**, 1318 (2006).

[18] P. Hohenberg and W. Kohn, "Inhomogeneous electron gas," Phys. Rev. **136**, B864 (1964).

[19] W. Kohn and L. J. Sham, "Self-consistent equations including exchange and correlation effects," Phys. Rev. **140**, A1133 (1965).

[20] J. J. Sakurai, *Advanced Quantum Mechanics*, Addison-Wesley Series in Advanced Physics (Addison-Wesley, 1967).

[21] J. W. Negele and H. Orland, *Quantum Many-Particle Systems*, Advanced Books Classics (Westview Press, 1998).

[22] R. Kanamoto, H. Saito, and M. Ueda, "Quantum phase transition in one-dimensional Bose-Einstein condensates with attractive interactions," Phys. Rev. A **67**, 013608 (2003).

[23] H. T. C. Stoof, D. B. M. Dickerscheid, and K. Gubbels, "Landau theory of phase transitions," in *Ultracold Quantum Fields* (Springer Netherlands, 2009) pp. 193–212.

[24] E. P. Gross, "Structure of a quantized vortex in boson systems," Nuovo Cimento **20**, 454 (1961).

[25] L. P. Pitaevskii, "Vortex lines in an imperfect Bose gas," Sov. Phys. JETP (USSR) **13**, 451 (1961).

[26] N. N. Bogoliubov, "On the theory of superfluidity," J. Phys. (USSR) **11**, 23 (1947).

[27] P. G. de Gennes, *Superconductivity of Metals and Alloys*, Frontiers in Physics (W. A. Benjamin, 1966).

[28] A. L. Fetter, "Nonuniform states of an imperfect Bose gas," Ann. Phys. (New York) **70**, 67 (1972).

[29] S. Tomonaga, "Remarks on Bloch's method of sound waves applied to many-fermion problems," Prog. Theor. Phys. **5**, 544 (1950).

[30] J. M. Luttinger, "An exactly soluble model of a many-fermion system," J. Math. Phys. **4**, 1154 (1963).

[31] D. C. Mattis and E. H. Lieb, "Exact solution of a many-fermion system and its associated boson field," J. Math. Phys. **6**, 304 (1965).

[32] H. Bethe, "Zur Theorie der Metalle," Z. Phys. **71**, 205 (1931).

[33] E. H. Lieb and W. Liniger, "Exact analysis of an interacting Bose gas. I. The general solution and the ground state," Phys. Rev. **130**, 1605 (1963).

[34] E. H. Lieb, "Exact analysis of an interacting Bose gas. II. The excitation spectrum," Phys. Rev. **130**, 1616 (1963).

[35] M. Gaudin, "Un systeme a une dimension de fermions en interaction," Phys. Lett. A **24**, 55 (1967).

[36] C. N. Yang, "Some exact results for the many-body problem in one dimension with repulsive delta-function interaction," Phys. Rev. Lett. **19**, 1312 (1967).

[37] C. J. Cramer, *Essentials of Computational Chemistry: Theories and Models*, 2nd ed. (Wiley, 2004).

[38] L. Cao, S. Krönke, O. Vendrell, and P. Schmelcher, "The multi-layer multi-configuration time-dependent Hartree method for bosons: Theory, implementation, and applications," J. Chem. Phys. **139**, 134103 (2013).

[39] V. J. Bolsinger, S. Krönke, and P. Schmelcher, "Beyond mean-field dynamics of ultra-cold bosonic atoms in higher dimensions: facing the challenges with a multi-configurational approach," J. Phys. B: At. Mol. Opt. **50**, 034003 (2017).

[40] C. Gattringer and K. Langfeld, "Approaches to the sign problem in lattice field theory," Int. J. Mod. Phys. A **31**, 1643007 (2016).

[41] F. Bruckmann, C. Gattringer, T. Kloiber, and T. Sulejmanpasic, "Corrigendum to "Dual lattice representations for $O(N)$ and $CP(N-1)$ models with a chemical potential" [Phys. Lett. B 749 (2015) 495–501]," Phys. Lett. B **751**, 595 (2015).

[42] F. Bruckmann, C. Gattringer, T. Kloiber, and T. Sulejmanpasic, "Two-dimensional $O(3)$ model at nonzero density: From dual lattice simulations to repulsive bosons," Phys. Rev. D **94**, 114503 (2016).

[43] F. Bruckmann, personal communication (2016).

[44] G. Franck and G. Hertz, "Über Zusammenstöße zwischen Elektronen und den Molekülen des Quecksilberdampfes und die Ionisierungsspannung desselben," Verh. D. Phys. Ges. **16**, 457 (1914).

[45] N. Bohr, "I. On the constitution of atoms and molecules," Philos. Mag. **26**, 1 (1913).

[46] A. Sommerfeld, "Zur Quantentheorie der Spektrallinien," Ann. d. Phys. **356**, 1 (1916).

[47] G. Tanner and K. Richter, "Semiclassical theory of helium atom," Scholarpedia **8**, 9818 (2013), revision #132323.

[48] D. Stone, "Einstein's unknown insight and the problem of quantizing chaos," Phys. Today **58**, 37 (2005).

[49] M. C. Gutzwiller, "Phase-integral approximation in momentum space and the bound states of an atom," J. Math. Phys. **8**, 1979 (1967).

[50] M. C. Gutzwiller, *Chaos in Classical and Quantum Mechanics*, Interdisciplinary Applied Mathematics (Springer New York, 1991).

[51] J. H. Van Vleck, "The correspondence principle in the statistical interpretation of quantum mechanics," Proc. Natl. Acad. Sci. **14**, 178 (1928).

[52] R. P. Feynman, "Space-time approach to non-relativistic quantum mechanics," Rev. Mod. Phys. **20**, 367 (1948).

[53] S. Tomsovic and E. J. Heller, "Semiclassical dynamics of chaotic motion: Unexpected long-time accuracy," Phys. Rev. Lett. **67**, 664 (1991).

[54] M. C. Gutzwiller, "Periodic orbits and classical quantization conditions," J. Math. Phys. **12**, 343 (1971).

[55] V. Ivrii, "100 years of Weyl's law," B. Math. Sci. **6**, 379 (2016).

[56] H. Weyl, "Über die Asymptotische Verteilung der Eigenwerte," Nachr. Ges. Wiss. Gött. Math.-Phys.: Kl. , 110 (1911).

[57] R. Balian and C. Bloch, "Distribution of eigenfrequencies for the wave equation in a finite domain. I. Three-dimensional problem with smooth boundary surface," Ann. Phys. (New York) **60**, 273 (1970).

[58] P. Cvitanović, R. Artuso, R. Mainieri, G. Tanner, and G. Vattay, *Chaos: Classical and Quantum* (Niels Bohr Inst., Copenhagen, 2016).

[59] J. B. Delos, "Semiclassical calculation of quantum mechanical wavefunctions," Adv. Chem. Phys. **65** (1986).

[60] J. B. Delos, "Catastrophes and stable caustics in bound states of Hamiltonian systems," J. Chem. Phys. **86**, 425 (1987).

[61] A. Holle, J. Main, G. Wiebusch, H. Rottke, and K. H. Welge, "Quasi-Landau spectrum of the chaotic diamagnetic hydrogen atom," Phys. Rev. Lett. **61**, 161 (1988).

[62] D. Wintgen, "Connection between long-range correlations in quantum spectra and classical periodic orbits," Phys. Rev. Lett. **58**, 1589 (1987).

[63] J. P. Pique, "Molecular dynamics and quantum chaos in small polyatomic molecules (CS_2, C_2H_2) through stimulated-emission pumping experiments and statistical Fourier-transform analysis," J. Opt. Soc. Am. B **7**, 1816 (1990).

[64] H.-J. Stöckmann and J. Stein, ""Quantum" chaos in billiards studied by microwave absorption," Phys. Rev. Lett. **64**, 2215 (1990).

[65] E. J. Heller, "Bound-state eigenfunctions of classically chaotic Hamiltonian systems: Scars of periodic orbits," Phys. Rev. Lett. **53**, 1515 (1984).

[66] R. A. Jalabert, "The semiclassical tool in mesoscopic physics," (1999), arXiv:cond-mat/9912038 .

[67] K. Richter, *Semiclassical Theory of Mesoscopic Quantum Systems*, Springer tracts in modern physics, Vol. 161 (Springer, Berlin, 2000).

[68] W. H. Miller, "Semiclassical methods in chemical physics," Science **233**, 171 (1986).

[69] E. M. Graefe and H. J. Korsch, "Semiclassical quantization of an N-particle Bose-Hubbard model," Phys. Rev. A **76**, 032116 (2007).

[70] M. L. Mehta, *Random Matrices*, 3rd ed., Pure and Applied Mathematics, Vol. 142 (Academic Press, 2004).

[71] O. Bohigas, M. J. Giannoni, and C. Schmit, "Characterization of chaotic quantum spectra and universality of level fluctuation laws," Phys. Rev. Lett. **52**, 1 (1984).

[72] M. V. Berry, "Semiclassical theory of spectral rigidity," P. Roy. Soc. Lond. A: Mat. **400**, 229 (1985).

[73] M. Sieber and K. Richter, "Correlations between periodic orbits and their rôle in spectral statistics," Phys. Scripta **2001**, 128 (2001).

[74] S. Heusler, S. Müller, P. Braun, and F. Haake, "Universal spectral form factor for chaotic dynamics," J. Phys. A: Math. Gen. **37**, L31 (2004).

[75] S. Müller, S. Heusler, P. Braun, F. Haake, and A. Altland, "Semiclassical foundation of universality in quantum chaos," Phys. Rev. Lett. **93**, 014103 (2004).

[76] M. Turek, *Semiclassics beyond the diagonal approximation*, Ph.D. thesis, Universität Regensburg (2004).

[77] M. Turek, D. Spehner, S. Müller, and K. Richter, "Semiclassical form factor for spectral and matrix element fluctuations of multidimensional chaotic systems," Phys. Rev. E **71**, 016210 (2005).

[78] S. Müller, S. Heusler, P. Braun, F. Haake, and A. Altland, "Periodic-orbit theory of universality in quantum chaos," Phys. Rev. E **72**, 046207 (2005).

[79] S. Müller, *Periodic-Orbit Approach to Universality in Quantum Chaos*, Ph.D. thesis, Universität Duisburg-Essen (2005).

[80] S. Heusler, S. Müller, P. Braun, and F. Haake, "Semiclassical theory of chaotic conductors," Phys. Rev. Lett. **96**, 066804 (2006).

[81] P. Braun, S. Heusler, S. Müller, and F. Haake, "Semiclassical prediction for shot noise in chaotic cavities," J. Phys. A: Math. Gen. **39**, L159 (2006).

[82] T. Nagao, P. Braun, S. Müller, K. Saito, S. Heusler, and F. Haake, "Semiclassical theory for parametric correlation of energy levels," J. Phys. A: Math. Theor. **40**, 47 (2007).

[83] S. Müller, S. Heusler, P. Braun, and F. Haake, "Semiclassical approach to chaotic quantum transport," New J. Phys. **9**, 12 (2007).

[84] S. Müller, S. Heusler, A. Altland, P. Braun, and F. Haake, "Periodic-orbit theory of universal level correlations in quantum chaos," New J. Phys. **11**, 103025 (2009).

[85] H. U. Baranger, R. A. Jalabert, and A. D. Stone, "Weak localization and integrability in ballistic cavities," Phys. Rev. Lett. **70**, 3876 (1993).

[86] H. U. Baranger, R. A. Jalabert, and A. D. Stone, "Quantum-chaotic scattering effects in semiconductor microstructures," Chaos **3**, 665 (1993).

[87] K. Richter and M. Sieber, "Semiclassical theory of chaotic quantum transport," Phys. Rev. Lett. **89**, 206801 (2002).

[88] S. Hikami, A. I. Larkin, and Y. Nagaoka, "Spin-orbit interaction and magnetoresistance in the two dimensional random system," Prog. Theor. Phys. **63**, 707 (1980).

[89] O. Zaitsev, D. Frustaglia, and K. Richter, "Semiclassical theory of weak antilocalization and spin relaxation in ballistic quantum dots," Phys. Rev. B **72**, 155325 (2005).

[90] P. Jacquod and R. S. Whitney, "Semiclassical theory of quantum chaotic transport: Phase-space splitting, coherent backscattering, and weak localization," Phys. Rev. B **73**, 195115 (2006).

[91] R. A. Jalabert and H. M. Pastawski, "Environment-independent decoherence rate in classically chaotic systems," Phys. Rev. Lett. **86**, 2490 (2001).

[92] A. Goussev, R. A. Jalabert, H. M. Pastawski, and D. A. Wisniacki, "Loschmidt echo," Scholarpedia **7**, 11687 (2012), revision #127578.

[93] P. W. Brouwer and S. Rahav, "Semiclassical theory of the Ehrenfest time dependence of quantum transport in ballistic quantum dots," Phys. Rev. B **74**, 075322 (2006).

[94] T. Hartmann, J. Michl, C. Petitjean, T. Wellens, J. D. Urbina, K. Richter, and P. Schlagheck, "Weak localization with nonlinear bosonic matter waves," Ann. Phys. (New York) **327**, 1998 (2012).

[95] G. Berkolaiko and J. Kuipers, "Transport moments beyond the leading order," New J. Phys. **13**, 063020 (2011).

[96] J. Kuipers and K. Richter, "Transport moments and Andreev billiards with tunnel barriers," J. Phys. A: Math. Theor. **46**, 055101 (2013).

[97] G. Berkolaiko and J. Kuipers, "Combinatorial theory of the semiclassical evaluation of transport moments. I. Equivalence with the random matrix approach," J. Math. Phys. **54**, 112103 (2013).

[98] R. S. Whitney and P. Jacquod, "Controlling the sign of magnetoconductance in Andreev quantum dots," Phys. Rev. Lett. **103**, 247002 (2009).

[99] T. Engl, J. Kuipers, and K. Richter, "Conductance and thermopower of ballistic Andreev cavities," Phys. Rev. B **83**, 205414 (2011).

[100] A. Goussev, D. Waltner, K. Richter, and R. A. Jalabert, "Loschmidt echo for local perturbations: non-monotonic cross-over from the Fermi-golden-rule to the escape-rate regime," New J. Phys. **10**, 093010 (2008).

[101] B. Gutkin, D. Waltner, M. Gutiérrez, J. Kuipers, and K. Richter, "Quantum corrections to fidelity decay in chaotic systems," Phys. Rev. E **81**, 036222 (2010).

[102] P. Borwein, *The Riemann Hypothesis: A Resource for the Afficionado and Virtuoso Alike*, CMS Books in Mathematics (Springer New York, 2008).

[103] J. Carlson, A. Jaffe, and A. Wiles, eds., *The Millennium Prize Problems* (American Mathematical Society and Clay Mathematics Institute, 2006).

[104] M. V. Berry and J. P. Keating, "The Riemann zeros and eigenvalue asymptotics," SIAM Rev. **41**, 236 (1999).

[105] J. Kuipers, Q. Hummel, and K. Richter, "Quantum graphs whose spectra mimic the zeros of the Riemann zeta function," Phys. Rev. Lett. **112**, 070406 (2014).

[106] R. Balian and C. Bloch, "Distribution of eigenfrequencies for the wave equation in a finite domain. II. Electromagnetic field. Riemannian spaces," Ann. Phys. (New York) **64**, 271 (1971).

[107] M. Brack and R. K. Bhaduri, *Semiclassical Physics*, Frontiers in Physics (Westview Press, 2003).

[108] D. Wintgen, K. Richter, and G. Tanner, "The semiclassical helium atom," Chaos **2**, 19 (1992).

[109] H. A. Weidenmüller, "Semiclassical periodic-orbit theory for identical particles," Phys. Rev. A **48**, 1819 (1993).

[110] Q. Hummel, *Semiclassical approach to systems of identical particles*, Diploma thesis, Universität Regensburg, Germany (2012).

[111] J. D. Urbina, J. Kuipers, S. Matsumoto, Q. Hummel, and K. Richter, "Multiparticle correlations in mesoscopic scattering: Boson sampling, birthday paradox, and Hong-Ou-Mandel profiles," Phys. Rev. Lett. **116**, 100401 (2016).

[112] L. H. Thomas, "The calculation of atomic fields," Math. Proc. Cambridge **23**, 542–548 (1927).

[113] P. Elliott, D. Lee, A. Cangi, and K. Burke, "Semiclassical origins of density functionals," Phys. Rev. Lett. **100**, 256406 (2008).

[114] R. F. Ribeiro, D. Lee, A. Cangi, P. Elliott, and K. Burke, "Corrections to Thomas-Fermi densities at turning points and beyond," Phys. Rev. Lett. **114**, 050401 (2015).

[115] S. Weinberg, *The Quantum Theory of Fields*, Vol. 1 (Cambridge University Press, 1995).

[116] L. S. Schulman, *Techniques and Applications of Path Integration* (Wiley, 1996).

[117] L. D. Faddeev and L. A. Takhtajan, *Hamiltonian Methods in the Theory of Solitons*, Springer Series in Soviet Mathematics (Springer, 1987).

[118] T. Engl, *A semiclassical approach to many-body interference in Fock-space*, Ph.D. thesis (2015).

[119] T. Engl, J. D. Urbina, and K. Richter, "The semiclassical propagator in fock space: dynamical echo and many-body interference," Philos. T. Roy. Soc. A **374** (2016).

[120] T. Engl, P. Plößl, J. D. Urbina, and K. Richter, "The semiclassical propagator in fermionic Fock space," Theor. Chem. Acc. **133**, 1563 (2014).

[121] T. Engl, J. Dujardin, A. Argüelles, P. Schlagheck, K. Richter, and J. D. Urbina, "Coherent backscattering in Fock space: A signature of quantum many-body interference in interacting bosonic systems," Phys. Rev. Lett. **112**, 140403 (2014).

[122] C. Chin, R. Grimm, P. Julienne, and E. Tiesinga, "Feshbach resonances in ultracold gases," Rev. Mod. Phys. **82**, 1225 (2010).

[123] S. Dettmer, D. Hellweg, P. Ryytty, J. J. Arlt, W. Ertmer, K. Sengstock, D. S. Petrov, G. V. Shlyapnikov, H. Kreutzmann, L. Santos, and M. Lewenstein, "Observation of phase fluctuations in elongated Bose-Einstein condensates," Phys. Rev. Lett. **87**, 160406 (2001).

[124] J. Billy, V. Josse, Z. Zuo, A. Bernard, B. Hambrecht, P. Lugan, D. Clement, L. Sanchez-Palencia, P. Bouyer, and A. Aspect, "Direct observation of Anderson localization of matter waves in a controlled disorder," Nature **453**, 891 (2008).

[125] H. Moritz, T. Stöferle, M. Köhl, and T. Esslinger, "Exciting collective oscillations in a trapped 1D gas," Phys. Rev. Lett. **91**, 250402 (2003).

[126] T. Kinoshita, T. Wenger, and D. S. Weiss, "Observation of a one-dimensional Tonks-Girardeau gas," Science **305**, 1125 (2004).

[127] B. Paredes, A. Widera, V. Murg, O. Mandel, S. Folling, I. Cirac, G. V. Shlyapnikov, T. W. Hansch, and I. Bloch, "Tonks-Girardeau gas of ultracold atoms in an optical lattice," Nature **429**, 277 (2004).

[128] T. Kinoshita, T. Wenger, and D. S. Weiss, "A quantum Newton's cradle," Nature **440**, 900 (2006).

[129] F. Serwane, G. Zürn, T. Lompe, T. B. Ottenstein, A. N. Wenz, and S. Jochim, "Deterministic preparation of a tunable few-fermion system," Science **332**, 336 (2011).

[130] G. Zürn, F. Serwane, T. Lompe, A. N. Wenz, M. G. Ries, J. E. Bohn, and S. Jochim, "Fermionization of two distinguishable fermions," Phys. Rev. Lett. **108**, 075303 (2012).

[131] A. N. Wenz, G. Zürn, S. Murmann, I. Brouzos, T. Lompe, and S. Jochim, "From few to many: Observing the formation of a Fermi sea one atom at a time," Science **342**, 457 (2013).

[132] M. Greiner, I. Bloch, O. Mandel, T. W. Hänsch, and T. Esslinger, "Exploring phase coherence in a 2D lattice of Bose-Einstein condensates," Phys. Rev. Lett. **87**, 160405 (2001).

[133] H. A. Gersch and G. C. Knollman, "Quantum cell model for bosons," Phys. Rev. **129**, 959 (1963).

[134] R. Folman, P. Krüger, J. Schmiedmayer, J. Denschlag, and C. Henkel, "Microscopic atom optics: From wires to an atom chip," (Academic Press, 2002) pp. 263–356.

[135] J. Reichel and V. Vuletic, *Atom Chips* (Wiley, 2011).

[136] B. Rauer, T. Schweigler, T. Langen, and J. Schmiedmayer, "Does an isolated quantum system relax?" in *Proceedings of the International School of Physics "Enrico Fermi"*, Vol. 191, edited by M. Inguscio, W. Ketterle, S. Stringari, and G. Roati (IOS Press, 2016) pp. 485–504.

[137] S. Gupta, K. W. Murch, K. L. Moore, T. P. Purdy, and D. M. Stamper-Kurn, "Bose-Einstein condensation in a circular waveguide," Phys. Rev. Lett. **95**, 143201 (2005).

[138] A. Turpin, J. Polo, Y. V. Loiko, J. Küber, F. Schmaltz, T. K. Kalkandjiev, V. Ahufinger, G. Birkl, and J. Mompart, "Blue-detuned optical ring trap for Bose-Einstein condensates based on conical refraction," Opt. Express **23**, 1638 (2015).

[139] W. Grandy, *Foundations of Statistical Mechanics: Equilibrium Theory*, Fundamental Theories of Physics (Springer Netherlands, 1987).

[140] H. J. Stöckmann, *Quantum Chaos: An Introduction* (Cambridge University Press, 2006).

[141] F. Haake, *Quantum Signatures of Chaos*, Springer Series in Synergetics (Springer Berlin, 2001).

[142] M. V. Berry and C. J. Howls, "High orders of the Weyl expansion for quantum billiards: Resurgence of periodic orbits, and the Stokes phenomenon," P. Roy. Soc. Lond. A: Mat. **447**, 527 (1994).

[143] L. L. Schiff, *Quantum Mechanics*, International Series in Pure and Applied Physics (McGraw-Hill, 1968).

[144] J. Rotman, *An Introduction to the Theory of Groups*, Graduate Texts in Mathematics (Springer New York, 1999).

[145] J. H. Davies, *The Physics of Low-Dimensional Semiconductors: An Introduction* (Cambridge University Press, 1998).

[146] C. Stephanos, T. Kopp, J. Mannhart, and P. J. Hirschfeld, "Interface-induced d-wave pairing," Phys. Rev. B **84**, 100510 (2011).

[147] E. Navarro-Moratalla, J. O. Island, S. Mañas-Valero, E. Pinilla-Cienfuegos, A. Castellanos-Gomez, J. Quereda, G. Rubio-Bollinger, L. Chirolli, J. A. Silva-Guillén, N. Agraït, G. A. Steele, F. Guinea, H. S. J. van der Zant, and E. Coronado, "Enhanced superconductivity in atomically thin TaS_2," Nat. Commun. **7**, 11043 (2016).

[148] W. J. Mullin and J. P. Fernández, "Bose–Einstein condensation, fluctuations, and recurrence relations in statistical mechanics," Am. J. Phys. **71**, 661 (2003).

[149] V. V. Kocharovsky, V. V. Kocharovsky, M. Holthaus, C. H. R. Ooi, A. Svidzinsky, W. Ketterle, and M. O. Scully, "Fluctuations in ideal and interacting Bose–Einstein condensates: From the laser phase transition analogy to squeezed states and Bogoliubov quasiparticles," Adv. Atom. Mol. Opt. Phy. **53**, 291 (2006).

[150] H. D. Ursell, "The evaluation of Gibbs' phase-integral for imperfect gases," Math. Proc. Cambridge **23**, 685–697 (1927).

[151] B. Kahn and G. E. Uhlenbeck, "On the theory of condensation," Physica **5**, 399 (1938).

[152] P. Grüter and F. Laloë, "Ursell operators in statistical physics I: Generalizing the Beth Uhlenbeck formula," J. Phys. I (France) **5**, 181 (1995).

[153] P. Grüter and F. Laloë, "Ursell operators in statistical physics II: Microscopic properties of a dilute quantum gas," J. Phys. I (France) **5**, 1255 (1995).

[154] P. Grüter, F. Laloë, A. E. Meyerovich, and W. Mullin, "Ursell operators in statistical physics III: Thermodynamic properties of degenerate gases," J. Phys. I (France) **7**, 485 (1997).

[155] M. Holzmann, P. Grüter, and F. Laloë, "Bose-Einstein condensation in interacting gases," Eur. Phys. J. B **10**, 739 (1999).

[156] J. N. Fuchs, M. Holzmann, and F. Laloë, "Ursell operators in statistical physics of dense systems: the role of high order operators and of exchange cycles," Eur. Phys. J. B **25**, 463 (2002).

[157] Q. Hummel, J. D. Urbina, and K. Richter, "Canonical description of 1D few-body systems with short-range interaction," (2016), arXiv:1603.02775 .

[158] C. Grosche, "Path integrals for two- and three-dimensional δ-function perturbations," Ann. d. Phys. **506**, 283 (1994).

[159] H. E. Camblong, L. N. Epele, H. Fanchiotti, and C. A. G. Canal, "Dimensional transmutation and dimensional regularization in quantum mechanics," Ann. Phys. (New York) **287**, 14 (2001).

[160] X.-W. Guan, M. T. Batchelor, and C. Lee, "Fermi gases in one dimension: From Bethe ansatz to experiments," Rev. Mod. Phys. **85**, 1633 (2013).

[161] M. Olshanii, "Atomic scattering in the presence of an external confinement and a gas of impenetrable bosons," Phys. Rev. Lett. **81**, 938 (1998).

[162] E. Haller, M. J. Mark, R. Hart, J. G. Danzl, L. Reichsöllner, V. Melezhik, P. Schmelcher, and H.-C. Nägerl, "Confinement-induced resonances in low-dimensional quantum systems," Phys. Rev. Lett. **104**, 153203 (2010).

[163] M. de Llano, A. Salazar, and M. A. Solis, "Two-dimensional delta potential wells and condensed-matter physics," Rev. Mex. Fis. **51**, 626 (2005).

[164] K. Huang and C. N. Yang, "Quantum-mechanical many-body problem with hard-sphere interaction," Phys. Rev. **105**, 767 (1957).

[165] M. Valiente, "Tan's distributions and Fermi-Huang pseudopotential in momentum space," Phys. Rev. A **85**, 014701 (2012).

[166] M. Gaudin, "Boundary energy of a Bose gas in one dimension," Phys. Rev. A **4**, 386 (1971).

[167] E. B. Manoukian, "Explicit derivation of the propagator for a Dirac delta potential," J. Phys. A: Math. Gen. **22**, 67 (1989).

[168] B. Geiger, J.-D. Urbina, Q. Hummel, and K. Richter, "Semiclassics in a system without classical limit: the few-body spectrum of two interacting bosons in one dimension," (2017), arXiv:1705.09637 .

[169] T. C. Dorlas, "Orthogonality and completeness of the Bethe ansatz eigenstates of the nonlinear Schroedinger model," Comm. Math. Phys. **154**, 347 (1993).

[170] M. Girardeau, "Relationship between systems of impenetrable bosons and fermions in one dimension," J. Math. Phys. **1**, 516 (1960).

[171] L. Tonks, "The complete equation of state of one, two and three-dimensional gases of hard elastic spheres," Phys. Rev. **50**, 955 (1936).

[172] C. N. Yang and C. P. Yang, "Thermodynamics of a one-dimensional system of bosons with repulsive delta-function interaction," J. Math. Phys. **10**, 1115 (1969).

[173] C. P. Yang, "One-dimensional system of bosons with repulsive δ-function interactions at a finite temperature T," Phys. Rev. A **2**, 154 (1970).

[174] T. Cheon and T. Shigehara, "Fermion-boson duality of one-dimensional quantum particles with generalized contact interactions," Phys. Rev. Lett. **82**, 2536 (1999).

[175] K. Suzuki, "Construction of Hermitian effective interaction in nuclei - general relation between Hermitian and non-Hermitian forms," Prog. Theor. Phys. **68**, 246 (1982).

[176] E. J. Lindgren, J. Rotureau, C. Forssén, A. G. Volosniev, and N. T. Zinner, "Fermionization of two-component few-fermion systems in a one-dimensional harmonic trap," New J. Phys. **16**, 063003 (2014).

[177] T. Busch, B.-G. Englert, K. Rzażewski, and M. Wilkens, "Two cold atoms in a harmonic trap," Found. Phys. **28**, 549 (1998).

[178] J. B. McGuire, "Interacting fermions in one dimension. I. Repulsive potential," J. Math. Phys. **6**, 432 (1965).

[179] M. Colomé-Tatché and D. S. Petrov, "Parametric excitation of a 1D gas in integrable and nonintegrable cases," Phys. Rev. Lett. **106**, 125302 (2011).

[180] W. G. Gibson, "Pade approximant method for the statistical thermodynamics of a quantum system. I. General formulation and simple examples," J. Phys. A: Math. Gen. **17**, 1877 (1984).

[181] E. Wigner, "On the quantum correction for thermodynamic equilibrium," Phys. Rev. **40**, 749 (1932).

[182] J. G. Kirkwood, "Quantum statistics of almost classical assemblies," Phys. Rev. **44**, 31 (1933).

[183] J. Clerk-Maxwell, "On the dynamical evidence of the molecular constitution of bodies," Nature **11**, 357 (1875).

[184] B. Geiger, (2016), (unpublished).

[185] M. Biberger, (2015), (unpublished).

[186] K. V. Kheruntsyan, D. M. Gangardt, P. D. Drummond, and G. V. Shlyapnikov, "Pair correlations in a finite-temperature 1D Bose gas," Phys. Rev. Lett. **91**, 040403 (2003).

[187] P. Deuar, A. G. Sykes, D. M. Gangardt, M. J. Davis, P. D. Drummond, and K. V. Kheruntsyan, "Nonlocal pair correlations in the one-dimensional Bose gas at finite temperature," Phys. Rev. A **79**, 043619 (2009).

[188] J. B. McGuire, "Study of exactly soluble one-dimensional N-body problems," J. Math. Phys. **5**, 622 (1964).

[189] A. G. Sykes, P. D. Drummond, and M. J. Davis, "Excitation spectrum of bosons in a finite one-dimensional circular waveguide via the bethe ansatz," Phys. Rev. A **76**, 063620 (2007).

[190] P. Calabrese and J.-S. Caux, "Dynamics of the attractive 1D Bose gas: analytical treatment from integrability," J. Stat. Mech.: Theory E. **2007**, P08032 (2007).

[191] B. Sutherland, "A brief history of the quantum soliton with new results on the quantization of the Toda lattice," Rocky Mt. J. Math. **8**, 413 (1978).

[192] M. Toda, *Theory of Nonlinear Lattices*, Springer Series in Solid-State Sciences (Springer Berlin, 1989).

[193] M. C. Gutzwiller, "The quantum mechanical Toda lattice, II," Ann. Phys. (New York) **133**, 304 (1981).

[194] M. Fowler and H. Frahm, "Quantization conditions for the periodic Toda chain: Inadequacy of Bethe-ansatz methods," Phys. Rev. B **39**, 11800 (1989).

[195] R. Siddharthan and B. Sriram Shastry, "Quantizing the Toda lattice," Phys. Rev. B **55**, 12196 (1997).

[196] S. Scarlatti and A. Teta, "Derivation of the time-dependent propagator for the three-dimensional Schrodinger equation with one point interaction," J. Phys. A: Math. Gen. **23**, L1033 (1990).

[197] G. E. Uhlenbeck and E. Beth, "The quantum theory of the non-ideal gas I. Deviations from the classical theory," Physica **3**, 729 (1936).

[198] V. I. Arnold, K. Vogtmann, and A. Weinstein, *Mathematical Methods of Classical Mechanics*, Graduate Texts in Mathematics (Springer New York, 1989).

[199] A. M. Ozorio de Almeida, *Hamiltonian Systems: Chaos and Quantization*, Cambridge Monographs on Mathematical Physics (Cambridge University Press, 1989).

[200] M. M. Nieto, "Quantum phase and quantum phase operators: some physics and some history," Phys. Scripta **1993**, 5 (1993).

[201] M. V. Berry and M. Tabor, "Calculating the bound spectrum by path summation in action-angle variables," J. Phys. A: Math. Gen. **10**, 371 (1977).

[202] T. Poston and I. Stewart, *Catastrophe Theory and its Applications*, Dover Books on Mathematics (Dover Publications, 1978).

[203] S. Sachdev, *Quantum Phase Transitions* (Cambridge University Press, 2011).

[204] L. D. Carr, ed., *Understanding Quantum Phase Transitions*, Series in Condensed Matter Physics (CRC Press, 2011).

[205] P. Stránskỳ, M. Macek, and P. Cejnar, "Excited-state quantum phase transitions in systems with two degrees of freedom: Level density, level dynamics, thermal properties," Ann. Phys. (New York) **345**, 73 (2014).

[206] L. Pitaevskii and S. Stringari, *Bose-Einstein Condensation and Superfluidity*, International Series of Monographs on Physics (Oxford University Press, 2016).

[207] Y. Castin, "Simple theoretical tools for low dimension Bose gases," J. Phys. IV (France) **116**, 89 (2004).

[208] R. Kanamoto, H. Saito, and M. Ueda, "Symmetry breaking and enhanced condensate fraction in a matter-wave bright soliton," Phys. Rev. Lett. **94**, 090404 (2005).

[209] R. Kanamoto, H. Saito, and M. Ueda, "Critical fluctuations in a soliton formation of attractive Bose-Einstein condensates," Phys. Rev. A **73**, 033611 (2006).

[210] J. G. Muga and R. F. Snider, "Solvable three-boson model with attractive δ-function interactions," Phys. Rev. A **57**, 3317 (1998).

[211] K. Sakmann, A. I. Streltsov, O. E. Alon, and L. S. Cederbaum, "Exact ground state of finite Bose-Einstein condensates on a ring," Phys. Rev. A **72**, 033613 (2005).

[212] C. Gardiner and P. Zoller, *Quantum Noise: A Handbook of Markovian and Non-Markovian Quantum Stochastic Methods with Applications to Quantum Optics*, Springer Series in Synergetics (Springer Berlin, 2004).

[213] J. R. Cary, D. Escande, and J. L. Tennyson, "Adiabatic-invariant change due to separatrix crossing," Phys. Rev. A **34**, 4256 (1986).

[214] H. Waalkens, J. Wiersig, and H. R. Dullin, "Elliptic quantum billiard," Ann. Phys. (New York) **260**, 50 (1997).

[215] M. V. Berry and K. E. Mount, "Semiclassical approximations in wave mechanics," Rep. Prog. Phys. **35**, 315 (1972).

[216] M. V. Berry and N. L. Balazs, "Evolution of semiclassical quantum states in phase space," J. Phys. A: Math. Gen. **12**, 625 (1979).

[217] G. Dvali, D. Flassig, C. Gomez, A. Pritzel, and N. Wintergerst, "Scrambling in the black hole portrait," Phys. Rev. D **88**, 124041 (2013).

[218] P. Hayden and J. Preskill, "Black holes as mirrors: quantum information in random subsystems," J. High Energy Phys. **2007**, 120 (2007).

[219] Y. Sekino and L. Susskind, "Fast scramblers," J. High Energy Phys. **2008**, 065 (2008).

[220] M. Abramowitz and I. A. Stegun, *Handbook of Mathematical Functions: with Formulas, Graphs, and Mathematical Tables*, Dover Books on Mathematics (Dover Publications, 1965).

[221] G. N. Watson, *A Treatise on the Theory of Bessel Functions*, 2nd ed., Cambridge Mathematical Library (Cambridge University Press, 1995).

[222] F. Dalfovo, S. Giorgini, L. P. Pitaevskii, and S. Stringari, "Theory of Bose-Einstein condensation in trapped gases," Rev. Mod. Phys. **71**, 463 (1999).

[223] M. A. Caprio, P. Cejnar, and F. Iachello, "Excited state quantum phase transitions in many-body systems," Ann. Phys. (New York) **323**, 1106 (2008).

[224] F. Leyvraz and W. D. Heiss, "Large-N scaling behavior of the Lipkin-Meshkov-Glick model," Phys. Rev. Lett. **95**, 050402 (2005).

[225] J. D. Urbina, personal communication (2017).

[226] M. Born and R. Oppenheimer, "Zur Quantentheorie der Molekeln," Ann. d. Phys. **389**, 457 (1927).

[227] P. W. Atkins and R. S. Friedman, *Molecular Quantum Mechanics*, 5th ed. (Oxford University Press, 2010).

[228] N. N. Bogoliubov and D. V. Shirkov, "The multiplicative renormalization group in the quantum theory of fields," Sov. Phys. JETP (USSR) **3**, 77 (1956).

[229] N. N. Bogoliubov and D. V. Shirkov, *Introduction to the Theory of Quantized Fields*, 2nd ed., Monographs and Texts in Physics and Astronomy, Vol. 3 (Interscience Publishers, 1959) authorized English Ed., Rev. and Enl. by the Authors.

[230] R. Landig, L. Hruby, N. Dogra, M. Landini, R. Mottl, T. Donner, and T. Esslinger, "Quantum phases from competing short- and long-range interactions in an optical lattice," Nature **532**, 476 (2016).

[231] B. Sundar and E. J. Mueller, "Lattice bosons with infinite-range checkerboard interactions," Phys. Rev. A **94**, 033631 (2016).

[232] A. I. Larkin and Y. N. Ovchinnikov, "Quasiclassical method in the theory of superconductivity," Sov. Phys. JETP (USSR) **28**, 1200 (1969).

[233] A. Kitaev, "Hidden correlations in the Hawking radiation and thermal noise," talk given at Fundamental Physics Prize Symposium (2014).

[234] I. L. Aleiner, L. Faoro, and L. B. Ioffe, "Microscopic model of quantum butterfly effect: Out-of-time-order correlators and traveling combustion waves," Ann. Phys. (New York) **375**, 378 (2016).

[235] B. Swingle and D. Chowdhury, "Slow scrambling in disordered quantum systems," Phys. Rev. B **95**, 060201 (2017).

[236] J. S. Cotler, D. Ding, and G. R. Penington, "Out-of-time-order operators and the butterfly effect," (2017), arXiv:1704.02979 .

[237] E. B. Rozenbaum, S. Ganeshan, and V. Galitski, "Lyapunov exponent and out-of-time-ordered correlator's growth rate in a chaotic system," Phys. Rev. Lett. **118**, 086801 (2017).

[238] J. Kurchan, "Quantum bound to chaos and the semiclassical limit," (2016), arXiv:1612.01278 .

[239] J. Michl, personal communication (2017).

[240] B. Geiger, personal communication (2017).

List of publications

- Q. Hummel, J. D. Urbina, and K. Richter, *The Weyl expansion for systems of independent identical particles*, J. Phys. A **47**, 015101 (2014).
- J. Kuipers, Q. Hummel, and K. Richter, *Quantum graphs whose spectra mimic the zeros of the Riemann zeta function*, Phys. Rev. Lett. **112**, 070406 (2014).
- T. Engl, J. D. Urbina, Q. Hummel, and K. Richter, *Complex scattering as canonical transformation: A semiclassical approach in Fock space*, Ann. d. Phys. **527**, 737 (2015).
- Q. Hummel, J. D. Urbina, and K. Richter, *Canonical description of 1d few-body systems with short range interaction*, (2016), arXiv:1603.02775 (to be submitted).
- J. D. Urbina, J. Kuipers, S. Matsumoto, Q. Hummel, and K. Richter, *Multiparticle correlations in mesoscopic scattering: Boson sampling, birthday paradox, and Hong-Ou-Mandel profiles*, Phys. Rev. Lett. **116**, 100401 (2016).
- B. Geiger, J. D. Urbina, Q. Hummel, and K. Richter, *Semiclassics in a system without classical limit: The few-body spectrum of two interacting bosons in one dimension*, (2017), arXiv:1705.09637 (accepted for publication in Phys. Rev. E).

Acknowledgements

Before I start I want to apologize for the excessiveness of the following, but personally speaking, for me this is one of the most important parts of this thesis.

I dedicate this work to my daughter, Ronja. She is the most valuable thing I have and the best thing I ever was able to introduce into this world. A single smile of her fills my world with light. There is no other process in this world for me that can compete with watching her develop from day to day.

I thank Vici, for she gave birth to the most precious thing in my life. I also thank her for never being afraid of thinking or acting outside the box. By a decision that seemed horrifying in the first place she opened the door for me to make this work happen and to find my way to my inner fate. Which brings me to the next person I am deeply grateful for.

Bianca, my love, who found her way into my life when I was at its bottom. I have one deep association with the unpredictable ways of this seemingly chaotic universe that lead me to her. Thinking back how I met this woman always reminds me of finding a rare blossom on the top of a mountain. She made this last period before finishing this work – which is commonly supposed to be the worst time of your life[3] – one of the best times of my life. I thank her for that with all my heart. With her I feel strong enough to look forward to whatever life will come up with in the future.

I greatly thank all my friends, too numerous to name them one by one. But my special thanks go to my old pals from my home town: Seppes, Günne, Mathi, Wolfi, Clemm and Schmau, as they made this world a home for me in times when I was risking to get forever lost in solitude.

I thank Susie, who supported me during the first years of my studies and for still being a good friend.

I also want to thank Lisa, who taught me humbleness and gratitude for my given reality.

My acknowledgements also go to Mim. She wouldn't understand a single word of this thesis but having her as a flat-mate makes a very good and delightful home for me and my daughter. I am grateful to her for supporting me during finishing this work so kindly and emphatically.

I especially thank my parents, who always supported me to find my way in their good-hearted and open-minded attitude. Due to them and with them I could become who I am now. I thank them for defining the initial conditions of my personal life the way they did.

[3] Indeed, it had a flavor of being caught in the middle of Zeno's paradox of Achilles and the tortoise. Luckily, in ignorance about the ongoing controversy, the belief in its resolution became reality in my personal case.

I thank my sister, Sonja, for our great childhood we have spent together and for loving me as a brother despite the differences in our characters, even when I am unable to show my love for her out of frustration from time to time.

I thank my Doktorvater Klaus for proposing the intriguing and at the same time challenging idea of applying semiclassics to many-body systems as subject of my diploma thesis and further for giving me the opportunity to try my best in continuing this project during my time as a PhD student. He gave one of my first lectures and thereby managed to attach my heart to theoretical physics. I further thank him for his open-minded attitude, always providing flexibility when I needed it. As his PhD student I always had the feeling of being free in deciding about the content of my work. Furthermore I thank him personally for always having a focus on not cutting out any aspects of life that others could possibly identify as peripheral in acts of inappropriate strictness. He was the right man with the right idea at the right time.

I want to thank Benni as a friend and also as a collaborator as he fitted in perfectly in both respects when he entered our little project. As a companion and co-musician he enriched my personal life a lot. As a colleague he was the most promising fit I could imagine to suck up all the ideas we had come up with so far in record time and for sure he is the perfect candidate to continue this project in the near future. He contributed a lot of essential ideas and calculations to this work and was never reluctant to provide them allowing me to use his contributions in my own interest. Besides that he also proofread this thesis, for which I am very grateful.

Last but by no means least, my special thanks go to Juan Diego – my supervisor, my colleague, my friend. First of all, I thank him as my supervisor for sharing his scientific experience with me and for always giving me the feeling of studying physics in an open-stage sense. I can not imagine anyone fitting better to my preferences regarding freedom of thoughts and intellect than him. He had a great influence on this work by throwing in important ideas many times. At the same time he would never be reluctant to step back from his own proposals when I had contrasting thoughts. This way he managed to set a stage for our scientific collaboration that allowed for what I would consider the most fruitful way of exchanging ideas. I am also extremely grateful to him for the colossal efforts he has taken in proofreading this thesis. Finally, I want to thank him for simply who he is. His way of never getting frustrated by dead ends and always having the focus on the bright sides of personal and scientific life kept me in line so many times when I was risking to sink into a bottomless abyss. He never got bored to push me up again. I thank him for lending me an ear whenever personal troubles were ahead. Besides, I will never forget the many situations as companions traveling, studying, talking bullshit, celebrating and pushing life to its limits in the very best sense. The only question about him that will persistently knock on my head until I go to my grave is: How the hell did he survive when he was too young to have a beard?

Cheers to all of you,

Quirin